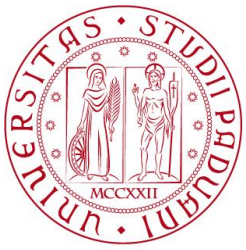

UNIVERSITÀ DEGLI STUDI DI PADOVA

UNIVERSITÀ DEGLI STUDI DI PADOVA
Dipartimento di Fisica e Astronomia "Galileo Galilei"

SCUOLA DI DOTTORATO DI RICERCA IN ASTRONOMIA
CICLO XXVIII

The ages of exoplanet hosts and field stars

Direttore della scuola: Ch.mo Prof. Giampaolo Piotto
Supervisore: Ch.mo Prof. Sergio Ortolani

Dottorando: Andrea Bonfanti

Abstract - Italian version

La tesi mira a valutare omogeneamente le età di stelle che ospitano pianeti e di generiche stelle di campo grazie alle tracce evolutive ed alle isocrone PARSEC (*PA*dova & T*R*ieste *S*tellar *E*volutionary *C*ode), v. 1.0.

Allo scopo, sono stati interamente sviluppati due algoritmi in linguaggio MatLab/Octave, basati su due differenti approcci statistici: l'uno frequentista, l'altro Bayesiano. Gli algoritmi sono stati testati su differenti campioni di stelle sintetiche per valutarne l'efficacia e metterne in evidenza i limiti.

Dopo di che abbiamo applicato gli algoritmi a due campioni di stelle appartenenti al medesimo range in tipo spettrale, essenzialmente stelle di sequenza principale di tipo G dei dintorni solari. Un campione è costituito da stelle che ospitano pianeti, mentre l'altro da generiche stelle di campo che non ospitano sistemi planetari, limitatamente alle nostre conoscenze.

Abbiamo trovato innanzitutto che le stelle ospitanti pianeti transitanti hanno una distribuzione in età molto simile alle loro omologhe per cui la velocità radiale ha rilevato la presenza di pianeti. Ciò suggerisce che questi due sottogruppi di stelle con pianeti risentono sostanzialmente dei medesimi effetti di selezione.

Infine, abbiamo messo a punto un confronto omogeneo tra stelle che ospitano o meno un sistema planetario. Gli istogrammi rappresentativi delle due distribuzioni in età presentano il picco nel medesimo intervallo [3; 3,5) miliardi di anni e la medesima mediana che è pari a 4,8 miliardi di anni.

L'affinità con l'età del Sole suggerisce che la nostra stella si trova nel tipico stato evolutivo che caratterizza le stelle G dei dintorni solari. D'altra parte, un'età mediana di 4.8 miliardi di anni risulta più vecchia rispetto a quella tipicamente assunta per il disco sottile, ove si trovano le stelle analizzate. La selezione in tipo spettrale introduce sicuramente un *bias*. È probabile, inoltre, che il nostro campionamento di stelle limitato ai soli dintorni solari non sia rappresentativo del disco nella sua interezza. Estendendo l'analisi a distanze tali da includere regioni giovani di intensa formazione stellare come il complesso del Toro-Auriga o la nebulosa di Orione, è lecito attendersi uno spostamento della distribuzione in età verso il dominio più giovane.

Abstract - English version

The thesis aims at homogeneously determining the ages of exoplanet hosts and generic field stars using stellar evolutionary tracks and isochrones computed with the *PA*dova & T*R*ieste *S*tellar *E*volutionary *C*ode (PARSEC), v. 1.0.

To achieve this goal, we fully developed two algorithms (MatLab/Octave language) based on two different statistical approaches: one is frequentistic, the other is Bayesian. The algorithms have been tested on several samples of synthetic stars, in order to evaluate their reliability and put in evidence their limits.

After that, we applied our custom-developed algorithms to two different samples of stars, belonging to the same spectral type range. They were essentially main-sequence G type stars located in the solar neighbourhood. One sample is made up of planet-hosting stars, while the other contains field stars that do not harbour planets, as far as we know.

First of all, we found that the age distribution of stars harbouring transiting planets is similar to that of stars whose planets have been discovered through the radial velocity technique. This suggests that these two subsets of stars with planets suffer essentially the same selection effects.

Finally we homogeneously compare planet-hosting stars with field stars. The histograms displaying the two age distributions peaks in the same age bin, i.e. [3, 3.5) Gyr, and have the same median age, that is 4.8 Gyr.

The median age is very similar to that of the Sun. On the one hand, this suggests that our star is in the typical evolutionary stage characterizing G-type stars of the solar neighbourhood. On the other hand, a median age of 4.8 Gyr results to be older than the typical age that is assumed for the thin disc, where the analyzed stars are located. The selection we made in spectral type does introduce a bias. Moreover, it is likely that the sampling of stars limited only to the solar neighbourhood is not representative of the entire thin disc. By extending the analysis to farther distances, so that to include young star-forming regions such as the Taurus-Auriga complex or the Orion Nebula, we expect to collect much more young stars.

Contents

List of Figures

List of Tables

Chapter 1

Introduction

Knowledge of stellar ages is a relevant issue in astrophysics, in fact it is at the base of stellar evolution. It is directly related to the history of our galaxy, the epoch of its formation and the phase of enrichment of various chemical elements. Low mass stars are long-lived objects, therefore they are particularly interesting, as tracers of the entire evolution of the Milky Way.

In the last decades, studying exoplanets and their hosts has acquired an increasing interest after the discover of the first exoplanet around a main sequence star in 1995 (Mayor and Queloz, 1995). More recently several Earth-sized exoplanets have been announced. In these cases, all the scientific community is very interested in assigning the accurate age to the planet-hosting stars, in order to assess the evolutionary stage of the hosted planets. This enables comparisons with the typical time-scales of biological evolution and an evaluation of the plausibility of the presence of life (see e.g. Kasting and Catling 2003). The research of biomarkers often passes through the thermal analysis of exoplanet atmospheres (Tinetti et al., 2015). Knowing planet age, we can also evaluate the timescales over which chemical reactions, tidal stripping or other atmospheric loss processes have act and compare the measured abundances of molecular species with the expected ones.

Another relevant issue is linked to the dynamics of exoplanetary systems (Laughlin and Chambers, 2001, Pätzold et al., 2004, Barker and Ogilvie, 2009). Many exoplanets are Hot Jupiters, i.e. close-in gaseous planets having masses comparable to that of Jupiter. Migration processes are typically invoked to justify the location of giant planets and the age of their star gives indication about migration timescales. Since the surface temperature of Hot Jupiters is very high, we can also estimate the hydrogen and helium evaporation rate. Developing a mass-radius relation as a function of age, then we can check whether planetary parameters are consistent with the model.

Another interesting topic linked to dynamics deals with the formation

and evolution of protoplanetary discs. It is very difficult to assign precise ages to the young stars still surrounded by debris discs. Reddening affects photometry, and stellar parameters would be derived by quite high uncertainties. Anyway, establishing a detailed timescale of disc evolution would enable to explore physical processes leading to the birth and evolution of the future planetary system.

Marzari (2014) explains that planet-planet scattering plays a major role in defining the architecture of planetary systems. It is likely that material is pushed out of the system both during the formation phase and in the following epochs. Actually, several free-floating planets (or nomad planets, see e.g. Strigari et al. 2012) have been discovered through the microlensing technique. These planets do not orbit around any stars and they may have been ejected from their original exoplanetary systems.

A consistent number of nomad planets may suggest whether we can justify those phenomena that are only addressed by dark matter, so far. In addition, the abundance of nomad planets would imply a descrete probability of encounters with planetary systems, which would lead to new instability phenomena.

Stability and possible evolutionary peculiarities of planet-hosting stars can be underlined by comparing their age distribution with that of field stars, not harbouring planets.

After giving an overview of the possible methods that are used for estimating stellar ages, this thesis describes the development of two different techniques based on stellar theoretical models that enable to infer the ages of stars. The corresponding algorithms have been fully tested and then applied to both a sample of exoplanet hosts and field stars. The major goals are to investigate the evolutionary stage of planet-hosting stars and compare their age distribution with that of field stars of the solar neighbourhood.

Chapter 2

Age determination methods

Computing the ages of field stars is a very difficult task. In astronomy there are parameters that can be directly obtained from observations, such as the magnitude of a star, while others are linked to observational quantities quite in a straightforward way. For instance, the effective temperature of a star can be obtained from its colour index.

Instead, facing the age problem requires the use of models, which link the observed properties with the evolutionary stage of a star. Unfortunately, the evolutionary stage is given by the nuclear burning phase and the composition of the stellar core, while we are almost obliged to investigate the global properties of the star at its surface. Thus we need proper age indicators. As pointed out by Soderblom (2010), a given property represents a so called "ideal" age indicator if:

- it is well defined and it can be measured for single stars;
- it is influenced only by age;
- it can be calibrated with known uncertainties;
- the relation between the indicator and age is invertible, so that age can be computed;
- by applying the relation to a coeval sample of stars, ages must result to be consistent.

Moreover, the age-indicator relation should be based on well known physics and such a relation should depend on as few assumptions as possible.

Such an *ideal* indicator does not exist. Each kind of star has its own problematics, so not necessarily all our available indicators can be applied. In addition, some indicators only cover a limited age range. We can distinguish the age indicators in three main cathegories.

1. Fundamental and semi-fundamental indicators. Physical processes underlying them are fully understood and observational data are available. Only few basic assumptions are required in the case of semi-fundamental indicators.

2. Evolutionary-model-based indicators. They are directly related to the internal composition of a star and its nuclear burning phase, providing the consequent observed stellar parameters.

3. Empirical indicators. Empirical relations between a given parameter and age hold. Even if the underlying physics is not necessarily fully understood, qualitative explanations about the phenomena may be given.

2.1 Fundamental and semi-fundamental indicators

The only age determined so far through a fundamental indicator is that of our Sun. It has been computed by analysing radioactive nuclides contained in the carbonaceous chondrites, which represent the most ancient material of our Solar System, formed at the epoch of its birth. According to Chaussidon (2007), its age is $4,567 \pm 1 \pm 5$ Myr, where the first uncertainty comes from measurement errors, while the second one is linked to systematics. Thus, the age of the Sun is known with very high precision and interestingly it is also the only star that does not reveal its age through its observational properties. We managed to establish its age only because we performed lab analyses of the Solar System material, which is not possible for any other star.

Two semi-fundamental indicators are also available: nucleo-cosmochronology and stellar kinematics.

2.1.1 Nucleo-cosmochronology

This method measures the abundances of radioactive nuclides present in the stellar spectra, which have a half life comparable with the ages of stars. Typically ^{238}U ($\tau_{1/2} = 4.47$ Gyr, characteristic line $\lambda = 4244.37$ Å) and ^{232}Th ($\tau_{1/2} = 14.05$ Gyr, characteristic line $\lambda = 4019.13$ Å) are used. This technique can be applied to metal-poor stars, characterized by spectra with high signal to noise ratio. In this way, the weak spectral lines of U and Th can be detected. It is necessary to assume the initial abundance of the decaying nuclides (and this may lead to biases), which is inferable from the rate of r-processes that follow any Supernova explosion. Nucleo-cosmochronological

targets are very old stars, born at the epoch of formation of the Galaxy. They are very distant, so that parallaxes measurements are usually unavailable and their luminosity cannot be computed.

The ages of stars computed through this technique may result to be older than the age of the Universe estimated by WMAP in 13.7 ± 0.2 Gyr. Typical uncertainties affecting ages are at least $\sim 20\%$. Ludwig et al. (2010) estimated that in favourable cases uncertainties are around 2.5 Gyr.

2.1.2 Stellar kinematics

This method can be applied to young stellar asociations and it requires to recover the 3D velocity vector of each star in terms of right ascension, declination and radial velocity. Stars belonging to the same association formed almost in the same place. By ideally rewind the motion of each star according to its own velocity vector, it is possible to establish the time required to move from the birth place (that is where the motion of all the stars converges) to the nowadays position. A basic assumption about the galactic potential which stars are subject to is needed, but this is not a critical point.

This technique suffers two limitations:

- orbiting around the galactic centre, massive objects perturb the regular motion of the associations, so that their motion can be constructed with high fidelity along time-scales lower than 100 Myr;
- the uncertainties characterizing the 3D velocity vector enable to reconstruct the stellar motion up to 20 Myr.

So the application of this technique is limited to stars not older than 20 Myr.

2.2 Model-dependent indicators

2.2.1 Isochrones

An isochrone is the locus of points representing coeval stars and it is defined according to our knowledge of stellar evolution. Given its theoretical origin, it is typically displayed on the Hertzsprung-Russell Diagram (HRD), but an analogous form on the observational cunterpart (i.e. the Colour-Magnitude Diagram, CMD) may also be provided. See Fig. 2.1 for a representation of theoretical isochrones on the CMD.

Stars belonging to a cluster are almost coeval and, neglecting second-order effects, they are located on a well defined region on the HRD. After superimposing isochrones having the same metallicity of the cluster, the isochrone

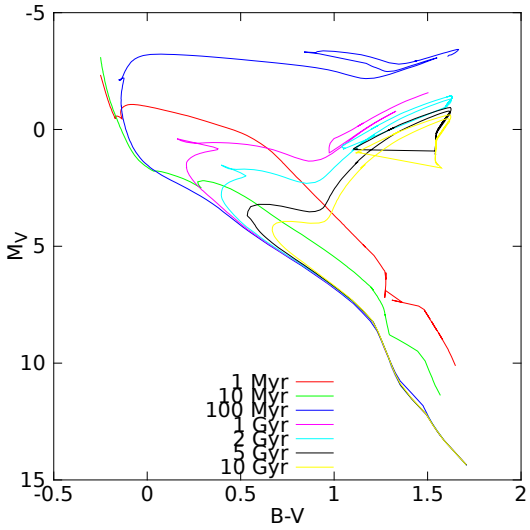

Figure 2.1: Different isochrones with solar metallicity represented on the CMD.

which best fits the global layout of the stars in the HRD expresses the cluster age. This technique is commonly called *isochrone fitting*. In the case of a single field star, instead, things are much more complicated. The star must be put on the HRD with its error bars in effective temperature $T_{\rm eff}$ and luminosity L. After that, the best isochrone having the same stellar metallicity must be selected in a proper way to account for the error box (*isochrone placement*). Several techniques can be implemented, based on a frequentistic or a Bayesian statistics and the inferred results show to be sensitive to the statistical treatment. In fact, the isochrone shapes are very complex, the relation between the position of a star on the HRD and its age is strongly non-linear and not necessarily univocal, and a star moves on the HRD with different speeds, depending on its evolutionary phase. Without taking these aspects into account while developing the algorithm could result in a biased age value.

Input parameters must be chosen according to the theoretical models in use. Isochrones typically report metallicity in terms of Z, while observational data are provided in terms of [Fe/H]. The conversion between the two indexes is no doubt a source of uncertainty, also because it depends on [α/Fe]. Stars with non-solar abundances (i.e. [α/Fe] $\neq 0$) may be result in a biased age value if this aspect is not taken into account. In fact, α-enhancement may produce remarkable changes on stellar evolution due to opacity effects, as pointed out by Marigo and Aringer (2009). Recovering stellar $T_{\rm eff}$ requires calibration processes from observational quantities as colour indexes or from

spectra. In the case of spectral analysis, temperature uncertainties arise because we try to characterize stellar atmosphere (which is not uniform), using only a global parameter, as $T_{\rm eff}$. This is an index of the total amount of energy emitted by the star, but it is not well representative of the atmospheric stratification and of the condition under which spectal lines form. Age is very sensitive to $T_{\rm eff}$ and any change in the adopted $T_{\rm eff}$ scale will affect age determination, also in a metallicity-dependent way. In fact, as pointed out by Holmberg et al. (2009), the consistency (both internal and with the $T_{\rm eff}$ scale and mix of elements adopted by theoretical models) in the choice of both the input $T_{\rm eff}$ and [Fe/H] is crucial to get reliable ages. Finally, L determination is sensitive to bolometric correction (BC). Several published table of BCs are reported in the literature, but — as emphasized by Torres (2010) — values given by an author can sensibly differ by the ones given by another author, depending on the arbitrary zero point, traditionally set using the Sun as reference. Because of these considerations, it is preferable to start from observational quantities, such as apparent magnitude, colour index and parallax and then derive the theoretical counterpart through interpolation in the isochrone grid. In this way, the internal consistency with the adopted models is preserved.

Determining ages by using isochrones is a very challenging task, especially in the case of main-sequence (MS) stars. During MS, stars quietly burn hydrogen in their core and their observational parameters vary on a very long time scale. As a consequence, MS isochrones are very close, even if they correspond to very different age values. Just to have an idea, MS isochrones with same metallicity differing by 2 Gyr are separated by 0.015 mag in $B-V$ and 0.08 mag in M_V. Such a closeness of the isochrones makes the age inference for MS stars very uncertain. This problem is particularly exacerbated in the low MS region, where different isochrones are almost overlapped because of the slow evolution of the stars located there (i.e. low mass stars). In addition, the error bars of such stars are typically big in fact photometric precision deteriorates for very dim stars and the widespread $B-V$ index loses its sensitivity to temperature when it becomes particularly red.

Furthermore, isochrones are affected by degeneracies. One is the age-metallicity degeneracy, therefore knowledge of stellar metallicity is crucial. Maintaining the metallicity fixed, the redder the colour, the older the age; maintaining the age fixed, the redder the colour, the higher the metallicity. As a consequence, a point on the CMD may be representative either of an old metal-poor star or of a young metal-rich star. Remaining in the MS, Fig. 2.2 shows that an isochrone characterized by $t = 1$ Gyr and [Fe/H]=0.05 is almost overlapped to the 3-Gyr-isochrone with [Fe/H]=0.

Another degeneracy is the age-mass degeneracy, occurring both in the

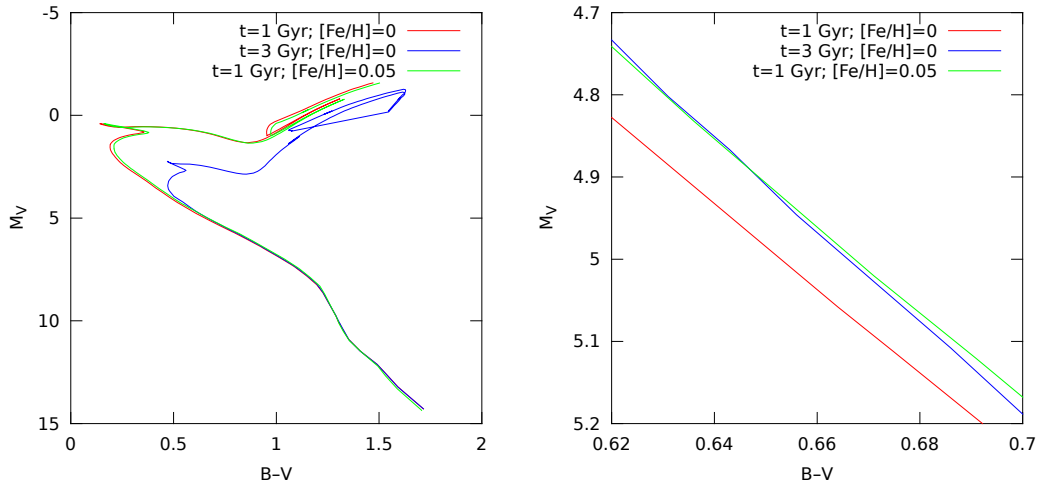

Figure 2.2: Isochrones of different ages and metallicities on the CMD showing the age-metallicity degeneracy in the MS. The zoom of the right-hand side panel shows that the 1-Gyr-isochrone with [Fe/H]=0.05 is almost overlapped to the 3-Gyr-isochrone with [Fe/H]=0.

turn-off (TO) region and near the zero-age-main-sequence (ZAMS). Degeneracies in the TO region are well clarified by Fig. 2.3, representing solar metallicity isochrones. Instead, age-mass degeneracy near the ZAMS can be understood considering that passing the Gyrs stars slowly go up along the MS occupying position where $\sim$ zero age more massive stars are. Left-hand side panel of Fig. 2.4 shows different evolutionary tracks, where more massive stars reaches the MS where luminosity is higher. The zoom on the right panel shows that the intersection point is either representative of a $1M_{\odot}$-star with $t = 6$ Gyr or of a $1.05M_{\odot}$ star with $t = 27.5$ Myr. This kind of degeneracy is also clear by looking at Fig. 2.1, where very young pre-MS isochrones (corresponding to an age of 1 or 10 Myr) intersect also very old isochrones representative of post-MS evolution. However, despite high age differences, differences in mass reported by the isochrones are often smaller than the typical uncertainties characterizing the available input mass values. In these cases, knowledge of other stellar parameters may help in better constraining ages.

2.2.2 White Dwarf cosmochronology

White dwarfs (WDs) represent the endpoint of the evolution of stars having masses up to $\sim 8M_{\odot}$. They are very compact objects, whose destiny is to become fainter and fainter, and then crystallized objects emitting no visible light: the so called black dwarf. In fact their main source of energy, which is

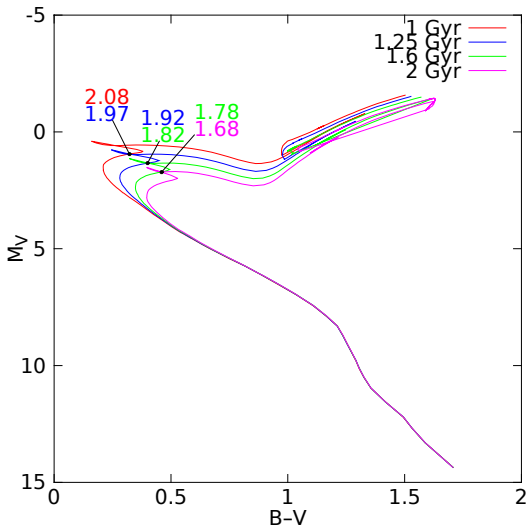

Figure 2.3: Different isochrones characterized by the same metallicity (solar in this case). Each couple of values in correspondence of the isochrone intersections in the TO region is representative of the stellar masses (in $M_{\odot}$) reported by the isochrones with the same colour. Given the overlap in the TO region, knowledge of stellar mass is crucial to remove such a degeneracy.

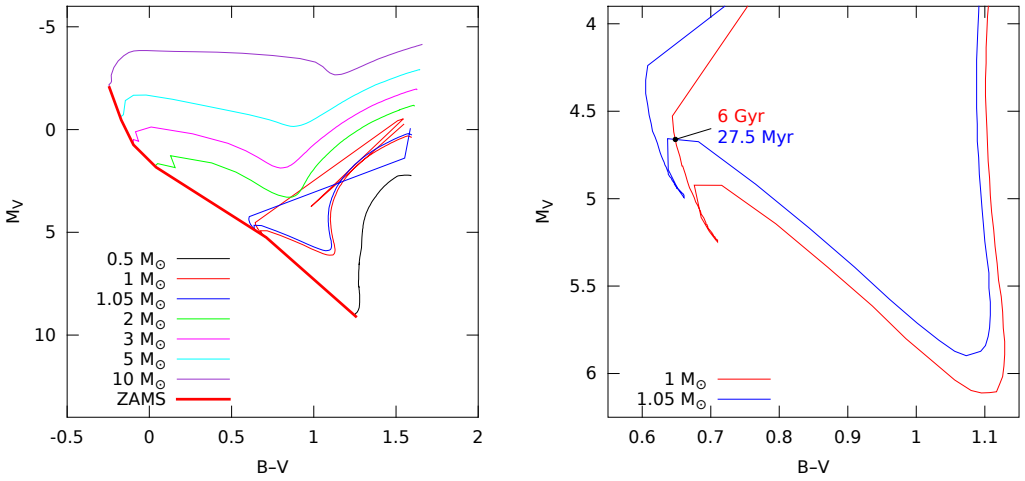

Figure 2.4: Left-hand side panel: evolutionary tracks corresponding to increasing masses going from bottom to top. Except for the 1-$M_{\odot}$-track and 1.05-$M_{\odot}$-track, the other tracks describe only the pre-MS evolutionary phase. The thick red line represents the ZAMS. The zoom on the right-hand side shows that stars of different masses pass through the same point on the CMD during different stages of their evolution.

the ion thermal energy, inevitably diminishes with time. As a consequence, knowledge of WDs parameters in conjunction with an appropriate cooling theory, enables to estimate their age. If they are members of a cluster, they may confirm the cluster age obtained in another way.

Typical WDs $T_{\rm eff}$ are around 10^4 K, while luminosities are 2-3 orders of magnitude less than solar luminosity. Therefore, even if the usefulness of WDs as cosmochronometers was already put in evidence by Schmidt (1959), the intrinsic faintness of WDs (especially of the coolest ones) has limited the application of any age determination technique for years. The mass of a WD is of the order of that of the Sun, while its dimension is comparable to that of planets. Therefore a WD is constituted by degenerate material characterized by densities ranging from 10^5 to 10^8 g/cm^3. Degenerate electrons are excellent conductors of heat, so they are able to efficiently thermalize almost all the WD. In fact, a WD can be thought as an isothermal sphere for the 99% of its mass surrounded by a thin, non-degenerate envelope. The temperature of the isothermal sphere ranges from $\sim 5 \cdot 10^6$ K to $\sim 2 \cdot 10^7$ K and then it abruptly drops only in the outer layer. As already mentioned, WDs can only cool off. In fact, nuclear burning in the core do not occur anymore and degenerate electron pressure prevent stellar contraction, i.e. gravitational energy release. In order to use WDs as cosmochronometers, it is necessary to establish its cooling rate, i.e. the rate with which heat flows from the hotter inner core to the thin, colder outer layer.

As also recalled by Fontaine et al. (2001) who present an interesting review about WDs as cosmochronometers, the total luminosity of a star $L = L(t)$ as a function of time t can be expressed through:

$$L(t) = \int_0^M \left(\epsilon - T \frac{\partial S}{\partial \rho}\bigg|_T \frac{\partial \rho}{\partial t} - c_V \frac{\partial T}{\partial t} \right) {\rm d}m \tag{2.1}$$

where ϵ is the global rate of energy production per unit mass (accounting for nuclear reactions and neutrino loss), the second addend in the integral represents the rate of gravitational energy release per unit mass (T is the temperature, S is the entropy, ρ is the density), while the third addend in the integral represents the rate of thermal energy loss per unit mass as well (c_V represents the specific heat at constant volume). The integral is computed over the entire stellar mass $M_\star$.

In the case of WDs, we can neglect the first and second term on the right-hand side of the equation and consider that the temperature T is essentially constant and given by the core temperature T_c. With these approximations,

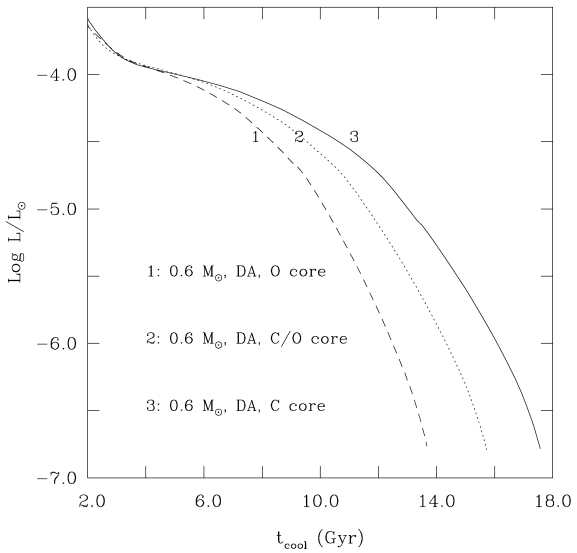

Figure 2.5: Cooling curves for 0.6 $M_{\odot}$ WDs with atmosphere made of hydrogen (DA) and with different core composition, as specified by the numbers from 1 to 3. Figure is taken from Fontaine et al. (2001).

from (2.1) we can obtain the cooling time $t_{\rm cool}$

$$t_{\rm cool} \simeq -\int_0^M c_V \mathrm{d}m \cdot \int_{L_1}^{L_2} \frac{\partial T_c}{\partial L} \frac{\mathrm{d}L}{L} \tag{2.2}$$

The first integral is related with the global amount of thermal energy of the star, while the second involves a relation between the core temperature T_c and the surface luminosity L. It can be computed by considering the thermodynamical mechanisms which predict the heat transfer from the core to the surface. As pointed out by Fontaine et al. (2001), $c_V(C) > c_V(O)$ in fact there are more ions in a gram of carbon than in a gram of oxygen, therefore starting from the same luminosity C-core WDs takes longer to cool off if compared with O-core WDs, as it is explained by Fig. 2.5.

A straightforward relation between $t_{\rm cool}$ and the major WDs parameters can be obtained only under further approximations:

- $c_V(e^-) = 0$, i.e. the specific heat is only due to ions;
- ions obey to a perfect gas law;
- strict radiative equilibrium holds in the partially degenerate envelope;
- radiative opacity χ in the envelope is described through a Kramers' law, i.e. $\chi \propto \rho T^{-7/2}$.

In this case one can recover the classic result of Mestel (1952):

$$t_{\rm cool}^{\rm Mestel} \propto A^{-1}\mu^{-2/7}M_{\star}^{5/7}L^{-5/7} \tag{2.3}$$

where A is the atomic weight of the core, μ is the mean molecular weight of the envelope, $M_{\star}$ and L are the WD mass and luminosity, respectively.

Actually, none of the last approximations are satisfactory for using WDs as cosmochronometers. Several aspects must be taken into account:

- sedimentation of C and/or O in the core, that makes the cooling time longer;
- redistribution of material between solid and liquid phases happening during the crystallization process;
- diffusion of the various atomic species;
- convective mixing;
- nuclear processes, such as picno-nuclear reactions or neutrinos loss.

Developing exhaustive theoretical models implies facing the problem of fitting WDs position with specific isochrones, rather than using a simply equation that gives $t_{\rm cool}$ in terms of WDs parameters. Thus, what has just been presented regarding isochrones in § 2.2.1 holds also here. In this context, isochrones have different shapes and occupy different position in the CMD, as it is shown in Fig. 2.6, for instance. Moreover, degeneracy problems happen in another region of the CMD, as presented by Fig. 2.7, where the intersections of the oldest WDs isochrones occur in correspondence of low luminosities.

2.2.3 Asteroseismology

Age is directly related to the nuclear burning phase, so the evolutionary stage of a star could be established if one could see the stellar core. Light, which constitutes the main information we can catch from a star, is radiated from the surface revealing nothing about its origin in the stellar centre. Given these assumptions, it seems impossible to investigate stellar interiors. Instead, since almost all the stars pulse, the modes of their oscillation give information about the internal structure of a star. Actually, asteroseismology analyses stellar oscillations as they were seismic waves.

There are different kind of modes. The simplest ones are radial modes, so that a star expands and contracts preserving its own spherical symmetry.

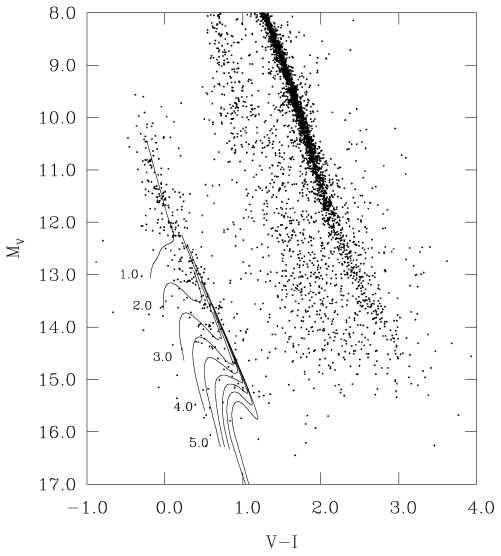

Figure 2.6: CMD of the globular cluster M4. It is clear the sequence of WDs on the left of the plot, where isochrones corresponding to different ages are superimposed. Ages increase from top to bottom and are specified in Gyr by numeric labels up to 5.0. The following values are not explicitely written to avoid confusion. [From Fontaine et al. (2001)].

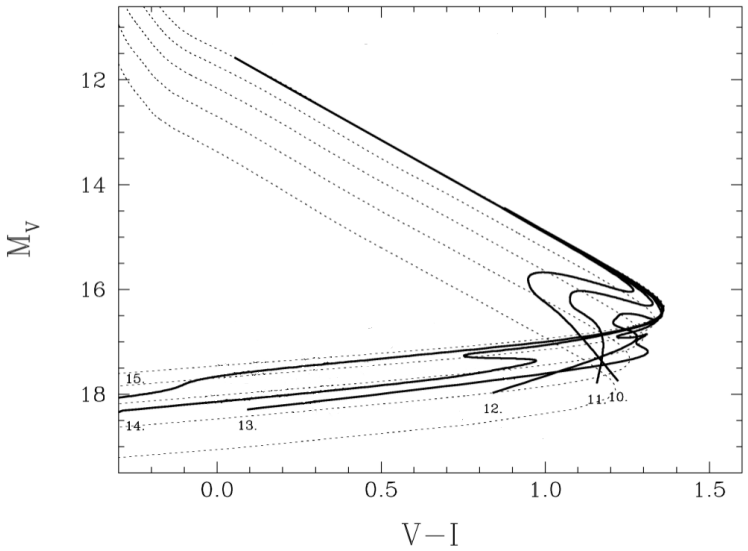

Figure 2.7: Adapted from Fontaine et al. (2001), this Figure represents five evolutionary tracks (dotted lines) of WDs with masses of 0.45, 0.6, 0.8, 1 and 1.2 $M_{\odot}$ (going from top to bottom). In addition old isochrones are displayed through solid lines and labelled with their ages (in Gyr). Degeneracies, that involve isochrones differing even by 5 Gyr, occur in the redder and fainter part of the CMD.

There are also non-radial modes, which are responsible of stellar deformation. Such a distorsion is described by eigenfunctions, which are proportional to spherical harmonics $Y_l^m(\theta, \phi)$.

$$Y_l^m(\theta, \phi) = N_l^m P_l^{|m|}(\cos\theta) e^{im\phi} \tag{2.4}$$

They are functions defined on a sphere, where θ is the colatitude, ϕ the longitude, l is the so called spherical degree, m the azimuthal order and N_l^m is a normalization constant depending on l and m. $P_l^m(\cos\theta)$ are the Legendre polynomials, defined according to

$$P_l^m(x) = (-1)^m (1-x^2)^{m/2} \frac{\mathrm{d}^m}{\mathrm{d}x^m} P_l(x) \tag{2.5}$$

Oscillations divide stellar surface in expanding and contracting regions which are getting colder and hotter, respectively. Different regions are separated by nodal lines, characterized by absence of motion. In polar coordinates nodes are recovered by imposing $P_l^m(\cos\theta) = 0$. l gives the total amount of nodal lines on the stellar surface, while m represents the number of nodal lines that are encountered moving along the equator. Radial pulsations are $l = 0$ modes; all the other modes are responsible of non-radial oscillations. In particular, if $l = 1$ we talk about dipole modes, $l = 2$ corresponds to quadrupole modes... Beyond l and m, modes are fully described using an additional index, n (radial overtone), which indicates the number of nodes inside the star. A mode with $n = 0$ is called fundamental mode. If $n = 1$ we talk about first overtone, if $n = 2$ second overtone, and so on. Apart from the identification through the triple (n,l,m), modes fall in two different cathegories: p-modes and g-modes, where p stands for pressure and g for gravity. They refer to the kind of force which brings the star back into its equilibrium configuration. In order to quantitatively distinguish p-modes from g-modes, it is necessary to introduce the concept of two different frequencies governing the propagation of pulsational modes. One of them is the Lamb frequency

$$L_l = \sqrt{l(l+1)} \frac{c_s}{r} \tag{2.6}$$

which represents the inverse of time requested to cover a horizontal distance equal to one wavelength, moving at the local speed of sound c_s. In eq. (2.6) r represents the radial coordinate. The other frequency, known as Brunt-Vaisälä frequency, indicates the rate a gas bubble vertically oscillates around its equilibrium position. It is defined by

$$N = \sqrt{g \left(\frac{1}{p_0 \gamma_1} \frac{\mathrm{d}p_0}{\mathrm{d}r} - \frac{1}{\rho_0} \frac{\mathrm{d}\rho_0}{\mathrm{d}r} \right)} \tag{2.7}$$

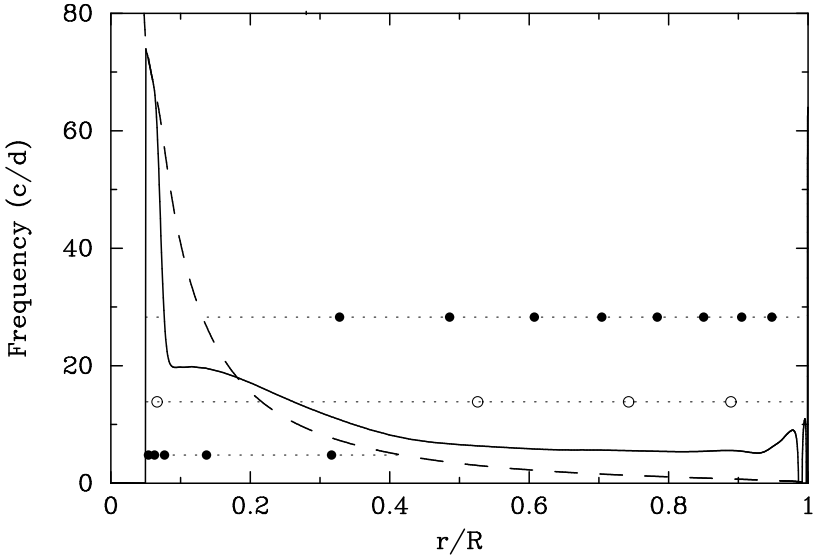

Figure 2.8: How oscillation modes propagate in the case of an evolved 2 $M_\odot$ star. Examples of stellar pulsation modes are represented through horizontal dotted lines. The behaviour of Lamb and Brunt-Vaisälä frequencies inside a star is figured out by dashed and solid lines, respectively. Because of their low frequencies, g-modes remain in the deep stellar interiors, so they are not easily detectable. Instead, p-modes take place near the surface and they can be observed. Intermediate frequency modes are able to tunnel through the evanescent region. They behave as g-modes in the deep interior and as p-modes near the surface. For they are called mixed modes. Figure is taken from Handler (2013).

where $\gamma_1 = \frac{\mathrm{d}\ln p}{\mathrm{d}\ln \rho}$ is the first adiabatic exponent, g is the local gravitational acceleration, r is the radial coordinate, p_0 and ρ_0 are the local pressure and density, respectively, in the unperturbed state. An oscillation with an angular frequency ω higher both than L_l and N is a p-mode, while an oscillation with ω lower both than L_l and N is a g-mode. Finally, if the oscillation frequency is between L_l and N, then the wave amplitude exponentially decreases and the region where it forms is called evanescent. g-modes form in the deeper stellar region, while p-modes take place near the stellar surface and may be observed. A representation of what has just been described is given in Fig. 2.8.

Assuming non-rotating stars, under asymptotic approximation the angular eigenfrequencies of p-modes result to be

$$\omega_{n,l} \simeq \Delta\omega_0 (n + \frac{l}{2} + \epsilon) - D_0 l(l+1) \tag{2.8}$$

while the periods of g-modes are

$$P_{n,l} \simeq \frac{P_0(n+\delta)}{\sqrt{l(l+1)}} \tag{2.9}$$

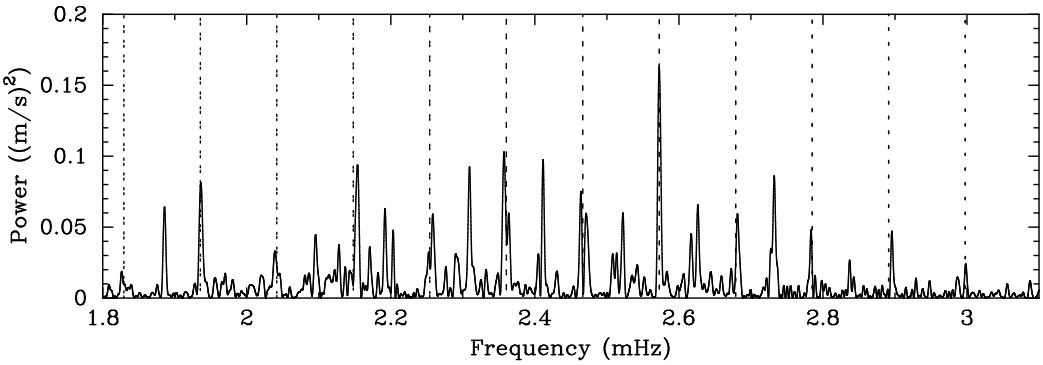

Figure 2.9: Oscillation power spectrum of α Centauri A. [From Handler (2013)]

$\Delta\omega_0$ is the inverse sound travel time required to pass through the entire star, D_0 is a frequency separation depending on the evolutionary state of the star, P_0 is the asymptotic period that is proportional to the integral of the Brunt-Vaisälä frequency N throughout the star, ϵ and δ are stellar structure parameters. Commenting eq. (2.8) and (2.9), it is clear that:

- maintaining l fixed, p-modes corresponding to consecutive values of n are equally spaced in the frequency space, while g-modes corresponding to consecutive n values are equally spaced in the period domain;
- maintainig n fixed, if $D_0 = 0$ all the p-modes having l values differing by 2 or multiples would be equally spaced in the frequency domain; in particular odd degree p-modes would occupy intermediate positions in between even degree ones.

Stellar oscillations generate motions and temperature variations on the stellar surface. This determines changes in luminosity, surface radial velocity and spectroscopic line profiles. Thus pulsating stars may be observed both spectroscopically and photometrically. Then a frequency analysis of the time series is performed, typically thanks to Fourier transforms. Since the stellar disc is not resolved, only the global effect of pulsation in luminosity or radial velocity can be observed. As a consequence, high spherical degree oscillations average into disc integrated measurements and the observed amplitudes are lower than the intrinsic ones. The observed amplitude diminishes according to $l^{-1/2}$. Because of this *geometric cancellation* only modes having $l \leq 2$ are typically detected. In exceptional cases, modes characterized by l up to 4 may also be observed.

Fig. 2.9 provides an example of the power spectrum of a solar-like oscillator as α-Centauri A. It shows equally spaced peaks (put in evidence by vertical dashed lines), which correspond to modes having the same l and

consecutive n, according to Eq. (2.8). Always as a consequence of this equation, signals in between the vertical dashed lines are modes having spherical degrees $l \pm 1$. Because of the effect of geometric cancellation, all these peaks are characterized by $l = 0$ or $l = 1$. The frequency difference between modes having $l = 0$ and consecutive n $\Delta\nu_0 = \nu_{n+1,0} - \nu_{n,0}$ is called large frequency separation. Further analysing Fig. 2.9, the majority of the peaks shows a splitting: they are characterized by spherical degrees l and $l + 2$. In fact, such modes have slightly different frequencies because of the term $D_0 \neq 0$ in Eq. (2.8). The frequency difference $\delta\nu_{02} = \nu_{0,l+2} - \nu_{0,l}$ between modes having l differing by 2 is called small frequency separation. The representation of $\delta\nu_{02}$ versus $\Delta\nu_0$ constitutes a sort of HR asteroseismic diagram. The comparison with theoretical models suggests mass and evolutionary stage of a star. Beyond the large frequency separation $\Delta\nu_0$, the oscillation power spectrum of a star is also characterized by the maximum frequency $\nu_{\max}$, which is the frequency of the maximum amplitude peak. Two scaling relations (Kjeldsen and Bedding, 1995) link $\Delta\nu_0$ and $\nu_{\max}$ to stellar surface gravity $g_\star$ and stellar mean density $\rho_\star$. In particular

$$\frac{\Delta\nu_0}{\Delta\nu_{0,\odot}} = \sqrt{\frac{\rho_\star}{\rho_\odot}} \tag{2.10}$$

$$\frac{\nu_{\max}}{\nu_{\max,\odot}} = \frac{g_\star}{g_\odot}\sqrt{\frac{T_{\mathrm{eff},\odot}}{T_{\mathrm{eff}}}} \tag{2.11}$$

By definition $\frac{\rho_\star}{\rho_\odot} = \frac{M_\star}{M_\odot}\left(\frac{R_\star}{R_\odot}\right)^{-3}$ and $\frac{g_\star}{g_\odot} = \frac{M_\star}{M_\odot}\left(\frac{R_\star}{R_\odot}\right)^{-2}$, so knowledge of $\Delta\nu_0$, $\nu_{\max}$ and T_{eff} enables to determine both stellar mass $M_\star$ and radius $R_\star$. As solar asteroseismic parameters Kjeldsen and Bedding (1995) adopt $\Delta\nu_\odot = 134.9$ μHz and $\Delta\nu_{\max} = 3050$ μHz, while Chaplin et al. (2014) adopt $\Delta\nu_\odot = 135.1$ μHz and $\Delta\nu_{\max} = 3090$ μHz.

Determining speed and intensity of oscillation modes require high precision photometry. Thus asteroseismic analyses are typically performed on luminous stars, especially giants. By deeply analysing the oscillation power spectrum and the individual oscillation frequencies, the inner density profile and the gradient of sound propagation speed can be recovered. In particular, low spherical order degree modes (luckily the ones we can detect) probe the deep interiors of stars. They suggest the central density of a star and, indirectly, its age. Ages that are determined in this way are based on the same models used for isochrones, therefore they are subjected to the same limitations.

2.3 Empirical indicators

Ages inferred from these indicators are recovered thanks to empirical relations between age and a given property of the star. Physics underlying these relations is not necessarily fully understood, even if a qualitative interpretation of the phenomena may be provided. These relations must be calibrated using stellar associations, moving groups or open clusters having ages that have already been computed though other methods, e.g. isochrone fitting. As a consequence, empirical indicators must be considered secondary with respect to model-dependent indicators.

It is difficult to properly extend the empirical relations in the domain of older ages because of the paucity of old coeval clusters, which are essential to perform the calibration. In any case, the indicators tend to become less sensible to age variations passing the Gyrs.

Four empirical age indicators will be described: gyrochronology, chromospheric activity, lithium depletion and X-ray luminosity. They are applicable to low mass stars, in fact their justification origins in the convective envelope which is present in this kind of stars.

2.3.1 Gyrochronology

In the convective envelope the material is ionized and so conductive. The interaction between convection and differential rotation determines even complex motions of the conductive cells, which magnify the pre-existent magnetic field **B** according to the dynamo model. Now, late type stars present an outflow of charged particles (generally called wind) and the presence of the magnetic field determines the co-rotation of the wind far away from the stellar surface. So a comparatively small amount of mass loss results in a proportionately high amount of angular momentum loss. According to this scenario, the rotational velocity of a star $v_{\rm rot}$ progressively diminishes following an inverse power-law relation $v_{\rm rot} \propto t^{-1/2}$, as already pointed out by the works of Kraft (1967) and Skumanich (1972). Recently, Collier Cameron et al. (2009) calibrated the following relation between rotational period P, colour $J-K$ and age t upon the Coma Berenices open cluster, whose age has been estimated in $t_{\rm CB} = 591$ Myr.

$$t = t_{\rm CB} \left(\frac{P}{9.71 + 10.68(J-K-0.528)} \right)^2 \tag{2.12}$$

Instead, Barnes (2010) introduced a simple non-linear model to describe the evolutionary spin-down of cool stars, which yields to the following relation

between the age t and the stellar rotational period P.

$$t = \frac{\tau}{k_C} \ln\left(\frac{P}{P_0}\right) + \frac{k_I}{2\tau}\left(P^2 - P_0^2\right) \tag{2.13}$$

Here $k_C = 0.646$ d/Myr, $k_I = 452$ Myr/d and P_0 is a free parameter ranging from 0.12 to 3.4 days ($P_0 = 1.1$ days corresponds to the initial rotational period of the calibrated solar mass model). τ represents the (global) convective turnover time which is a function of the colour index $B - V$ and whose values are tabulated in Barnes and Kim (2010). The measurement of the stellar rotational period P should be the starting point for gyrochronology. P can be recovered studying the photometric modulation due to spots that, for instance, characterizes solar-type stars. As reported by Guinan and Engle (2009), photometric modulation is easily detectable in young stars (say $t < 1.5$ Gyr) also from ground-based surveys, which enable photometric precision of the order of ~ 5 mmag. Instead, for older solar-type stars, spots cover not more than 1% of the entire stellar surface, so P determination through photometry is very difficult. High precision photometry is requested and it can be reached thanks to space missions.

The application of gyrochronology suffers several limitations:

- Sometimes amplitude light variations are too low to be detected, so P cannot be inferred. In such cases, if we deal with a statistically significant sample of stars, the problem can be overtaken by using spectroscopic $v \sin i$ value. i is the angle between the stellar spin axis and the line of sight, so $v \sin i$ represents the lower limit for the rotational velocity v of a star. Assuming a random orientation of stellar spin axes, the mean rotational velocity of a star $\bar{v}$ is expected to be greater than $v \sin i$ by a factor $\frac{4}{\pi}$. If the stellar sample to be analyzed is numerous, gyrochronological ages inferred from $\bar{v}$ can be considered statistically reliable.

- Stars belonging to the same cluster are globally coeval, but their rotational periods may present significant dispersion. $P \propto t^{1/2}$ is calibrated on slow rotators, therefore faster rotators result to be younger than they are.

- Different clusters having the same or similar ages do not show identical period distribution, which introduces further uncertainties about gyrochronological relations. Other parameters, such as chemical composition, may influence age, but they do not enter current gyro calibrations.

- Star-disc locking during pre-MS and different initial rotational velocity of protostellar nebula influence ZAMS velocity of stars. Magnetic braking progressively spins down stars. The faster their rotational velocity, the more effective the spin down, so that faster rotators are spun down quicker than slower ones. As a consequence, all the stars have approximately the same rotational velocity after few Gyrs. Fig. 2.10 taken from Denissenkov (2010) shows rotational velocity convergence, regardless of the initial rotational velocity.

Further uncertainties are related to the application of gyrochronological relations to field stars. Period-age relations are essentially calibrated upon cluster stars. Barnes (2009), Brown (2014), Kovács (2015) showed that isochronal ages are considerably greater than gyro-ages if field stars are analyzed. In other words, Kovács (2015) stresses that, apparently, non-clusters field stars have significantly lower slow-down rates than their cluster counterparts. Van Saders et al. (2016) confirm the presence of unexpectedly rapid rotators among stars that are more evolved than the Sun.

We can conclude that, if on the one hand slow rotating stars are actually old, on the other hand faster rotators are not necessarily young. The correctness of gyro calibrations exploring the fast-rotators regime is still a matter of debate. For instance, Van Saders et al. (2016) suggest that if field star evolution were modelled through a weakened magnetic braking, then the gyro relations would retrieve ages that would be consistent with isochronal or asteroseismic ages.

2.3.2 Magnetic activity

Stellar magnetic fields $\mathbf{B}$ are generated by the dynamo mechanism and reveal themselves through the so called chromospheric activity (CA). According to processes still not known, neither for the Sun, non-thermal energy deposits in the stellar chromosphere and corona. Chromospheric properties are inferable by analysing strong absorption lines, such as Hα, Mg II h and k lines, Ca II H and K lines and the Ca II infrared triplet. Although these lines are easily detectable, it is not so easy to disentangle the chromospheric component of the flux (which is the true CA signal) from the photospheric (or basal) one.

Also CA scales proportional to $t^{-1/2}$ as rotation does. Actually, the link between rotation and activity is causal, as pointed out by Skumanich (1972). In fact, the decrease in rotational velocity due to angular momentum loss weakens the dynamo mechanism, which is the source of $\mathbf{B}$. The weaker $\mathbf{B}$, the weaker CA. Rotational velocity and convective zone depth correlates with CA, acting in opposite direction. On the one hand, high rotational velocities

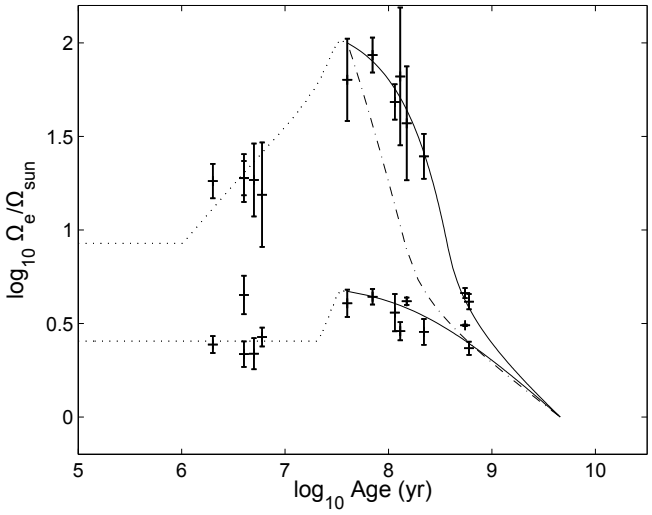

Figure 2.10: Evolution of stellar angular velocity Ω for different models, that have been developed by Denissenkov (2010). The upper solid line is representative of the rotation of the radiative envelope that is totally decoupled to that of the convective core. The point-dashed line in the middle represents partial coupling between core and envelope increasing with time, while the bottom solid line holds for core and envelope rotationally coupled. Finally point curves describe the evolution of the star during the pre-MS phase with star-disc locking still present. Regardless of the initial rotational velocity, Ω converges towards low values after a few Gyr.

characterizing high $T_{\rm eff}$ stars favour plasma mixing in the convection zone, which strengthen **B**. On the other, dynamo processes acting thanks to the deep convective zone in low $T_{\rm eff}$ stars enhance **B**, as well.

A typical indicator of the stellar CA is represented by $\log R'_{\rm HK}$, which expresses the ratio between the chromospheric flux measured in the cores of the Ca II H and K lines and the total bolometric flux. In order to properly define $\log R'_{\rm HK}$, one may introduce Mount-Wilson S_{MWO} index, which has become the standard measure of stellar CA, since O.C. Wilson started a long-term monitoring program of the activity of MS stars in 1966. It is defined (Vaughan et al., 1978, Duncan et al., 1991) as

$$S_{MWO} = \alpha \frac{N_H + N_K}{N_R + N_V} \tag{2.14}$$

where:

- N_H and N_K are the number of counts in the triangular bandpasses H and K with a FWHM of 1.09 Å, centred in the Ca II H and K cores (located at 3968.47 Å and 3933.66 Å, respectively);
- N_R and N_V are the number of counts in the 20 Å continuum bandpasses R and V centred at 3901.07 Å and 4001.07 Å, respectively, after a time normalisation and a sky correction;
- $\alpha = 2.4$ is a calibration factor.

In the literature the mean $S_{\rm HK}$ value is usually given. It represents the mean magnetic activity level of a star averaged over a long period. In fact, chromospheric emission is influenced by rotation modulation or flares, and also can have relatively large cyclic variations. Middelkoop (1982) provided a formula that converts $S_{\rm HK}$ into $R_{\rm HK} \propto \frac{F_{\rm HK}}{\sigma T_{\rm eff}^4}$, where $F_{\rm HK}$ is the total flux coming from both H and K bands. The default conversion is

$$R_{\rm HK} = 1.34 \cdot 10^{-4} C_{\rm cf} S_{\rm HK} \tag{2.15}$$

$C_{\rm cf}$ is a standard conversion factor determined by Middelkoop (1982) as well, which depends upon $B-V$ colour index. In fact, $S_{\rm HK}$ is sensible to the integrated emission in the R and V bands, which is related to the stellar spectral type. It holds

$$\log C_{\rm cf} = 1.13(B-V)^3 - 3.91(B-V)^2 + 2.84(B-V) - 0.47 + \delta(B-V) \tag{2.16}$$

If $x \equiv 0.63 - (B-V)$, $\delta(B-V)$ is a corrective term defined by

$$\delta(B-V) = \begin{cases} 0.135x - 0.814x^2 + 6.03x^3 & \text{if } x > 0 \\ 0 & \text{if } x < 0 \end{cases} \tag{2.17}$$

Stellar magnetic activity is specifically reflected by the chromospheric component of the flux measured in the core of Ca II H and K lines. Thus Noyes et al. (1984) introduced the parameter $R'_{\rm HK}$, which is given by the ratio between the chromospheric emission (obtained by subtracting the photospheric component to the total flux) and the total bolometric flux in the H and K line cores. So

$$R'_{\rm HK} = R_{\rm HK} - R_{\rm HK,phot} \tag{2.18}$$

where the photospheric (or basal) term is estimated through

$$\log R_{HK,\rm phot} = -4.898 + 1.918(B-V)^2 - 2.893(B-V)^3 \tag{2.19}$$

Starting from the index given by eq. (2.18), Mamajek and Hillenbrand (2008) calibrated an age-activity relation based on the data of nine star clusters with known age. They derived the following fit

$$\log t = -38.053 - 17.912 \log R'_{\rm HK} - 1.6675 \log^2 R'_{\rm HK} \tag{2.20}$$

which holds for the range between -5.1 and -4 in $\log R'_{\rm HK}$. The standard deviation of age is $\sim 16\%$ for $\log R'_{\rm HK} < -4.3$. Activity-age relations like the one given in (2.20) give reliable ages only in the case of young stars. In fact, Ca II emission saturates for stars older than $\sim$ 3-4 Gyr, therefore it becomes insensitive both to rotation and age for older stars. In addition, multiple $\log R'_{\rm HK}$ measurements taken on long cadence observations should be used, to ensure to trace the effective average chromospheric activity of a star.

2.3.3 Lithium depletion

The lithium depletion phenomenon is another consequence of the presence of a convective envelope. Because of convective motions, Li may be transported downwards, where hotter temperatures fuse it, depleting its content. Li depletion is observed in solar type stars, with the Sun that constitutes an extreme case. In fact, its Li content is 200 times less than Li content found in the primordial material of our Solar System.

According to Fu et al. (2015), pre-MS phase plays a key role in determining Li abundance. Three main mechanisms act: convective overshooting (OV), late mass accretion and photo-evaporation of circumstellar gas induced by extremely ultraviolet radiation (EUV photo-evaporation). Stars are initially fully convective and Li is efficiently burned when they reach the effective Li-burning temperature of $\sim 4 \cdot 10^6$ K (i.e. the temperature required to consume the entire Li content in $\sim 10^7$ yrs). As the central region heats

up, the core becomes radiative, but surface Li depletion can go ahead thanks to overshooting, which extends the mixed outer convective envelope into the hotter stellar interior. Consistently with the observational evidences, soon after the formation of the radiative core the size of the OV region is $\Lambda_e \approx 1.5 H_p$ (where H_p is the pressure scale height), and then it scales proportionally to the mass of the outer convective region until the typical value estimated for the Sun $\Lambda = 0.3 H_p$ (Christensen-Dalsgaard et al., 2011) is reached. Under these conditions, OV is so efficient that the photospheric Li is significantly depleted after few Myr.

Recent observations of late pre-MS stars (De Marchi et al., 2010, Spezzi et al., 2012) suggest that residual disc accretion processes may last longer than previously believed: at least some tenths of Myr and even up to the early MS phase (De Marchi et al., 2011). The residual accreting material keeps the original Li content, so that it tends to restore the Li abundance. This restoring effect is modulated by EUV photo-evaporation, that is produced by high energy stellar photons (λ = 10-121 nm). In fact, such photons heat the circumstellar disc gas enough to let it escape from stellar gravitational potential. The lack of residual circumstellar material gradually turns off the late accretion processes. According to this scenario the accreting mass rate declines following relation (2.21):

$$\dot{M} = \dot{M}_0 \left(\frac{t}{\tau_{\rm acc}} \right)^{-\eta} \tag{2.21}$$

where $\dot{M}_0 \sim 2 \cdot 10^{-8}\ M_\odot {\rm yr}^{-1}$ is a reasonable initial mass loss rate according to Hartmann et al. (1998), $\tau_{\rm acc} \sim 10^5$ yrs and $\eta = 0.9$. Instead, the disc mass loss due to EUV photo-evaporation is given by (Dullemond et al., 2007):

$$\dot{M}_{\rm EUV} \sim k \left(\frac{\Phi_{\rm EUV}}{10^{41}\ \ {\rm s}^{-1}} \frac{M_\star}{M_\odot} \right)^{0.5} \tag{2.22}$$

where $k = 4{\cdot}10^{-10}\ M_\odot {\rm yr}^{-1}$, $\Phi_{\rm EUV}$ is the EUV photon luminosity (photons$\cdot$s^{-1}) produced by the central star and $M_\star$ is the stellar mass. $\Phi_{\rm EUV}$ is a function of $T_{\rm eff}$ and $R_\star$ and it typically spans a range from 10^{38} to 10^{42} photons$\cdot$s^{-1}. At an age of $\sim$ 60 Myr, the residual accretion is prevented by EUV evaporation. In summary, the combination of these three effects tends to level out the photospheric Li abundance of stars of whatever mass just after the pre-MS phase at a value that is lower than the initial Li content. After that, during the MS phase, Li is significantly depleted by burning at the base of the convective envelope only if stellar mass $M_\star \lesssim 0.6\ M_\odot$. The temporal evolution of surface Li content in both the pre-MS and MS phase is displayed in Fig. 2.11, taken from Fu et al. (2015).

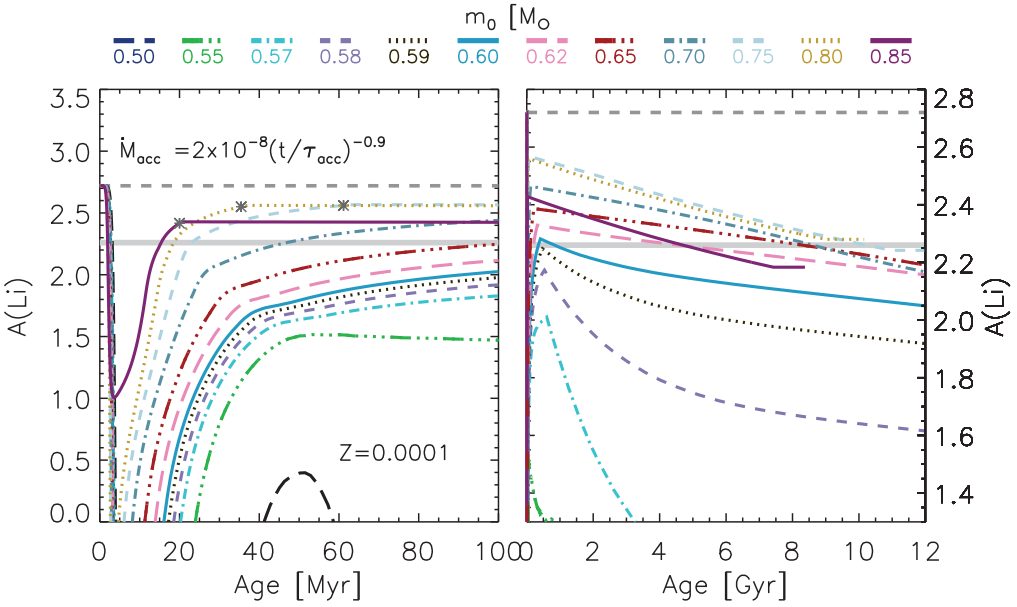

Figure 2.11: The Li abundance $A(\mathrm{Li})$ is plotted versus stellar age for both the pre-MS (left-hand side panel) and MS (right panel) phase. We recall that $A(\mathrm{Li}) = 12 + \log[n(\mathrm{Li})/n(\mathrm{H})]$, where n is the atomic number density. [From Fu et al. (2015)].

Li I abundance is usually inferred from the equivalent width of the $\lambda =$ 6708 Å line. Spectroscopic analysis of this line is not so easy, because it is typically blended with other lines and, in case of Li-poor-stars, such a line has an equivalent width $W_\lambda < 2$ mÅ. Moreover, since Li ionization potential is quite low, the most abundant form of stellar lithium is Li II. However, its characteristic line at $\lambda = 6103$ Å is often undetectable. Thus, the typically analyzed $\lambda = 6708$ Å line is strongly influenced by $T_{\rm eff}$. In addition, absence of local thermodynamical equilibrium (LTE) may not be negligible. Anyway, Li I line is typically evident in very young stars, where $W_\lambda > 100$ mÅ. In particular, Li I is often used to recognize T-Tauri stars.

2.3.4 X-ray luminosity

Solar-like stars have coronae emitting in soft X-rays regime. At those wavelengths stellar emission is entirely non-thermal, so the corona produces high contrast signals. Nevertheless, the signal is quite weak and difficult to detect, except for young or nearby stars. X-ray emission L_X tends to diminish with age and it is particularly strong for pre-MS and ZAMS stars. Therefore, X-ray luminosity is especially suitable to distinguish very young stars. In fact, several studies on solar type stars with large age spread, led e.g. by Dorren and Guinan (1994), Güdel et al. (1997), Guinan et al. (2003), Ribas et al.

(2005), have shown that at the ZAMS the Sun was rotating 10 times faster than nowadays. The higher the rotational velocity $v_{\star,\mathrm{rot}}$, the more vigorous the magnetic dynamo and stronger the coronal emissions in X-rays and far UV rays. As an example, despite our Sun at the ZAMS was 30% dimmer than today, it had an X and UV flux 100-1000 times stronger than today.

Güdel et al. (1997) firstly proposed $L_X \propto t^{-3/2}$, which was then confirmed by Giardino et al. (2008). Since $L_X \propto v^2_{\star,\mathrm{rot}}$, such a scaling relation suggests a stellar spin-down proportional to $t^{-3/4}$, which is steeper than the power-law $t^{-1/2}$ proposed by Skumanich (1972). Actually, stars with the same age and similar masses may present large spread in L_X, as already pointed out by e.g. Stern et al. (1995), Micela et al. (1996), Micela (2002). The observed spread in L_X is linked to the different rotational velocity with which stars come to MS, because of the different star-disc coupling during the pre-MS phase. In addition, X-ray emission saturates at high levels like chromospheric emission and the measured L_X decline depends on the X-ray wavelengths because of changes in the coronal structure and in its temperature.

Thanks to the project *Sun in Time*, which monitors several G0-5 V stars regarding their ground-based photometry, spectroscopy, magnetic activity and X and UV flux, Guinan and Engle (2009) fit the following $\log L_X$-t relation for solar-type stars

$$\log L_X = 31.84 - 3.338 t^{0.2176} \tag{2.23}$$

where L_X is expressed in erg/s, while the age t in Gyr. This equation disregards uncertainties on the fitted coefficients, which are fully reported in Fig. 2.12. This Figure shows the X-ray luminosity L_X of solar type stars of different ages, which were usually estimated from membership to nearby clusters. X-ray luminosities of solar-age-stars differ by ~ 3 orders of magnitude with respect to the youngest stars. Fig. 2.13, instead, shows the solar fluxes in different wavelength intervals versus age, as inferred from the studies of solar-type stars. The fluxes are normalized to the corresponding mean flux values of the present Sun. It is striking that at the Sun's birth hard X-ray emission (λ = 1-20 Å) was ~ 1000 times higher than today.

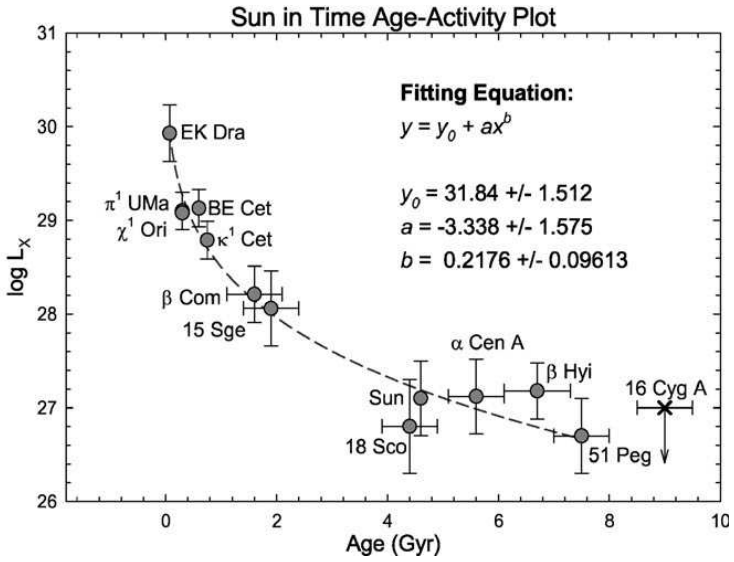

Figure 2.12: Coronal X-ray (0.2-2.5 keV) luminosity L_X [erg/s] of solar-type stars plotted versus age, as taken from Guinan and Engle (2009). The least-squares fit to the data is shown through dashed lines and the coefficients of the relation are also provided. The emission difference between the youngest and oldest stars spans more than three orders of magnitude.

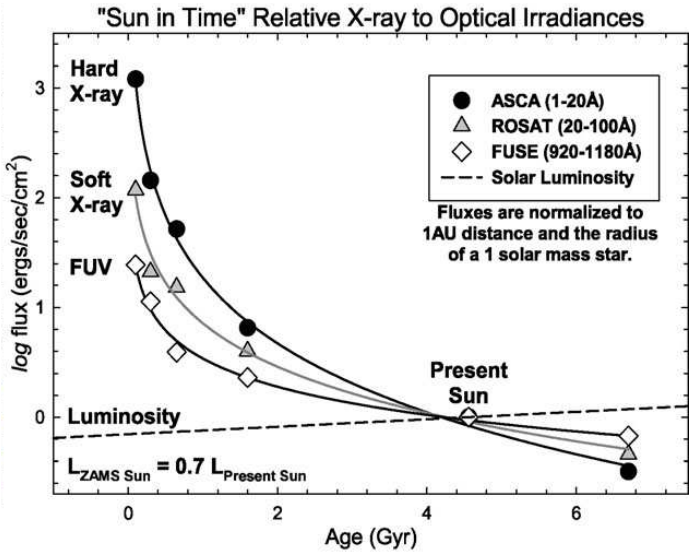

Figure 2.13: Fluxes at different wavelengths as inferred for the Sun history, on the basis of studies of solar-type stars. Flux values are normalized to the corresponding flux values of the present Sun. The dashed line represents the bolometric luminosity evolution of the Sun. The Figure is taken from Guinan and Engle (2009), who took spectral irradiance data from Ribas et al. (2005).

Chapter 3

Theoretical models and algorithms

3.1 Padova isochrones

Computation of stellar ages has been done thanks to PARSEC (*PA*dova & T*R*ieste *S*tellar *E*volutionary *C*ode) isochrones and evolutionary tracks, which are available at the CMD web interface.[1] All technical details are specified in Bressan et al. (2012); here we briefly summarize the key aspects. Theoretical models span a metallicity range from $Z = 0.0005$ to $Z = 0.070$ and a mass range from 0.1 $M_\odot$ to 12 $M_\odot$. They include the pre-MS phase, so zero age begins with the birth of a star and covers a range up to $\log t = 10.13 \Rightarrow t \approx 13.5$ Gyr.

Solar abundances are generally taken from Grevesse and Sauval (1998), except for some chemical elements, whose references are reported in Tab. 3.1. With these assumptions, the present day solar metallicity results to be $Z_\odot = 0.01524$. Microscopic diffusion is taken into account following the algorithm of Salasnich (1999) and the diffusion coefficients are computed according to Thoul et al. (1994). As a result, the initial solar metallicity $Z_{\mathrm{ini},\odot} = 0.01774$. The helium content Y is assumed to increase with Z, according to $Y = Y_p + \frac{\Delta Y}{\Delta Z} Z$, where $Y_p = 0.2485$ (Komatsu et al., 2011) is the primordial He abundance, while the helium-to-heavy elements enrichment ratio $\frac{\Delta Y}{\Delta Z} = 1.78$, that is derived from solar calibration considering that $Z_{\mathrm{ini},\odot} = 0.01774$ and $Y_{\mathrm{ini},\odot} = 0.28$.

Main solar parameters upon which isochrones are calibrated are $L_\odot = 3.846 \cdot 10^{33}$ erg/s, $R_\odot = 6.9598 \cdot 10^{10}$ cm, $T_{\mathrm{eff},\odot} = 5778$ K (all consistent with Guenther et al., 1992). According to Girardi et al. (2008), $M_{\mathrm{bol},\odot} =$

[1] CMD input form: `http://stev.oapd.inaf.it/cgi-bin/cmd`

Table 3.1: Specific references for solar abundances adopted by PARSEC

Element	Reference	Element	Reference
Li	Caffau et al. (2011)	K	Caffau et al. (2011)
C	Caffau et al. (2010)	Fe	Caffau et al. (2011)
N	Caffau et al. (2009)	Eu	Mucciarelli et al. (2008)
O	Caffau et al. (2008)	Hf	Caffau et al. (2008)
P	Caffau et al. (2007)	Os	Caffau et al. (2011)
S	Caffau and Ludwig (2007)	Th	Caffau et al. (2008)

4.770 mag and, through interpolation in the isochrone grid, it turns out that $BC_\odot = -0.063$ mag, $B - V_\odot = 0.667$ and $\log g_\odot = 4.432$. A complete overview of solar parameters adopted by Padova isochrones is given by Bonfanti et al. (2015, Table 1).

Convective energy transfer is treated according to mixing length theory (MLT, see Böhm-Vitense, 1958). Mixing length parameter $\alpha_{\rm MLT}$ is set through solar model calibration and results to be $\alpha_{\rm MLT} = 1.74$. Overshooting is taken into account, as well, both above the convective core (see Bressan et al., 1981) and below the convective envelope (according to Alongi et al., 1991, Bressan et al., 1993). Its reference parameter is the mean path Λ taken by a convective bubble *across* the convective border, expressed in terms of a pressure scale height. This choice differs from the typical convention used in the literature where the mean bubble path taken only *beyond* the convective border is considered. Just to have a rough idea, $\Lambda = 0.5$ in the Padova formalism corresponds to a pressure scale height ~ 0.25 according to the definition often found in the literature. Anyway, the overshoot parameter Λ is not constant, but it depends on mass. This dependence is particularly evident for MS stars in the mass range between 1.0 and 1.5 $M_\odot$. Therefore overshooting from the convective core (resp. from the convective envelope) is described through a variable Λ_c (resp. Λ_e) parameter. Indicating with M_1 and M_2 ($M_1 < M_2$) two limiting masses that vary according to the initial chemical composition of the model, $\Lambda_c = 0$ for $M < M_1$, $\Lambda_c = \Lambda_{\rm max} = 0.5$ for $M > M_2$ and it varies smoothly from 0 to $\Lambda_{\rm max}$ in the $M_1 < M < M_2$ mass regime. Similarly, $\Lambda_e = 0.05$ for $M < M_1$, $\Lambda_e = 0.7$ for $M > M_2$ and it varies smoothly from 0.05 to 0.7 in the intermediate mass regime. As recalled by Bressan et al. (2012), the overshoot from the convective envelope has almost negligible effects on the evolutionary stages of stars unlike the overshoot in the central region.

In order to compute ages, we used different grids of PARSEC isochrones (version 1.0), each one characterized by its own metallicity. Theoretical

isochrones report the metallicity in terms of Z, while we usually deal with the observational counterpart [Fe/H]. Considering that the relation between Z and [Fe/H] is exponential, to guarantee linearly spaced [Fe/H] values, it is necessary to take Z values in geometric progression. In particular, to have isochrone grids differing at most by δ[Fe/H] = 0.05, we select Z values belonging to a geometric progression with common ratio 1.115 from 0.0005 up to 0.00945 and then all the values from 0.010 to 0.070 at steps of 0.001. We adopted the following Z-[Fe/H] relation

$$Z = 10^{[\mathrm{Fe/H}]-1.817} \tag{3.1}$$

which is a reduced version of the one proposed by Straniero et al. (1992)

$$\log Z = [\mathrm{Fe/H}] + \log 0.6369 f_\alpha + 0.3631 - 1.658 \tag{3.2}$$

where $\log f_\alpha = [\alpha/\mathrm{Fe}]$. Relation (3.2) becomes (3.1) if $f_\alpha = 1 \Rightarrow [\alpha/\mathrm{Fe}] = 0$, i.e. stars have solar α-enhancement. This hypothesis is reasonable, in fact all the analyzed stars are essentially disc stars farther not more than a few hundreds of parsecs and, in any case, except for just a few stars, no detailed spectroscopic analyses in terms of α-elements abundance are carried out. In addition, the zero-point of the metallicity scale has been changed from -1.658 to -1.817, so that [Fe/H]=0 for $Z = Z_\odot = 0.01524$, consistently with Padova isochrones.

Each grid of isochrones reports stellar age values from $\log t = 6$ to $\log t = 10.1$ (where t is in years) at steps of 0.05. We used the UBVRI-JHK photometric system; the bolometric corrections for the majority of stars ($T_{\mathrm{eff}} > 4000$ K) are mostly based on the ATLAS9 ODFNEW models described in Girardi et al. (2008). No circumstellar dust corrections are performed, also because they would affect only oxygen-rich or carbon-rich stars with a high mass loss rate, i.e. red supergiants or thermally-pulsing asymptotic giant branch (TP-AGB) stars, which are not our targets. Therefore, also any selection of the BCs for carbon stars proposed by the web interface and based either on Loidl et al. (2001) or Aringer et al. (2009) does not affect the final results. We also maintained the default value of $\eta_{\mathrm{Reiners}} = 0.2$, that describes tha mass loss rate of red giant branch (RGB) star.

Finally, initial mass function (IMF) for single star has been set to Chabrier (2001) lognormal, while interstellar extinction to $A_V = 0$. In fact, data about interstellar extinction for field stars are not usually available and, anyway, target stars are not farther than a few hundreds of parsecs, so that reddening is negligible. Just to have an idea, Casagrande et al. (2011) carried out a re-analysis of the Geneva-Copenagen survey, which contains 16,682 nearby F and G stars of the solar neighbourhood. The colour excess $E(B-V) = 0$ for 75% of them.

```
# File generated by CMD 2.4 (http://stev.oapd.inaf.it/cmd) on Sat Nov 24 10:55:23 CET 2012
# PARSEC isochrones, stable release v1.0
# Basic reference: Bressan et al. (2012, MNRAS in press, arXiv:1208.4498)
# Warning: the TP-AGB phase is not included! TP-AGB tracks are in preparation by Marigo et al.
# Photometric system: <i>UBVRIJHK</i> (cf. Maiz-Apellaniz 2006 + Bessell 1990)
# BCs of Carbon stars derive from Loidl et al. (2001, A&A 342, 531)
# O-rich circumstellar dust ignored
# C-rich circumstellar dust ignored
# IMF: Chabrier (2001) lognormal
# On RGB, assumed Reimers mass loss with efficiency eta=0.2
# Kind of output: isochrone tables
#       Isochrone  Z = 0.01700  Y = 0.27900    [M/H] = 0.067  eta_R = 0.200  Age =  1.0000e+06 yr
#   Z  log(age/yr)    M_ini  M_act  logL/Lo  logTe  logG  mbol  U     B     V     R     I     J     H     K     int_IMF  stage
    0.017000     6.0000 0.10000000   0.1000 -1.2062 3.4940 3.5662 7.785  13.340 11.743 10.095 8.856  7.309  5.907  5.374  5.100  1.57040203   0
    0.017000     6.0000 0.12000000   0.1200 -1.0959 3.4994 3.5565 7.510  12.910 11.355 9.727  8.517  7.012  5.644  5.110  4.840  1.74782515   0
    0.017000     6.0000 0.13678978   0.1368 -1.0168 3.5036 3.5514 7.312  12.610 11.078 9.466  8.275  6.800  5.456  4.919  4.653  1.87379706   0
    0.017000     6.0000 0.14000000   0.1400 -1.0025 3.5044 3.5501 7.276  12.556 11.029 9.419  8.231  6.762  5.422  4.885  4.619  1.89584959   0
    0.017000     6.0000 0.14810064   0.1481 -0.9701 3.5065 3.5507 7.195  12.426 10.909 9.307  8.128  6.674  5.346  4.807  4.543  1.94897318   0
    0.017000     6.0000 0.19716123   0.1972 -0.8004 3.5192 3.5559 6.771  11.709 10.257 8.699  7.575  6.210  4.950  4.404  4.150  2.20929670   0
    0.017000     6.0000 0.18809053   0.1881 -0.8298 3.5169 3.5557 6.845  11.835 10.372 8.806  7.672  6.291  5.018  4.473  4.218  2.16780996   0
    0.017000     6.0000 0.18322349   0.1832 -0.8444 3.5156 3.5539 6.881  11.901 10.431 8.861  7.721  6.331  5.052  4.508  4.251  2.14448190   0
    0.017000     6.0000 0.17132814   0.1713 -0.8835 3.5125 3.5515 6.979  12.070 10.584 9.003  7.850  6.439  5.143  4.600  4.341  2.08397698   0
    0.017000     6.0000 0.24260345   0.2426 -0.6770 3.5311 3.5703 6.463  11.151 9.750  8.228  7.150  5.870  4.670  4.114  3.869  2.38394117   0
    0.017000     6.0000 0.22266515   0.2227 -0.7285 3.5258 3.5635 6.591  11.378 9.959  8.424  7.328  6.010  4.785  4.235  3.986  2.31341982   0
    0.017000     6.0000 0.20450160   0.2045 -0.7793 3.5211 3.5583 6.718  11.611 10.170 8.619  7.503  6.151  4.901  4.354  4.102  2.24109650   0
    0.017000     6.0000 0.29757386   0.2976 -0.5520 3.5459 3.5934 6.150  10.561 9.210  7.728  6.700  5.526  4.396  3.826  3.590  2.54156017   0
    0.017000     6.0000 0.27541295   0.2754 -0.6005 3.5399 3.5840 6.271  10.795 9.424  7.926  6.877  5.660  4.501  3.937  3.698  2.48368859   0
    0.017000     6.0000 0.25478178   0.2548 -0.6484 3.5343 3.5759 6.391  11.019 9.629  8.116  7.049  5.792  4.607  4.048  3.805  2.42317200   0
    0.017000     6.0000 0.30000001   0.3000 -0.5467 3.5466 3.5942 6.137  10.535 9.187  7.706  6.680  5.511  4.384  3.814  3.578  2.54750419   0
    0.017000     6.0000 0.32195401   0.3220 -0.5009 3.5525 3.6026 6.022  10.326 9.011  7.559  6.545  5.394  4.275  3.693  3.466  2.59819126   0
```

Figure 3.1: Part of an isochrone grid, as downloaded from the CMD web interface.

To summarize, for each metallicity value the grid of isochrones lists stellar age, mass, effective temperature, bolometric luminosity, surface gravity, bolometric magnitude and absolute magnitudes in the Johnson-Cousin photometric system. Fig. 3.1 reports a part of an isochrone grid as illustrative purpose.

3.1.1 The impact of stellar model input physics on ages

The reliability of the output ages inferred from isochrones is impacted by the input physics of the theoretical models and by the adopted chemical abundances. In this subsection we briefly discuss the reasonability of PARSEC assumptions and how their change may impact the resulting ages.

The initial chemical composition is one of the main input when developing stellar models. As reported by Lebreton et al. (2014), different elements enter different chemical processes with different level of importance. For instance, nuclear reaction rates are most related to the abundance of H (during MS) and then of heavier elements such as He, C, O, etc. The opacity is mainly determined by H, He, Fe, O and Ne, while microscopic diffusion involves all the chemical elements. Instead, there are also elements such as ^{6,7}Li, ^{9}Be or ^{13}C that do not influence the stellar structure very much.

According to PARSEC solar model, the helium-to-metals enrichment ratio $\frac{\Delta Y}{\Delta Z} = 1.78$. The solar mixture is based on the abundances reported by Grevesse and Sauval (1998, GS98) (which would imply $(Z/X)_{\odot} = 0.0229$), except for some elements, whose abundances are essentially taken from Caffau (CAF10, see Table 3.1). Actually, several more up-to-date abundance tables are available, like the ones from Asplund et al. (2009, AGSS09) or

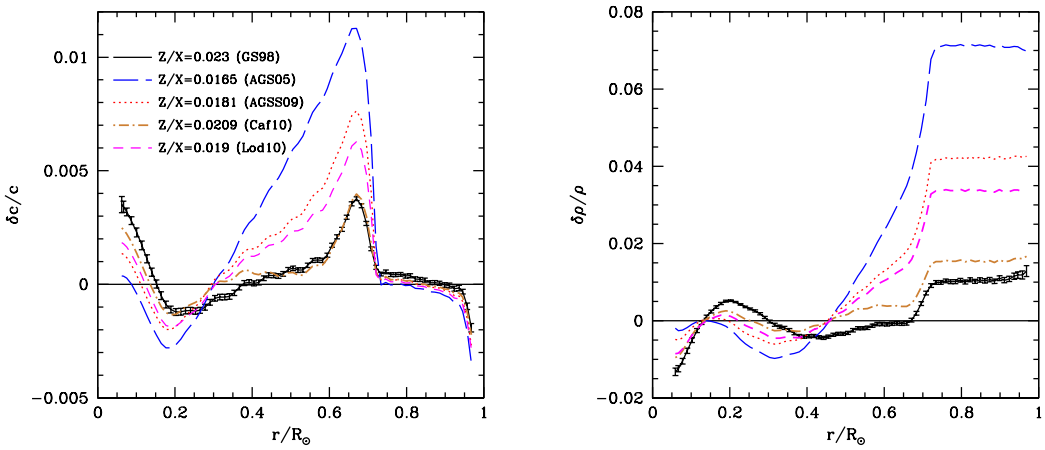

Figure 3.2: Different models trying to reproduce the sound propagation speed c and the density profile ρ of the Sun, as inferred from helioseismology. *Left-hand side panel*. Relative difference in the sound propagation speed $\frac{\delta c}{c}$. *Right-hand side panel*. Relative difference in density $\frac{\delta \rho}{\rho}$. In both the two panels, quantities are plotted versus the radial distance from the core, expressed in terms of fraction of solar radius. Different models are considered, namely Grevesse and Sauval (1998, GS98), Asplund et al. (2005, AGS05), Asplund et al. (2009, AGSS09), Caffau et al. (2010, 2011, CAF10), Lodders et al. (2009, LOD10). Horizontal 0-line represents perfect agreement with the values inferred from helioseismic observations. For the sake of clarity, error bars are shown only for one model. Plots are taken from Basu and Antia (2013).

Lodders et al. (2009), which are derived from 3D model atmospheres. Basu and Antia (2013) tested several models based on different solar mixtures to find the ones that fit the structure of the Sun coming from helioseismology best. The results of the analysis are shown in Fig. 3.2. Both the GS98 and CAF10 models show a similar degree of agreement with the Sun, both in terms of internal sound propagation speed and density. Despite e.g. AGSS09 model is more recent, however it is less consistent in reproducing the solar structure derived from helioseismology. Therefore, so far the choice by Bressan et al. (2012) is reasonable considering our ability of modelling internal sound propagation speed and density profile in the Sun.

As mentioned above, the input chemistry (H and He abundances, solar mixtures, α-element enhacement) affects the nuclear reaction rates and the stellar opacity. Proton-proton chain (p-p chain) reaction rate is constrained by helioseismology with an uncertainty of $\pm 15\%$ (degl'Innocenti et al., 1998). Regarding the CNO cycle, instead, Broggini et al. (2010) extrapolated its reaction rate in the low energy domain where stellar nuclear reactions take place (typically from a few Kev to less than 0.1 Mev), starting from the measurements taken with the LUNA device (see e.g. Formicola and LUNA Collaboration 2002). Predictions about nuclear reaction rates are also in-

fluenced by the so called screening factor due to electrons. In fact, the interaction between positive nuclei in nuclear reactions occurs in presence of electrons. The electron cloud surroundings the nuclei slightly reduces the Coulomb repulsive barrier between nuclei, so that nuclear reaction rates are enhanced. Considering the typical uncertainties in deriving nuclear reaction rates, Lebreton et al. (2014) estimated the age impacts at most $\sim 9\%$ and $\sim 4\%$ for the p-p chain and the CNO cycle, respectively. Such age impacts occur for stars with $\sim 1 M_{\odot}$, while in other mass domains age variations are significantly less.

Radiative opacity is expressed through the Rosseland opacity κ, that is a function of stellar temperature, density and chemical composition. Uncertainties on these quantities impact κ. Bailey et al. (2015) were able to reproduce typical solar interior conditions in laboratory (essentially in terms of electron temperature and density) and they measured the wavelength-resolved iron opacity of the generated plasma. The measured values result to be higher than the predicted one. According to the authors, iron accounts for a quarter of the total opacity at the solar radiation/convection boundary and its enhanced opacity leads to a κ increase of $\sim$ 1-2%. On the whole, all the uncertainties related to stellar temperature, density and chemical composition impact κ and then age. Lebreton et al. (2014) computed that increasing κ by 10%, the resulting isochronal age would be increased by 6% to 14%. Qualitatively, age increases because the higher the opacity, the lower the luminosity, and therefore the longer the MS lifetime.

In general, as summarized by Lebreton et al. (2014), changes in opacities may be due to different sources:

- uncertainty on the solar mixture. The smaller the $(Z/X)_{\odot}$, the smaller Z and Y (if $\frac{\Delta Y}{\Delta Z}$ is constant), and this implies higher X. Because of the opacity increase due to H, isochronal ages result to be higher.

- α-elements enhancement: age generally decreases if evaluated using α-enhanced models, but the entity of the variation depends also on [Fe/H].

- uncertainty on metallicity. At constant $\frac{\Delta Y}{\Delta X}$, increasing [Fe/H] produces two competing effects: on the one side, Y increases, which implies lower age values; on the other side, the opacity increases, which reduces the luminosity and implies higher ages. In low-mass stars the most important role is played by bound-bound and bound-free opacities due to metals, so that ages are evaluated globally higher. Instead, in high-mass stars, opacity is less affected by the metal increase since free-free opacities are predominant. Therefore, the Y increase is the prominent

factor and this implies younger ages. Quantitatively, [Fe/H] variations by ± 0.1 dex imply age differences up to 8%.

- uncertainty on the He abundance. Generally speaking, increasing Y increases also the mean molecular weight, which leads to higher luminosities and therefore smaller isochronal ages.

- uncertainty on $\frac{\Delta Y}{\Delta Z}$. Increasing the helium-to-metals enrichment ratio produces models richer in He, which yield to the determination of lower isochronal ages because of the Y increase.

Changing either the helium content by ± 0.03 dex or the $\frac{\Delta Y}{\Delta Z}$ ratio from +2 to +5 may lead to age variations up to 20-30%.

Staying in the context of chemical abundances, microscopic atomic diffusion (also referred to element diffusion) is responsible of depleting stellar surface of metals. The net effect is that the present-day Z of a star differs from the one the star had at its birth. This impact the choice of the theoretical grid of isochrones to be chosen to compute age. This specific topic is faced in § 3.2.1, while here we briefly examine the theoretical counterpart of the element diffusion. Transport of chemical elements inside low-mass stars (spectral types from G to K) are led by pressure (gravitational settling), temperature and concentration gradients. In hotter A-F stars radiative forces play also an important role. In any case, the net effect of element diffusion is to push heavy elements towards the core, while the hydrogen abundance increases at the surface. The increase of the central helium abundance enhances the stellar luminosity, which imply a shorter MS phase. Lebreton et al. (2014) report that implementing element diffusion in stellar evolutionary models leads to an estimation of lower isochronal ages by a few percent.

Another thorny factor entering the input picture of stellar models is the mixing length parameter $\alpha_{\rm MLT}$, which describes the efficiency of energy transport through convection in stars. For decades, the solar $\alpha_{\rm MLT,\odot}$ has been used for every star, whatever its mass. Recently, Trampedach and Stein (2011) investigated the $\alpha_{\rm MLT}$ variations for solar chemical composition stars using 3D surface convection simulations. They found that for masses decreasing from 1.5 to 0.7 $M_\odot$, $\alpha_{\rm MLT}$ increases from 1.7 to 2.2, with $\alpha_{\rm MLT,\odot}$ around 1.7-1.8. In addition, very recent 3D radiative hydrodynamic simulations (Magic et al., 2015) show that the derived mixing length parameter differs from the one computed through simpler 1D simulations. In particular, $\alpha_{\rm MLT}$ ranges between 1.7 and 2.3, basically dependent on stellar mass. Magic et al. (2015) prove that the higher the $T_{\rm eff}$ and/or [Fe/H], the lower $\alpha_{\rm MLT}$; the higher the $\log g$, the higher $\alpha_{\rm MLT}$. Apart from MLT, also other theories that take the multi-spatial scale nature of convection into account have been developed.

Among them, it is worth to cite the Full Spectrum of Turbulence theory (FST, by Canuto and Mazzitelli 1991, Canuto et al. 1996). FST requires a convective-scale parameter, as the MLT approach, however the inferred convective flux differ from the one obtained using the MLT.

Anyway, despite the different values that $\alpha_{\rm MLT}$ may assume, Lebreton et al. (2014) show that the $\alpha_{\rm MLT}$ impact on isochrones is small, confirming what already stated by Castellani et al. (1999). In fact, stars hotter than ~ 7000 K (say $M \gtrsim 1.8 M_{\odot}$) are not impacted at all, since such stars have too thin convective envelopes to consider convection remarkable. The maximum effect for a change in $\alpha_{\rm MLT}$ takes place for stars in the range 1.2-1.5 $M_{\odot}$, but even for ± 0.20 dex $\alpha_{\rm MLT}$ perturbation, the age relative variation does not exceed $\sim 3\%$. Therefore, adopting $\alpha_{\rm MLT} = \alpha_{\rm MLT,\odot} = 1.74$ for every stars as Bressan et al. (2012) is reasonable. Computing tracks with variable $\alpha_{\rm MLT}$ may be considered in future releases of the evolutionary code.

Two other main phenomena are essential to produce realistic evolutionary models: overshooting and rotation. MS stars with masses greater than $\sim 1.2 M_{\odot}$ develop a convective core because the efficiency of the CNO burning cycle strongly depends on temperature. Core overshooting consists in convective bubbles still moving in the radiative envelope, beyond the extension of the convective core. Including the expected core overshooting in models increases the effective size of the mixed core. This provides more fuel to stars, so that its MS life lengthens.

The overshooting distance can be quantified through the $\alpha_{\rm ov}$ parameter, that is generally expressed in terms of a reference pressure scale-height H_p. Left-hand side panel of Fig. 3.3 actually shows that models involving overshooting result in longer MS phase, that ends at higher luminosities and lower $T_{\rm eff}$. As a result, overshooting is not negligible for stars with $M_{\star} \gtrsim 1.2 M_{\odot}$. Its impact on ages has been estimated by Lebreton et al. (2014) in $\sim 30\%$ for a 1.5 $M_{\odot}$. The impact decreases with stellar mass, anyway it still amounts around $\sim 10\%$ at 20 $M_{\odot}$ (see the right-hand side panel of Fig. 3.3).

Rotation is another process that enter stellar evolution. It influences many physical processes involving angular momentum and matter transport, so that its treatment is very complex (see e.g. Maeder et al. 2013, Meynet et al. 2013, Mathis 2013). The consequent modifications of internal angular velocity and chemical composition profile also due to differential rotation, strongly impact age-dating. In fact, as reported by Lebreton et al. (2014), rotationally induced mixing provides additional fresh hydrogen to the stellar core. The net effect is that the mass of the stellar core results to be higher, similarly to what is produced by the convective overshooting. Actually, different studies led by Talon et al. (1997), Eggenberger et al. (2010), Marques et al. (2013), Goupil and Talon (2002) agree that for $M_{\star} \gtrsim 1.8 M_{\odot}$, the effect

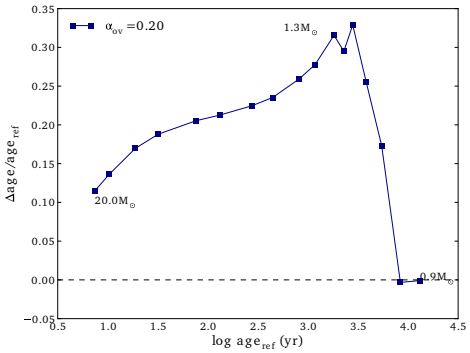

Figure 3.3: *Left-hand side panel.* Evolutionary tracks of different stellar masses with no overshooting (solid lines) and with overshooting quantified through $\alpha_{\rm ov} = 0.2H_p$ (dashed lines). For masses greater than $\sim 1.2M_\odot$, overshooting lengthens the MS phase by $\sim 20\%$. Such stars present a convective core, that is responsible of the characteristic "double hook" of the tracks on the HRD. In each track, the end of the MS occurs at the left hook. As a consequence of the overshooting, the MS phase ends at higher luminosities and lower $T_{\rm eff}$. *Right-hand side panel.* Relative differences in the isochronal ages of stars evaluated considering models with $\alpha_{\rm ov} = 0.2H_p$, with respect to reference models, where overshooting is not taken into account. Computing ages using models with implemented overshooting leads to higher age estimations, from $+10\%$ to $+30\%$, except for low mass stars ($M_\star \lesssim 1M_\odot$). The Figures are taken from Lebreton et al. (2014).

of rotationally-induced mixing is roughly equivalent to the effect of a core overshooting with $\alpha_{\rm ov} \approx 0.1H_p$. As a consequence, implementing rotation in evolutionary models allows to decrease the amount of needed core overshooting to reproduce observations to $\alpha_{\rm ov} \lesssim 0.10H_p$. Instead, ignoring rotation, the core overshooting parameter amounts at ~ 0.15-$0.20H_p$. Thanks to data provided by Ekström et al. (2012), Lebreton et al. (2014) estimated that ages computed through models that take stellar rotation into account may differ up to $\sim 30\%$. Age differences are slightly less (however remarkable) for metal-poor models. Rotation does not strongly impact isochronal ages only in the domain of low-mass stars, i.e. $M_\star \lesssim 1.1M_\odot$. The influence of rotation on stellar ages is clarified by Fig. 3.4.

The impact of different physical/chemical inputs entering theoretical models is synthesized by Fig. 3.5, taken from Lebreton et al. (2014). Taking the mean impact on age, that has been averaged over the possible stellar masses and metallicities, it is clear that the helium abundance, the choice of the helium-to-metals enrichment ratio and the treatment of overshooting and rotation are the most important factors that impact the isochronal age.

In the worst cases relative differences may amount up to $\sim 40\%$. On the one hand, the evaluation of the age of an individual star might differ from another estimation if different theoretical models are used for age computation.

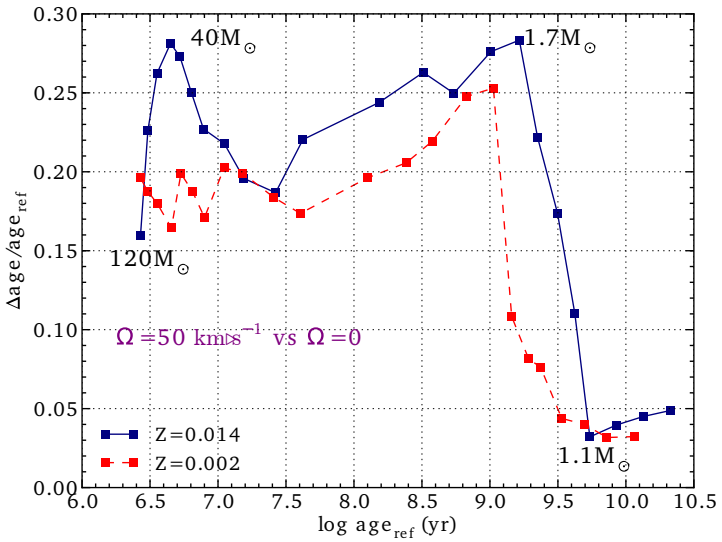

Figure 3.4: Relative age difference arising when stellar rotation is taken into account by theoretical models. In this case, an angular rotational velocity $\Omega = 50$ km/s is assumed, while the reference model does not consider rotation. High age differences (up to $\sim 30\%$) characterize all the stars with $M_\star \gtrsim 1.3M_\odot$. For $M_\star \gtrsim 1.7M_\odot$ the impact on age is almost constant regardless the mass, and it is slightly influenced by the metallicity. Only in the $M_\star \lesssim 1.1M_\odot$ regime, the implementation of rotation in models does not affect the isochronal age in a remarkable way. [From Lebreton et al. (2014)].

On the other hand, it is worth to emphasize that the algorithms we developed use additional parameters such as the stellar surface gravity, density (inferred from observations), rotational velocity and magnetic activity beyond the "classical ones" (i.e. magnitudes in different bands, metallicity and distance) to compute stellar ages. Therefore, the present work constitutes the best attempt to establish the age of individual stars so far. Even more so, in this thesis we will develop global age comparisons between samples of stars. We are more interested in the relative shape of the age distribution of a sample with respect to the other. Since the comparisons are homogeneous regarding the age derivation techniques, then our results can be judged statistically reliable.

3.2 Isochrone placement implementation

The basic idea of the isochrone placement technique is to properly compare the mutual position of a star and of theoretical isochrones on the CMD, in order to derive a reliable age for such a star.

Before starting describing the algorithm, it is worth to present some preliminary considerations.

3.2.1 Element diffusion

The interaction between different chemical species in stars characterized by a convective envelope leads to a progressive surface depletion of elements heavier than hydrogen, that sink downwards. The characteristic time-scale for the diffusion of an element is (Chaboyer et al., 2001):

$$\tau_{\rm diff} \simeq K \frac{M_{\rm CZ}}{M_\star T_{\rm CZ}^{3/2}} \tag{3.3}$$

where $M_\star$ is the stellar mass, $M_{\rm CZ}$ the mass of the convective envelope, $T_{\rm CZ}$ the temperature at the base of the convective zone and K is a constant referring to the chemical element taken into account. Diffusion acts in the same direction of the temperature and pression gradients and in the opposite direction with respect to the chemical concentration gradient. For further details see Burgers (1969) and Chapman and Cowling (1970, 3rd ed.).

Fig. 3.6 shows the surface metallicity evolution with time $Z = Z(t)$ for stars of different masses, as inferred from specific tables of Padova evolutionary tracks (Leo Girardi, private communication) reporting the surface metallicity content of a star time by time. This Figure assumes an initial surface metallicity $Z_{\rm ini} = 0.017$ for all the stars. In any cases, independently

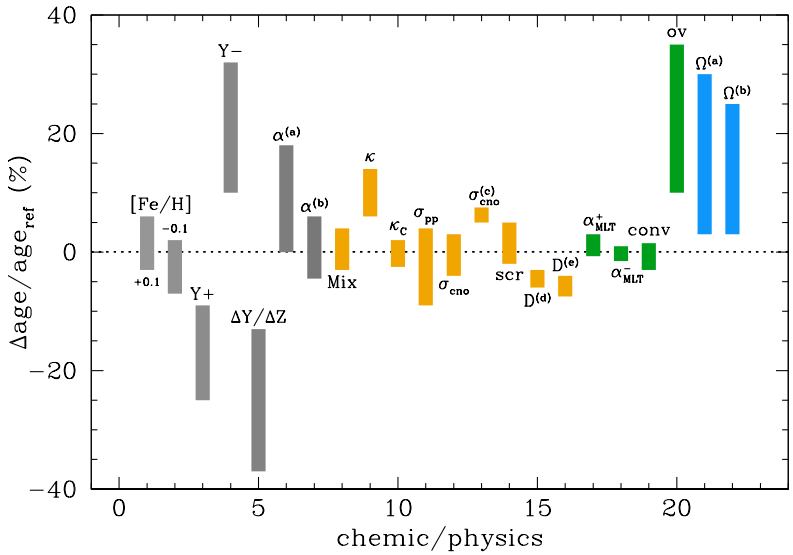

Figure 3.5: Variations of different input parameters entering theoretical evolutionary models are considered to test their impact on isochronal ages. The chemical/physical inputs are labelled through progressive numbers along the x-axis. All the variations are evaluated with respect to the solar calibrated model and they are the following: [1,2] δ[Fe/H]$= \pm 0.1$ dex; [3,4] $\delta Y = \pm 0.03$ dex; [5] $\delta \frac{\Delta Y}{\Delta Z} = +3$; [6] $\delta(\alpha\text{-enhancement}) = +0.4$ dex at [Fe/H]=0; [7] $\delta(\alpha\text{-enhancement}) = +0.4$ at [Fe/H]$= -1$; [8] solar mixture taken from AGSS09, instead that from GN93; [9] opacity variation $\frac{\delta\kappa}{\kappa} = 0.1$; [10] conductive opacity taken from Iben (1975) instead that from Cassisi et al. (2007); [11] p-p chain reaction rate variation $\frac{\delta\sigma_{\rm pp}}{\sigma_{\rm pp}} = -0.15$; [12] ^{14}N$(p,\gamma)^{15}$O reaction rate taken from LUNA (Formicola et al., 2004) instead that from NACRE (Angulo et al., 1999), at [Fe/H]=0; [13] same as [12], but now [Fe/H]$=-2$; [14] nuclear reaction rates variations due to the screening factor (screening vs. no screening); [15] atomic diffusion vs. no diffusion; [16] no diffusion vs. diffusion with diffusion velocities increased by 20%; [17,18] $\delta\alpha_{\rm MLT} = \pm 0.2$ dex; [19] convection implemented following the Mixing Length Theory (MLT) vs. convection implemented following the Full Spectrum of Turbulence theory (FST); [20] convective core overshooting quantified by $\alpha_{\rm ov} = 0.2 H_p$ vs. no overshooting; [21]: rotation implemented considering a stellar angular velocity $\Omega = 50$ km/s vs. no rotation, at [Fe/H]=0; [22]: same as [21], but now [Fe/H]$=-1$.

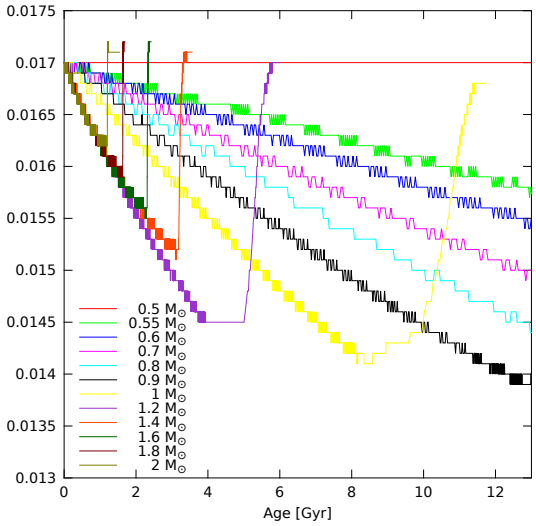

Figure 3.6: Temporal evolution of the surface metallicity of stars having the same initial metallicity (in this case $Z_{\rm ini} = 0.017$), but different masses. The ruggedness of the curves is due to discrete steps in the model and has been smoothed thanks to piecewise polynomial interpolation during the algorithm implementation.

from $Z_{\rm ini}$, it turns out that low mass stars up to 0.5 $M_\odot$ exhibit constant Z during their entire life, as well as stars more massive than ~ 2 $M_\odot$. In the intermediate mass range, instead, Z diminishes during the MS phase. After that, as the convective envelope deepens, the consequent mixing of elements makes the star as metallic as it was at its birth, approximately.

The online available Padova isochrone grids are identified only through $Z_{\rm ini}$, while we know only the present day metallicity of a star, of course. Typical targets of this work are late spectral type stars with masses around 1 $M_\odot$. This is the mass range where the difference between Z and $Z_{\rm ini}$ may also be sensible, depending on the evolutionary stage of a star. Therefore, as already shown by Bonfanti et al. (2015, Fig. 4), neglecting the element diffusion effect may result in older age derivations, especially for intermediate age stars. For instance, using the $Z = Z_\odot = 0.01524$ grid of isochrones to compute the age of a solar star (i.e. a star having exactly the same properties of our Sun), the isochrone placement gives an age $t = 5.1 \pm 2.8$ Gyr, which differs from the real solar age $t = 4.5 \pm 0.1$ Gyr that one would have obtained if he had correctly used the $Z = Z_{\rm ini,\odot} = 0.01774$ grid of isochrones.

Thanks to the specific set of evolutionary tracks provided by Girardi, we built up a piecewise 3$^{\rm rd}$-degree-polynomial interpolation of the different curves $Z_{k,l} = Z_{k,l}(t)$, for any given stellar mass and $Z_{\rm ini}$ (represented through the subscripts l and k, respectively). In this way, it is possible to infer what

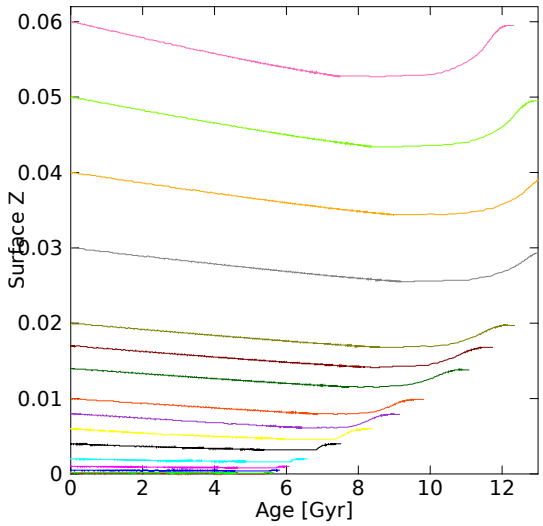

Figure 3.7: Temporal evolution of the surface metallicity Z of stars of the same mass (1 $M_{\odot}$ in this case), but with different $Z_{\rm ini}$.

$Z_{\rm ini}$ of a given star was, starting from its present Z and a first raw guess of its age and mass, after an iterative process. In fact, at first iteration, the isochrone grid identified by the present day metallicity of the star is employed, in order to derive a first guess for stellar age ($t_{1,\star}$) and mass ($M_{1,\star}$). Then, the interpolated curves $Z_{k,M_{1,\star}}(t)$ describing the temporal metallicity evolution of stars with mass $M_{1,\star}$ and different $Z_{\rm ini}$ (identified by the subscript k) are taken into account. By inserting $t_{1,\star}$ in $Z_{k,M_{1,\star}}(t)$, one finds the metallicity that a given $Z_{\rm ini}$-star has at the age $t_{1,\star}$. The two $Z_{k_1,M_{1,\star}}(t_{1,\star})$ and $Z_{k_2,M_{1,\star}}(t_{1,\star})$ values that are the nearest to the present day $Z_{\star}$ enable to infer the first guess for the initial metallicity of the star ($Z_{1,{\rm ini},\star}$), after linear interpolation. By selecting the grid of isochrones characterized by $Z_{1,{\rm ini},\star}$, new output values for stellar age and mass are obtained. The just described algorithm is repeated iteratively until a convergence in the $Z_{{\rm ini},\star}$ values is reached. Fig. 3.7 represents temporal evolution of surface Z for stars of 1 $M_{\odot}$ with different initial metallicity values.

3.2.2 Distinguishing pre-MS stars from older ones

As already presented, the CMD shows degeneracies between pre-MS isochrones and older ones. Despite the geometric overlap on the diagram, very young stars sensibly differ from older ones in terms of e.g. rotational velocity, chromospheric activity and mean stellar density. We complemented pure isochrone analysis with evolutionary information coming from parameters

linked to these three properties in order to better constrain age. In particular, we computed up to 3 age values (namely t_v, $t_{\rm HK}$ and t_ρ) through age-scaling relations to preliminary evaluate the ensemble of isochrones to be used in the following age computation; here follow the details.

Stars are subjected to rotational decline, as a consequence of angular momentum loss through coronal magnetic winds (Kraft, 1967, Skumanich, 1972). Thus pre-MS stars are expected to rotate much more faster than MS stars. There are essentially two independent approaches to derive stellar rotational velocity v. Especially in the case of late spectral type stars, spots are spread throughout the stellar surface. They identified magnetically active regions that prevent hot convective bubble coming from inner stellar parts to reach the surface. As a consequence, these regions are colder than the surrounding surface and they appear darker. By performing high precise photometry on a sufficiently long timescale, the stellar flux appears to be characterized by an almost periodic photometric modulation because stellar rotation periodically puts spots along the line of sight. The period of the inferred light curve corresponds to the stellar rotational period P. If the stellar radius $R_\star$ is known from e.g. interferometry or stellar models, then it is possible to compute $v = \frac{2\pi R_\star}{P}$.

However, the most widespread index linked to stellar rotation is the spectroscopic $v \sin i$, where i is the angle between the stellar spin axis and the line of sight. If the stellar disc is ideally divided in vertical slices, the ones that "are approaching" the observer because of stellar rotation will emit blue-shifted flux, while the others red-shifted flux. As a result, spectral lines appear broader and suggest how fast the star is spinning. If a star is edge-on with respect to the line of sight, then exactly v can be recovered; if the star is pole-on, no rotational line broadening is observed and this method fails. In all the intermediate cases only the component of the stellar rotational velocity parallel to the line of sight (i.e. $v \sin i$) can be recovered. Degeneracy with i cannot be removed if the rotational period P is unknown. However, considering a random space orientation of stellar spin axes, it can be proven that the probability density function $p(i)\mathrm{d}i = \sin i \mathrm{d}i$. Thus, the expectation value for $\sin i$ is $< \sin i >= \frac{\pi}{4}$ and so $\bar{v} = \frac{4}{\pi} v \sin i$ represents a good reference value for the stellar spin.

We used relation (2.13) developed by Barnes (2010) to infer a reference gyrochronological age t_v. P_0 was set equal to 1.1 days, as the standard solar model. P was computed by combining $\bar{v}$ with the input stellar radius $R_\star$ (available once stellar $T_{\rm eff}$ and L were recovered from the isochrones). Considering that the global convective turnover time τ appears at denominator of (2.13), the gyro-relation was employed only for stars with $0.443 < B - V \leq 1.631$ (i.e. $3.5096 \leq \log T_{\rm eff} < 3.8081$), so that $\tau \neq 0$,

as reported by Barnes and Kim (2010). Meibom et al. (2015) suggest that gyro-ages with precision around 10% can be inferred for stars up to 2.5 Gyr, so we considered t_v as reference gyro age only if $t_v < 2.5$ Gyr, otherwise we set $t_v = 2.5$ Gyr.

Stellar chromospheric activity is usually quantified by $\log R'_{\rm HK}$ index, which comes from $S_{\rm HK}$ in the way already shown in § 2.3.2. Baliunas et al. (1995b) report $S_{HK,\odot} = 0.179$ averaged over 25 yrs, while Hall et al. (2007) report $S_{HK,\odot} = 0.171$ averaged over 13 yrs. By weighting these two values upon their respective time spans, we obtain our reference S mean value for the Sun, i.e. $< S >_\odot = 0.1762$, which implies $< \log R'_{HK,\odot} >= -4.912$ if $B - V_\odot = 0.667$ is assumed. According to Henry et al. (1996) and Baliunas et al. (1995a), over the past 400 years $S_{MW,\odot}$ has varied from 0.145 (at Maunder minimum) to 0.215 during some observations at the peak of the 11-year solar cycle. This implies a solar maximum range in $\log R'_{\rm HK}$ going from -5.105 to -4.753. With respect to the $< \log R'_{HK,\odot} >$ mean value, an excursion a little less than 0.2 dex is expected in the chromospheric activity of Sun-like stars.

We took relation (2.18) and we slightly shifted it, so that the adopted $< \log R'_{HK,\odot} >$ gives the age of the Sun. Such a relation is represented in Fig. 3.8, which shows that low $\log R'_{\rm HK}$ values characterize old stars. In computing any stellar age coming from magnetic activity ($t_{\rm HK}$), we add a conservative threshold of 0.17 dex to the $\log R'_{\rm HK}$ index to be sure that a given star cannot be younger than the resulting $t_{\rm HK}$. We maintain $t_{\rm HK}$ as a valid age value if $t_{\rm HK} < 500$ Myr, otherwise we set $t_{\rm HK} = 500$ Myr.

The third information giving hints about age is the stellar mean density $\rho_\star$. As it is shown by the evolutionary track in Fig. 3.9, $\rho_\star$ progressively increases during the pre-MS phase until the star reaches the ZAMS. Mean stellar density is maintained almost constant during the MS and then it starts decreasing when a star leaves the MS and becomes a red giant. Therefore, a pre-MS star has a very different mean density, if compared with a MS star. As can be caught by Fig. 2.1, for stars under the TO (i.e. stars dimmer than $M_V \sim 5$), isochrones characterized by some tenths of Myr are close to the oldest MS-isochrones. $\rho_\star$ may help in distinguishing very old from very young stars, removing the degeneracy due to the isochrone closeness on the CMD. In particular, among pre-MS ages, we set t_ρ as the reference age value such that $\rho < \rho_\star$ for $t < t_\rho$.

It is not always possible to compute all the three reference age values t_v, $t_{\rm HK}$ and t_ρ. Anyway, the maximum among the available t_v, $t_{\rm HK}$ and t_ρ represents the value up to which all the younger isochrones are discarded before the development of the isochrone placement.

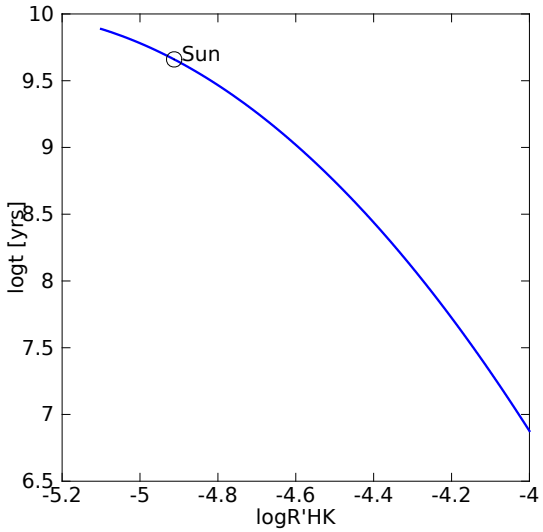

Figure 3.8: Mamajek and Hillenbrand (2008) relation that reproduces the age of a star as a function of its activity. Such a relation has been slightly shifted so it matches solar parameters adopted by Padova isochrones. In this way, the constant shift results to be -38.092 instead of -38.053 that is reported in (2.20). It is clear that a high activity level (i.e. high $\log R'_{\rm HK}$) characterizes young stars.

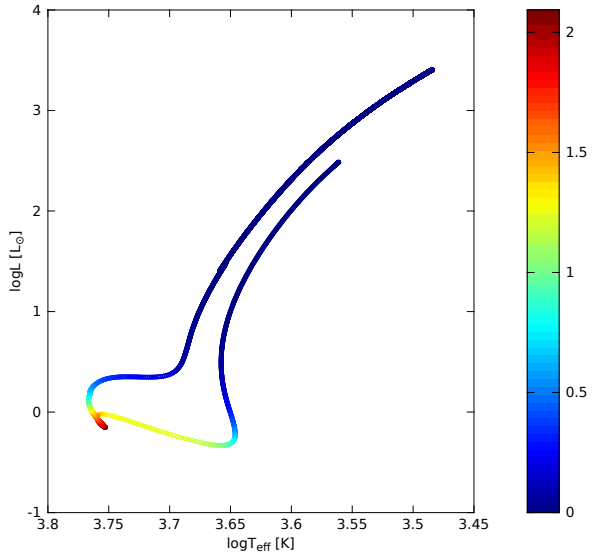

Figure 3.9: 1-$M_{\odot}$-evolutionary track on the HRD. The colorbar is representative of the stellar mean density $\rho_{\star}$ [g/cm^3]. Stellar density gradually increases until the star reaches the ZAMS and then it will start decreasing when the star leaves the MS.

3.2.3 The algorithm

In § 2.2.1 it has already been emphasized that isochrone degeneracies occur in different part of the CMD and that mass knowledge is essential for removing them. We analyzed stars from several databases, which often list the stellar mass $M_\star$, besides various stellar properties such as $T_{\rm eff}$ or bolometric luminosity L. However, as already explained, different authors obtain them through different methods and/or calibration processes, which are not likely consistent with the theoretical isochrones in use. So it is preferable to start from observational quantities and then infer all the other needed input parameters consistently with the theoretical models (*observational approach*). Sometimes, stellar parameters deriving in a straightforward way from observations are not available. Thus, in order to compute stellar age, the forced choice of using $T_{\rm eff}$ or L already present in the literature database must be taken (*spectroscopic approach*). In this case, one should be aware that the input parameters are not necessarily autoconsistent with the colour-temperature scale or the BCs adopted by the isochrones. This may also create wrong age results!

According to the *observational approach*, the input parameters required by the algorithm are:

- V magnitude;
- $B-V$ colour index;
- [Fe/H];
- $\log g$;
- π parallax or $\frac{a}{R_\star}$ (observationally available in the case of transiting planet hosts) or $\rho_\star$ (observationally available from asteroseismology).

[Fe/H] enables to choose the proper grid of isochrones identified by Z, thanks to relation (3.1). After interpolation in the isochrone grid, $T_{\rm eff}$ is inferred from $B-V$. The parallax π gives the stellar distance d and, combining it with V, one obtains the absolute magnitude:

$$M_V = V - 5\log d + 5 \tag{3.4}$$

Through interpolation in the isochrone grid, L can be recovered, as well. Thanks to the Stefan-Boltzmann law it is then possible to compute the stellar radius:

$$\frac{R_\star}{R_\odot} = \sqrt{\frac{L}{L_\odot}\left(\frac{T_{\rm eff}}{T_{\rm eff,\odot}}\right)^{-4}} \tag{3.5}$$

The logarithm of the surface gravity $\log g$ is a proxy for the stellar mass $M_\star$ and it is usually available from spectroscopic analyses. Alternatively, if asteroseismology has been performed, $\log g$ may be also recovered by inverting the scaling relation (2.11)[2]. From the definition of the stellar surface gravity, one obtains the stellar mass:

$$\frac{M_\star}{M_\odot} = \frac{g}{g_\odot}\left(\frac{R_\star}{R_\odot}\right)^2 \tag{3.6}$$

Knowledge of distance d is not fundamental to infer all input stellar parameters, if the ratio $\frac{a}{R_\star}$ (a is the planetary semimajor axis) is known through observations. This is only the case of stars harbouring planets that are detected through transit method. In fact, as specified by Winn (2010, eqs. (13) to (19)), the ratio $\frac{a}{R_\star}$ is linked to the transit duration and the planet orbital period. By re-arranging Kepler III law in the way shown e.g. by Sozzetti et al. (2007), such a ratio results to be linked to the stellar mean density $\rho_\star$:

$$\rho_\star = \frac{3\pi}{G}\left(\frac{a}{R_\star}\right)^3 \frac{1}{P^2} \tag{3.7}$$

By combining together stellar mean density and surface gravity, it is possible to recover both the stellar radius and mass.

$$\begin{cases} \frac{R_\star}{R_\odot} = \frac{g}{g_\odot}\left(\frac{\rho_\star}{\rho_\odot}\right)^{-1} \\ \frac{M_\star}{M_\odot} = \left(\frac{g}{g_\odot}\right)^3\left(\frac{\rho_\star}{\rho_\odot}\right)^{-2} \end{cases} \tag{3.8}$$

Using $R_\star$ and $T_{\rm eff}$, it is possible to compute L thanks to Stefan-Boltzmann law, without any information about distance.

Sometimes we are forced to follow the *spectroscopic approach* because of the lack of input data. In this case, the reference diagram is the $\log T_{\rm eff}$-$\log g$ diagram, because only [Fe/H], $T_{\rm eff}$ and $\log g$ are available in the worst case. Tab. 3.2 summarizes the alternative sets of input parameters required by our algorithm. The algorithm has been developed so that $\log g$ is essential in the *observational approach*. Giving a proxy for $M_\star$, we emphasize its importance

[2]Besides the asteroseismic $\nu_{\rm max}$, relation (2.11) contains also $T_{\rm eff}$. One may ask whether it is possible either to directly take the asteroseismic $\log g$ given in the literature (where the authors use their own $T_{\rm eff}$ value) or it is better to calibrate $T_{\rm eff}$ from $B-V$ using isochrones, before entering it in (2.11). After error propagation in (2.11), the $T_{\rm eff}$ contribution in the $\log g$ uncertainty results to be $\Delta \log g \approx \frac{1}{5}\frac{\Delta T_{\rm eff}}{T_{\rm eff}}$, which implies $\Delta \log g < 0.01$ for a solar-type stars, also assuming a huge uncertainty $\Delta T_{\rm eff} \sim 200$ K. The $\log g$ variation, that is smaller than the typical measurement errors, suggest that simply taking asteroseismic $\log g$ directly from the literature is a safe choice.

Input parameters	*Observational approach*	*Spectroscopic approach*
[Fe/H]	■	■
V	■	
$B-V$	■	
$\log g$	■	■
π	●	
$\frac{a}{R_\star}$	●	✓
$\Delta\nu$, $\nu_{\max}$	●	✓
$T_{\rm eff}$		■
$v \sin i$	✓	✓
$\log R'_{\rm HK}$	✓	✓

Table 3.2: Input parameters accepted by the isochrone placement algorithm. Essential parameters are denoted through ■, while useful but not essential ones are denoted through ✓. Referring to the *Observational approach* column, at least one of the parameters indicated through the ● symbol is also required.

because it enables to disentangle some isochrone degeneracies on the CMD. Age determination without any input $\log g$ is possible in any case, however the resulting age uncertainty is considerably higher.

If interpolation in the isochrone grid is required, internal uncertainties on bolometric magnitude and $T_{\rm eff}$ are assumed equal to 0.03 mag and 1%, respectively. Then, any other input uncertainty is derived after error propagation. Once that all the needed input parameters have been established, star position must be compared with respect to the isochrones in the HRD. Directly using the theoretical values tabulated in the grid is the easiest choice, but it could result in bad age estimation. To have an idea, let us consider Fig. 3.10 (left-hand side panel) where synthetic stars exactly belonging to the 3.2-Gyr-isochrone are shown on the CMD. Three different isochrones are plotted putting in evidence the discrete dots, whose coordinates are listed in the theoretical isochrone grid. Then dots are simply linked through lines during plotting. Even if each star is exactly on the 3.2-Gyr-isochrone (as the isochrone line shows), nevertheless some of them are closer to the dots belonging to other isochrones of the grid. Thus, performing the calibration between CMD and HRD using the discrete values listed in the isochrone grid may lead to an umprecise estimation of theoretical parameters. The result is shown in the right panel of Fig. 3.10, where the stars do not belong to their isochrone anymore.

To solve the problem, the interpolation process between CMD and HRD,

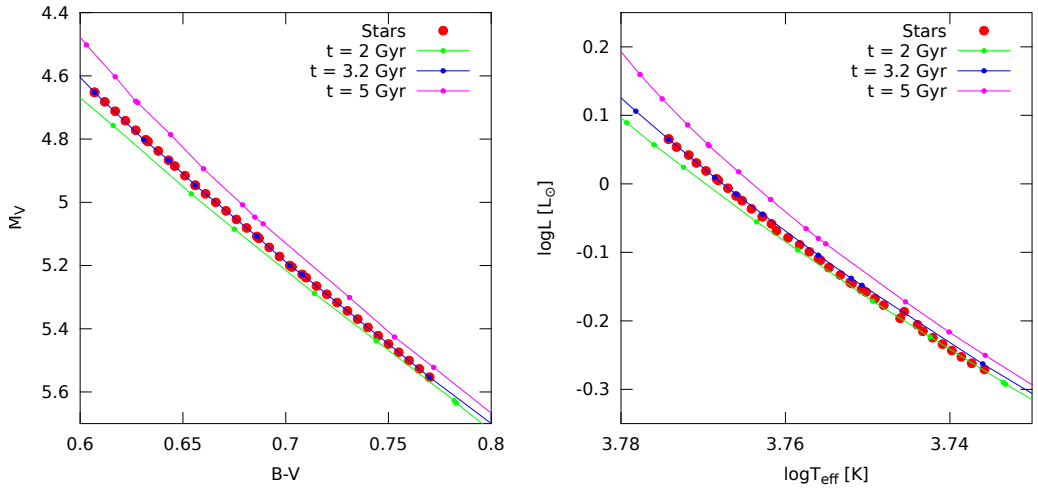

Figure 3.10: *Left-hand side panel.* Synthetic stars exactly belonging to the 3.2-Gyr-isochrones displayed on the CMD with other two reference isochrones. They have been used to test the calibration process CMD $\rightarrow$ HRD. Directly using the values tabulated in the isochrone grid results in a not satisfactory calibration, as right-hand side panel shows.

and the following operations needed to recover age have been based on a custom-built sequence of theoretical parameters (*Is* sequence), based on the available grid of isochrone. Given a star with metallicity $Z_\star$ and a grid of isochrones characterized by $Z_\star$, for each isochrone of the grid we consider the point tabulated in the grid that is closer to the star on the CMD (say A). By connected it with the following in the isochrone grid (B) through a line, we obtain a line segment (AB), like the ones that enable to display the isochrones in Fig. 3.10. Through linear interpolation, we recovered the theoretical parameters of that point belonging to AB and having the minimum distance from the star (in terms of point-line distance). In this way, we built variable grids of theoretical parameters depending on the star to be analyzed, which are more suitable to compare the star position on the CMD/HRD with respect to the theoretical isochrones. Using these new reference theoretical values *Is*, the result of the interpolation between CMD and HRD is shown in Fig. 3.11 and it is satisfactory.

The *Is* sequence is then used to compute stellar age and all the relevant stellar parameters, according to Padova evolutionary models. The key steps of the algorithm are the following:

1. If either $v \sin i$, $\log R'_{\rm HK}$ or $\rho_\star$ are available, at least one among t_v, $t_{\rm HK}$ or t_ρ can be computed, as described in § 3.2.2. Isochrones younger than the maximum value among t_v, $t_{\rm HK}$ and t_ρ are discarded and not used

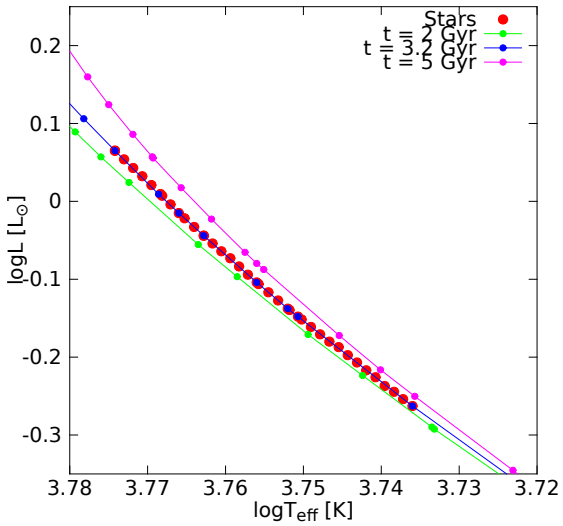

Figure 3.11: Stars on the HRD deriving from the ones exactly belonging to the 3.2-Gyr-isochrone on the CMD. By performing the calibration using a suitable grid of theoretical values (obtained through linear interpolation from the ones originally tabulated in the isochrone grid), the result is satisfactory.

in the age computation.

2. Each set of theoretical values reported at a given i^{th} row of *Is* is smoothed through a bidimensional Gaussian window function, whose σs are given by the extensions of the stellar error bars in $\log T_{\text{eff}}$ and $\log L$:

$$\mathcal{G}(\log T_{\text{eff},i}, \log L_i) = \frac{e^{\frac{1}{2}\left[\left(\frac{\log T_{\text{eff},i} - \log T_{\text{eff}}}{\Delta \log T_{\text{eff}}}\right)^2 + \left(\frac{\log L_i - \log L}{\Delta \log L}\right)^2\right]}}{2\pi \Delta \log T_{\text{eff}} \Delta \log L} \tag{3.9}$$

Variables with subscript i refer to theoretical values, while the others are the input stellar parameters.

3. Once that the input stellar parameters are available, the most probable stellar age should be indicated by the nearest isochrone in the 4-D $\log T_{\text{eff}}$-$\log L$-$\log g$-M plane $\mathcal{P}$. So a different weight (i.e. a measure of the probability that a star has a given age) should be attributed to the different isochrones. Actually, this weight should not be based only on the simple geometric distance evaluated in $\mathcal{P}$ between the star and the theoretical model. In fact, some evolutionary stages are intrinsically less probable to be observed, because a star spends little time in those phases. For example, if a star is equally distant from a pre-MS isochrone

and a MS isochrone, it is likely that we are dealing with a MS star, because a star lays on the MS for most of its life. Taking the theoretical track describing the evolution of a star with mass $M_\star$, we define the stellar evolutionary speed as

$$v_{\rm evo} = \sqrt{\left(\frac{\log T_{\rm eff,2} - \log T_{\rm eff,1}}{t_2 - t_1}\right)^2 + \left(\frac{\log L_2 - \log L_1}{t_2 - t_1}\right)^2} \qquad (3.10)$$

$(\log T_{\rm eff,1}, \log L_1)$ is the point of the track that is nearest to the star, while $(\log T_{\rm eff,2}, \log L_2)$ is the points occurring later in time; t_1 and t_2 correspond to ages when the star assumes such parameters.

Considering both the geometric distance of a star from the theoretical models and the variability of the stellar evolutionary speed $v_{\rm evo}$, we attributed the weight p_i to the $i^{\rm th}$ row of the *Is* isochrone grid:

$$p_i = \left[\left(\frac{\log T_{\rm eff,i} - \log T_{\rm eff}}{\Delta \log T_{\rm eff}}\right)^2 + \left(\frac{\log L_i - \log L}{\Delta \log L}\right)^2 + \left(\frac{\log g_i - \log g}{\Delta \log g}\right)^2 + \right.$$
$$\left. + \left(\frac{M_i - M}{\Delta M}\right)^2 + \log^2\left(\frac{v_{\rm ref}}{v_{\rm evo}}\right)\right]^{-1} \qquad (3.11)$$

$v_{\rm evo}$ is normalized with respect to $v_{\rm ref}$, which corresponds to the minimum evolutionary speed registered on the entire track. The more the geometric distance between the star and the theoretical model, the less p_i. The higher the theoretically predicted evolutionary speed of the star, the less p_i.

4. The generic stellar property $X_\star$ evaluated according to Padova evolutionary models is computed through the following weighted mean:

$$X_\star = \frac{\sum_i X_i \mathcal{G}(T_{\rm eff,i}, L_i) p_i}{\sum_i \mathcal{G}(T_{\rm eff,i}, L_i) p_i} \qquad (3.12)$$

The corresponding uncertainty is given by

$$\Delta X_\star = \sqrt{\frac{\sum_i (X_i - X_\star)^2 \mathcal{G}(T_{\rm eff,i}, L_i) p_i}{\sum_i \mathcal{G}(T_{\rm eff,i}, L_i) p_i}} \qquad (3.13)$$

Previous formula are given considering the *observational approach*. In the case of the *spectroscopic approach*, $\log g$ is used instead of $\log L$ in equations (3.9) and (3.10). Given the lack of input data, p_i is built considering only the contributions given by $\log T_{\rm eff}$, $\log g$ and $v_{\rm evo}$.

In order to take element diffusion into account, after that $t_\star$ and $M_\star$ have been derived thanks to (3.12), the algorithm is repeated iteratively according to what has already been described in § 3.2.1 until convergence in age determination is reached.

3.3 Bayesian estimation implementation

In a Bayesian statistical context it is required to get the posterior probability density functions (the so called *pdf*s) of the parameters of interest. If the evolutionary model input parameters are collected in a vector $\mathbf{p}$ and the observational data in a vector $\mathbf{q}$, isochrones provide a map from the parameter space $\mathbf{p}$ to the data space $\mathbf{q}$. Finding a *pdf* requires to invert such a relation, i.e. determining the theoretical parameters once that observational data are available.

Following the prescriptions of Jørgensen and Lindegren (2005), we assume $\mathbf{q} = (\log T_{\rm eff}, \log L, [\mathrm{Fe/H}])$ and $\mathbf{p} = (t, Z, M_\star)$. $\log T_{\rm eff}$ and $\log L$ can either directly come from literature databases (if the *spectroscopic approach* is followed), or they are inferred from their observational counterparts (i.e. $B - V$ and M_V) through the calibration CMD $\rightarrow$ HRD, already presented in § 3.2.3.

Treating t, Z and $M_\star$ as random variables, the posterior (joint) probability density function is

$$f(t, Z, M_\star) \propto f_0(t, Z, M_\star)\mathcal{L}(t, Z, M_\star) \tag{3.14}$$

where f_0 is the prior *pdf* and $\mathcal{L}$ the likelihood function. $f(t, Z, M_\star)\mathrm{d}t\mathrm{d}Z\mathrm{d}M_\star$ is the fraction of stars with age within $[t,\ t + \mathrm{d}t]$, metallicity within $[Z,\ Z + \mathrm{d}Z]$, mass within $[M_\star,\ M_\star + \mathrm{d}M_\star]$. The constant of proportionality is chosen so that $\iiint f(t, Z, M_\star)\mathrm{d}t\mathrm{d}Z\mathrm{d}M_\star = 1$. By integrating over Z and $M_\star$, one obtains $f(t)$ that is the posterior *pdf* of the age.

The stellar age is recovered from $f(t)$, synthesizing the *pdf* through proper statistical indexes. Possible choices are related to the mean μ_t or the median m_t of the distribution. The mean is the centroid of the area under $f(t)$, while the median is the value bisecting the area under $f(t)$. Jørgensen and Lindegren (2005) showed that both μ_t and m_t suffer the bias of artificially centering the age distribution. Instead the most natural choice is that referring to the mode $\hat{t}$, that is the value representing the peak of the *pdf*. According to the Bayesian age estimation implemented by Jørgensen and Lindegren (2005), the mode suffers the bias of preferentially selecting the outmost age values available in the isochrone grid. In § 4.1 we will show that if information

coming e.g. from stellar rotational velocity is taken into account, then this bias is mitigated.

Assuming independent Gaussian observational errors $\sigma_n^{\rm obs}$ for each $q_n^{\rm obs}$, the likelihood function is given by

$$\mathcal{L}(t, Z, M_\star) = \prod_{n=1}^{3} \frac{1}{\sqrt{2\pi}\sigma_n^{\rm obs}} \cdot \exp\left(-\frac{\chi^2}{2}\right) \tag{3.15}$$

where

$$\chi^2 = \sum_{n=1}^{3} \left(\frac{q_n^{\rm obs} - q_n(t, Z, M_\star)}{\sigma_n^{\rm obs}}\right)^2 \tag{3.16}$$

Following the suggestion of Jørgensen and Lindegren (2005), the prior *pdf* has been set as

$$f_0(t, Z, M_\star) = \psi(t)\phi(Z)\xi(M_\star) \tag{3.17}$$

where $\psi(t)$ is the prior star formation rate (SFR), $\phi(Z)$ is the prior metallicity distribution, and $\xi(M_\star)$ is the prior initial mass function (IMF). Since our main purpose is estimating stellar ages, we considered $\psi(t)$ to be flat, not to introduce a priori biases on the derived ages. In the case of precise spectroscopic measurements (say $\sigma_{\rm [Fe/H]} \approx 0.05$ dex), the likelihood acts as a narrow window function that substantially suppresses the contribution of $\phi(Z)$, selecting it only on a small interval. Thus, if the hypothesis holds, $\phi(Z)$ may be considered flat, as well. As IMF, we assumed a decreasing power-law $\xi(M_\star) \propto M_\star^{-2.7}$ (Kroupa et al., 1993), so that the *pdf* of the age t results to be

$$f(t) \propto G(t) = \iint \mathcal{L}(t, Z, M_\star)\xi(M_\star)\mathrm{d}Z\mathrm{d}M_\star \tag{3.18}$$

As a preliminary way of testing whether the stellar input parameters matches the theoretical values tabulated in the isochrone grid, we evaluated the condition

$$\min\chi_i^2 < \chi_{0.99}^2 \tag{3.19}$$

where χ_i^2 is evaluated through (3.16) considering the theoretical values tabulated at the $i^{\rm th}$ row of the isochrone grid. Instead, $\chi_{0.99}^2 = 11.345$ is the 99th percentile of the χ^2-distribution with three degrees of freedom (that are [Fe/H], $\log T_{\rm eff}$, $\log L$). If condition (3.19) does not hold, then there is less than 1% probability that the given input parameters are actually real. In this case, they are probably the result of error measurements, therefore we avoid computing ages of such stars.

If the preliminary condition given by (3.19) is satisfied, the Bayesian estimation algorithm selects all the available isochrone grids characterized

by a metallicity within the $[[\mathrm{Fe/H}] - 3.5\sigma_{[\mathrm{Fe/H}]}, [\mathrm{Fe/H}] + 3.5\sigma_{[\mathrm{Fe/H}]}]$ interval. After that, $G(t)$ is obtained by estimating its values at different ages t_j:

$$G(t_j) = \sum_k \sum_l \mathcal{L}(t_j, Z_k, M_{\star j,k,l}) \xi(M_{\star j,k,l})(M_{\star j,k,l+1} - M_{\star j,k,l}) \qquad (3.20)$$

Finally we smoothed $G(t)$ through a polynomial interpolation and we normalized it so that the maximum peak is 1, obtaining $\tilde{G}(t)$. As shown by Jørgensen and Lindegren (2005), under certain regularity conditions, it is possible to prove that the outmost age values t_1 and t_2 for which $\tilde{G}(t_1) = \tilde{G}(t_2) = \tilde{G}_{\mathrm{lim}} = 0.61$ define the bounds of the 68% confidence interval.

Chapter 4

Results and publications

4.1 Test of the algorithms

To estimate the reliability of both our isochrone placement and Bayesian estimation techniques, we generate huge samples of synthetic stars (i.e. stars having an a priori known age) to check whether our algorithms retrieve the correct age value. In particular, we built a sample of:

- 928 stars exactly belonging to the $\log t = 9.5$-isochrone $\rightarrow$ 3.2 Gyr (synthetic sample 9.5: *SS9.5*);
- 825 stars exactly belonging to the $\log t = 9.75$-isochrone $\rightarrow$ 5.6 Gyr (synthetic sample 9.75: *SS9.75*).

We also introduced a random Gaussian perturbation on the input $B-V$, M_V and $\log g$ of the synthetic stars, considering Gaussian distributions with $3\sigma = 1\%$ of the unperturbed values, obtaining the perturbed counterparts of the synthetic samples (*SS9.5p* and *SS9.75p*).

Given the high nominal age values of our synthetic samples, we reasonably assume that the supposed $v \sin i$ of the stars enables to discard all the isochrones younger than 2.5 Gyr. Therefore all the tests involving synthetic stars are performed without considering the youngest isochrones.

According to its original implementation, the isochrone placement technique requires only one grid of isochrones, i.e. the one having the same metallicity of the star to be analyzed. On the other hand, several grids of isochrones enter as input theoretical values in the Bayesian estimation technique, because we originally followed the implementation by Jørgensen and Lindegren (2005). One could reasonably expect that the output Bayesian ages will result more scattered around the true age, due to the numerous input grids. Thus, we also implemented the possibility of computing ages through the

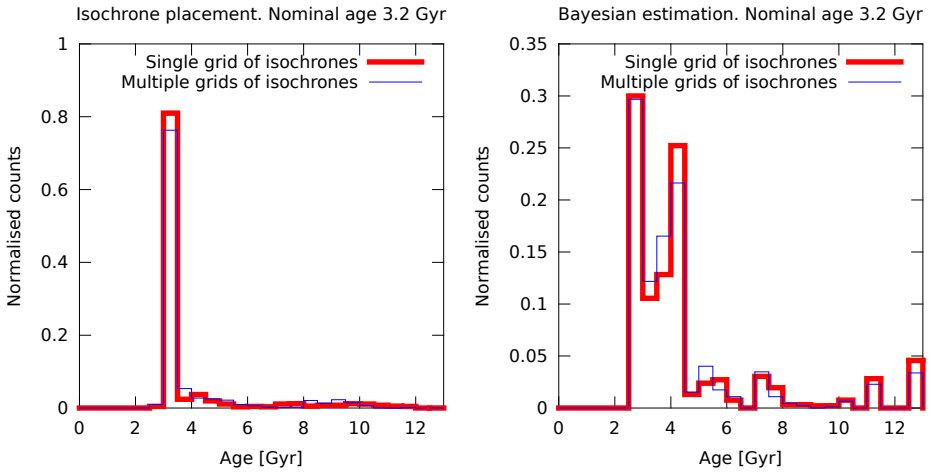

Figure 4.1: *Left-hand side*. Age distribution of the *SS9.5* stars inferred from the isochrone placement, both in the case of a single input grid of isochrones (red bars) and in the case of multiple input grids of isochrones (blue bars). *Right-hand side*. Same kind of comparison as in the left-hand side panel, but this time the Bayesian estimation technique has been used. In both panels, no sensible scatter effects are present.

isochrone placement, using grids of isochrones of different metallicity, within the $[[\mathrm{Fe/H}] - 3.5\sigma_{[\mathrm{Fe/H}]}, [\mathrm{Fe/H}] + 3.5\sigma_{[\mathrm{Fe/H}]}]$ interval, as the Bayesian implementation does. At the same time, we also developed a reduced Bayesian algorithm that requires in input only one grid of isochrones corresponding to the metallicity of the star.

As a preliminary test, we checked whether multiple input grids of isochrones (i.e. grids with different metallicity) actually impact the derived ages. Left-hand side panel of Fig. 4.1 shows the age distribution of the stars belonging to the *SS9.5* sample inferred from the isochrone placement both using a single grid and multiple grids of isochrones. Right panel of Fig. 4.1 shows the same kind of comparison, but this time the Bayesian estimation technique has been used. Fig. 4.2 shows the same comparison tests as in Fig. 4.1, but the *SS9.75* sample has been employed in this case.

Both from Figures 4.1 and 4.2, it is clear that the usage of multiple grids of isochrones centred at the expected [Fe/H] value of the star, does not impact very much the output age, in terms of the expectation value. On the other hand, the uncertainties affecting the results are sensibly higher.

The isochrone placement and the Bayesian estimation techniques address the age uncertainties quite in a different way. In these particular tests, we are dealing with stars exactly belonging to an isochrone, nevertheless the age relative uncertainties carried out by the Bayesian estimation technique have

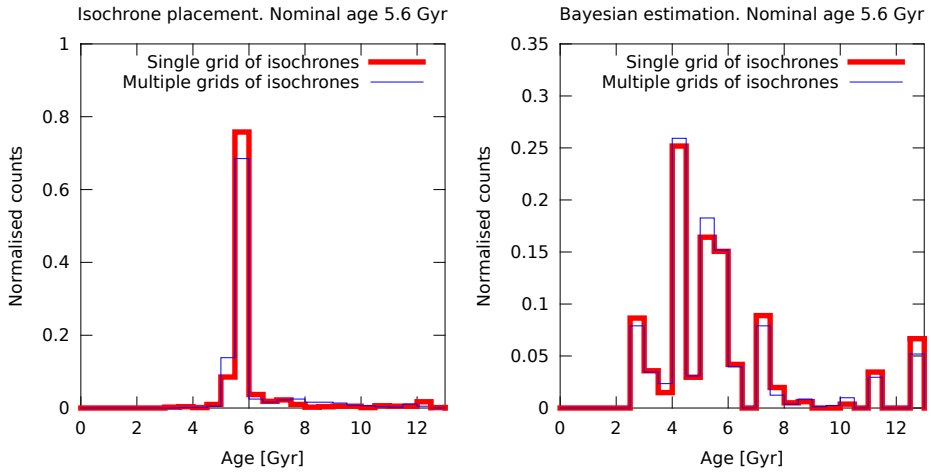

Figure 4.2: Same kind of comparisons as in Fig. 4.1, but this time in the case of the *SS9.75* sample of stars.

quite high median values, i.e. $\sim 30\%$ (*SS9.5*) and $\sim 40\%$ (*SS9.75*), both for the single and multiple grids approach. Instead, the age median uncertainties obtained by the isochrone placement are smaller and they increase by a factor of 4, passing from $\sim 3\%$ of the single grid implementation to $\sim 12\%$ of the multiple grids implementation. The small amount of age uncertainty is not surprising in this case, since we are considering stars exactly belonging to an isochrone. The age of real stars will be reasonably affected by higher errors. Moreover, we recall that the given age uncertainties are internal and based upon the error propagation of the input data. In other words, age uncertainties do not take the uncertainties due to stellar theoretical models into account. This means that the age uncertainty of a star is likely higher than the formal one given by our isochrone placement algorithm. Maybe, the formal error given by the Bayesian estimation technique is better representative of the realistic age uncertainty of a star.

Besides this aspect, the goals of this section are also to:

- compare the synthetic ages coming from the isochrone placement and the Bayesian estimation, to see if one technique should be preferred to the other;
- evaluate how the determination of stellar ages is influenced by the position of the stars on the CMD.

A direct comparison between the output ages obtained through the isochrone placement and the Bayesian estimation techniques is given by Fig. 4.3. The

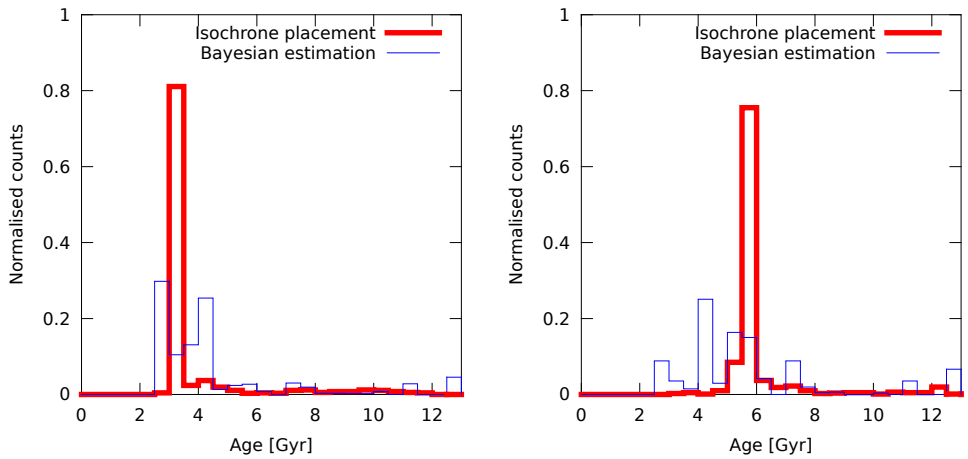

Figure 4.3: Age distributions of the *SS9.5* sample (left-hand side panel) and of the *SS9.75* sample (right-hand side panel) inferred from isochrone placement (red bars) and Bayesian estimation (blue bars).

left-hand side and the right-hand side panels report the age distributions of the *SS9.5* and the *SS9.75* samples, respectively. In both cases, the isochrone placement algorithm selects the expected age value for $\sim 80\%$ of the stars. Instead, the age distributions inferred from Bayesian estimation are less peaked, and their modal values underestimate the age. A similar comparison involving the perturbed synthetic sample is shown in Fig. 4.4. As expected, in this case the histogram bars are distributed over a wide age range. The age distributions coming from the isochrone placement are bell-shaped, mimicking the Gaussian perturbations of the input parameters. For the nominal age $t = 3.2$ Gyr, the ensemble of the age distribution derived from the Bayesian estimation is centred around the expected bin, even if the peak is at 2.8 Gyr (left-hand side panel of Fig. 4.4). Instead, from right-hand side panel of the same Figure, it comes out that the Bayesian estimation technique underestimates the age, in the case of perturbed input values. Table 4.1 synthesizes the relevant properties of the age distributions.

We can further comment the results given by the Bayesian estimation technique. In the case of the *SS9.75* and *SS9.75p* samples (age distributions represented through blue bars in the right-hand side panels of Figures 4.3 and 4.4), the nominal age of 5.6 Gyr is far away from the two outmost age bins, i.e. [2.5, 3) and [12.5, 13) Gyr. Thus, any extreme age comes out as a consequence of the bias already pointed out by Jørgensen and Lindegren (2005), according to which the mode tends to attribute the outmost age values available in the

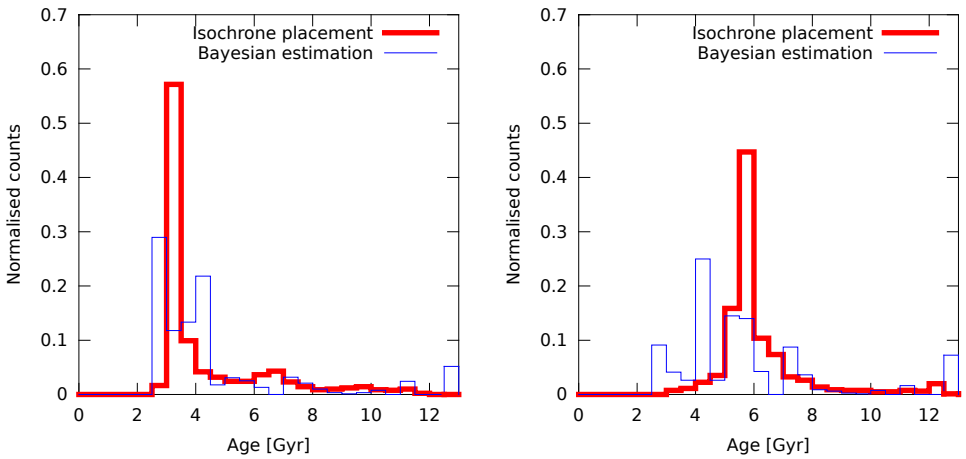

Figure 4.4: Same as Fig. 4.3, but for the perturbed synthetic samples.

	Unperturbed input				Perturbed input			
	3.2 Gyr		5.6 Gyr		3.2 Gyr		5.6 Gyr	
	Mode	Median	Mode	Median	Mode	Median	Mode	Median
Isochrone placement	3.2	3.2	5.6	5.6	3.2	3.3	5.6	5.7
Bayesian estimation	2.8	3.6	4.1	5.1	2.8	3.6	4.1	5.1

Table 4.1: Mode and median of the age distributions of the synthetic samples of stars. All the tabulated values are expressed in Gyr.

isochrone grid. According to a Montecarlo analysis developed by the authors, this bias involves $\sim 70\%$ of their sample of synthetic stars. We mitigated this effect, in fact, by inserting the check in terms of $v \sin i$, the bias is limited to $\sim 15\%$ of the analyzed synthetic stars.

The reliability of the output age depends also on the position of a star on the CMD. Fig. 4.5 represents the ages of the synthetic stars as a function of their absolute magnitude M_V, which is a proxy of the position of the star along an isochrone. The age differs sensibly from the expected one in the cases of very dim stars (low-MS region) and very bright stars (RGB region). Given that the analyzed stars are synthetic, problems are due to errors in the interpolation scheme, which enables to retrieve all the needed input parameters. In the very low MS-region, interpolation is difficult because not many points are available in the grid, since we are just at the beginning of the isochrones. Instead, in the RGB region:

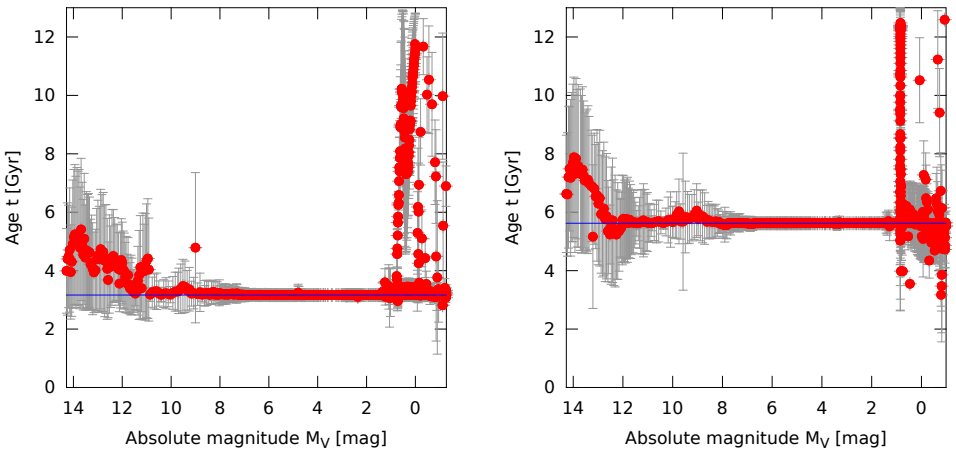

Figure 4.5: Ages of the stars belonging to the *SS9.5* sample (left-hand side panel) and to the *SS9.75* sample (right-hand side panel) as a function of stellar absolute magnitude, that is a proxy of stellar position along an isochrone. In the case of synthetic stars, the best determination is achieved for MS stars. Instead, for very-low MS stars or RGB stars, a worse age determination arises either because of the paucity of points in the isochrone grids or the highly not-linear shape of the isochrones on the CMD.

- isochrones have a strongly not-linear shape and overlap in several points;
- stars rapidly move on the CMD due to their fast evolution, so quite a large CMD area is covered by just a few grid points.

As a consequence, the interpolation process can lead also to completely wrong ages.

In the regions of the MS and of the TO and, especially, for $2 \lesssim M_V \lesssim 8$, the age is very well determined because the shape of the isochrones is linear. But this happens only because here we are dealing with synthetic stars having input parameters exactly corresponding to the theoretical ones. So, what has just been described is a way of testing the capability of the algorithms to perform the correct interpolation in the grid, which is, however, a caveat to produce correct output age values. In the case of real stars, all the input parameters required by the algorithm likely differ from the theoretical ones. Because of the closeness of MS isochrones, the ages of MS stars are expected to be characterized by a quite high uncertainty.

We have just pointed out the intrinsic problems of determining the ages either of very dim or very bright stars. So, it is worth to conclude the comparison between the isochrone placement and the Bayesian estimation by comparing the age distributions deriving from the two techniques for a subsample

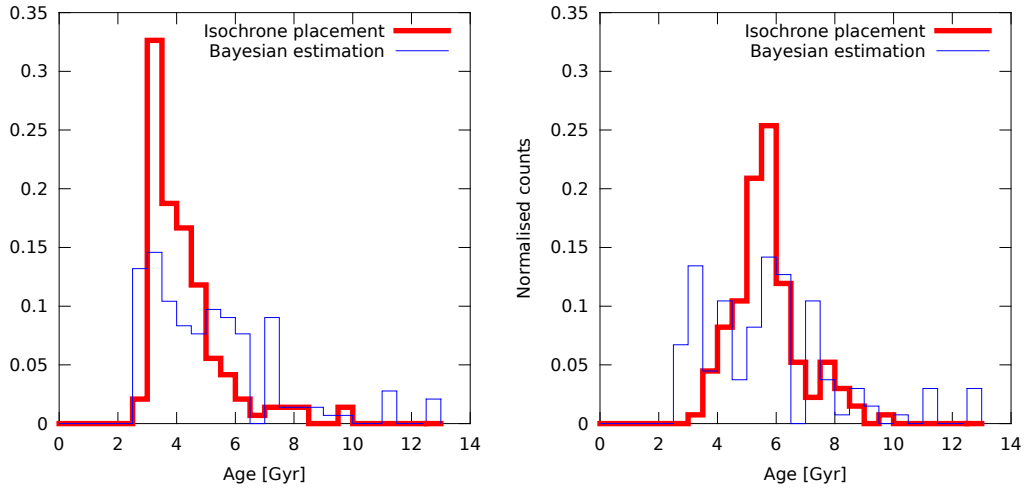

Figure 4.6: Age distributions of the subset of stars with $4 < M_V < 8$ taken from the *SS9.5p* sample (left-hand side panel) and the *SS9.75p* sample (right-hand side panel). The analysis has been carried out both with the isochrone placement and the Bayesian estimation algorithms.

of our synthetic stars with $4 < M_V < 8$. In fact, we have just observed that in this range our algorithms give reliable ages, thanks to the ordered position and shape of the isochrones on the CMD. In addition, this absolute magnitude range implies considering stars of late spectral types, which are the most numerous in the universe and very interesting to be studied, e.g. regarding the possibility of hosting habitable planets. Given the perturbations in the input parameters, we chose *SS9.5p* and *SS9.75p* as target samples, because they simulate stars characterized by likely observational uncertainties, which scatter the stars around the nominal age isochrones. Their consequent age distributions, inferred from both the isochrone placement and the Bayesian estimation, allow to build a realistic comparison of the strength of the two algorithms in the magnitude range with relevant astrophysical importance. Fig. 4.6 shows the result of our analysis, that is quantitatively summarized by Table 4.2.

The isochrone placement technique gives distributions that are peaked around the nominal age values and result to be less scattered over the age range. The median age of the *SS9.75p* sample is consistent with the nominal age, while in the case of the *SS9.5p* sample the skewness due to the cut of the youngest isochrones brings the median at 3.9 Gyr. The modal values deriving from the Bayesian estimation are consistent with the expected age, but the inferred age distributions have a higher variability. For both the two samples, the median age uncertainty as derived from the isochrone placement

	SS9.5p		*SS9.75p*	
	Mode	Median	Mode	Median
Isochrone placement	3.2	3.9	5.7	5.6
Bayesian estimation	3.1	4.6	5.6	5.6

Table 4.2: Main statistical indexes describing the age distributions of our perturbed synthetic subsamples of stars having $4 < M_V < 8$, deriving both from the isochrone placement and the Bayesian estimation. Tabulated values are expressed in Gyr.

is ~ 1.2 Gyr, while the Bayesian estimation gives it enhanced by a factor of 2.

Our isochrone placement allows to retrieve a better age estimation, so we decided to employ it in the following analyses. We further test the algorithm by considering a sample of Kepler stars analyzed by Silva Aguirre et al. (2015). They made a complete asteroseismological analysis based on the individual oscillation frequencies of the stars, so that the resulting ages are judged very reliable. The age estimation by Silva Aguirre et al. (2015) versus ours is represented in Fig. 4.7.

The data are in very good agreement, which is quantified by the linear correlation coefficient $\rho_{\rm BP} = 0.95$. The line of best fit according to the least-square method is represented in green. Our algorithm tends to slightly overestimate the older ages, but we are not able to conclude whether this is an intrinsic effect or it is linked to the paucity of the statistical sample. In any case, this comparison constitutes a good validation test for our isochrone placement.

Another aspect it is worth to deepen is how a variation in the input parameters propagates onto the output ages. It is very difficult to make a priori predictions, since the relations between the input parameters and age is strongly not linear and isochrones spacing changes for different locations on the CMD. Just to have an idea, we performed simulations employing the Sun as reference star and then we check how its age changes, by varying the main input parameters. We alternatively supposed a variation in V and $B-V$ of ± 0.01 mag and in $\log g$ of ± 0.01 dex, as it is specified in Tab. 4.3. V and $B-V$ variations simulate photometric uncertainties. They may either come from measurement errors or they can be due to blendings with other field stars, especially in the cases of dim stars with low galactic latitude.

It is not very easy to take the age variations under control. They could be either negligible or of the order of even $\sim 40\%$ for small input perturbations.

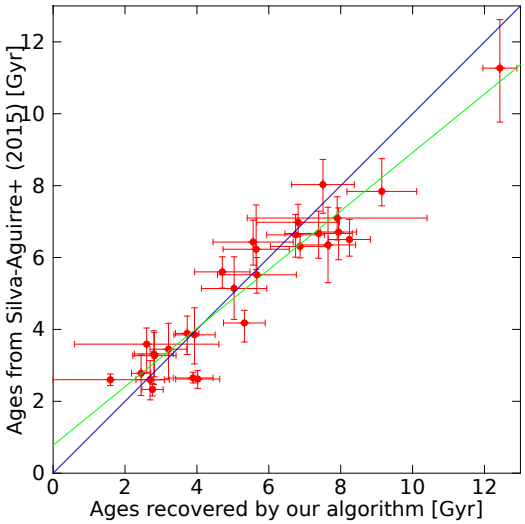

Figure 4.7: Ages reported by Silva Aguirre et al. (2015) are plotted versus our estimation through the isochrone placement. The blue line is the bisector, representing exact correspondence between the two determinations. The green line is obtained from least square regression and is characterized by $\rho_{\rm BP} = 0.95$. Given the error bars, we found good agreement between the two age determinations.

Sun	t [Gyr]
Unperturbed input	4.5 ± 0.1
$\Delta V = 0.01$ mag	4.2 ± 0.9
δ	-6.7%
$\Delta V = -0.01$ mag	4.5 ± 0.7
δ	0%
$\Delta(B-V) = +0.01$ mag	5.3 ± 1.2
δ	$+17.8\%$
$\Delta(B-V) = -0.01$ mag	2.7 ± 1.3
δ	-40%
$\Delta \log g = +0.01$ dex	4.2 ± 0.9
δ	-6.7%
$\Delta \log g = -0.01$ dex	4.3 ± 1.0
δ	-4.4%

Table 4.3: Impact of the input parameters on the output ages. Right column specifies the solar age after the perturbation of the input parameter reported on the left column. δ represents the percentual age variation with respect to the reference solar age.

This emphasizes that determining the ages of MS stars is not a trivial task because of the closeness of the isochrones. Moreover, the uncertainties characterizing the ages derived from perturbed input parameters are an order of magnitude higher than the one accompanying the solar reference value. This happens because the input perturbations trigger artificial stars, and the big uncertainties reflect the difficulty of properly matching the input data with the theoretical parameters.

4.2 Data analysis

Main goals of the data analysis consist in determining the age distributions of planet-hosting stars (both coming from radial velocity and transit surveys) and then comparing the evolutionary state of the entire ensemble of planet-hosting stars with the one inferred for stars of the solar neighbourhood having consistent distances and spectral types. In principle, photometric surveys should not suffer some biases, in fact:

- target stars are not necessarily inactive, unlike in spectroscopic surveys, where well-defined and sharp lines are required to give satisfactory results. However, high intrinsic stellar variability plays against photometric analysis, as well;

- target stars are not necessarily slow-rotators, unlike in radial velocity surveys, where rotation broadens the spectroscopic lines and reduces their depth, making the analysis less precise.

On the other hand, the transit method is affected by other systematic effects. The host stars are expected to be close-in and preferentially edge-on, even if spin-orbit misalignment occurs in some exoplanetary systems (see e.g. Schlaufman 2010, Huber et al. 2013).

Considering all these sources of biases, it is worth to evaluate whether target stars of photometric surveys actually differ from the ones of spectroscopic surveys, in terms of evolutionary stage. Once that this aspect will have been clarified, then a homogeneous comparison with field stars will enable to investigate possible evolutionary peculiarities of stars with planets.

4.2.1 Analysed samples

We performed our analysis by taking stellar parameters from two main sources:

1. SWEET-Cat: a catalogue of stellar parameters for stars with planets[1] (Santos et al., 2013). It lists stellar coordinates, V magnitude, parallax, mass and the classical parameters coming from spectroscopy, i.e. [Fe/H], microturbulence velocity, $\log g$ and $T_{\rm eff}$. As reference input parameters for deriving stellar ages, we directly took parallax π, [Fe/H] and $\log g$. We complemented these data with $\log R'_{\rm HK}$, $v \sin i$, $\rho_\star$ (observationally available in the case of transiting-planet hosts, as inferred thanks to (3.7)). In addition, if available, we took V magnitude and $B-V$ colour index from Maxted et al. (2011), otherwise we collected V from SWEET-Cat and $B-V$ from `exoplanets.org`[2]. As reported by Maxted et al. (2011), surveys aiming at discovering planets through transits are typically characterized by poor quality optical photometry. For stars brighter than $V \approx 12$, photometry is usually available from Tycho catalogues[3], even if the catalogues are completed up to $V \approx 11$ and photometry rapidly deteriorates for $V \gtrsim 9.5$. Instead, Maxted et al. (2011) performed high-quality photoelectric optical photometry for some transiting-planet hosts, therefore we decided to use their photometry if available.

   Among Sweet-Cat stars, we selected 61 transiting-planet host stars (TPH). Among them, we also considered the sub-sample made of 43 stars brighter than $V = 12$ (BTPH). This criterion takes into account that future photometric missions with the aim of characterizing exoplanets, such as CHEOPS (Broeg et al., 2013) or PLATO (Rauer et al., 2014), will target bright stars. Furthermore, we selected from Sweet-Cat as well 274 planet-hosting stars, whose planets were detected through radial velocity technique (spectroscopic host: SH). The union of the TPH and SH catalogues (335 stars) constitutes our reference catalogue of stars with planets (SWP).

2. The Geneva Copenhagen Survey of the Solar Neighbourhood. It is a survey of late spectral type dwarf stars (F, G and K stars) essentially nearer than 200 pc and magnitude limited at $V \approx 8.3$ mag. We considered the most up-to-date results by Casagrande et al. (2011), who re-analyzed the stars previously taken into account by Nordström et al. (2004), Holmberg et al. (2007, 2009). In order to perform homogeneous comparisons with our SWP, we selected those MS stars having $T_{\rm eff}$ between 4500 K and 6300 K, within a range of 0.45 dex in $\log L$, whose

[1] `https://www.astro.up.pt/resources/sweet-cat/`

[2] The Site of California and Carnegie Program for Extrasolar Planet Search: Exoplanets Data Explorer. `http://exoplanets.org/table`.

[3] `http://heasarc.nasa.gov/W3Browse/all/tycho2.html`

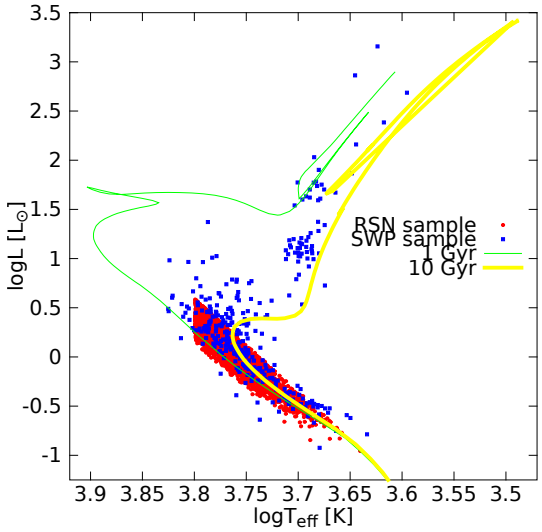

Figure 4.8: All the planet-hosting stars we analyzed in this thesis (SWP sample) and the solar neighbourhood MS stars in the same spectral type range taken from the Geneva Copenhagen survey (RSN sample) represented on the HRD. Two isochrones with solar metallicity are superimposed as reference.

minimum and maximum values were -1.24 dex and 0.63 dex, respectively. In this way, we remained with 3713 stars that build up our reduced solar neighbourhood (RSN) catalogue.

A representation of the two different kind of samples we analyzed (SWP and RSN) is given on the HRD thanks to Fig. 4.8. We can appreciate that in both cases we essentially deal with G stars, with a small amount of K stars.

4.2.2 The ages of stars

We derived the ages of the stars belonging to the TPH catalogue, by applying our isochrone placement algorithm. The result is shown in Fig. 4.9. The BTPH is a sub-sample of the TPH catalogue, therefore we superimposed its age distribution (grey bars) to the age distribution of the TPH (blue bars). The median ages of the BTPH and TPH samples are ~ 4.2 and ~ 5 Gyr, respectively.

Brighter stars are on average younger, consistently with the age inferred for the BTPH sample. One of the three stars younger than 1 Gyr, namely WASP-18 ($t = 0.9 \pm 0.2$ Gyr) appears too blue for its metallicity, so we checked its input parameters. We used [Fe/H]=0.19, $V = 9.273$ and $B-V = 0.484$, while instead Southworth et al. (2009), for instance, adopt [Fe/H]=0, $V = 9.30$ and $B - V = 0.44$. According to Southworth et al. (2009) input

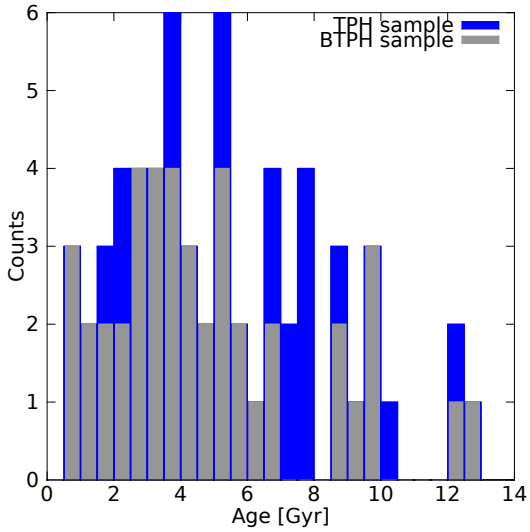

Figure 4.9: Age distribution of the BTPH (grey bars) superimposed to the entire TPH sample (blue bars).

parameters, WASP-18 would be located again on the bluer side of the MS of PARSEC models. Its isochrone placement age would be even lower than before, i.e. $t = 0.2^{+0.3}_{-0.2}$ Gyr. Southworth et al. (2009) suggest an age between 0 and 2 Gyr, that is consistent with both our two determinations. Anyway, since any of the two sets of input stellar parameters do not fully agree with the theoretical models, we caution that its age estimation is not necessarily reliable.

As a term of comparison for the TPH, we derived the age distribution of the SH sample, that is displayed in Fig. 4.10. It peaks in the [3 3.5) Gyr bin and its median is ~ 4.8 Gyr, which is very close to the solar age value.

The comparison between Figures 4.9 and 4.10 suggests good consistency between the age distribution. This statement is quantitatively supported by a Kolmogorov-Smirnov (KS) test. We obtained high p-values (0.5 for the TPH-SH comparison and 0.3 for the BTPH-SH comparison), indicating not to reject the null hypothesis, according to which the samples come from the same distribution. We can conclude that even if, in principle, photometric and spectroscopic targets could be chosen according to different criteria, however the confirmation of a candidate transiting planet requires the application of both the transit and radial velocity methods. Therefore, similar biases characterize the two kind of samples.

Our second step is to investigate whether the age distribution of all the SWP is compatible with that of generic field stars not harbouring planets.

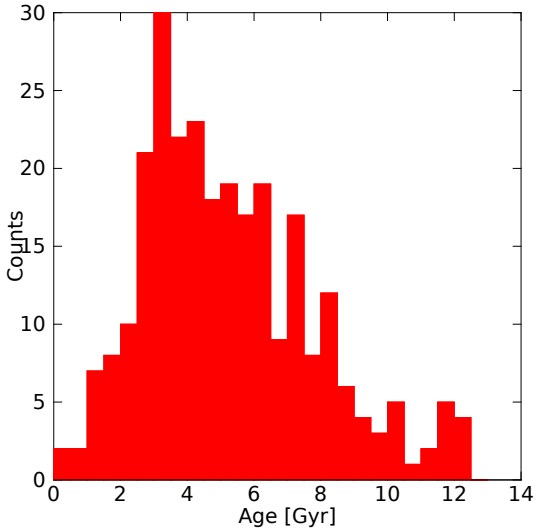

Figure 4.10: Age distribution of the stars belonging to the SH catalogue.

The SWP are essentially G type stars closer than 200 pc, therefore the stars belonging to the RSN catalogue represent an interesting sample to be compared. The RSN catalogue does not report all the input parameters required by our algorithms to retrieve ages. However, Casagrande et al. (2011) (C11 from here on) computed the ages of the different stars of the Geneva Copenhagen survey. Even if they followed their own method, nevertheless we refer to Bonfanti et al. (2016) to demonstrate that C11 ages are statistically consistent with the ones deriving from our isochrone placement technique for that subsample for which all the input parameters were available.

Fig. 4.11 shows the comparison between the age distribution of the SWP, as inferred from our isochrone placement and the age distribution of the RSN sample, built up using the age values by C11. The two histograms both have the same peak in the [3, 3.5) Gyr bin and the same median $t \sim 4.8$ Gyr. The RSN age distribution is slightly less peaked, anyway their consistency is also enforced by the quite high KS p-value= 0.2.

At this stage one may ask whether our isochrone placement has actually given accurate age distributions for these G-type stars. As shown in § 4.1, we fully tested our algorithms, but considering only two particular synthetic age values. Now, instead, we want to deal with a synthetic sample that is comparable with both our SWP and RSN catalogues in terms of $T_{\rm eff}$, L, metallicity, distance and magnitudes.

We generated about half a million of stars, that are spread throughout the allowable ranges in $T_{\rm eff}$, L, metallicity. Then, we imposed the selection

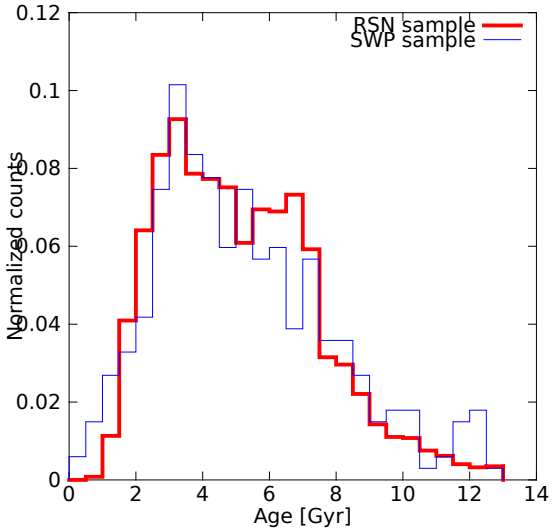

Figure 4.11: Comparison of the age distributions of the RSN sample (3713 stars) and of the SWP sample (335). The histograms exhibit the same mode ([3, 3.5) Gyr bin) and median (~ 4.8 Gyr).

effects characterizing both the SWP and RSN samples, so to obtain a set of a thousand synthetic stars (synthetic stars of the solar neighbourhood: *SSN*) mimicking the properties of all the real stars we analyzed. After that we computed the age of this *SSN* sample thanks to our isochrone placement, to further evaluate its reliability.

The distribution of the true age of the SSN sample is represented through red thick stairs in Fig. 4.12. The superimposed blue thin stairs are representative of the age distribution that comes from the isochrone placement computation. The consistency of the histograms confirms the reliability of the isochrone placement technique.

Further analysing the age distributions of the planet-hosting stars and of the stars of the solar neighbourhood in Fig. 4.11, we point out that:

1. the median $t \sim 4.8$ Gyr of the SWP age distribution is very similar to the solar age value ($t_\odot \approx 4.6$ Gyr, according to Chaussidon 2007), but it differs by ~ 1.5 Gyr from the youngest peak of the histogram, due to the skewness towards older ages. According to their metallicities, there is no evidence that stars with $t > 9$ Gyr have population II properties. If we exclude this contamination, we may argue whether such a skew distribution reflects a prolonged star formation history (Rocha-Pinto et al., 2000) or it is due to an asymmetric propagation of errors.

2. the median age of ~ 4.8 Gyr appears older than that currently assumed

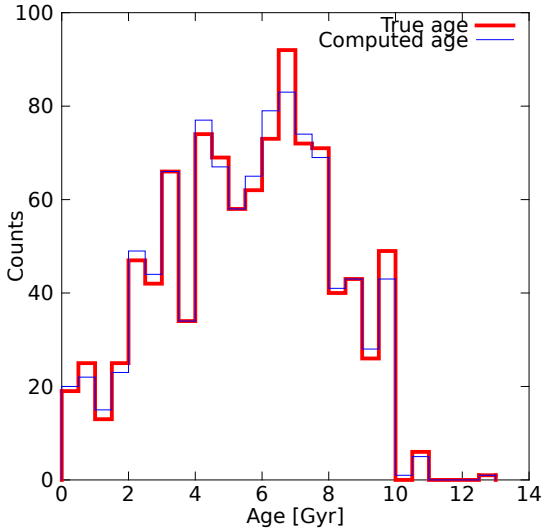

Figure 4.12: Comparison between the age distributions of the *SSN* sample. The red histogram represents the true synthetic age, while the blue one has been derived after the aplication of the isochrone placement to each star.

for most of the thin disc population, where planet-hosting stars and the RSN sample are located. In fact, as summarized by Allende Prieto (2010), Reddy et al. (2006) say that thin disc stars span a range between 1 and 9 Gyr, with the majority of them younger than 5 Gyr. Holmberg et al. (2009) and Haywood (2008) set an older upper limit for the thin disc ages, however they both agree that most of these stars are younger than 4-5 Gyr. Rocha-Pinto et al. (2000), using a different approach based on the stellar activity as age indicator, found three different peaks in the local star formation history, with the highest at very young ages below 1 Gyr. We caution that we limited our sample primarily to G-type stars. The other point is that we are sampling a very limited inter-arms volume (essentially < 200 pc), as most of the recent studies based on single star age measurements. The literature does not present detailed studies of the ages of single disc stars far away from the solar neighbourhood. Thus, this lack of information does not allow us to perform a complete comparison between the evolutionary properties of our samples and those of the entire galactic disc. The extension of the stellar analysis to a distance larger than 200 pc would include younger active star-forming regions, such as the Orion Nebula or Taurus-Auriga complex. As a consequence, in deeper surveys we expect to include significantly younger stars.

Astronomy & Astrophysics manuscript no. AgeAA
June 18, 2015

Revising the ages of planet-hosting stars

A. Bonfanti[1,2], S. Ortolani[1,2], G. Piotto[1,2], and V. Nascimbeni[1,2]

[1] Dipartimento di Fisica e Astronomia, Università degli Studi di Padova, Vicolo dell'Osservatorio 3, I-35122 Padova, Italy
[2] Osservatorio Astronomico di Padova, INAF, Vicolo dell'Osservatorio 5, I-35122 Padova, Italy

ABSTRACT

Aims. This article aims to measure the age of planet-hosting stars (SWP) through stellar tracks and isochrones computed with the *PA*dova & T*R*ieste *S*tellar *E*volutionary *C*ode (PARSEC).
Methods. We developed algorithms based on two different techniques for determining the ages of field stars: *isochrone placement* and *Bayesian estimation*. Their application to a synthetic sample of coeval stars shows the intrinsic limits of each method. For instance, the Bayesian computation of the modal age tends to select the extreme age values in the isochrones grid. Therefore, we used the isochrone placement technique to measure the ages of 317 SWP.
Results. We found that $\sim$ 6% of SWP have ages lower than 0.5 Gyr. The age distribution peaks in the interval [1.5, 2) Gyr, then it decreases. However, $\sim$ 7% of the stars are older than 11 Gyr. The Sun turns out to be a common star that hosts planets, when considering its evolutionary stage. Our SWP age distribution is less peaked and slightly shifted towards lower ages if compared with ages in the literature and based on the isochrone fit. In particular, there are no ages below 0.5 Gyr in the literature.

1. Introduction

Knowledge of the ages of stars with planets (SWP) is important for studying several aspects of the evolution of planetary systems, such as dynamical interactions among planets (see e.g. Laughlin & Chambers (2001)) and tidal effects induced by SWP (see e.g. Pätzold et al., 2004 Barker & Ogilvie, 2009). See Hut (1980), Hut (1981) for a theoretical approach regarding tides. Moreover, SWP ages enable assessment of the evolution of the atmosphere of the hosted planets caused by chemical reactions occurring on the planets themselves and by the consequences of tidal stripping or other atmospheric loss processes. Knowledge of the stellar ages is also useful for selecting candidates for planet detections.

Most of the known SWP are main sequence G-K type stars that belong to the nearby disk field population. It is very well known that determining the ages of these stars is difficult because of the degeneracy of parameters and the slow evolution of the observational quantities. The current uncertainties are higher than the accuracy needed for these studies.

The age is not a direct observable, so its computation should use models or a combination of models and empirical relations. Methods based on isochrones from stellar evolutionary models are often used, but other methods are also applied, based on empirical relations, such as gyrochronology and activity indices. Asteroseismology will be a very promising technique when more specific data is available, and in specific cases, the chemical analysis (the so-called chemiochronology) can be applied as well. See Soderblom (2010) for a broad review on this topic.

Most of the ages of SWP come from individual sources and different methodologies. A recent discussion of the ages of nearby field stars is presented in Haywood et al. (2013), while specific analyses of SWP have been published by Saffe et al. (2005) and Takeda et al. (2007). Finally Brown (2014) presents a new study based on a new geometrical approach for interpolating the grids of isochrones, and he shows that the results from gyrochronology give systematically younger ages.

In this paper we focus on the ages derived by using isochrones. To determine the age of a stellar cluster using isochrones, it is necessary to put its stars on the Hertzsprung-Russel diagram (HRD) and evaluate — among the isochrones having the metallicity of the cluster — which isochrone best fits the layout of the stars on the diagram (*isochrone fitting*). Instead, determining the age of a field star, in particular a MS star, is much more complex. The statistical treatment of the data plays a crucial role in the analysis, and it is necessary to face the problem of the degeneracy of parameters. Two different methods are typically applied: the *isochrone placement* and the *Bayesian estimation* (Jørgensen & Lindegren (2005), da Silva et al. (2006), Pont & Eyer (2004)).

The isochrone placement technique consists in putting a star on the HRD together with its error bars in $\log T_{\rm eff}$ and $\log L$ and in properly selecting the best isochrone to account for the error box. Instead, the Bayesian estimation technique requires getting a posterior probability density function (*pdf*) of the age of a star, assuming an a priori star formation rate, an a priori metallicity distribution, and an a priori initial mass function (IMF).

We note that sometimes statistical instruments such as Markov Chain Monte Carlo (MCMC) have been applied in the literature. MCMC tools are able to sample *pdf*s (without obtaining an explicit expression for them), in order to infer parameters in Bayesian ambit. It can happen that useful parameters for computating stellar ages are recovered via MCMC tools and then used to compute the age through χ^2-minimization-based methods. Algorithms where a preliminary Bayesian approach is followed by a frequentistic one are not strictly Bayesian.

The paper is organized in the following way. In § 2 the input data and the isochrones we used are presented; in § 3 the implementation of isochrone placement and Bayesian estimation techniques is described; in § 4 the results obtained are discussed; while § 5 reports a summary of our work.

Table 1. Solar parameters adopted by the isochrones.

Solar data	Value	Source
$Z_\odot$	0.01524	Caffau et al. (2008)
$Z_{\mathrm{ini},\odot}$	0.01774	Bressan et al. (2012)
$L_\odot$ [erg/s]	$(3.846 \pm 0.005) \cdot 10^{33}$	Guenther et al. (1992)
$R_\odot$ [km]	695980 ± 100	Guenther et al. (1992)
$T_{\mathrm{eff},\odot}$ [K]	5778 ± 8	from $L_\odot$ and $R_\odot$
$M_{\mathrm{bol},\odot}$ [mag]	4.770	Girardi et al. (2008)
$BC_\odot$ [mag]	−0.063	interpolation
$B-V_\odot$ [mag]	0.667	in the isochrones
$\log g_\odot$ [cgs]	4.432	grid
$M_{V,\odot}$ [mag]	4.833	from $M_{\mathrm{bol},\odot}$ and $BC_\odot$
$V_\odot$ [mag]	−26.739	from $M_{V,\odot}$ and $d_{\oplus-\odot}$

2. The data

First of all, this section presents the input data that were used to test the reliability of the developed algorithms. The last two subsections are dedicated to describing the sample of SWP and of the theoretical models used to characterize the SWP. From here on, all the photometric parameters are expressed in the Johnson system.

2.1. The 3.2 Gyr synthetic stars catalogue

We built a catalogue of 927 synthetic stars located on an isochrone with initial [Fe/H]=0 and $\log t = 9.5$ ($t \approx 3.2$ Gyr). To each of them we attributed a distance d, its uncertainty Δd, and an uncertainty on $\log g$ $\Delta \log g$, generating random numbers from normal distributions with means $\bar{d} = 135$ pc, $\overline{\Delta d} = 0.1\bar{d}$, and $\overline{\Delta \log g} = 0.1$ dex, respectively. The uncertainty on [Fe/H] is Δ[Fe/H] = 0.05. All these values are typical of the stars belonging to the SWP catalogue that is described below.

2.2. SWP Catalogue

All the planetary and stellar parameters of SWP were collected from *The Site of California and Carnegie Program for Extra-solar Planet Search: Exoplanets Data Explorer*[1] (Wright et al. (2011)). After having discarded binaries and stars without measurements of the apparent V magnitude, $B-V$ colour index, parallax π from Hipparcos, [Fe/H], and $\log g$, we considered the remaining 326 stars that constitute our SWP catalogue. These stars are represented on the CMD in Fig. 1 with the two 1-Gyr-isochrones corresponding to the minimum ($Z = 0.00318$) and the maximum ($Z = 0.054$) metallicity of the sample. Increasing the metallicity, the isochrones go towards redder colours. Some stars are located to the left of the $Z = 0.00318$ 1-Gyr-isochrone. These are anomalous because they are expected on the right-hand side, considering their higher metallicity.

2.3. The isochrones

The theoretical models employed to determine the ages of the stars are the PARSEC[2] isochrones (version 1.0) by Bressan et al. (2012), corresponding to the solar parameters listed in Table 1. The different sequences of isochrones are identified by the metallicity of a star at the moment of its birth: Z_{ini}.

[1] `http://exoplanets.org/exotable/exoTable.html`

[2] The web interface called CMD 2.5 input form is available at `http://stev.oapd.inaf.it/cgi-bin/cmd`

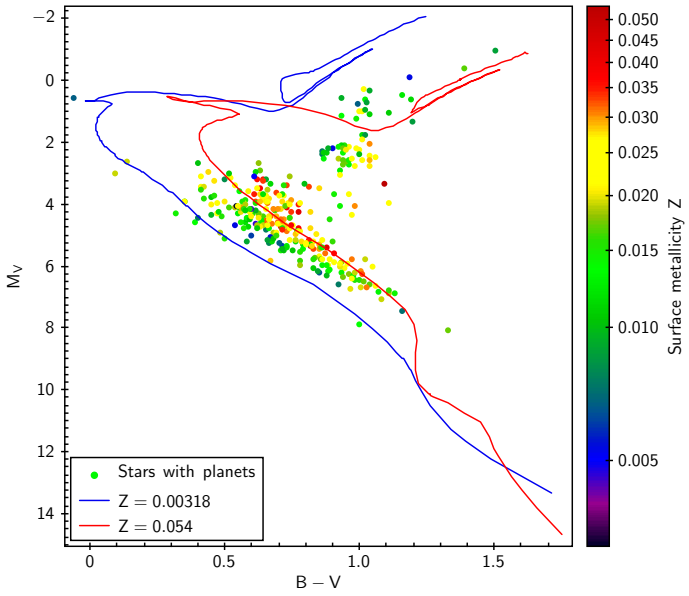

Fig. 1. SWP on the CMD. The colour of the points is representative of the metallicity Z of the stars. As reference, the 1-Gyr-isochrones corresponding to the extreme metallicity values of the sample are also represented.

We used sequences spaced by 0.05 in $\log t$ (with t in years) starting from $\log t = 6$ up to $\log t = 10.1$.

Considering the solar sequence of isochrones identified by $Z_{\mathrm{ini}} = Z_{\mathrm{ini},\odot} = 0.01774$ as reported by Bressan et al. (2012) (note that this value is different from the present one, which is $Z_\odot = 0.01524$), the interpolation between the $\log L/L_\odot$ and M_{bol} tabulated values yields the correspondence $1L_\odot \rightarrow M_{\mathrm{bol}} = 4.770$. We also computed the differences between the absolute bolometric and V magnitudes given by the grid (which correspond to the bolometric corrections in the V band BC $= M_{\mathrm{bol}} - M_V$ adopted by the authors), and finally, we looked for the BC value that gave $T_{\mathrm{eff}} = T_{\mathrm{eff},\odot}$ and $L = L_\odot$. The interpolation gives a bolometric correction for the Sun $\mathrm{BC}_\odot = -0.063$. Finally, $\log g_\odot$ and $B-V_\odot$ come from the interpolation in the solar isochrone grid, as well.

As already said, the parameter that identifies a given sequence of isochrones is the metallicity Z, which is linked to [Fe/H] by an exponential relation[3] , which assumes the form

$$Z = 10^{[\mathrm{Fe/H}]-1.817}. \quad (1)$$

3. Age determination methods

3.1. Preliminary considerations

Deriving the ages of stars by making use of theoretical models requires knowledge of the stellar mass M. In fact, since isochrones corresponding to different age values can be very close on the HRD, M can help in the selection of the one that fits the input data best. In some cases, there is even a degeneracy between the age t and the mass M of a given star. Figure 2, which shows the solar metallicity evolutionary tracks of 1 and

[3] A reference relation between Z and [Fe/H] is $\log z = [\mathrm{Fe/H}] + \log(0.6369 f_\alpha + 0.3631) - 1.658$ proposed by Straniero et al. (1992). It takes the possibility of α-enhancement into account, where $\log f_\alpha = [\alpha/\mathrm{Fe}]$. (1) is a reduced version of this equation considering $f_\alpha = 1 \Rightarrow [\alpha/\mathrm{Fe}] = 0$, i.e. assuming a solar α-enhancement. Moreover, the constant −1.658 is substituted with −1.817 so that $Z = Z_\odot = 0.01524$ for [Fe/H]=0.

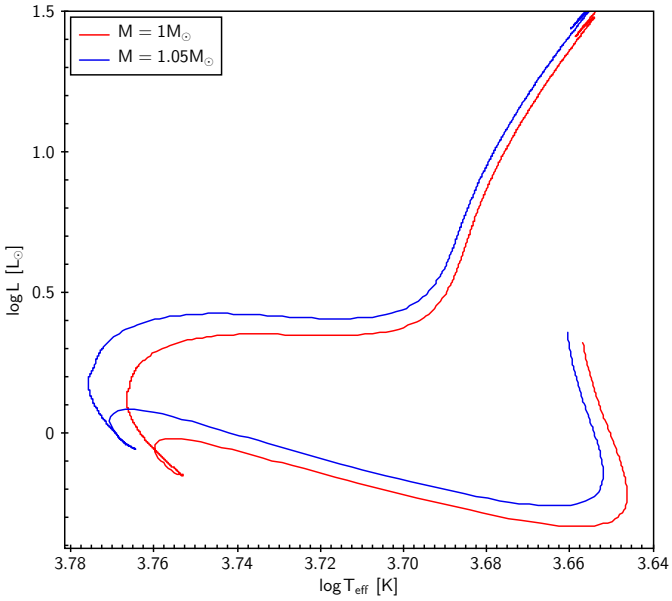

Fig. 2. Solar metallicity evolutionary tracks of 1 and 1.05 $M_\odot$ star on the HRD. Their intersection point is representative of the degeneracy between stellar mass and age. See text for further details.

1.05 $M_\odot$, clarifies the situation: the stellar parameters ($\log T_{\rm eff}$, $\log L$) = (3.7662, 0.0839) corresponding to the intersection of the two tracks are representative either of a 1 $M_\odot$ star with an age of 6.34 Gyr or of a 1.05 $M_\odot$ with an age of 26.8 Myr, so the knowledge of the stellar mass is fundamental to correctly establishing the evolutionary stage of any given star.

In the particular case where the comparison is between ages of a pre-main sequence (PMS) star and a MS star, it is also possible to remove the degeneracy considering that PMS stars are particularly active if compared with MS stars, and this implies that they have very high rotational velocities and cromospheric activity indices. Considering $\log R'_{HK}$ as reference index for the cromospheric activity, we took the age-activity relation by Mamajek & Hillenbrand (2008) and we slightly shifted it, so that solar values adopted by the isochrones of Padova match the model. According to this relation $\log R'_{HK} = -4.48$ for an age $t = 500$ Myr and $\log R'_{HK} = -4.27$ for $t = 100$ Myr. The typical variation between the highest and lowest peaks in activity and the average level is ~ 0.2 dex for a solar type star; in fact the present mean solar $\log R'_{HK,\odot} = -4.91$, while it was $\log R'_{HK,\odot,\rm Maunder} = -5.105$ during the Maunder minimum. To be conservative we assume that if

$$\log R'_{HK,\star} < -4.65, \tag{2}$$

then the star has an age $t > 500$ Myr, while if

$$\log R'_{HK,\star} < -4.47, \tag{3}$$

then the star has an age $t > 100$ Myr.

As mentioned before, another indicator of the activity of a star is its rotational velocity. According to the study of Denissenkov (2010), a star younger than 500 Myr at the very least has an angular velocity $\Omega_\star \gtrsim 2.65\Omega_{e,\odot}$, while a star younger than 100 Myr has, at least, $\Omega_\star \gtrsim 4\Omega_{e,\odot}$, where $\Omega_{e,\odot} = 2.86 \cdot 10^{-6}$ rad/s is the present angular velocity of the solar envelope. In the absence of the $\log R'_{HK,\star}$ value, and assuming $\frac{4}{\pi} v \sin i$ as the mean probable rotational velocity of a star, we conclude that a star has an age $t > 500$ Myr, if

$$\Omega_\star < 7.579 \cdot 10^{-6} \quad \text{rad/s}, \tag{4}$$

while its age is greater than 100 Myr, if

$$\Omega_\star < 1.144 \cdot 10^{-5} \quad \text{rad/s}. \tag{5}$$

Besides many other parameters, the databases we examined often reported the stellar mass M, but all these parameters were derived by different authors following different calibration procedures. To make as few assumptions as possible and to produce input parameters that enter a picture that is self-consistent with the theoretical values reported by the isochrones, we decided to start from the values of

- visual magnitude V,
- colour index $B - V$,
- parallactic distance d,
- metallicity [Fe/H], and
- spectroscopic $\log g$,

which are available in the literature, and then to compute all the other needed parameters (i.e. the stellar mass M using the stellar effective temperature $T_{\rm eff}$, luminosity L, and radius R), according to the calibrations that can be inferred from the values tabulated in the isochrones.

The results are sensitive to the bolometric corrections (BCs). Several published tables of bolometric corrections are reported in the literature, but — as pointed out by Torres (2010) — values given by an author can differ noticeably from the ones given by another author depending on the arbitrary zero point (traditionally set using the Sun as reference) that each author adopts. Moreover, there is sometimes no internal consistency between $V_\odot$, $M_{\rm bol,\odot}$, and $\rm BC_\odot$.

For these reasons we obtained the correspondence between M_V and $\log L$ by interpolating the values of the isochrone grids and inferring the BCs from the photometric values tabulated in the isochrones. Assuming an internal uncertainty on the apparent bolometric magnitude equal to 0.03 mag, the uncertainty ΔL is associated to L through error propagation. The correspondence between $B - V$ and $\log T_{\rm eff}$ is obtained from the isochrones as well. An internal uncertainty of 1% is attributed to the resulting $T_{\rm eff}$ value.

From the parameters just derived, we can now compute the estimates of R and M that are used as input data in the isochrone placement technique:

$$R = \sqrt{\frac{L}{\left(\frac{T_{\rm eff}}{5778}\right)^4}} \tag{6}$$

$$M = \frac{g}{10^{4.43}} R^2. \tag{7}$$

In these equations L and M are in solar unities, $T_{\rm eff}$ is in K, and g is in cm/s^2. After applying the error propagation, all the data are accompanied by the respective uncertainties.

Another aspect that has been investigated is the temporal evolution of the surface stellar metallicity Z due to atomic diffusion. The interaction between different chemical species leads to a surface depletion of elements heavier than hydrogen, which sink downwards. The characteristic timescale for the diffusion of an element is (Chaboyer et al. (2001))

$$\tau_{\rm diff} \simeq K \frac{M_{\rm CZ}}{M T_{\rm CZ}^{3/2}} \tag{8}$$

where M is the stellar mass, $M_{\rm CZ}$ the mass of the surface convective zone, $T_{\rm CZ}$ the temperature at the base of the convective zone, and K a constant referring to the chemical element being

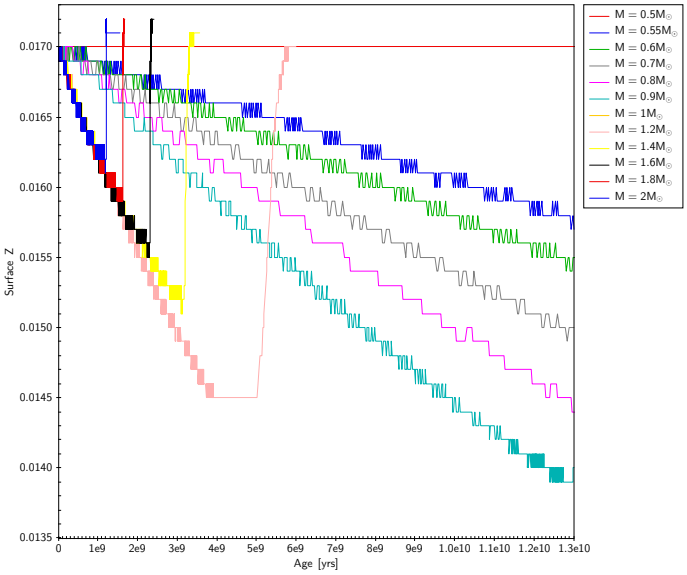

Fig. 3. Evolution with time of the surface metallicity Z for stars of different masses characterized by the same initial metallicity $Z_{\rm ini} = 0.017$. The ruggedness of the curves is due to the discrete steps in the model, and it has been smoothed while implementing our routines.

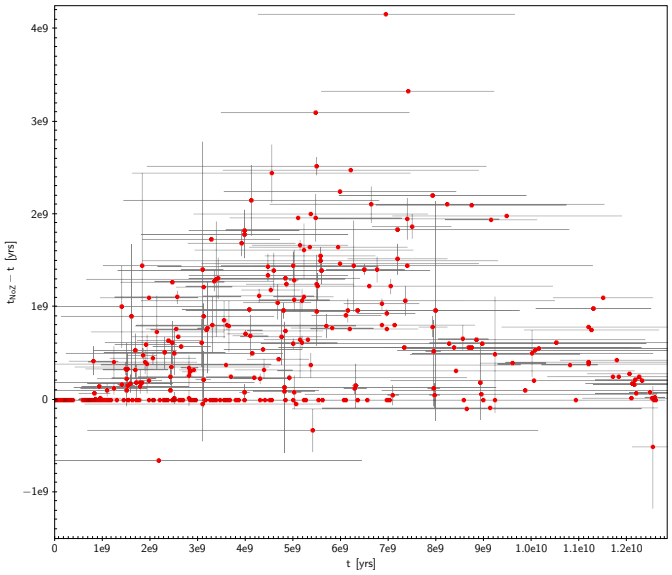

Fig. 4. SWP ages computed through the isochrone placement technique. The difference $t_{\rm noZ} - t$ between the ages $t_{\rm noZ}$ computed without taking the surface metallicity Z evolution into account and the ages t computed considering such an effect, is plotted versus t. If the algorithm does not take into account that the sequences of isochrones are identified by the initial stellar metallicity, while we only know the present value, then the ages obtained are biased towards older values, especially for intermediate-age stars.

taken into account. The direction of this process is parallel to the temperature and pressure gradients, while it is antiparallel to the chemical concentration gradient. For further information see Burgers (1969) and Chapman & Cowling (1970).

We considered several stellar evolutionary tracks, kindly provided by Leo Girardi, which illustrate the evolution of stars of different masses and initial metallicities on the HRD. Such tracks give the surface Z in correspondence of any given age, so we built up different $Z_{k,l} = Z_{k,l}(t)$ functions depending on the stellar initial metallicity and mass (identified by the subscripts k and l, respectively). We observed that atomic diffusion is not negligible for stars having masses between 0.5 and 2 $M_{\odot}$. In this mass range, the surface metallicity decreases with the time during the MS phase and then increases as the envelope convection deepens, becoming constant once the initial metallicity value $Z_{k,l}(0)$ is reached. As a consequence, the initial decrease followed by the increase in $Z_{k,l}(t)$ spans a shorter time scale for higher masses, where the evolution is faster. An example of the temporal evolution of Z for stars of different masses, but characterized by the same initial metallicity, is shown in Fig 3.

The evolution of the atmospheric chemical composition has a non-negligible effect. For instance, if we take a solar star (i.e. with the current luminosity and temperature of the Sun) with a present metallicity equal to $Z_{\odot} = 0.01524$ and employ the sequence of isochrones characterized by such metallicity without taking into account that the metallicity value that identifies the isochrones is the one that a star had when it was born and not the present one, then we get an age $t = 5.1 \pm 2.8$ Gyr instead of the $t = 4.5 \pm 0.1$ Gyr that we obtain if we adopt the initial metallicity value $Z_{\rm ini,\odot} = 0.01774$ to select the isochrones.

Adopting the present-day atmospheric chemical composition in selecting the isochrones for the age computation of field stars generally produces a result that is slightly biased towards older ages, especially for intermediate-age stars, as shown in Fig. 4. In fact, higher metallicity isochrones are redder than lower ones for every age, and in the MS the older a star, the redder it is. Since considering the initial chemical composition of a star implies selection of an equally or higher metallic grid of isochrones, we expect $t_{\rm noZ} - t \geq 0$ for MS stars. Among pre-MS isochrones, instead, older isochrones are bluer for a given metallicity: in this case, we expect negative differences. The three stars in Fig. 4 with evident $t_{\rm noZ} - t < 0$ are peculiar because their colours are too red for their luminosity and metallicity. They are located in a region where there are both old and pre-MS isochrones. Furthermore, they do not have activity indices to disentangle between young and old ages; in these conditions, the code may give $t_{\rm noZ} < t$. This result could be eliminated by iterating the isochrone placement twice and using in the second iteration only those isochrones that differ $\pm\Delta t$ from the age value t recovered by the first iteration. We are considering implementating this in the near future.

3.2. Isochrone placement

The input data characterizing each star for which we want to establish the age are listed below:

$$Z \quad V \quad \mathrm{BC} \quad B-V \quad d \quad \Delta d \quad T_{\rm eff} \quad \Delta T_{\rm eff} \quad L \quad \Delta L \quad g \quad \Delta g \quad M \quad \Delta M.$$

To determine the age and the other parameters, such as effective temperature, luminosity, gravity, and mass, of a given star according to the theoretical models, we first considered the sequence of isochrones *Is* characterized by the present metallicity of the star $Z_{\star}$. If $\log R'_{HK}$ or $v \sin i$ of a star was available (which happens for the 94% of the stars that belong to the SWP catalogue) and relations (2) or (4) were satisfied, we discarded all the rows reporting ages lower than 500 Myr from the sequence *Is*. If, instead, relations (2) and (4) did not hold, but relations (3) or (5) were satisfied, we discarded all the age values available in the isochrone grids lower than 100 Myr (activity cleaning).

Then, for each isochrone in the *Is* sequence, we considered the point on the CMD with the minimum distance from the given

star and computed all its corresponding theoretical values by interpolation through the isochrone grid values. We thus built our reduced grid of isochrones *Is'*. After that, we developed the following procedure:

1. For each row $i = 1, 2, \ldots, \bar{n}$ of *Is'* (from here on, the subscript i will always represent the row index of *Is'*), multiply the theoretical value reported in the i^{th} row of *Is'* (we refer to it as the generic variable X_i that indicates, time by time, $T_{\rm eff}$, L, M, or g) by the bidimensional Gaussian distribution (window function):

$$\mathcal{G}(L_i, T_{\rm eff,}{}_i) = \frac{e^{-\frac{1}{2}\left[\left(\frac{\log T_{\rm eff,}{}_i - \log T_{\rm eff}}{\Delta \log T_{\rm eff}}\right)^2 + \left(\frac{\log L_i - \log L}{\Delta \log L}\right)^2\right]}}{2\pi \Delta \log T_{\rm eff} \Delta \log L}. \quad (9)$$

   In this way we can consider that the probability that a given stellar parameter corresponds to the value reported by a certain row of *Is'* decreases with increasing distance on the HRD between the star and the isochrone itself, but — at the same time — the isochrones falling out of the error bars in $\log T_{\rm eff}$ and $\log L$ are not discarded definitely.
2. Compute the weight

$$p_i = \left[\left(\frac{\log L - \log L_i}{\Delta \log L}\right)^2 + \left(\frac{\log T_{\rm eff} - \log T_{\rm eff,}{}_i}{\Delta \log T_{\rm eff}}\right)^2 + \left(\frac{M - M_i}{\Delta M}\right)^2 + \left(\frac{\log g - \log g_i}{\Delta \log g}\right)^2\right]^{-1} \quad (10)$$

   that must be attributed to X_i, so that the similarity between the stellar and the theoretical M and $\log g$ values is also taken into account. The greater the likeness between the stellar and the theoretical data, the bigger p_i.

Clearly, in the previous equations all the data with the subscript i are taken from the isochrones, while the others are the input stellar parameters.

Through weighted means, it is now possible to compute the age of a given star and its temperature, luminosity, mass, and gravity according to the Padova evolutionary models. According to what has just been described, the generic stellar parameter expressed by $X_\star$ results in:

$$X_\star = \frac{\sum_{i=1}^{\bar{n}} X_i \mathcal{G}(L_i, T_{\rm eff,}{}_i) p_i}{\sum_{i=1}^{\bar{n}} \mathcal{G}(L_i, T_{\rm eff,}{}_i) p_i}. \quad (11)$$

The corresponding uncertainty is given by

$$\Delta X_\star = \sqrt{\frac{\sum_{i=1}^{\bar{n}} (X_i - X_\star)^2 \mathcal{G}(L_i, T_{\rm eff,}{}_i) p_i}{\sum_{i=1}^{\bar{n}} \mathcal{G}(L_i, T_{\rm eff,}{}_i) p_i}}. \quad (12)$$

Making use of these first guesses for $t_\star$ and $M_\star$, among the $Z_{k,M_\star}$ functions describing the evolution in metallicity of a star with $M = M_\star$, we looked for the one where $Z(t_\star) = Z_\star$, from which we recovered the initial metallicity $Z_{\rm ini,\star}$ that a star of age $t_\star$ had at its birth if the present metallicity is $Z_\star$. After that, we considered the sequence of isochrones corresponding to the just estimated metallicity $Z_{\rm ini,\star}$ and we iterated all these operations until a convergence in the stellar age value was reached.

3.3. Bayesian estimation

As presented by Jørgensen & Lindegren (2005), determining stellar ages from isochrones requires a comparison between observational and theoretical data, according to the stellar evolutionary model adopted. If the model-relevant parameters are collected in a vector $\mathbf{p}$, while the observational data are collected in a vector $\mathbf{q}$, the theoretical model gives a map from the parameter space $\mathbf{p}$ to the data space $\mathbf{q}$. Determining stellar ages represents the inverse problem, i.e. finding a map from $\mathbf{q}$ to $\mathbf{p}$; here we considered $\mathbf{p} = (\tau, Z, m)$ (where τ is the age and m is the mass) and $\mathbf{q} = ([\text{Fe/H}], \log T_{\rm eff}, \log L)$.

In Bayesian statistics, the parameters that have to be estimated (in our case τ, Z and m) are treated as random variables, and their posterior (joint) probability density function is

$$f(\tau, Z, m) \propto f_0(\tau, Z, m) \mathcal{L}(\tau, Z, m) \quad (13)$$

where f_0 is the prior probability density function and $\mathcal{L}$ the likelihood function. The value given by $f(\tau, Z, m)\mathrm{d}\tau\mathrm{d}Z\mathrm{d}m$ represents the fraction of stars with age inside $[\tau, \tau + \mathrm{d}\tau]$, metallicity inside $[Z, Z + \mathrm{d}Z]$ and mass inside $[m, m + \mathrm{d}m]$. The constant of proportionality must be chosen so that $\int\int\int f(\tau, Z, m)\mathrm{d}\tau\mathrm{d}Z\mathrm{d}m = 1$. The integration of f with respect to Z and m gives $f(\tau)$, which is the posterior pdf that a star has the age τ. Assuming the mode as the statistical index that synthesizes the function, the best estimate for the age is the value that maximizes $f(\tau)$. Other plausible choices are those referring to the most probable age of a star considering the mean of the pdf (corresponding to the centroid of the area under $f(\tau)$) or the median, which, instead, is the value that bisects the area under $f(\tau)$. As already pointed out by Jørgensen & Lindegren (2005) — who considered a sample of 2968 synthetic stars in order to evaluate the best criterion to assess age in Bayesian statistics — the mean and the median suffer the bias of attributing an age that is in the centre of the sequence of age values reported by the isochrone grid employed. On the other hand, the mode tends to assign the extreme age values of the isochrone grid to the stars: in particular, selection of extreme ages arises for 2031 stars over the 2968 of their entire sample, which corresponds to a frequency of $\sim 70\%$. In § 4 we confirm the behaviour of these three statistical indices by applying the Bayesian statistics to the stars of both the 3.2 Gyr catalogue and the SWP catalogue.

Assuming independent Gaussian observational errors $\sigma_n^{\rm obs}$ for each $q_n^{\rm obs}$, the likelihood function is given by

$$\mathcal{L}(\tau, Z, m) = \prod_{n=1}^{3} \frac{1}{\sqrt{2\pi}\sigma_n^{\rm obs}} \cdot \exp(-\chi^2/2) \quad (14)$$

where

$$\chi^2 = \sum_{n=1}^{3} \left(\frac{q_n^{\rm obs} - q_n(\tau, Z, m)}{\sigma_n^{\rm obs}}\right)^2. \quad (15)$$

Following the suggestion of Jørgensen & Lindegren (2005), we assumed

$$f_0(\tau, Z, m) = \psi(\tau)\phi(Z)\xi(m) \quad (16)$$

where $\psi(\tau)$ is the a priori star formation rate (SFR), $\phi(Z)$ the a priori metallicity distribution, and $\xi(m)$ the a priori IMF. As one of our purposes is that of studying possible evolutionary peculiarities of our stellar samples, we assume that the prior SFR $\psi(\tau)$ is flat. Regarding the metallicity prior $\phi(Z)$, the spectroscopically determined [Fe/H] values we employed are very reliable (for

example, ∼ 85% of the stars belonging to the SWP catalogue has $\sigma_{[Fe/H]} < 0.08$ dex, with the majority of them that having $\sigma_{[Fe/H]} = 0.03$ dex) and, since for very high accuracy metallicities (say $\sigma_{[Fe/H]} \sim 0.05$ dex) the likelihood function acts as a narrow window function that substantially suppresses the contribution of $\phi(Z)$, we consider a flat $\phi(Z)$ (see Pont & Eyer (2004) for a detailed discussion about the choice of the prior distributions). Assuming also that $\xi(m) = m^{-2.7}$, which is representative of the empirical IMF at around 1 $M_\odot$ (Kroupa et al. (1993)), it is possible to obtain $f(\tau)$ as

$$f(\tau) \propto G(\tau) = \int\int \mathcal{L}(\tau, Z, m)\, \xi(m)\, \mathrm{d}m\, \mathrm{d}Z. \quad (17)$$

Implementing the algorithm of the Bayesian determination of age, we first check that the condition

$$\min \chi_i^2 < \chi_{0.99}^2 \quad (18)$$

is satisfied; $\chi_{0.99}^2$ is the 99$^{\mathrm{th}}$ percentile value of the chi-square distribution that in our case is 11.345, because we have three degrees of freedom (d.o.f). Since the probability that $\chi^2 \leq 11.345$ for a 3 d.o.f. chi-square distribution is 99%, relation (18) states that we do not evaluate ages for stars whose input parameters have less than 1% probability (according to chi-square distribution) to actually be those measured. These stars are characterized by data points that are far away from any isochrone, so their pdfs turn out to be meaningless.

If the preliminary condition given by (18) is satisfied, then we numerically evaluate $G(\tau)$ considering a set of sequences of isochrones taken at constant steps of 0.05 dex in [Fe/H] within the interval whose bounds are empirically fixed at $\pm 3.5\sigma_{[Fe/H]}$ from the stellar metallicity, where $\sigma_{[Fe/H]}$ is the uncertainty on [Fe/H]. Let m_{jkl} be the initial mass value read at line l of the isochrones grid of age τ_j and metallicity Z_k, then

$$G(\tau_j) = \sum_k \sum_l \mathcal{L}(\tau_j, Z_k, m_{jkl}) \xi(m_{jkl})(m_{jkl+1} - m_{jkl}). \quad (19)$$

Once we have obtained the vector $G(\tau)$ of components $G(\tau_j)$, we find the component that assumes the maximum value (say $G(\tau_{\bar{j}})$) and divide each component by $G(\tau_{\bar{j}})$, obtaining the normalized function $\tilde{G}(\tau)$. After we have smoothed $\tilde{G}$ through a polynomial interpolation, the most probable age $\hat{\tau}$ attributed to the star is the value that maximizes $\tilde{G}$ (modal value). We also compute the mean age as the age coordinate of the centroid of the area under $\tilde{G}$ and the median age as the age value that bisects the area under $\tilde{G}$.

As described by Jørgensen & Lindegren (2005), it is possible to prove that $\tilde{G}_{\mathrm{lim}} = 0.61$ sets the 68% confidence level of $\hat{\tau}$, so we provide a 68% confidence interval $[\tau_1, \tau_2]$ to be the shortest interval such that $\tilde{G}(\tau) < 0.61$ outside it.[4]

4. Discussion of the results

4.1. Isochrone placement vs. Bayesian estimation

The first aim of the paper is to compare the reliability of the developed algorithms in the computation of ages of field stars. To reach this goal, we applied these algorithms taking the 3.2 Gyr synthetic stars one by one. Then we checked the correspondence $(B-V, M_V) \rightarrow (\log T_{\mathrm{eff}}, \log L)$ representing each star on both the colour magnitude diagram (CMD) and the HRD. The calibration is correct if a star has the same relative position with respect to the same reference isochrones on both the two diagrams. Finally, we checked to what extent the global age distribution of the entire sample is consistent with the expected age of 3.2 Gyr attributed to the stars a priori. The calibration between observational and theoretical parameters is perfect except for the RGB region, where the intersection between different isochrones makes it difficult; this will have consequences on the age determination.

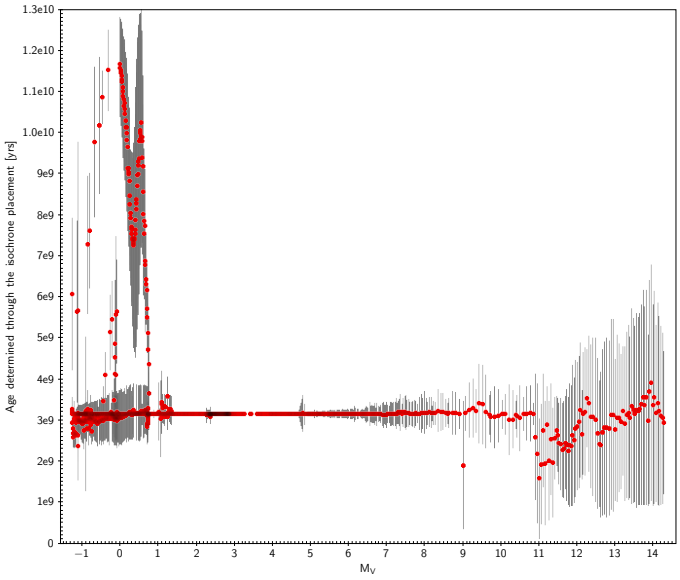

Fig. 5. Ages of the 3.2 Gyr synthetic stars determined through the isochrone placement technique plotted versus their absolute magnitude M_V.

In fact, the representation of the age of these stars determined with the isochrone placement technique versus their absolute magnitude M_V (Fig. 5) shows that — as expected — the majority of the stars fall in the horizontal region between 3 and 3.5 Gyr, but some deviations occur for very low and very high magnitudes. The ages of some very bright stars (in the RGB phase) can be imprecise because of the difficulties linked to the calibration between observational and theoretical stellar parameters owing to the particular shape of the isochrones in that region. Instead, the errors for the ages obtained for the faintest stars deals with the intrinsic difficulties in estimating the ages of low MS stars, even if the calibration from the CMD to the HRD is well done. Just to summarize, the algorithm implementing the isochrone placement technique gives reliable ages, except for

- some stars in the RGB phase, whose ages could also be completely wrong;
- low MS stars, with the obtained ages that can differ up to 50% from the correct value.

We decided to further analyse the ages of the synthetic stars belonging only to the MS (i.e. stars having $4 < M_V < 8$), because they are the most common one amongst the SWP. In addition, since extremely young ages can be discarded considering the stellar activity, the ages are obtained by removing the theoretical isochrones with ages lower than 500 Myr from the fit procedure.

The histogram in Fig. 6 shows a comparison between the age distributions computed with the isochrone placement technique and the Bayesian estimation, which adopts the mode as synthesis index. It also reports the mean error bars associated to the

[4] Since $f(\tau)$ can have multiple maxima, it may happen that $f(\tau)$ is locally below 0.61 inside $[\tau_1, \tau_2]$

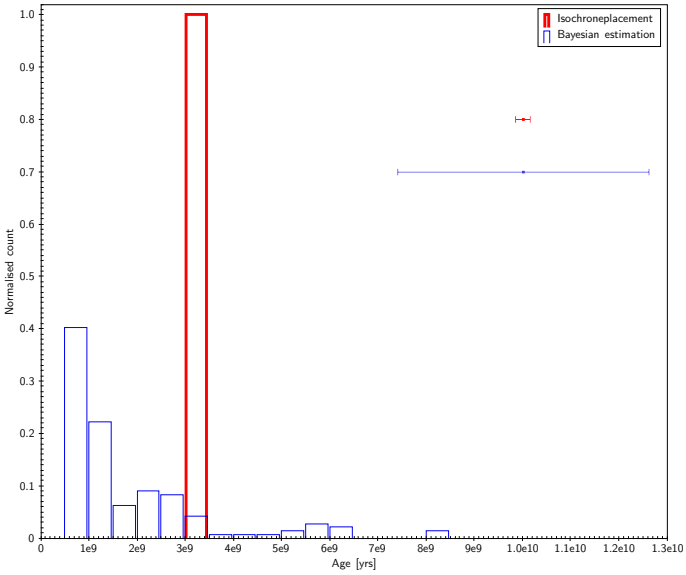

Fig. 6. Isochrone placement vs. modal Bayesian ages. Age distribution of the 3.2 Gyr synthetic stars having $4 < M_V < 8$.

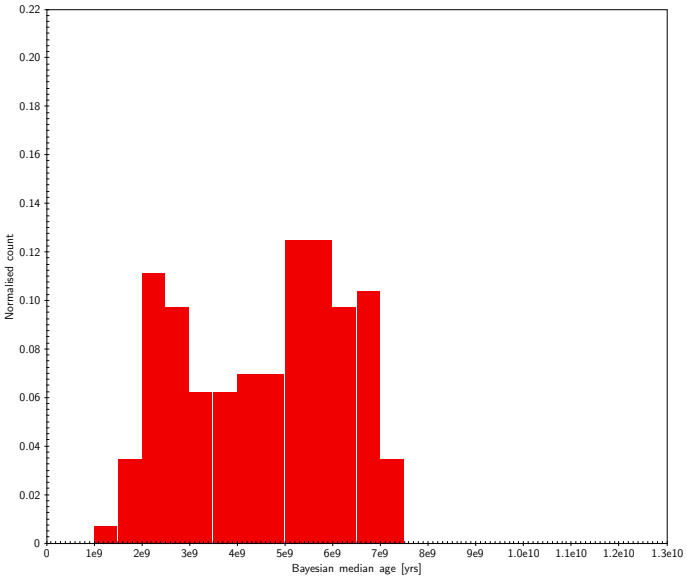

Fig. 8. Bayesian estimation. Median age distribution of the 3.2 Gyr synthetic stars.

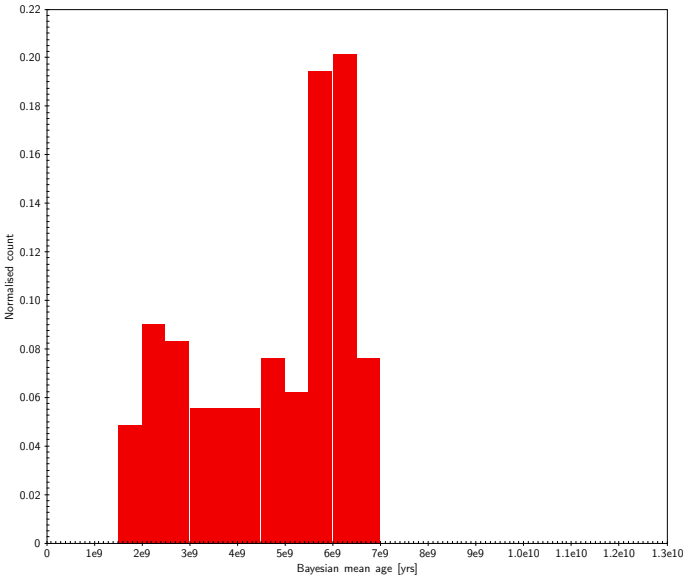

Fig. 7. Bayesian estimation. Mean age distribution of the 3.2 Gyr synthetic stars.

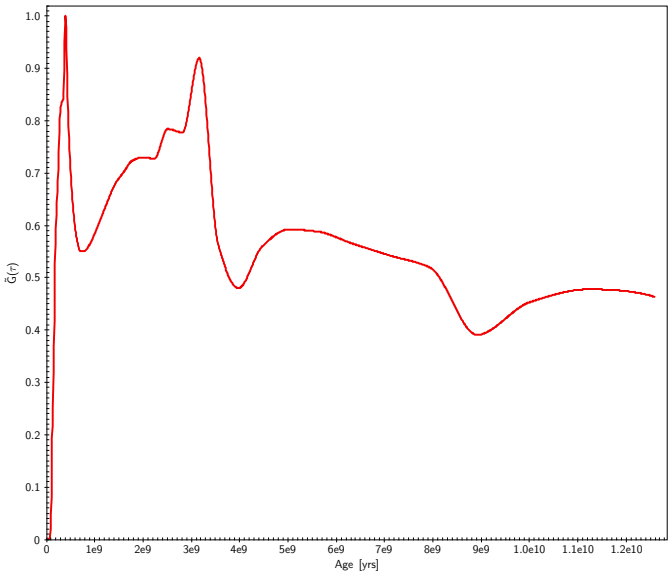

Fig. 9. Bayesian $\tilde{G}(\tau)$ of a 3.2 Gyr synthetic star, which is representative of the presence of spurious peaks corresponding to low age values.

results. Figures 7 and 8 show the age distributions of the same synthetic stars as were obtained through the Bayesian estimation technique that adopts the mean and the median as synthesis indices, respectively.

The isochrone placement turns out to be the most reliable technique, since all the stars fall in the bin [3, 3.5] Gyr (which contains the value of age of 3.2 Gyr a priori attributed to these stars) with a typical uncertainty in the age determination of $\sim$ 0.15 Gyr, corresponding to an error of $\sim$ 5%.

On the other hand, using the Bayesian statistics, the distribution derived from the modal age values presents the main peak in correspondence of [0.5, 1] Gyr. This is the outmost interval of the isochrone grid, and it is representative of an age that is lower than the correct one. Finally, the distribution obtained using the mean and the median as synthesis indices of the Bayesian pdfs are quite similar, essentially spanning an age range from 1 to 7 Gyr. The determination of ages through the mean or the median is therefore not very accurate, and confirming the conclusion by Jørgensen & Lindegren (2005) and by Takeda et al. (2007), these statistical indices tend to select ages in the middle of the sequence of age values reported by the isochrone grids, centralizing the distribution.

The mode is definitely the indicator to be preferred and its tendency to select the extremes in age values in the isochrone grids could be partially mitigated operating a proper numerical filtering. In fact, in some cases — an example of one of them is shown in Fig. 9 — the Bayesian pdf shows peaks corresponding to very low ages. Dealing with synthetic stars, in this context we can recognize such peaks as spurious, and we realize that they hide the presence of the peak centred at $\sim$ 3 Gyr, which indicates the correct age. However, if no a priori indication is given about the ages of stars (the ordinary situation if the scientific aim is to determine of the ages of field stars), it is not possible to select the true peak.

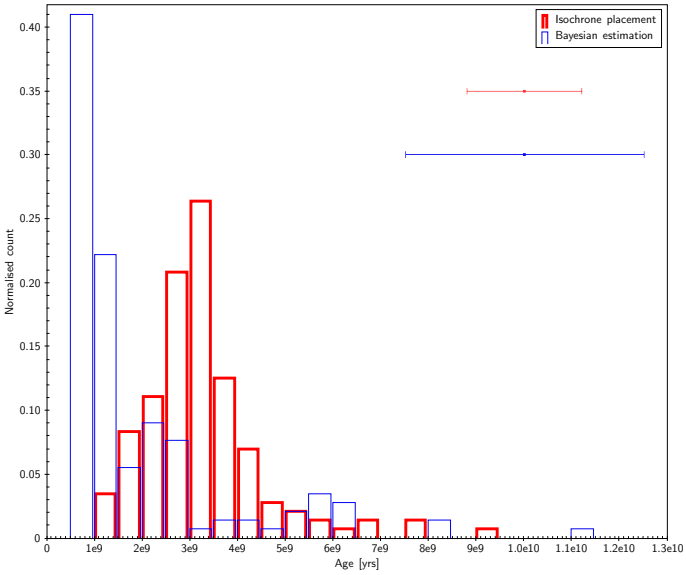

Fig. 10. Isochrone placement vs. modal Bayesian ages. Age distribution of the perturbed synthetic stars with $4 < M_V < 8$.

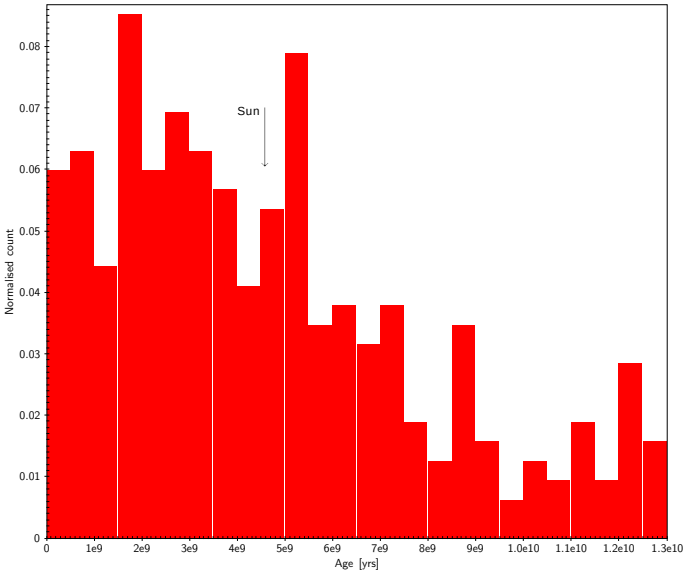

Fig. 11. Isochrone placement. SWP age distribution (317 stars).

Finally, we introduced a random Gaussian perturbation in the input M_V, $B - V$ and $\log g$ of the synthetic stars, considering Gaussian distributions with $3\sigma = 1\%$ of the unperturbed values. We show the age distributions deriving from the isochrone placement and the modal Bayesian age in Fig. 10. As expected, the distributions are broader and the mean error bars of the output results are higher. The mean age value of the isochrone placement does not change. The behaviour of the two techniques is similar to what we have just said about the ages derived from unperturbed input values.

In conclusion, the isochrone placement technique is the method chosen to compute the ages of the SWP.

4.2. Stars with planets ages

We analysed all the 326 stars belonging to the SWP Catalogue. Only nine of them have been removed because their observational parameters were not consistent with the theoretical ones. The age distribution of the remaining 317 stars determined using the isochrone placement technique is presented in Fig. 11. About 6% of the stars are younger than 0.5 Gyr, and then the distribution reaches a peak at [1.5, 2) Gyr and after that it generally decreases. There is a non-negligible number of stars ($\sim 7\%$) older than 11 Gyr. All the parameters of these stars are presented in Table 4.

The histogram of Fig. 11 shows that there are SWP with all possible ages, with a preponderance of stars with ages $< \sim 6$ Gyr. The median value ($\sim$ 4 Gyr) appears slightly lower than the age of the Sun. Of course, older MS stars are fainter (making it more difficult to identify planets). It is not obvious that there is a selection bias for the ages in Fig. 11. Very old or very young stars can have large uncertainties in age because the oldest isochrones overlap the pre-MS region. The frequency of stars in the [0, 0.5) Gyr bin is still an open question. The majority of the youngest SWP are hot Jupiter (HJs) hosts, and they tend to have high rotational velocity, so the check of activity did not discard the youngest isochrones. Actually, it might happen that such high rotational velocity does not reflect the stellar activity, while it can be due to the spin-up induced by the HJ, as suggested for example by Poppenhaeger & Wolk (2014). Without definite indications from activity indices, another way to disentangle pre-MS from post-MS isochrones is to consider the stellar density $\rho_\star$, which is observationally available in the case of SWP detected through the transit method (see e.g. Sozzetti et al. (2007)). Here, $\rho_\star$ gives indications of the evolutionary stage of a star, and it has been used, for instance, by Rouan et al. (2012) to reject an extremely low age for CoRoT-23. We are planning of inserting this kind of check in the future development of our algorithm.

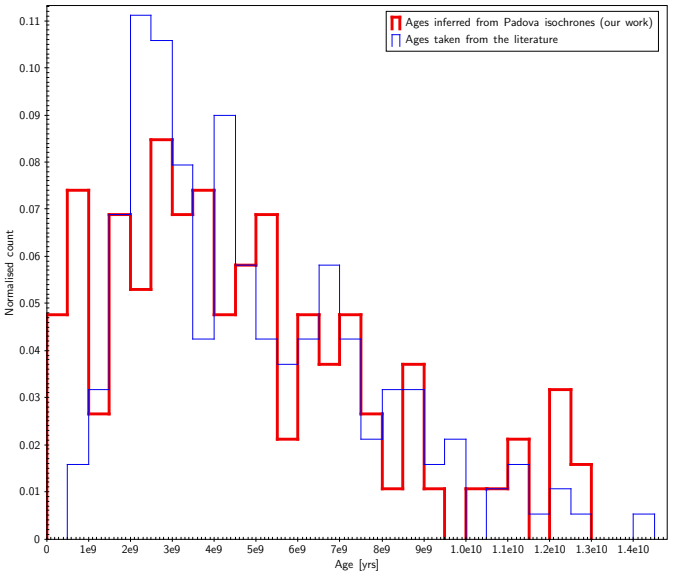

Fig. 12. Comparison between the SWP age distribution derived here and coming from the literature (189 stars).

The literature reports the ages of 189 SWP, estimated using isochrones, but with different theoretical models and techniques. The superimposition of the consequent literature age distribution on what is found here is shown in Fig. 12. The two distributions are quite in agreement for ages older than $\sim$ 4.5 Gyr, while we found more stars in the domain of younger ages. In particular, in our sample, $\sim$ 5% of the stars has an age between 0 and 0.5 Gyr, while no stars in the literature fall in this first bin.

The difference $t_{\rm Lett} - t$ between the ages found in the literature and the values computed here is represented in Fig. 13,

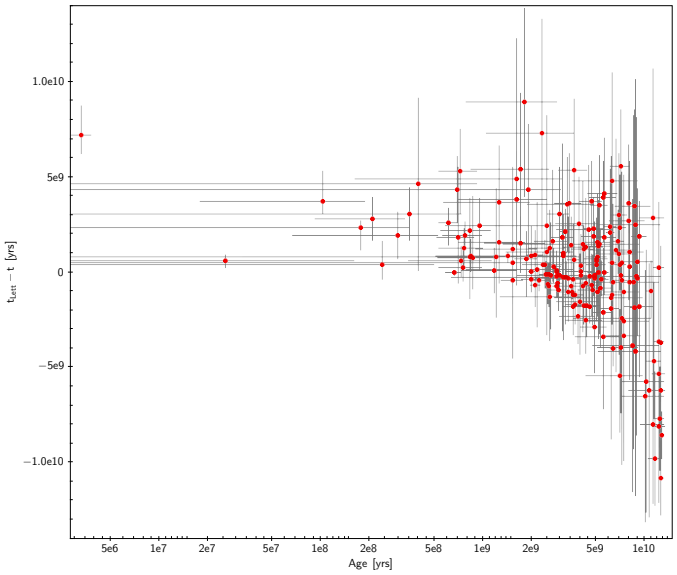

Fig. 13. $t_{\rm Lett} - t$ vs. t for the 189 SWP found in the literature.

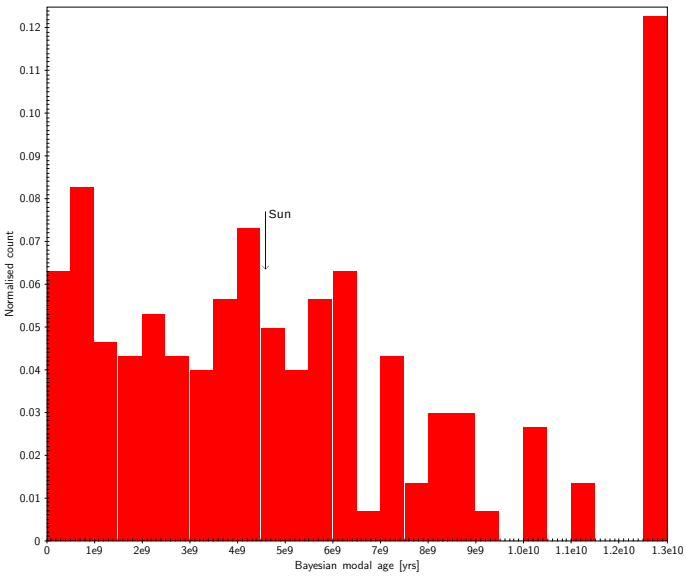

Fig. 14. Bayesian estimation. SWP modal age distribution (302 stars).

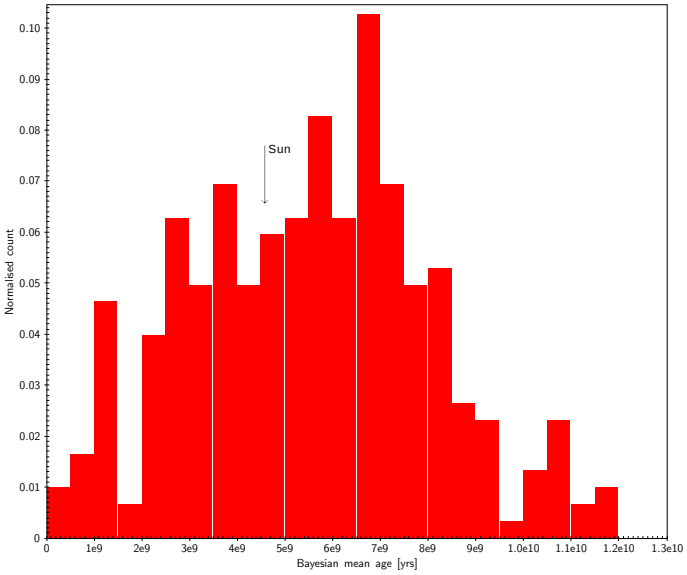

Fig. 15. Bayesian estimation. SWP mean age distribution (302 stars).

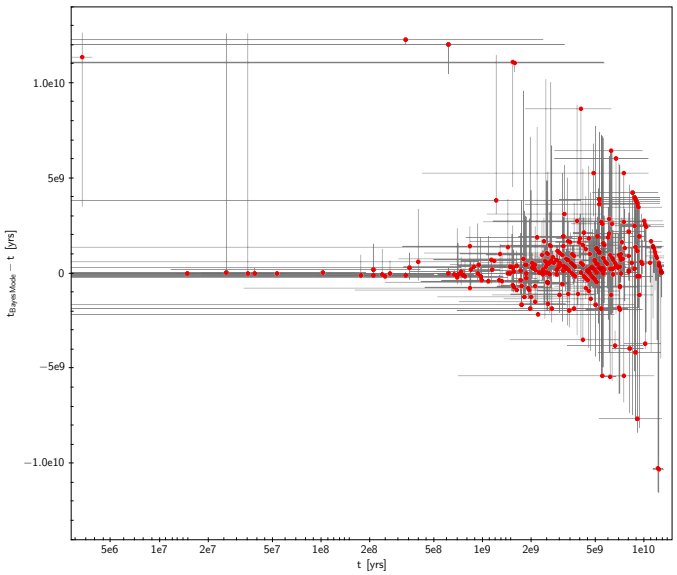

Fig. 16. $t_{\rm BayesMode} - t$ vs. t (302 stars).

which shows a wide spread in the age values. We provide new ages, which have the advantage of being derived using the same method and the same set of isochrones, and therefore useful for statistical investigations. Our age distribution in Fig. 12 is broader than in the literature. Our data show an overabundance of young stars. Some young stars in the literature are judged to be older by our technique. This may happen for stars located on the red side of the isochrone interval, where the locus of the old isochrones is very near to the pre-MS one.

Just for completeness, we also show the age distributions of 302 stars belonging to the SWP catalogue from the modal Bayesian estimation. Given that we find high frequencies in the first and in the last age bin of Fig. 14, it is again clear that the mode always tends to assign extreme age values to the stars. Figure 15 again suggests that the mean always produces a distribution centred on the middle of the age range. We avoid reporting the age distribution of SWP inferred from the median Bayesian age value, because it is very similar to Fig. 15 where the mean is employed as reference statistical index.

Figure 16 shows the difference $t_{\rm BayesMode} - t$ between the modal Bayesian age $t_{\rm BayesMode}$ and the age t computed through the isochrone placement represented versus t. Apart from the effect of the mode of attributing the most extreme age values available in the isochrone grids (visible from the locus of points in the upper right part of the figure), the other Bayesian-estimated age values appear slightly biased towards older ages. The median of the isochrone placement age distribution is $\sim$ 4 Gyr and the mean error is $\sim$ 1.15 Gyr, while the Bayesian modal age distribution has a median of $\sim$ 4.25 Gyr, and the mean error is $\sim$ 1.75 Gyr. This behaviour of the method contrasts with what is reported by Haywood et al. (2013), who used both a χ^2 minimization (somewhat comparable to our isochrone placement technique, even if they considered the χ^2 minimization simply on the ($T_{\rm eff}$, M_V) plane) and the Bayesian technique described by Jørgensen & Lindegren (2005) to compute the ages of nearby field stars. In their paper, the Bayesian technique does give younger ages, so we again emphasize the crucial role played

by the details within the specific method implemented to compute the ages of field stars.

In the upper left-hand side of Figures 13 and 16 there is a single isolated point, which is the star CoRoT-23. The paper that discusses its detection (Rouan et al. (2012)) reports $V_\star = 15.63$ mag and $B_\star = 16.96$ mag. $V_\star$ also agrees with the magnitude reported by `exoplanets.eu`[5]. Instead, `exoplanets.org` reports $V_\star = 16.96$ mag. Since `exoplanets.org` reports $B - V_\star = 1.33$ (same value as inferred from Rouan et al. (2012)), it is likely that $B_\star = 16.96 \neq V_\star$. However, after applying the isochrone placement with the new photometry, our code does not converge on any age value. This new photometry, in fact, moves the star farther out from the set of isochrones. This means that, first of all, there is a problem in the source of the photometry. Moreover, CoRoT-23 is a peculiar system considering its age and the orbital eccentricity of the hosted planet (see Rouan et al. (2012)). As already said, taking the observational $\rho_\star$ into account may help give a better answer to this problem.

Either way, using $V_\star = 16.96$ mag, we obtained an isochrone placement age $t_{\star,\mathrm{Isoc}} = 3.3$ Myr, while the Bayesian estimation gives $t_{\star,\mathrm{Bayes}} = 11.3$ Gyr. This is why CoRoT-23 appears as an outlier in Fig. 16. Thus $t_{\star,\mathrm{Bayes}} \gg t_{\star,\mathrm{Isoc}}$ because, even if the Bayesian pdf had a peak corresponding to a very low age, such a peak was judged as a spike by the smoothing through the polynomial interpolation, so it was erased. The next major peak was then at 11.3 Gyr.

Finally, we considered the work of Brown (2014), who used different isochrones and gyrochronological relations to assess the ages of a sample of SWP. We found 24 SWP in common with Brown (2014). The difference $t_{\mathrm{BrownYY}} - t$ between the ages t_{BrownYY} computed by Brown using the YY isochrones (Demarque et al. (2004)) and the ages t computed here through the isochrone placement are represented versus t in Fig. 17. Considering the small sample of stars, the spread is consistent with the uncertainties of the ages of MS stars. The outlier in the upper left-hand side in Fig. 17 is WASP-2. It is in the pre-MS region of the CMD, but we do not have any activity index, which could allow us to discard the youngest isochrones.

As stated by Brown (2014) in his paper, isochrones tend to give ages older than gyrochronology. If, instead, we employ our determination of the SWP ages t through the isochrone placement technique, we find that isochrones can also give ages younger than gyrochronology as clarified by Fig. 18, where the gyrochronological ages $t_{\mathrm{BrownGyro}}$ obtained from the relation of Barnes (2010) are used. Considering the typical age uncertainties, the agreement with Brown's gyrochronological ages is very good with a lower dispersion if compared with the ages derived from YY models. It is likely that those stars, which turn out to be the oldest from the isochrone placement, do not have an accurate gyrochronological age considering that the age from the rotational velocity to age is very uncertain after some billion years.

4.3. Impact of the input parameters on the output ones

In this section we briefly discuss the sensitivity of the output parameters derived through the isochrone placement technique to the parameters assumed as input. We simulated the Sun, adopting the input parameters listed in the input column of Table 2. These are the same parameters as the isochrones we used to fit of the Sun. We attributed the typical uncertainties of the SWP catalogue stars to them, i.e. $\Delta \log g = 0.1$ dex, ΔL comes from the error propagation of $\Delta m_{\mathrm{bol}} = 0.03$ mag and $\bar{\Delta} d \sim 7\%$; we have $\Delta L \sim 17\%$, $\Delta R \sim 10\%$, and $\Delta M \sim 40\%$. The output parameters obtained according to the isochrones are shown in the output column of Table 2. They are consistent with the expected

[5] `http://exoplanets.eu`: The Extrasolar Planets Encyclopaedia.

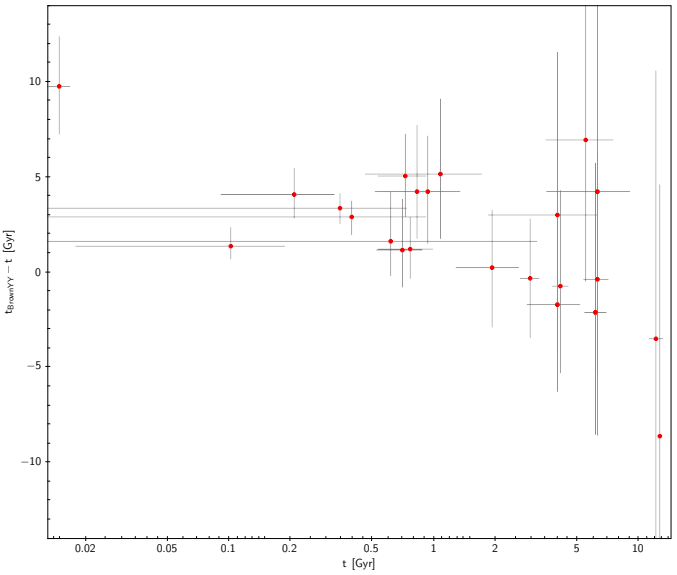

Fig. 17. $t_{\mathrm{BrownYY}} - t$ vs. t for the 24 SWP in common with Brown (2014).

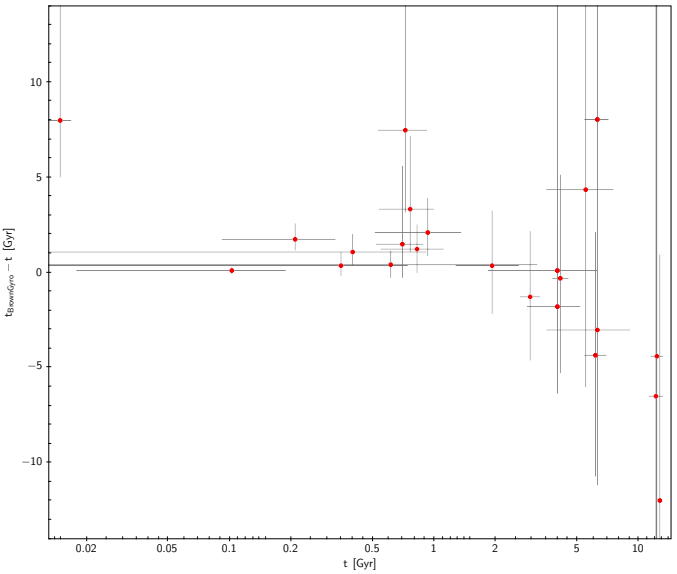

Fig. 18. $t_{\mathrm{BrownGyro}} - t$ vs. t for the 24 SWP in common with Brown (2014).

Table 2. *Sun* parameters

Parameters	Input	Output
[Fe/H]	0	
V	−26.739	
d [AU]	1 ± 7%	
$B - V$	0.667	
$\log g$ [cgs]	4.432 ± 0.1	4.432 ± 0.002
T_{eff} [K]	5778 ± 1%	5778 ± 3
L [$L_\odot$]	1.00 ± 0.17	1.0001 ± 0.0005
R [$R_\odot$]	1.00 ± 0.10	1.000 ± 0.001
M [$M_\odot$]	1.00 ± 0.44	1.003 ± 0.002
t [Gyr]		4.5 ± 0.1

solar parameters, and among them, the age is correct and characterized by very high precision.

To evaluate how changes in both the photometry and the spectroscopy propagate into the results, we perturbed the input V and $B-V$ of the Sun alternatively by ± 0.01 mag and $\log g$ by ± 0.01 dex. Table 3 presents what we obtained, also listing the percentual variations Δ_{oo} of the output data assuming as reference values the output values obtained without any perturbation of the input parameters.

Table 3 shows that a variation of only 0.01 mag in V or $B-V$ can lead to variations in the mean output values up to $\sim 40\%$ in the age and up to $\sim 2\%$ in the other parameters. This level of sensitivity for the derived age to the input photometry is understandable considering that we chose a MS star to perform these tests. In this region of the HRD, the isochrones are very close, so that even a small variation in magnitude and colours completely moves onto an isochrone that corresponds to a different age value. It is reasonable that if the star were in a different region of the HRD, where the isochrones are not so closed, the change in age induced by the perturbation of the input photometry would not be evident like this. Anyway, a very precise photometry is required in order to attribute the correct age to a star. On the other hand, even a slight perturbation in the input $\log g$ by only 0.01 dex induces a variation in the ages up to $\sim 7\%$, while the variations in the other parameters can be considered almost negligible.

A final observation concerns the uncertainties accompanying the age values reported in Table 3, which also turn out to be an order of magnitude greater than the uncertainty of the output age of the unperturbed Sun. This is because the perturbations trigger so-called artificial stars, and the big uncertainties reflect the difficulty of properly matching all the input parameters in the isochrone grids, where parameters referring to stars that are supposed to exist are tabulated. On the other hand, since the physics underlying the isochrones is well performed and the Sun does exist, entering with consistent input stellar properties gives high precision output.

5. Conclusions

In this paper we uniformly derived the ages of 317 planet-hosting stars. We checked the reliability and accuracy of two techniques (isochrone placement and Bayesian estimation) from a sample of 3.2 Gyr synthetic stars. We found that the isochrone placement technique produces the expected age value. Instead, the estimation of age through the Bayesian statistics (using an explicit probability density function) suffers the problem of primarily selecting the extreme age values available in the isochrones grid if we adopt the modal value of the pdf. It is worth emphasizing that this bias is present, although we used stars with well-defined ages. The mean or the median values of the pdf produce a bias towards the middle of the available age range and the age dispersion is large.

We found that $\sim 6\%$ of the stars with planets are younger than 0.5 Gyr: the reliability of this frequency will be subject to further investigations. The age distribution shows a peak in correspondence of the bin [1.5, 2) Gyr, then it decreases and $\sim 7\%$ of the stars are older than 11 Gyr. Approximately 60% of the stars in this sample are younger than 5 Gyr.

We found that a perturbation of the input V or $B-V$ by only 0.01 mag can lead to variations up to 40% in the estimated age of a MS Sun-like star. These are the typical uncertainties that characterize the stars in our sample. Instead, a perturbation in the input $\log g$ by 0.01 dex can lead to variations up to 7% in the estimated age. The final accuracy depends on the combination of the input errors. Important uncertainties and biases can also be produced by the adopted stellar models, in particular by treating the element diffusion. We found that one of the most important consequences of the element diffusion is the choice of the correct isochrone metallicity because the initially metallicity can be considerably higher than the metallicity of the stellar atmosphere after some billion years for solar-type stars. If this effect is ignored, the ages can be overestimated up to about 25%.

Finally, we confirmed the presence of some stars with planets located on the left-hand side of the solar main sequence (as also noted by Brown (2014)) and suggested further photometric observations to identify the source of the problem. Once the observational data is confirmed, we will investigate the nature using models that implement rotation. In fact, in the typical range of luminosities of MS stars with planets, MS isochrones that consider rotation are bluer than models that do not take rotation into account, as can be seen in Yang et al. (2013).

Acknowledgements. We thank the anonimous referee for the useful, thoughtful and deep comments that helped us in improving our paper. V. N. acknowledges partial support from INAF-OAPd through the grant "Analysis of HARPS-N data in the framework of GAPS project" (#19/2013) and "Studio preparatorio per le osservazioni della missione ESA/CHEOPS" (#42/2013). This research has made use of the Exoplanet Orbit Database and the Exoplanet Data Explorer at exoplanets.org.

References

Baraffe I., Chabrier G., Barman T. S., Selsis F., Allard F., Hauschildt P. H. 2005, A&A, 436, L47
Barker A.J. & Ogilvie G.I., 2009, MNRAS, 395, 2268-2287. doi:10.1111/j.1365-2966.2009.14694.x
Barnes S.A., 2010, ApJ, 722, 222
Barnes S.A., Kim Y.-C., 2010, ApJ, 721, 675
Bressan A., Marigo P., Girardi L., Salasnich B., Dal Cero C., Rubele S., Nanni A. 2012, MNRAS 427, 127-145
Broeg C., Fortier A., Ehrenreich D., Alibert Y., Baumjohann W., Benz W., Deleuil M., Gillon M., Ivanov A., Liseau R., Meyer M., Oloffson G., Pagano I., Piotto G., Pollacco D., Queloz D., Ragazzoni R., Renotte E., Steller M., Thomas N., the CHEOPS team 2013. arXiv:1305.2270v1
Brown D.J.A., 2014. arXiv:1406.4402v1
Burgers J.M., 1969, Flow equations for composite gases, Academic Press
Caffau E., Steffen M., Sbordone L., Ludwig H.G., Bonifacio P., 2007, A&A 473, L9
Chaboyer B., Fenton W.H., Nelan J.E., Patnaude D.J., Simon F.E. 2001, ApJ, 562:521-527
Chapman S., Cowling T.G., 1970, The mathematical theory of non-uniform gases, Cambridge University Press
da Silva L., Girardi L., Pasquini L., Setiawan J., von der Lühe O., de Medeiros J. R., Hatzes A., Döllinger M. P., Weiss A. 2006, A&A 458, 609-623. doi:10.1051/0004-6361:20065105
Demarque P., Woo J.-H., Kim Y.-C., Yi S.K., 2004, ApJS, 155, 667
Denissenkov P.A. 2010, ApJ, 719,28:44
Fortney J. J., Marley M. S., Barnes J. W. 2007, ApJ, 659,1661:1672. doi:10.1086/512120
Guenther D.B., Demarque P., Kim Y.C., Pinsonneault M.H., 1992, ApJ, 387, 372
Girardi L., Dalcanton J., Williams B., de Jong R., Gallart C., Monelli M., Groenewegen M.A.T., Holtzman J.A., Olsen K.A.G., Seth A.C., Weisz D.R., 2008, Publications of the Astronomical Society of the Pacific, 120:583-591
Haywood M., Di Matteo P., Lehnert M. D., Katz D., Gómez A., 2013, A&A 560, A109. doi:10.1051/0004-6361/201321397
Hubbard W. B., Hattori M. F., Burrows A., Hubeny I., Sudarsky D. 2007, Icarus, 187, 358
Hut P., 1980, A&A, 92, 167-170
Hut P., 1981, A&A, 99, 126-140
Jørgensen B. R., Lindegren L. 2005, A&A 436, 127-143. doi:10.1051/0004-6361:20042185
Kroupa P., Tout C.A., Gilmore G. 1993, MNRAS, 262, 545
Laughlin G. & Chambers J.E., 2001, ApJ, 551, L109-L113
Liu K., Bi S.L., Li T.D., Liu Z.E., Tian Z.J., Ge Z.S. arXiv:1406.4402v1
Mamajek E.E. & Hillenbrand L.A. 2008, ApJ, 687:1264-1293
Michaud G., Fontaine G., Baudet G., 1984, ApJ, 282, 206

Table 3. Output parameters after the perturbation of the *Sun*.

Sun	t [Gyr]	$T_{\rm eff}$ [K]	L [$L_\odot$]	R [$R_\odot$]	M [$M_\odot$]	$\log g$ [cgs]
Reference data	4.5 ± 0.1	5778	1.0001	1.000	1.003	4.432
$\Delta V = +0.01$	4.2 ± 0.9	5780	0.991	0.995	1.005	4.438
$\Delta_{\rm oo}$	-6.7%	$+0.03\%$	-0.9%	-0.5%	$+0.2\%$	$+0.1\%$
$\Delta V = -0.01$	4.5 ± 0.7	5783	1.008	1.002	1.004	4.431
$\Delta_{\rm oo}$	0%	$+0.09\%$	$+0.8\%$	$+0.2\%$	$+0.1\%$	-0.02%
$\Delta(B-V) = +0.01$	5.3 ± 1.2	5756	1.002	1.009	0.991	4.420
$\Delta_{\rm oo}$	$+17.8\%$	-0.4%	$+0.2\%$	$+0.9\%$	-1.2%	-0.3%
$\Delta(B-V) = -0.01$	2.7 ± 1.3	5819	0.995	0.983	1.028	4.458
$\Delta_{\rm oo}$	-40%	$+0.7\%$	-0.5%	-1.7%	$+2.5\%$	$+0.6\%$
$\Delta \log g = +0.01$	4.2 ± 0.9	5783	0.999	0.998	1.006	4.436
$\Delta_{\rm oo}$	-6.7%	$+0.09\%$	-0.1%	-0.2%	$+0.3\%$	$+0.09\%$
$\Delta \log g = -0.01$	4.3 ± 1.0	5781	1.000	0.999	1.005	4.434
$\Delta_{\rm oo}$	-4.4%	$+0.05\%$	-0.01%	-0.1%	$+0.2\%$	$+0.05\%$

Pätzold M., Carone L., Rauer H., 2004, A&A 427, 1075-1080

Pont F. & Eyer L. 2004, MNRAS, 351, 487

Poppenhaeger K., Wolk S.J. 2014, A&A 565, L1. doi:10.1051/0004-6361/201423454

Rouan D., Parviainen H., Moutou C., Deleuil M., Fridlund M., Ofir A., Havel M., Aigrain S., Alonso R., Auvergne M., et al., 2012, A&A 537, A54

Saffe C., Gómez M., Chavero C., 2005, A&A 443, 609-626. doi:10.1051/0004-6361:20053452

Seager S., Kuchner M., Hier-Majumder C. A., Militzer B. 2007, ApJ 669:1279-1297

Soderblom D. R., Annu. Rev. Astro. Astrophys., 2010.48:581-629

Sozzetti A., Torres G., Charbonneau D., Latham D.W., Holman M.J., Winn J.N., Laird J.B., O'Donovan F.T., 2007, ApJ, 664:1190-1198

Straniero O., Chieffi A., Salaris M. 1992, Mem. S.A.It. vol. 63, n. 2, pag. 315-320

Takeda G., Ford E.B., Sills A., Rasio F.A., Fischer D.A., Valenti J.A 2007, ApJ Supplement Series 168:297-318

Torres G. 2010, The Astronomical Journal, 140:1158-1162. doi:10.1088/0004-6256/140/5/1158

Winn J. N. 20 Mar 2011, arXiv:1001.2010v4

Wright J. T., Fakhouri O., Marcy G. W., Han E., Feng Y., Johnson J. A., Howard A. W., Fischer D. A., Valenti J. A., Anderson J., Piskunov N. 11 Feb 2011, arXiv:1012.5676v3

Wright J. T., Gaudi B. S. 11 Oct 2012, arXiv:1210.2471v2

Yang W., Bi S., Meng X., Liu Z., 2013, ApJ 776:112. doi:10.1088/0004-637X/776/2/112

Table 4. SWP parameters determined through Padova isochrones.

Star	t (Gyr)	Δt (Gyr)	$T_{\rm eff}$ (K)	$\Delta T_{\rm eff}$ (K)	L ($L_\odot$)	ΔL ($L_\odot$)	M ($M_\odot$)	ΔM ($M_\odot$)	$\log g$ (cm/s^2)	$\Delta \log g$ (cm/s^2)	R ($R_\odot$)	ΔR ($R_\odot$)
WASP-26	0.7	0.2	6245	7	1.603	0.001	1.15	0.005	4.422	0.004	1.084	0.003
HD 1502	2.5	0.1	5059	13	9.75	0.03	1.59	0.01	3.41	0.01	4.07	0.03
HD 2039	4.4	0.8	5935	64	2.18	0.02	1.2	0.03	4.22	0.03	1.4	0.04
HIP 2247	10.5	2.6	4692	9	0.212	0.001	0.72	0.01	4.6	0.01	0.7	0.01
HD 2638	1.9	2.6	5160	24	0.407	0.004	0.89	0.02	4.58	0.02	0.8	0.01
HAT-P-16	0.8	0.2	6326	12	2.125	0.002	1.25	0.01	4.36	0.01	1.22	0.01
HD 3651	4.6	2.9	5284	29	0.51	0.005	0.91	0.02	4.53	0.02	0.85	0.01
HD 4208	6.6	2.1	5717	33	0.71	0.004	0.86	0.02	4.5	0.03	0.86	0.01
HD 4308	1.6	4.0	5714	61	1.03	0.01	0.95	0.05	4.38	0.02	1.04	0.03
HD 4203	6.3	1.0	5666	43	1.68	0.01	1.12	0.03	4.22	0.03	1.35	0.03
HD 4313	2.0	0.1	5006	25	13.9	0.1	1.72	0.03	3.29	0.03	4.9	0.1
HD 4732	2.3	0.2	4994	32	14.8	0.2	1.61	0.05	3.22	0.03	5.1	0.1
HD 5319	3.6	0.4	4941	40	8.2	0.1	1.4	0.1	3.4	0.04	3.9	0.1
HD 5388	5.5	0.5	6195	78	4.43	0.02	1.11	0.03	3.98	0.04	1.8	0.1
HD 5891	1.5	0.1	4915	23	32.9	0.2	1.87	0.04	2.9	0.02	7.9	0.1
HD 6434	12.2	0.8	5907	71	1.208	0.004	0.83	0.03	4.31	0.01	1.029	0.004
HIP 5158	4.9	3.7	4592	11	0.185	0.001	0.74	0.01	4.63	0.02	0.68	0.01
HD 6718	6.0	2.4	5818	57	1.07	0.01	0.98	0.04	4.42	0.04	1.01	0.02
HD 7199	9.5	2.4	5349	38	0.7	0.01	0.93	0.02	4.42	0.03	0.98	0.02
HD 7449	2.4	1.5	6070	45	1.24	0.01	1.04	0.03	4.45	0.02	1.01	0.01
HD 7924	3.0	1.8	5216	13	0.364	0.001	0.81	0.01	4.6	0.01	0.74	0.01
HD 8535	2.1	0.9	6200	50	1.85	0.01	1.17	0.02	4.36	0.02	1.18	0.02
HD 8574	5.0	0.1	6065	6	2.335	0.001	1.144	0.003	4.21	0.03	1.39	0.01
HD 9446	2.0	1.5	5771	28	0.924	0.005	1.03	0.02	4.48	0.02	0.96	0.01
WASP-18	0.2	0.3	6188	10	1.442	0.002	1.14	0.01	4.45	0.01	1.047	0.004
HD 10180	3.9	1.1	5962	47	1.48	0.01	1.09	0.02	4.35	0.04	1.14	0.03
HD 10647	3.2	1.2	6128	41	1.57	0.01	1.08	0.03	4.39	0.03	1.1	0.02
HD 10697	7.1	0.1	5715	26	2.84	0.01	1.129	0.005	4.01	0.02	1.72	0.04
HD 11506	1.6	0.9	5833	28	1.17	0.01	1.12	0.02	4.43	0.02	1.06	0.01
HD 11977	1.2	0.4	5001	32	60.1	0.5	2.0	0.2	2.7	0.1	10.4	0.2
HAT-P-32	0.1	0.1	6594	6	2.251	0.001	1.221	0.004	4.395	0.003	1.152	0.002
HD 12661	1.8	0.5	5765	14	1.104	0.003	1.11	0.01	4.43	0.01	1.05	0.01
alpha Ari	3.4	1.9	4563	26	79.2	1.0	1.4	0.2	2.3	0.1	14.3	0.2
HAT-P-29	0.3	0.2	6137	7	1.6	0.001	1.2	0.01	4.412	0.004	1.121	0.003
HD 13931	6.8	0.6	5868	24	1.49	0.01	1.04	0.01	4.3	0.03	1.18	0.02
WASP-33	0.04	0.01	7268	3	5.23	0.005	1.539	0.001	4.298	0.001	1.445	0.002
HD 16175	3.2	0.2	6048	35	3.3	0.01	1.34	0.01	4.12	0.03	1.66	0.04
81 Cet	2.5	0.9	4825	41	60.0	0.8	1.6	0.2	2.5	0.1	11.1	0.3
HD 16760	1.3	0.9	5518	11	0.58	0.002	0.93	0.01	4.56	0.01	0.835	0.005
iota Hor	1.5	0.6	6148	31	1.68	0.01	1.17	0.01	4.38	0.02	1.14	0.01
HD 17156	4.1	0.4	5997	27	2.5	0.01	1.23	0.01	4.19	0.02	1.47	0.02
HD 18742	2.9	0.2	5009	22	11.9	0.1	1.48	0.03	3.28	0.02	4.6	0.1
WASP-11	8.7	3.5	4884	16	0.28	0.002	0.77	0.02	4.58	0.02	0.74	0.01
HIP 14810	8.7	2.0	5535	51	0.99	0.01	0.98	0.02	4.35	0.03	1.08	0.03
HAT-P-25	11.2	1.9	5099	18	0.478	0.003	0.86	0.01	4.47	0.02	0.89	0.01
HD 20794	11.2	1.8	5610	25	0.645	0.003	0.8	0.01	4.47	0.02	0.85	0.02
HD 20782	5.6	1.2	5878	35	1.22	0.01	1.01	0.02	4.38	0.03	1.07	0.02
HD 20868	8.4	3.7	4811	14	0.255	0.002	0.76	0.02	4.59	0.02	0.73	0.01
WASP-22	0.2	0.1	6105	3	1.2498	5.0E-4	1.101	0.004	4.472	0.002	1.001	0.001
epsilon Eri	1.4	1.7	5100	16	0.335	0.002	0.83	0.01	4.61	0.01	0.74	0.01
HD 23127	4.8	0.6	5843	52	3.01	0.03	1.26	0.04	4.06	0.02	1.71	0.03
HD 23079	5.1	1.0	6003	36	1.372	0.005	1.01	0.02	4.37	0.04	1.08	0.02
HD 22781	7.3	3.1	5170	18	0.322	0.002	0.74	0.02	4.6	0.02	0.71	0.01
HD 23596	5.0	0.7	5953	48	2.63	0.03	1.2	0.04	4.14	0.03	1.53	0.04
HD 24040	4.8	0.8	5917	52	1.81	0.01	1.14	0.02	4.27	0.02	1.28	0.03
HD 25171	4.9	0.8	6125	51	1.92	0.01	1.08	0.02	4.28	0.04	1.23	0.03
HD 27894	2.2	4.2	4898	55	0.37	0.01	0.89	0.03	4.52	0.03	0.85	0.03
XO-3	2.0	1.0	6634	11	7.04	0.01	1.41	0.03	3.97	0.03	2.01	0.01
HD 28254	7.9	0.2	5607	19	2.13	0.01	1.1	0.01	4.1	0.02	1.54	0.03
HD 28185	4.8	4.4	5609	41	1.18	0.01	1.0	0.1	4.33	0.03	1.15	0.03
epsilon Tau	0.7	0.1	4878	8	81.9	0.4	2.6	0.1	2.65	0.01	12.7	0.1
HD 28678	4.3	1.1	4828	46	21.3	0.3	1.3	0.1	2.9	0.1	6.6	0.2
HD 30177	4.8	1.5	5607	47	1.04	0.01	1.06	0.02	4.38	0.03	1.09	0.02
HD 30562	4.4	0.6	5983	37	2.82	0.01	1.25	0.03	4.14	0.02	1.57	0.03
HD 30856	4.7	0.9	4952	31	8.5	0.1	1.3	0.1	3.34	0.04	4.0	0.1
HD 33142	3.3	0.4	5005	41	9.0	0.1	1.4	0.1	3.39	0.03	4.0	0.1
HD 33283	3.6	0.6	5985	57	4.37	0.02	1.39	0.04	3.99	0.03	1.95	0.04
HD 32518	6.4	1.5	4599	41	46.4	0.9	1.2	0.1	2.4	0.1	10.8	0.3
HD 33636	2.5	1.1	5979	28	1.08	0.003	1.01	0.02	4.46	0.02	0.97	0.01
HD 290327	11.8	1.2	5525	20	0.747	0.004	0.86	0.01	4.41	0.01	0.95	0.02
HD 37124	11.8	1.2	5763	22	0.839	0.003	0.81	0.01	4.41	0.01	0.92	0.02
HD 39091	3.4	0.6	6013	18	1.532	0.004	1.11	0.01	4.35	0.01	1.15	0.01
HD 37605	1.8	1.0	5380	13	0.602	0.002	0.98	0.01	4.52	0.01	0.89	0.01
HD 38801	4.8	0.3	5338	59	3.7	0.1	1.28	0.02	3.83	0.02	2.3	0.1
HD 40307	7.0	4.2	4948	19	0.24	0.002	0.7	0.02	4.63	0.02	0.67	0.01
WASP-49	1.1	0.6	5809	11	0.73	0.002	0.94	0.01	4.55	0.01	0.845	0.004
HD 43197	3.1	2.0	5469	35	0.74	0.01	1.02	0.02	4.47	0.03	0.96	0.02
HD 43691	3.1	2.5	5920	34	2.24	0.02	1.21	0.04	4.19	0.02	1.44	0.03
HD 44219	9.6	0.7	5749	45	1.83	0.01	1.01	0.01	4.17	0.02	1.37	0.03
HD 45364	3.4	2.7	5540	31	0.562	0.004	0.88	0.02	4.55	0.03	0.82	0.01
CoRoT-19	0.7	0.7	6066	23	1.239	0.003	1.09	0.01	4.46	0.01	1.01	0.01
HD 45350	7.0	0.9	5683	39	1.43	0.01	1.06	0.02	4.27	0.03	1.24	0.02
HD 45652	6.0	2.9	5348	38	0.62	0.01	0.94	0.03	4.48	0.03	0.92	0.02

Table 4. continued.

Star	t (Gyr)	Δt (Gyr)	$T_{\rm eff}$ (K)	$\Delta T_{\rm eff}$ (K)	L ($L_\odot$)	ΔL ($L_\odot$)	M ($M_\odot$)	ΔM ($M_\odot$)	$\log g$ (cm/s^2)	$\Delta \log g$ (cm/s^2)	R ($R_\odot$)	ΔR ($R_\odot$)
6 Lyn	2.8	0.2	4994	15	14.9	0.1	1.46	0.02	3.17	0.03	5.2	0.1
CoRoT-18	0.03	0.34	5364	18	0.7	0.003	0.94	0.01	4.429	0.005	0.97	0.01
HD 47186	5.5	0.6	5736	21	1.219	0.005	1.05	0.01	4.35	0.01	1.12	0.01
7 CMa	4.6	0.7	4790	27	11.3	0.1	1.3	0.1	3.18	0.03	4.9	0.1
CoRoT-12	12.5	0.4	5370	7	0.753	0.001	0.894	0.004	4.38	0.02	1.0	0.02
CoRoT-7	6.9	2.7	5226	22	0.462	0.003	0.86	0.02	4.53	0.03	0.83	0.01
CoRoT-13	12.5	0.4	5605	52	1.45	0.01	0.95	0.02	4.2	0.01	1.26	0.01
HD 49674	1.8	1.2	5702	28	0.96	0.01	1.07	0.02	4.46	0.02	1.01	0.01
HD 50499	2.7	0.6	6102	54	2.25	0.02	1.25	0.01	4.27	0.03	1.35	0.03
CoRoT-14	0.03	0.13	5204	32	0.67	0.01	0.98	0.01	4.42	0.01	1.01	0.02
HD 50554	3.3	1.4	6036	52	1.37	0.01	1.06	0.03	4.4	0.04	1.07	0.03
HD 52265	2.6	0.6	6163	41	2.08	0.01	1.21	0.02	4.31	0.03	1.27	0.03
HAT-P-24	2.4	0.7	6487	47	2.54	0.01	1.18	0.02	4.3	0.03	1.26	0.02
HAT-P-9	0.8	0.8	6358	40	2.17	0.01	1.25	0.03	4.36	0.02	1.21	0.01
HAT-P-33	4.2	0.6	5843	110	5.4	0.7	1.3	0.1	3.9	0.1	2.1	0.3
HD 63454	2.7	3.3	4788	20	0.242	0.003	0.79	0.02	4.62	0.02	0.72	0.01
XO-5	12.1	0.9	5409	40	0.93	0.01	0.93	0.01	4.33	0.01	1.08	0.01
HD 63765	7.2	3.6	5483	42	0.58	0.01	0.85	0.03	4.51	0.04	0.84	0.02
XO-2	2.1	1.4	5412	21	0.671	0.004	1.01	0.02	4.5	0.02	0.93	0.01
HD 65216	1.7	0.5	5718	8	0.716	0.001	0.95	0.01	4.53	0.01	0.864	0.003
HD 66428	4.1	1.4	5773	55	1.28	0.01	1.09	0.02	4.37	0.03	1.13	0.03
HAT-P-30	0.8	0.2	6329	11	2.069	0.002	1.24	0.01	4.37	0.01	1.199	0.005
HD 68988	1.0	0.4	5919	11	1.297	0.002	1.16	0.01	4.42	0.01	1.08	0.01
HD 69830	11.2	1.7	5396	15	0.596	0.002	0.84	0.02	4.47	0.01	0.88	0.01
HD 70642	1.9	1.1	5732	23	0.917	0.004	1.04	0.02	4.47	0.02	0.97	0.01
HD 72659	7.0	0.7	5956	43	2.16	0.01	1.07	0.02	4.19	0.02	1.38	0.02
HD 73256	2.5	2.3	5532	36	0.74	0.01	1.01	0.03	4.49	0.03	0.94	0.02
HD 73526	7.9	0.3	5675	33	2.21	0.01	1.09	0.01	4.1	0.03	1.54	0.04
HD 73534	5.8	0.9	5006	44	3.41	0.04	1.22	0.05	3.71	0.03	2.5	0.1
HAT-P-13	6.2	0.8	5731	35	1.95	0.01	1.14	0.03	4.19	0.02	1.42	0.02
4 UMa	12.3	0.7	4554	59	37.0	1.1	0.94	0.03	2.45	0.01	9.4	0.03
HD 74156	4.3	0.6	6074	48	3.08	0.01	1.24	0.03	4.12	0.02	1.59	0.03
WASP-36	0.7	0.2	6333	7	1.4292	5.0E-4	1.061	0.004	4.461	0.004	0.995	0.002
HD 75898	4.0	0.4	5998	38	2.24	0.01	1.21	0.01	4.23	0.03	1.39	0.03
HD 76700	6.9	0.8	5694	44	1.69	0.01	1.1	0.02	4.22	0.03	1.34	0.03
WASP-13	12.59	0.01	5625	42	1.44	0.02	0.94	0.02	4.2072	1.0E-4	1.241	1.0E-4
HD 81040	5.5	1.8	5707	31	0.78	0.005	0.92	0.02	4.48	0.03	0.91	0.01
HD 81688	6.5	3.2	4847	55	54.5	1.0	1.1	0.2	2.4	0.1	10.5	0.3
HD 82943	1.3	0.5	6022	21	1.503	0.004	1.18	0.01	4.4	0.01	1.13	0.01
HD 82886	3.4	0.6	5105	45	11.9	0.1	1.3	0.1	3.26	0.04	4.4	0.1
HD 83443	3.3	1.6	5497	28	0.77	0.01	1.02	0.02	4.47	0.02	0.97	0.01
HD 85390	5.6	3.7	5186	26	0.389	0.004	0.82	0.02	4.57	0.03	0.77	0.01
HD 85512	8.2	3.3	4555	6	0.1339	5.0E-4	0.62	0.01	4.68	0.01	0.589	0.003
HD 86081	5.2	0.7	5905	40	2.43	0.01	1.19	0.03	4.16	0.03	1.5	0.03
HD 86264	1.4	0.1	6589	15	4.011	0.005	1.416	0.003	4.21	0.01	1.54	0.01
BD -08 2823	8.7	3.5	4721	12	0.211	0.001	0.72	0.01	4.61	0.02	0.69	0.01
HD 87883	9.1	3.5	4956	24	0.325	0.004	0.8	0.02	4.56	0.02	0.77	0.01
HD 88133	5.0	0.1	5466	28	3.7	0.1	1.28	0.01	3.87	0.02	2.1	0.1
HD 89307	6.3	0.3	5960	12	1.377	0.002	0.99	0.01	4.34	0.02	1.1	0.01
WASP-43	0.2	0.6	4371	8	0.104	0.001	0.63	0.01	4.73	0.01	0.563	0.004
HAT-P-22	12.2	0.9	5358	37	0.79	0.01	0.91	0.01	4.37	0.01	1.01	0.01
24 Sex	2.3	0.3	5048	44	13.6	0.1	1.6	0.1	3.27	0.03	4.8	0.1
HD 90156	5.9	1.5	5719	24	0.746	0.003	0.89	0.02	4.49	0.02	0.88	0.01
HD 92788	2.3	1.3	5838	47	1.25	0.01	1.12	0.02	4.4	0.03	1.1	0.02
HD 93083	5.4	4.7	5035	43	0.38	0.01	0.85	0.03	4.54	0.03	0.81	0.02
BD -10 3166	5.2	3.4	5257	40	0.56	0.01	0.94	0.03	4.5	0.03	0.9	0.02
HD 95089	2.3	0.2	5007	37	13.2	0.1	1.61	0.05	3.27	0.03	4.8	0.1
47 UMa	5.1	1.0	5951	48	1.61	0.01	1.08	0.02	4.31	0.04	1.19	0.03
WASP-34	12.2	0.8	5567	45	0.98	0.01	0.91	0.02	4.34	0.01	1.05	0.01
HD 96063	3.6	0.7	5103	47	11.0	0.1	1.3	0.1	3.29	0.04	4.3	0.1
HD 96167	5.1	0.3	5665	20	3.8	0.1	1.26	0.03	3.93	0.04	2.0	0.1
HD 96127	5.4	2.4	3955	35	503.4	20.7	1.2	0.2	1.1	0.1	48.1	1.8
HD 97658	3.8	2.6	5190	17	0.34	0.002	0.78	0.02	4.61	0.02	0.72	0.01
HD 98219	4.0	0.8	4960	46	9.6	0.2	1.3	0.1	3.31	0.05	4.2	0.1
HD 99109	4.1	2.7	5268	30	0.54	0.01	0.94	0.02	4.51	0.03	0.88	0.02
HD 99706	2.8	0.2	4904	16	13.1	0.1	1.53	0.03	3.21	0.02	5.03	0.05
HD 100655	0.9	0.2	4918	8	40.8	0.3	2.2	0.1	2.89	0.02	8.8	0.1
HD 100777	5.3	1.3	5590	29	0.92	0.01	1.01	0.02	4.41	0.02	1.02	0.01
HD 101930	5.4	4.4	5147	39	0.43	0.01	0.87	0.03	4.54	0.03	0.83	0.02
HIP 57274	8.4	3.7	4660	11	0.211	0.001	0.74	0.02	4.6	0.02	0.71	0.01
HD 102117	5.5	0.9	5740	41	1.38	0.01	1.08	0.02	4.32	0.02	1.19	0.02
HD 102195	5.5	3.5	5281	32	0.489	0.005	0.88	0.03	4.53	0.03	0.84	0.01
HD 102272	9.2	1.9	4778	37	21.9	0.3	1.0	0.1	2.77	0.05	6.8	0.2
HD 102329	2.0	0.3	4867	42	16.1	0.2	1.8	0.1	3.16	0.04	5.7	0.1
HD 102956	2.4	0.2	5016	50	9.9	0.1	1.62	0.04	3.4	0.04	4.2	0.1
HD 103197	2.5	2.0	5236	18	0.467	0.003	0.92	0.02	4.55	0.02	0.83	0.01
HD 104067	10.1	2.9	4974	14	0.311	0.002	0.77	0.01	4.56	0.02	0.75	0.01
HD 106252	7.2	1.0	5870	36	1.31	0.01	0.99	0.02	4.34	0.03	1.11	0.02
HD 106270	4.0	0.1	5498	32	5.2	0.1	1.35	0.02	3.76	0.03	2.5	0.1
HD 107148	4.3	1.2	5795	55	1.38	0.01	1.11	0.02	4.34	0.03	1.17	0.03
HD 108147	1.7	0.7	6229	39	1.9	0.01	1.19	0.02	4.36	0.02	1.18	0.02
HD 108863	2.2	0.2	4940	31	13.9	0.2	1.68	0.04	3.24	0.03	5.1	0.1
HD 108874	7.5	0.8	5630	24	1.066	0.005	1.0	0.01	4.36	0.03	1.09	0.02

Table 4. continued.

Star	t (Gyr)	Δt (Gyr)	$T_{\rm eff}$ (K)	$\Delta T_{\rm eff}$ (K)	L ($L_\odot$)	ΔL ($L_\odot$)	M ($M_\odot$)	ΔM ($M_\odot$)	$\log g$ (cm/s^2)	$\Delta \log g$ (cm/s^2)	R ($R_\odot$)	ΔR ($R_\odot$)
HD 109246	2.5	0.7	5890	21	1.155	0.004	1.07	0.01	4.43	0.02	1.03	0.01
HAT-P-36	11.3	1.2	5467	44	1.12	0.01	0.96	0.01	4.27	0.03	1.18	0.03
WASP-41	4.0	2.2	5564	28	0.642	0.004	0.91	0.02	4.52	0.03	0.86	0.01
HD 111232	11.7	1.4	5648	30	0.7	0.003	0.8	0.02	4.45	0.02	0.88	0.01
HD 114386	6.6	3.8	4913	18	0.286	0.003	0.78	0.02	4.59	0.02	0.74	0.01
HD 114783	9.8	3.0	5074	23	0.397	0.003	0.83	0.02	4.53	0.02	0.81	0.01
HD 116029	3.5	0.5	4906	40	9.7	0.1	1.4	0.1	3.34	0.03	4.3	0.1
70 Vir	8.0	0.1	5618	66	2.9	0.1	1.08	0.01	3.92	0.02	1.88	0.05
HD 117207	4.5	1.7	5732	53	1.16	0.01	1.06	0.03	4.38	0.03	1.09	0.03
HD 117618	5.0	0.8	5995	39	1.63	0.01	1.08	0.02	4.32	0.03	1.19	0.02
HAT-P-3	0.9	0.3	5221	5	0.455	0.001	0.931	0.004	4.567	0.003	0.824	0.002
HD 121504	1.7	0.9	6088	41	1.61	0.01	1.17	0.02	4.38	0.02	1.14	0.02
HAT-P-26	8.0	1.8	5093	11	0.359	0.001	0.8	0.01	4.56	0.01	0.771	0.005
HD 125595	10.0	3.0	4708	16	0.223	0.002	0.74	0.02	4.6	0.01	0.704	0.005
WASP-39	12.0	0.9	5470	11	0.68	0.01	0.85	0.01	4.43	0.01	0.92	0.02
WASP-14	1.5	0.6	6499	45	2.61	0.01	1.25	0.02	4.31	0.02	1.28	0.02
HD 128311	1.7	2.5	4917	17	0.296	0.003	0.84	0.01	4.6	0.02	0.75	0.01
HD 130322	4.6	3.3	5425	35	0.557	0.005	0.9	0.03	4.53	0.02	0.85	0.01
WASP-37	6.2	2.7	5879	51	0.84	0.01	0.87	0.03	4.48	0.04	0.89	0.02
HD 131496	4.5	0.4	4827	19	8.6	0.1	1.34	0.03	3.31	0.02	4.2	0.05
HD 131664	2.6	1.0	5921	42	1.47	0.01	1.15	0.02	4.37	0.03	1.15	0.02
HD 134987	4.7	0.7	5822	39	1.49	0.01	1.11	0.01	4.32	0.03	1.2	0.02
11 UMi	3.9	0.9	4140	16	243.4	3.6	1.4	0.1	1.61	0.04	30.4	0.5
HD 136118	5.3	0.6	6135	37	3.03	0.01	1.15	0.03	4.12	0.03	1.54	0.03
HD 136418	4.7	0.6	4987	29	6.9	0.1	1.26	0.05	3.44	0.03	3.5	0.1
HAT-P-4	6.1	0.7	5805	57	2.74	0.01	1.17	0.04	4.06	0.03	1.65	0.04
HD 137510	3.1	0.2	6032	44	4.33	0.01	1.41	0.01	4.02	0.02	1.91	0.03
HD 139357	7.0	2.0	4457	41	73.5	1.7	1.1	0.1	2.2	0.1	14.4	0.4
HD 137388	7.4	3.9	5182	35	0.47	0.01	0.88	0.03	4.51	0.03	0.85	0.02
HD 330075	0.1	0.5	4977	45	0.46	0.01	0.91	0.02	4.47	0.02	0.91	0.03
HD 141937	1.2	0.7	5891	18	1.108	0.003	1.09	0.01	4.46	0.01	1.01	0.01
HD 142245	3.3	0.4	4858	34	11.4	0.1	1.5	0.1	3.24	0.03	4.8	0.1
HD 142415	1.5	0.9	5918	24	1.153	0.005	1.09	0.02	4.45	0.02	1.02	0.01
rho CrB	9.1	1.0	5911	54	1.76	0.01	0.97	0.02	4.21	0.05	1.27	0.04
XO-1	2.2	1.4	5742	27	0.849	0.004	1.0	0.02	4.49	0.02	0.93	0.01
HD 145457	2.6	0.4	4785	37	40.5	0.5	1.5	0.1	2.67	0.04	9.3	0.2
14 Her	3.6	2.0	5349	29	0.64	0.01	0.98	0.02	4.48	0.02	0.93	0.01
HD 145377	2.6	1.3	5987	50	1.42	0.01	1.12	0.03	4.39	0.03	1.11	0.02
WASP-38	0.4	0.5	6321	22	1.624	0.003	1.14	0.02	4.43	0.01	1.06	0.01
HAT-P-2	0.8	0.2	6671	23	3.42	0.01	1.37	0.01	4.28	0.01	1.39	0.01
HD 147018	7.4	1.8	5528	31	0.78	0.01	0.94	0.02	4.43	0.04	0.97	0.02
HD 148156	1.0	0.4	6150	20	1.822	0.004	1.23	0.01	4.37	0.01	1.19	0.01
HD 148427	3.55	0.04	5029	15	6.05	0.03	1.43	0.01	3.56	0.01	3.25	0.03
HD 149026	2.9	0.3	6110	50	2.78	0.02	1.301	0.005	4.2	0.02	1.49	0.03
HD 150706	0.3	0.3	5958	8	1.043	0.001	1.07	0.01	4.49	0.01	0.96	0.003
HD 149143	7.1	0.3	5745	31	2.28	0.01	1.12	0.01	4.11	0.03	1.53	0.04
HD 152581	8.6	2.1	4995	44	13.5	0.2	1.0	0.1	3.0	0.1	4.9	0.1
HD 154345	3.1	0.4	5558	5	0.609	0.001	0.907	0.004	4.54	0.01	0.843	0.002
HD 153950	4.5	0.6	6111	53	2.24	0.01	1.15	0.01	4.24	0.04	1.34	0.03
HD 155358	0.3	2.0	5933	49	2.1	0.01	1.11	0.05	4.2	0.02	1.37	0.03
HD 154672	7.0	0.6	5754	37	1.85	0.01	1.1	0.01	4.2	0.03	1.37	0.03
HD 154857	5.6	0.2	5729	36	4.5	0.1	1.14	0.01	3.81	0.01	2.17	0.04
HD 156279	7.4	1.9	5453	30	0.71	0.01	0.93	0.02	4.45	0.03	0.95	0.01
HD 156668	8.8	3.5	4859	15	0.278	0.002	0.78	0.02	4.58	0.02	0.75	0.01
HD 156411	4.4	0.2	5921	64	5.4	0.1	1.23	0.02	3.84	0.02	2.2	0.1
HAT-P-14	0.7	0.4	6684	43	3.41	0.01	1.37	0.02	4.29	0.02	1.38	0.02
HD 158038	3.7	0.5	4837	38	10.2	0.1	1.4	0.1	3.27	0.04	4.6	0.1
HD 159868	6.1	0.4	5593	54	3.8	0.1	1.16	0.02	3.87	0.02	2.1	0.1
mu Ara	5.7	0.6	5815	40	1.81	0.01	1.13	0.02	4.24	0.03	1.33	0.02
HD 162020	1.7	1.5	4756	7	0.23	0.001	0.79	0.01	4.63	0.01	0.708	0.004
TrES-3	1.8	1.5	5613	18	0.581	0.003	0.89	0.01	4.57	0.01	0.81	0.01
TrES-4	2.8	0.1	6308	24	4.39	0.01	1.374	0.001	4.08	0.02	1.76	0.04
HD 163607	8.91	0.01	5541	2	2.316	0.001	1.0719	2.0E-4	4.024	0.002	1.65	0.01
HD 164509	1.5	0.2	5865	7	1.15	0.001	1.103	0.004	4.44	0.01	1.041	0.003
HD 164922	5.2	2.3	5467	34	0.69	0.01	0.95	0.02	4.48	0.03	0.93	0.02
HAT-P-31	0.6	0.1	6380	5	2.2391	4.0E-4	1.269	0.003	4.357	0.002	1.227	0.002
HAT-P-5	11.5	1.0	5005	20	2.0	0.1	1.02	0.03	3.88	0.04	1.9	0.1
HD 168443	10.8	0.6	5585	83	2.082	0.003	1.0	0.01	4.05	0.04	1.5	0.1
HD 168746	11.2	1.4	5661	37	1.05	0.01	0.91	0.02	4.33	0.02	1.07	0.02
42 Dra	9.0	2.1	4384	31	146.6	2.7	1.0	0.1	1.8	0.1	20.9	0.6
HD 169830	2.82	0.03	6300	23	4.703	0.005	1.39	0.01	4.06	0.01	1.81	0.02
HD 170469	8.6	0.5	4990	28	2.5	0.1	1.11	0.02	3.84	0.03	2.1	0.1
HD 171028	6.1	0.5	5787	81	4.9	0.2	1.06	0.03	3.76	0.03	2.3	0.1
CoRoT-16	12.1	1.0	5021	16	0.395	0.002	0.82	0.01	4.51	0.01	0.826	0.003
HD 171238	2.5	1.6	5596	26	0.762	0.004	1.0	0.02	4.5	0.02	0.93	0.01
CoRoT-23	0.0033	5.0E-4	3704	32	0.201	0.003	0.4	0.02	3.96	0.04	1.09	0.03
CoRoT-11	1.5	4.0	4994	39	2.42	0.04	1.5	0.2	4.0	0.1	2.07	0.05
CoRoT-9	12.1	1.0	5380	40	0.64	0.01	0.86	0.02	4.44	0.01	0.909	0.005
HD 173416	1.5	0.6	4777	21	80.5	0.5	1.8	0.1	2.46	0.04	13.1	0.2
HD 175541	2.51	0.03	5162	17	9.55	0.02	1.54	0.02	3.44	0.01	3.85	0.04
TrES-1	1.5	1.1	5281	10	0.434	0.002	0.88	0.01	4.58	0.01	0.789	0.005
HD 177830	5.3	0.9	4789	48	5.2	0.1	1.3	0.1	3.51	0.05	3.3	0.1
TrES-2	5.1	0.8	5891	19	1.053	0.003	0.96	0.01	4.43	0.01	0.99	0.01

Table 4. continued.

Star	t (Gyr)	Δt (Gyr)	$T_{\rm eff}$ (K)	$\Delta T_{\rm eff}$ (K)	L ($L_\odot$)	ΔL ($L_\odot$)	M ($M_\odot$)	ΔM ($M_\odot$)	$\log g$ (cm/s^2)	$\Delta \log g$ (cm/s^2)	R ($R_\odot$)	ΔR ($R_\odot$)
Kepler-21	3.55	0.03	6203	5	5.281	0.001	1.311	0.003	3.95	0.05	1.99	0.04
Kepler-20	12.5	0.3	5432	42	0.74	0.01	0.88	0.02	4.403	0.004	0.958	0.002
HD 179079	7.3	0.4	5678	72	2.43	0.01	1.12	0.01	4.07	0.03	1.6	0.1
HD 180314	0.9	0.6	4977	31	39.8	0.7	2.3	0.1	2.94	0.04	8.5	0.2
HD 179949	1.9	0.3	6215	15	1.954	0.003	1.2	0.01	4.35	0.01	1.21	0.01
HD 180902	3.0	0.2	5026	27	9.3	0.1	1.49	0.03	3.39	0.02	4.0	0.1
HD 181342	3.6	0.5	4992	49	8.4	0.1	1.4	0.1	3.4	0.04	3.9	0.1
HD 181720	12.6	0.2	5888	108	1.91	0.02	0.86	0.02	4.134	0.002	1.29	0.003
HD 181433	8.6	3.6	4912	25	0.34	0.005	0.83	0.02	4.54	0.02	0.8	0.01
CoRoT-3	1.2	2.8	5066	51	3.3	0.1	1.6	0.2	3.9	0.1	2.4	0.1
HD 183263	4.8	0.8	5874	59	1.81	0.02	1.15	0.02	4.26	0.03	1.3	0.04
HAT-P-7	1.5	0.2	6659	49	5.24	0.01	1.49	0.01	4.13	0.02	1.72	0.03
HD 231701	3.5	0.2	5873	63	7.3	0.1	1.41	0.03	3.75	0.03	2.6	0.1
HD 187123	5.6	0.9	5855	40	1.45	0.01	1.06	0.02	4.32	0.02	1.17	0.02
Kepler-40	0.04	0.02	7744	8	7.25	0.01	1.656	0.002	4.298	0.002	1.499	0.004
HD 187085	3.6	0.3	6117	27	2.06	0.01	1.17	0.01	4.28	0.02	1.28	0.02
HAT-P-11	1.6	1.5	4747	9	0.242	0.001	0.82	0.01	4.62	0.01	0.729	0.004
Kepler-17	0.6	2.5	5407	53	1.78	0.02	1.4	0.1	4.2	0.03	1.53	0.04
xi Aql	2.4	0.7	4796	17	45.1	0.3	1.5	0.1	2.64	0.03	9.7	0.1
HD 189733	6.2	3.4	5038	21	0.327	0.003	0.8	0.02	4.58	0.02	0.75	0.01
HD 190228	5.0	0.5	5352	30	4.4	0.2	1.18	0.04	3.73	0.02	2.4	0.1
HD 190647	8.3	0.5	5656	60	2.19	0.02	1.08	0.01	4.09	0.03	1.54	0.04
HAT-P-34	0.8	0.3	6778	32	4.46	0.01	1.47	0.03	4.23	0.01	1.54	0.02
Qatar-1	8.9	3.7	4757	16	0.256	0.002	0.78	0.02	4.58	0.02	0.74	0.01
HD 192263	1.8	0.8	4965	7	0.299	0.001	0.821	0.005	4.61	0.01	0.74	0.003
GJ 785	1.0	0.6	5179	11	0.396	0.003	0.88	0.005	4.589	0.004	0.782	0.002
HD 192310	10.0	2.5	5136	17	0.398	0.003	0.81	0.02	4.53	0.02	0.8	0.01
HD 192699	2.5	0.1	5136	15	11.12	0.03	1.5	0.01	3.36	0.01	4.22	0.03
TrES-5	9.2	1.8	5087	14	0.42	0.002	0.85	0.01	4.51	0.01	0.84	0.01
HAT-P-23	12.6	0.2	4830	5	2.829	0.005	0.987	0.005	3.663	0.005	2.41	0.01
WASP-2	0.015	0.002	4747	46	0.56	0.01	1.05	0.02	4.36	0.02	1.11	0.04
HD 197037	0.3	0.3	6357	15	1.561	0.002	1.11	0.01	4.45	0.004	1.034	0.004
WASP-7	0.2	0.2	6562	13	2.434	0.002	1.27	0.01	4.37	0.01	1.21	0.01
18 Del	1.1	0.1	5005	35	35.7	0.3	2.0	0.1	2.94	0.03	8.0	0.2
HD 200964	2.7	0.3	5105	42	11.3	0.1	1.47	0.05	3.33	0.03	4.3	0.1
BD +14 4559	9.0	3.4	4980	19	0.339	0.003	0.81	0.02	4.55	0.02	0.78	0.01
HD 202206	1.1	0.6	5745	17	1.024	0.003	1.1	0.01	4.45	0.01	1.02	0.01
HD 204313	5.5	0.8	5761	26	1.22	0.01	1.04	0.01	4.36	0.02	1.11	0.01
HD 204941	5.2	3.9	5079	23	0.304	0.002	0.76	0.02	4.61	0.02	0.72	0.01
HD 205739	2.8	0.2	6276	41	3.52	0.01	1.329	0.003	4.15	0.02	1.59	0.04
HAT-P-17	6.9	1.9	5273	11	0.465	0.002	0.85	0.02	4.54	0.02	0.82	0.01
HD 206610	2.1	0.3	4907	36	18.1	0.2	1.7	0.1	3.12	0.03	5.9	0.1
HD 208487	3.1	0.6	6119	32	1.78	0.01	1.14	0.01	4.34	0.03	1.19	0.02
HD 209458	4.0	1.2	6084	63	1.77	0.01	1.11	0.02	4.3	0.1	1.2	0.04
HD 210277	7.9	2.0	5566	50	0.99	0.01	0.98	0.02	4.37	0.04	1.07	0.03
HD 210702	2.1	0.1	5027	32	12.8	0.1	1.69	0.03	3.31	0.02	4.7	0.1
HD 212771	3.0	0.4	5064	45	13.5	0.1	1.4	0.1	3.22	0.04	4.8	0.1
HD 215497	10.1	2.8	5082	24	0.43	0.004	0.85	0.02	4.5	0.02	0.85	0.01
HAT-P-8	0.3	0.4	6697	38	3.05	0.01	1.33	0.02	4.33	0.01	1.3	0.02
tau Gru	4.2	0.6	5996	56	3.39	0.02	1.28	0.04	4.07	0.03	1.71	0.04
HD 216437	5.2	0.6	5909	31	2.28	0.01	1.17	0.03	4.18	0.04	1.44	0.03
HD 216770	4.5	2.3	5413	33	0.65	0.01	0.96	0.02	4.49	0.03	0.92	0.02
51 Peg	3.3	1.2	5882	48	1.35	0.01	1.1	0.02	4.38	0.03	1.12	0.03
HAT-P-1	1.9	0.6	6029	24	1.473	0.005	1.14	0.02	4.39	0.01	1.12	0.01
HD 217107	3.1	1.5	5717	50	1.14	0.01	1.1	0.02	4.4	0.03	1.09	0.02
HD 217786	6.5	0.8	6027	42	1.73	0.01	1.02	0.01	4.28	0.03	1.21	0.02
WASP-21	5.5	2.0	6074	58	1.17	0.01	0.93	0.03	4.42	0.04	0.98	0.02
HD 240210	10.9	1.8	4833	28	11.9	0.1	1.0	0.1	3.05	0.04	4.9	0.1
HD 219828	5.0	0.7	5938	42	2.64	0.01	1.2	0.04	4.14	0.04	1.54	0.04
HD 220773	6.3	0.1	5852	14	3.32	0.01	1.156	0.002	4.0	0.01	1.78	0.01
14 And	3.2	2.1	4783	39	56.1	0.8	1.4	0.2	2.5	0.1	10.9	0.3
HD 221287	0.8	0.5	6307	22	1.859	0.005	1.19	0.01	4.39	0.01	1.14	0.01
WASP-4	0.9	0.4	5758	7	0.8	0.002	1.0	0.01	4.52	0.01	0.901	0.004
HD 222155	7.9	0.1	5834	17	2.94	0.04	1.05	0.01	4.0	0.01	1.7	0.1
HAT-P-6	6.3	0.2	5720	54	3.9	0.1	1.13	0.02	3.85	0.03	2.1	0.1
kappa And	0.2	0.2	10942	19	72.8	0.3	2.45	0.01	4.067	0.003	2.38	0.01
WASP-5	0.8	0.3	5819	6	0.95	0.002	1.055	0.004	4.489	0.004	0.961	0.003
HD 224693	3.7	0.5	5960	70	4.06	0.03	1.37	0.03	4.01	0.03	1.9	0.1

Astronomy & Astrophysics manuscript no. AAtransitsCitet
November 12, 2015

Age consistency between exoplanet hosts and field stars

A. Bonfanti[1,2], S. Ortolani[1,2], and V. Nascimbeni[2]

[1] Dipartimento di Fisica e Astronomia, Università degli Studi di Padova, Vicolo dell'Osservatorio 3, I-35122 Padova, Italy
[2] Osservatorio Astronomico di Padova, INAF, Vicolo dell'Osservatorio 5, I-35122 Padova, Italy

ABSTRACT

Context. Transiting planets around stars are discovered mostly through photometric surveys. Unlike radial velocity surveys, photometric surveys do not tend to target slow rotators, inactive or metal-rich stars. Nevertheless, we suspect that observational biases could also impact transiting-planet hosts.
Aims. This paper aims to evaluate how selection effects reflect on the evolutionary stage of both a limited sample of transiting-planet host stars (TPH) and a wider sample of planet-hosting stars detected through radial velocity analysis. Then, thanks to uniform derivation of stellar ages, a homogeneous comparison between exoplanet hosts and field star age distributions is developed.
Methods. Stellar parameters have been computed through our custom-developed isochrone placement algorithm, according to Padova evolutionary models. The notable aspects of our algorithm include the treatment of element diffusion, activity checks in terms of $\log R'_{HK}$ and $v \sin i$, and the evaluation of the stellar evolutionary speed in the Hertzsprung-Russel diagram in order to better constrain age. Working with TPH, the observational stellar mean density $\rho_\star$ allows us to compute stellar luminosity even if the distance is not available, by combining $\rho_\star$ with the spectroscopic $\log g$.
Results. The median value of the TPH ages is $\sim$ 5 Gyr. Even if this sample is not very large, however the result is very similar to what we found for the sample of spectroscopic hosts, whose modal and median values are [3, 3.5) Gyr and $\sim$ 4.8 Gyr, respectively. Thus, these stellar samples suffer almost the same selection effects. An analysis of MS stars of the solar neighbourhood belonging to the same spectral types bring to an age distribution similar to the previous ones and centered around solar age value. Therefore, the age of our Sun is consistent with the age distribution of solar neighbourhood stars with spectral types from late F to early K, regardless of whether they harbour planets or not. We considered the possibility that our selected samples are older than the average disc population.

Key words. stars: fundamental parameters, stars: evolution, (stars:) Herztsprung-Russell and C-M diagrams, stars:planetary systems

1. Introduction

Computing ages of field stars is very challenging because the age is not a direct observable. Thanks to models, information about the age comes from the composition and evolutionary state of the core of a star, while we are mostly limited to observing the properties at the surface. Several techniques can be applied.

Using the stellar effective temperature $T_{\rm eff}$ and luminosity L as input values, age can be computed through interpolation in the grids of isochrones (isochrone placement). Instead, gyrochronology (see e.g. Barnes & Kim 2010) is an empirical technique that allows the determination of stellar ages considering that the rotational speed of stars declines with time because of magnetic braking. Asteroseismology (see Handler 2013 for a review) is a very promising technique because the individual oscillation frequencies are directly linked to the inner density profile and the sound propagation speed in the stellar core. These frequencies are recovered through detailed analyses and high-precision photometry, which facilitates the determination of very precise, though model-dependent, ages. If it is not possible to investigate each oscillation mode, asteroseismic studies simply give global parameters i.e. the large frequency separation $\Delta\nu$ and the frequency of maximum power $\nu_{\rm max}$, which are linked to the stellar mean density $\rho_\star$ and surface gravity $\log g$ (see e.g. Kjeldsen & Bedding 1995). In this case, asteroseismology loses part of its strength. Input $T_{\rm eff}$, $\rho_\star$ and $\log g$ again require isochrones to compute ages as in Chaplin et al. (2014), however, asteroseismic $\log g$ is known with better precision if compared with the spectroscopic value, for instance. For a broad review about different age computation methods, see Soderblom (2010).

Since $T_{\rm eff}$ and L can be usually recovered for many stars, in this paper we compute the ages of transiting-planet host stars (TPH) in a homogeneous way via isochrones. Knowledge of stellar ages is particularly important in the context of planet-hosting stars (SWP). The age distribution of SWP tells us whether planets are preferentially hosted by young or old stars. This is related to the dynamical stability of the systems and with the mutual influence between planets and hosting star; see e.g. Pätzold et al. (2004), Barker & Ogilvie (2009), Debes & Jackson (2010). Moreover, ages for exoplanet host stars enable a comparison with typical timescales of biological evolution and an assessment of the plausibility of the presence of life (see e.g. Kasting & Catling 2003).

The paper is organised in the following way: §2 describes the characteristics of our stellar sample and the isochrones. §3 presents the central aspects of our algorithm, §4 shows the results, and §5 summarizes our work.

2. The data

2.1. Planet-hosting stars catalogues

We analysed the ages of those stars whose planets were discovered through the transit method. In principle, these kinds of stars should not suffer from biases: (1) The stars that are chosen are not necessarily inactive, unlike in radial velocity surveys,

where spectroscopic analysis requires sharp and well-defined lines. However, we caution that it is indeed more difficult to detect transits for stars with a large amplitude of intrinsic variability. (2) These TPH stars are not necessarily slow rotators, unlike in radial velocity surveys. In fact, rotation broadens the lines and reduces their depth, making spectroscopic analysis less precise, however, once a possible transit signal is detected, spectroscopic validation is required to confirm such a planet. Therefore, stars belonging to photometric surveys must also be suitable for spectroscopic analyses if exoplanet validation is expected, so almost the same biases are expected. In fact, in the case of transiting planet hosts, there are other systematic selection effects. Transiting-planet hosts are expected to be preferentially edge-on, even if spin-orbit misalignment occurs in some exoplanetary systems. Gravity darkening or differential rotation (von Zeipel 1924, Maeder 1999) could affect stellar observables. In addition, the hosted planets are very close to their own star.

We selected 61 transiting-planet hosts from SWEET-Cat, a catalogue of stellar parameters for stars with planets[1] (Santos et al. 2013), to obtain our transiting-planet hosts (TPH) catalogue. Among the stars of this catalogue, we further consider only those stars brighter than $V = 12$ and this inevitably introduces a further source of bias. This criterion takes into account that future photometric missions with the aim of characterizing exoplanets, such as CHEOPS (Broeg et al. 2013) or PLATO (Rauer et al. 2014), will investigate bright stars. This led us to the Bright Transiting-Planet Hosts (BTPH) catalogue, which is composed of 43 stars. The metallicity [Fe/H] and the logarithm of the surface gravity $\log g$ are always available from Sweet-Cat. If available, we took V magnitude and $B - V$ colour index from Maxted et al. (2011), otherwise we collected V from SWEET-Cat and $B-V$ from The Site of California and Carnegie Program for Extrasolar Planet Search: Exoplanets Data Explorer.[2] As reported by Maxted et al. (2011), the target stars of surveys that aim to discover exoplanets through transits are typically characterized by optical photometry of poor quality in the range V=8.5-13 mag. For stars brighter than $V \approx 12$, optical photometry is usually available from Tycho catalogue, nevertheless, this catalogue is only complete up to $V \approx 11$ and photometric accuracy rapidly deteriorates for $V \gtrsim 9.5$. The authors give high-quality photoelectric optical photometry for planet-hosting stars (mostly WASP discoveries), so we decided to use these data if available.

We also built a catalogue of 274 planet-hosting stars whose planets were detected through radial velocity method (Spectroscopic hosts: SH catalogue) from SWEET-Cat.

2.2. Solar neighbourhood catalogues

We built a catalogue of F-G-K main sequence stars (MS-stars) belonging to the solar neighbourhood (SN catalogue) by taking stellar data from the re-analysis of the Geneva-Copenhagen survey by Casagrande et al. (2011). It is a survey of late-type dwarf stars that are magnitude limited at $V \approx 8.3$; the authors computed the ages for these stars. In particular, we collected the 7044 stars with available ages, belonging to the MS. The MS containing the F-G-K stars has been indentified by selecting a strip going from $T_{\rm eff} \approx 4500$ K to $T_{\rm eff} \approx 7100$ K, within a range of 0.45 dex in $\log L$, whose minimum and maximum values are -1.24 dex and 0.63 dex, respectively. We further removed F type stars, i.e stars with $T_{\rm eff} > 6300$ K, from the SN catalogue. This way we remained with 3713 stars (Reduced Solar Neighbourhood catalogue; RSN) belonging to the same spectral type range of planet-hosting stars. Among useful input parameters to compute stellar ages through our own algorithm, Casagrande et al. (2011) give only metallicity, which is inferred from Strömgren photometry; distance, according to the new reduction of the *Hipparcos* parallaxes (van Leeuwen 2007); and V magnitude for each star. We complemented this information by cross-matching the entire Geneva-Copenhagen survey with the catalogue of cool late-type stars by Valenti & Fischer (2005), which also provides precise spectroscopic measurements of surface gravity $\log g$ and projected rotational velocity $v \sin i$. This led to the Valenti Fischer Solar Neighbourhood catalogue (VF-SN catalogue), which contains 825 stars.

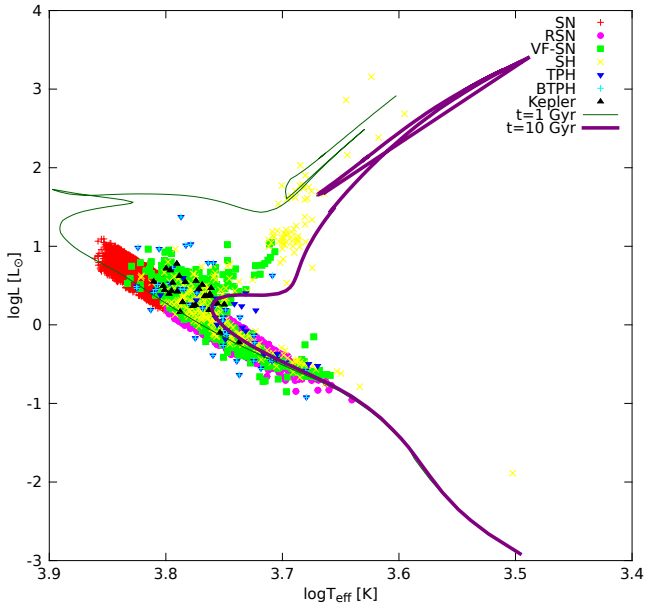

Fig. 1. Stars belonging to our custom-built catalogues are represented on the HRD. Two solar metallicity isochrones, corresponding to 1 Gyr and 10 Gyr, are shown as reference. Since BTPH is a subsample extracted from TPH, all the cyan crosses representng the BTPH stars are superimposed on part of the blue reverse triangles representing the TPH stars.

A brief overview of our custom-built catalogues used in the paper is given in Table 1. In Fig. 1 stars, belonging to our catalogues are represented on the HRD with two solar metallicity isochrones as reference.

2.3. Isochrones

To compute the ages of stars we used isochrones taken from Padova and Trieste Stellar Evolutionary Code (PARSEC, version 1.0)[3] by Bressan et al. (2012). We queried isochrones identified by $\log t$ in the range between 6 and 10.1 (t in years) at steps of 0.05 dex. These isochrones include the pre-MS phase, so the given ages must be considered as starting from the birth of a star and not since the zero age main sequence (ZAMS). Specific details about the solar parameters adopted by the isochrones are already reported by Bonfanti et al. (2015). Here, we recall the relation between metallicity Z and [Fe/H], i.e.

$$Z = 10^{[\mathrm{Fe/H}]-1.817} \quad (1)$$

[1] https://www.astro.up.pt/resources/sweet-cat/
[2] http://exoplanets.org/table
[3] http://stev.oapd.inaf.it/cgi-bin/cmd

Table 1. Overview of our custom-built catalogues

Catalogue	# stars	log g source	Reference	
TPH: Transiting planet hosts	61	spectroscopy	SWEET-Cat	
BTPH: Bright transiting planet hosts	43	spectroscopy	SWEET-Cat	
SH: Spectroscopic hosts	274	spectroscopy	SWEET-Cat	
SN: Solar neighbourhood	7044	not available	Casagrande et al. (2011)	[(a)] see §4.1
RSN: Reduced solar neighbourhood	3713	not available	Casagrande et al. (2011)	
VF-SN: Valenti Fischer solar neighbourhood	825	spectroscopy	Casagrande et al. (2011) + Valenti & Fischer (2005)	
Kepler sample[a]	29	asteroseismology	Silva Aguirre et al. (2015)	

3. Age determination methods

Computing the age of a field star through isochrones requires us to put the star on a suitable plane with its error bars. Traditionally, HRD is chosen, so $T_{\rm eff}$ and L are the reference quantities. Several catalogues in the literature already report $T_{\rm eff}$ or L, but they were obtained by different authors through different processes and/or calibration techniques. For instance, $T_{\rm eff}$ and L are not likely to be consistent with the colour-temperature scale or the bolometric corrections (BCs) adopted by the isochrones. Therefore, we prefer to start from quantities coming from observations in a straightforward way, where possible. Our reference input quantities to compute stellar ages are V magnitude, $B-V$ colour index, [Fe/H] metallicity, spectroscopic $\log g$, and parallactic distance d, which can be substituted by the $\frac{a}{R_\star^3}$ parameter coming from transit, as better specified in § 3.1.

3.1. Isochrone placement: Preliminary considerations

Starting from observational quantities, $T_{\rm eff}$ can be inferred from colour index (e.g. $B-V$), while L is determined thanks to the magnitude in a given band (say V), its corresponding bolometric correction BC_V and the distance d of the star recovered from parallax π. In the particular case where a star hosts a transiting planet, we are able to compute L, even if d is not available. In fact, the ratio between the orbital period P and the transit duration allows us to recover $a/R_\star$, where a is the planet semimajor axis and $R_\star$ is the stellar radius (see e.g. Winn (2010)). Rearranging Kepler III law in the manner shown by Sozzetti et al. (2007), the mean stellar density results to be

$$\rho_\star = \frac{3\pi}{G}\left(\frac{a}{R_\star}\right)^3 \frac{1}{P^2} \tag{2}$$

where G is the universal gravitational constant. Combining the spectroscopic $\log g$ with $\rho_\star$, one can solve a system of two equations in the two variables $R_\star$ and $M_\star$. One obtains

$$\begin{cases} \frac{R_\star}{R_\odot} = \frac{g}{g_\odot}\left(\frac{\rho_\star}{\rho_\odot}\right)^{-1} \\ \frac{M_\star}{M_\odot} = \left(\frac{g}{g_\odot}\right)^3\left(\frac{\rho_\star}{\rho_\odot}\right)^{-2} \end{cases} \tag{3}$$

Finally, the stellar luminosity L is given by

$$\frac{L}{L_\odot} = \left(\frac{R}{R_\odot}\right)^2\left(\frac{T_{\rm eff}}{T_{\rm eff,\odot}}\right)^4 \tag{4}$$

In Bonfanti et al. (2015) we have already pointed out that on the right-hand side of the main sequence (in the lower temperature region) or around the turn-off (TO) very old and very young isochrones are close and can even overlap. According to Fig. 2, the 1-Myr- and 10-Myr-isochrones interesect older isochrones in the TO region. The intersection points are representative of a degeneracy between pre-MS and MS isochrones on the CMD. In fact, the photometry alone cannot disentagle young and old ages, and other information is needed.

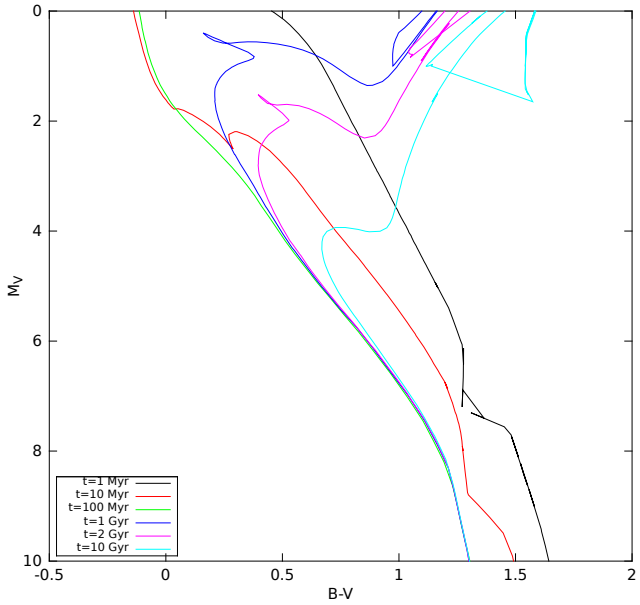

Fig. 2. Isochrones of solar metallicity: pre-MS isochrones are located on the right-hand side of the MS (in this region ages increase from right to left on the diagram) and they intersect older isochrones around the TO. The ages of MS isochrones increase from left to right on the diagram.

So far, the only exoplanet candidate orbiting around a pre-MS is PTFO 8-8695b, as reported by van Eyken et al. (2012) and then investigated by Barnes et al. (2013). Thus, we do not expect to find pre-MS stars among our samples of stars with planets. Anyway, our algorithm is built to compute ages of any kind of star and we decided to perform the activity checks that are described in the following. In this way, we do not put any a priori conditions on the evolutionary stage of the planet-hosting stars. Possible pre-MS interlopers in our planet-hosting stars samples would be very low-mass stars with long pre-MS lifetimes. Twenty-two stars out of the 335 SWP have masses lower than 0.8 $M_\odot$. In principle, they could be pre-MS stars and the checks performed by our algorithm may help in recognizing them.

In the case of late spectral type stars, such as those analysed in this paper, very young stars are chromospherically very active with respect to older stars and typically rotate faster, so we performed activity checks in terms of $\log R'_{HK}$ and $v \sin i$, trying to remove the degeneracy between pre-MS and MS isochrones. We evaluated three age scales through three independent methods to

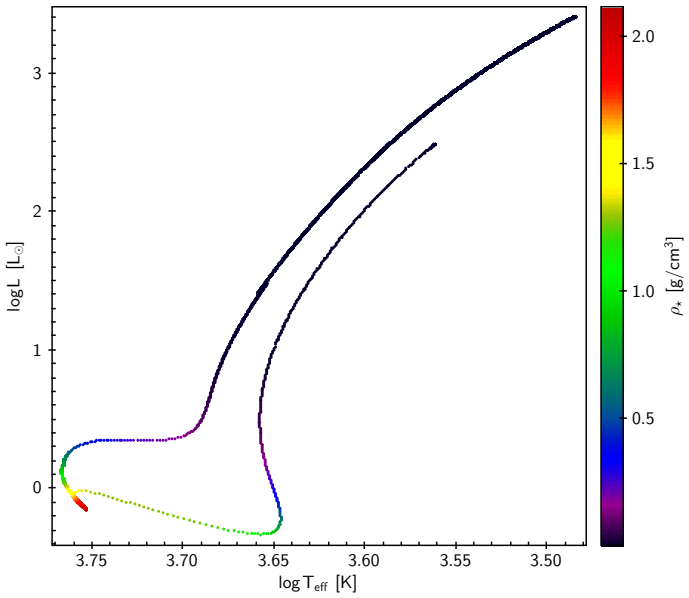

Fig. 3. Evolutionary track of a star with $M = 1M_{\odot}$ and $Z = Z_{\odot}$. Even if the oldest MS isochrones are close to pre-MS isochrones, however, $\rho_{\star}$ in the MS is sensibly higher with respect to the pre-MS phase. As a consequence, the mean stellar density enables us to discard unlikely age values according to $\rho_{\star}$.

decide on the ensemble of isochrones to be used in the following computation.

1. We considered the age-activity relation by Mamajek & Hillenbrand (2008) and we set a conservative threshold of 0.2 dex corresponding to the typical difference between the highest and lowest peaks in activity and the average level for a solar-type star. Inserting $\log R'_{HK}$ in the relation, we evaluated the corresponding age: τ_{HK} represents this age if it was younger than 500 Myr, otherwise $\tau_{HK} = 500$ Myr.
2. Meibom et al. (2015) proved that the gyrochronological relation by Barnes (2010) holds up to 2.5 Gyr, so we applied this relation employing $\frac{4}{\pi} v \sin i$ as the expected stellar rotational velocity to obtain the gyro age τ_v. We set $\tau_v = 2.5$ Gyr, if the resulting gyro age was older than 2.5 Gyr.
3. There is other information that may suggest whether a star located under the TO on the right-hand side of the MS is very young or very old, and this is $\rho_{\star}$. Figure 3 shows the evolutionary track of a 1 $M_{\odot}$ star with solar metallicity. Starting from the birth of a star, $\rho_{\star}$ increases in approaching the MS. After the TO, $\rho_{\star}$ clearly decreases so that post-MS stars have a mean stellar density similar to that of pre-MS stars. So, for $M_V > 5$, corresponding to the luminosity of the TO of the oldest isochrone in the CMD, pre-MS isochrones differ from older isochrones in terms of $\rho_{\star}$. Among pre-MS ages, τ_{ρ} is the threshold age value such that for $t < \tau_{\rho}$ isochrones report mean stellar density $\rho < \rho_{\star}$.

The maximum value among τ_{HK}, τ_v and τ_{ρ} represents the age up to which all the younger isochrones are discarded before the computation of stellar age.

3.2. Isochrone placement: Implementation

The isochrone placement technique enables the determination of the ages of field stars, as well as all the other stellar parameters, such as $T_{\rm eff}$, L, $\log g$, $M_{\star}$, $R_{\star}$, according to stellar evolutionary models. This technique was already described in Bonfanti et al. (2015), but several improvements have been made, such as the new kind of activity checks described above and the possibility of computing the age without any input distance d, if we have stellar density measurements. We also solved some problems linked to numerical stability convergence for which the previous algorithm sometimes gave fictitious young ages. In fact, in the previous version of the algorithm some input data were loaded in single precision, instead of double precision. Sometimes, it could happen that single precision were not sufficient to perform the correct computation of stellar parameters. Moreover, we make this new version more flexible, since it also enables to use input asteroseismic global parameters or only spectroscopic parameters if photometry is not available. Here, we briefly summarize the key aspects.

To make as few assumptions as possible and to start from input data directly obtained from observations, our algorithm requires

- visual magnitude V;
- colour index $B - V$;
- metallicity [Fe/H];
- spectroscopic $\log g$;

and the distance d or $a/R_{\star}$. If d is available, it is possible to infer $T_{\rm eff}$ from $B - V$ and L from the absolute magnitude M_V via interpolation in the isochrone grid. Then $R_{\star}$ is known thanks to Stefan-Boltzmann law (Eq. 4) and finally $M_{\star}$ can be computed by combining $R_{\star}$ with $\log g$. If, instead, d is not available, which can occur for some TPH, first we compute $\rho_{\star}$ through (2) and then we recover $M_{\star}$ and $R_{\star}$ via relations (3). After that, we obtain the correspondence between $B - V$ and $T_{\rm eff}$ through interpolation in the isochrone grid. Finally, we compute L from $T_{\rm eff}$ with (4). Once all the input parameters are available, it is possible to derive stellar properties according to Padova theoretical models by properly weighting each isochrone in the manner already described in Bonfanti et al. (2015). With the new version of the algorithm, we improved the weighting scheme to take the evolutionary speed of a star into account. In fact, the probability that a star is a given age does not only depend on the simple distance between the star and the given isochrone in the HRD, but it is also influenced by the time spent by a star in a given evolutionary stage. For instance, pre-MS evolution is quicker than the MS one. This means that a star rapidly changes its properties during the first tenths of Myr of its life, instead, it remains in the MS for Gyrs with parameters variations detectable on longer timescales. As a consequence, given a star on the HRD, located at the same distance with respect to a pre-MS and a MS isochrone, the probability of dealing with a MS star is higher. To quantify this aspect, we considered the theoretical stellar evolutionary track characterized by the same input metallicity and mass of the star, and we evaluated its evolutionary speed by

$$v_{\rm evo} = \sqrt{\left(\frac{\log L_2 - \log L_1}{t_2 - t_1}\right)^2 + \left(\frac{\log T_{\rm eff,2} - \log T_{\rm eff,1}}{t_2 - t_1}\right)^2} \qquad (5)$$

where $(\log T_{\rm eff,1}, \log L_1)$ is the point on the track, that is nearer to the star, while $(\log T_{\rm eff,2}, \log L_2)$ is the point that occurs later in time on the track, and t_1 and t_2 are the epochs reported by the track. The greater $v_{\rm evo}$, the less is the probability to find a star in such an evolutionary stage. We normalized $v_{\rm evo}$, with respect to a reference speed value $v_{\rm ref}$ for a given track, that is the lowest speed registered on the entire track. In this way, the evolutionary speed can be easily interpreted as a multiple of a reference speed

with which a star goes along its track and the contribution to be added to the weight is unitless, like the others. So the weight p_i to be attributed to the $i^{\rm th}$ isochrone results to be

$$p_i = \left[\left(\frac{\log L - \log L_i}{\Delta \log L}\right)^2 + \left(\frac{\log T_{\rm eff} - \log T_{{\rm eff},i}}{\Delta \log T_{\rm eff}}\right)^2 + \left(\frac{M_\star - M_{\star,i}}{\Delta M_\star}\right)^2 + \left(\frac{\log g - \log g_i}{\Delta \log g}\right)^2 + \log^2\left(\frac{v_{\rm ref}}{v_{\rm evo}}\right)\right]^{-1} \quad (6)$$

Sometimes photometry is not available and only spectroscopic analyses have been carried out. We caution that the given spectroscopic input temperature has been inevitably subjected to a calibration process, which can bring biases. Anyway, to compute ages in such cases we can use spectroscopic [Fe/H], $T_{\rm eff}$ and $\log g$. In this case, the algorithm works in the $\log g$-$\log T_{\rm eff}$ plane following the same prescriptions as in the HRD. This time the weight is simply given by

$$p_i = \left[\left(\frac{\log g - \log g_i}{\Delta \log g}\right)^2 + \left(\frac{\log T_{\rm eff} - \log T_{{\rm eff},i}}{\Delta \log T_{\rm eff}}\right)^2 + \log^2\left(\frac{v_{\rm ref}}{v_{\rm evo}}\right)\right]^{-1} \quad (7)$$

where this time the evolutionary speed of the star $v_{\rm evo}$ and its reference value $v_{\rm ref}$ are evaluated in the $\log g$-$\log T_{\rm eff}$ plane instead of the HRD.

If global asteroseismological indexes, i.e. $\Delta\nu$ and $\nu_{\rm max}$, are available, $\log g$ and $\rho_\star$ may also be computed by inverting the following scaling relations:

$$\Delta\nu = \sqrt{\frac{M_\star}{M_\odot}\left(\frac{R_\star}{R_\odot}\right)^{-3}}\,\Delta\nu_\odot \quad (8)$$

$$\nu_{\rm max} = \frac{g}{g_\odot}\left(\frac{T_{\rm eff}}{T_{{\rm eff},\odot}}\right)^{-\frac{1}{2}}\nu_{{\rm max},\odot} \quad (9)$$

$\Delta\nu_\odot = 135.1\ \mu$Hz and $\nu_{{\rm max},\odot} = 3090\ \mu$Hz as reported by Chaplin et al. (2014). Knowledge of both $\log g$ and $\rho_\star$ enables us to compute $M_\star$ and $R_\star$. Given that $T_{\rm eff}$ is available, L may also be recovered using (4). Even if an accurate asteroseismological analysis based on the study of individual frequency enables precise determination of the stellar evolutionary stage, however, combining information from global asteroseismic parameters and from spectroscopy gives a complete set of input data useful for our isochrone placement. Once the star is located on the HRD, it is then possible to compute its age and its parameters according to Padova evolutionary models. Our algorithm takes element diffusion into account.

If known, stellar multiplicity has been pointed out through a flag at the column *Bin* of Table 2. In these cases, the literature already reports data referred to the specific star we analysed. We caution that if some unresolved binaries were present in our samples, such stars would appear more luminous than they are. If located in the MS region, they would erroneously be judged as older.

Another critical point deals with reddening. In the case of SWP, we do not deeply check whether the different sources give photometry de-reddened or not because neither *SWEET-Cat* nor the *Exoplanets Data Explorer* report any reddening information. We explicitely account for reddening in the case of those TPH listed in Maxted et al. (2011), who report the colour excess $E(B-V)$. Anyway, by a posteriori catalogue cross-matching, we were able to recover $E(B-V)$ index for 154 stars out of the 335 SWP, and we found that more than 80% of them has $E(B-V) = 0$. Similarly, $\sim$ 90% of the stars belonging to the VF-SN catalogue have $E(B-V) = 0$. Considering also that the analysed stars are essentially inside the Local Bubble, whose extension varies between $\sim$ 80 and 200 pc from the Sun (Sfeir et al. 1999), we expect that the effect of reddening does not significantly impact our resulting statistics.

4. Results

4.1. Test of the algorithm

Silva Aguirre et al. (2015) analysed a sample of Kepler exoplanet host stars (Kepler sample from here on). They performed a complete asteroseismological analysis of the individual oscillation frequencies, recovered thanks to the high signal-to-noise ratio of their observations. Among other fundamental properties, they derived the ages of their sample of stars, claiming a median error of 14%. As a result of high reliability attributed to a complete asteroseismological analysis, comparing the results given by our isochrone placement with those reported by Silva Aguirre et al. (2015) represents a good validation test for our algorithm. The authors observe that the majority of these stars are older than the Sun because of selection effects. In particular, stellar pulsations characterized by high signal-to-noise ratio are preferentially detected in F-type stars (ages $\sim$ 2-3 Gyr) and in old G-type stars (ages $\sim$ 6 Gyr). Thus, aim of this section is to test the accuracy of our algorithm, without comparing the evolutionary stage of the Kepler sample with other stars.

We analysed 29 over 33 stars of the Kepler sample, for which both $\Delta\nu$ and $\nu_{\rm max}$ were available. We have just considered the global asteroseismic parameters, deriving input $\log g$ and $\rho_\star$ by inverting (8) and (9). Spectroscopic [Fe/H] and $T_{\rm eff}$ were reported by Silva Aguirre et al. (2015). If available, $v \sin i$ was employed to perform checks as described in point 2 in § 3.1.

Our age determination is in good agreement with the analysis of Silva Aguirre et al. (2015), as shown in Fig. 4. The linear correlation coefficient $r = 0.95$ and the reduced $\chi^2/26 = 1.5$ confirm that a linear least-squares regression well describe the data scatter and is consistent with the extension of our error bars. The least-squares line represented in green (thicker line) shows that our method slightly overestimate the age in the domain of the oldest stars.

4.2. The ages of the exoplanet hosts

The BTPH catalogue is a subset of the TPH catalogue. In Fig. 5, we superimposed the age distribution of the 43 stars belonging to the BTPH catalogue (grey bars) to the age distribution of the all TPH (blue bars). The medians of the distributions are $\sim$ 4.2 Gyr and $\sim$ 5 Gyr for the BTPH and for the TPH, respectively. One of the three stars younger than 1 Gyr, namely WASP-18 ($t = 0.9 \pm 0.2$ Gyr), appears too blue for its metallicity, so we investigated the input parameters of this star. Southworth et al. (2009) analysed the properties of WASP-18, adopting $V = 9.30$ and $B-V = 0.44$, instead of $V = 9.273$ and $B-V = 0.484$, which are the values we used. In addition they started from [Fe/H]=0, as reported by Hellier et al. (2009), which sensibly differs from [Fe/H]=0.19, which we took from SWEET-Cat. With the input parameters used by Southworth et al. (2009), WASP-18 is again located on the bluer side out of the MS, and our isochrone placement gives $t = 0.2^{+0.3}_{-0.2}$ Gyr. Southworth et al. (2009) considered different sets of evolutionary models and they concluded that

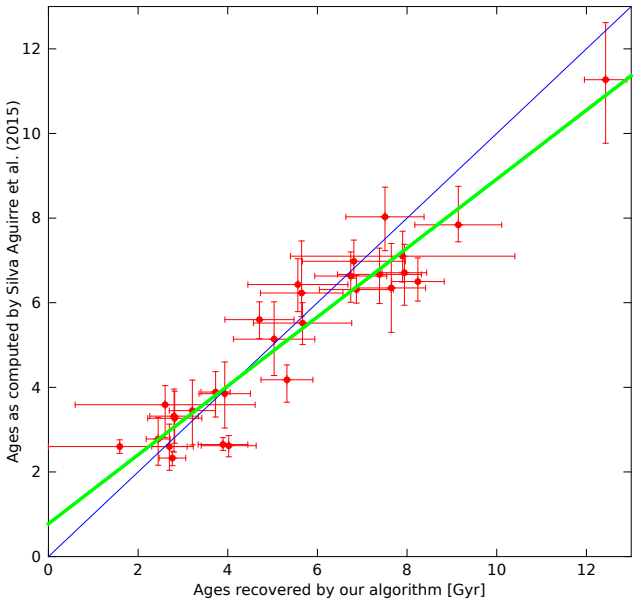

Fig. 4. Ages of the Kepler sample. The least-squares line that regress the data is represented with a thick green line, while the thin blue line is the bisector representing the exact correspondence between the data.

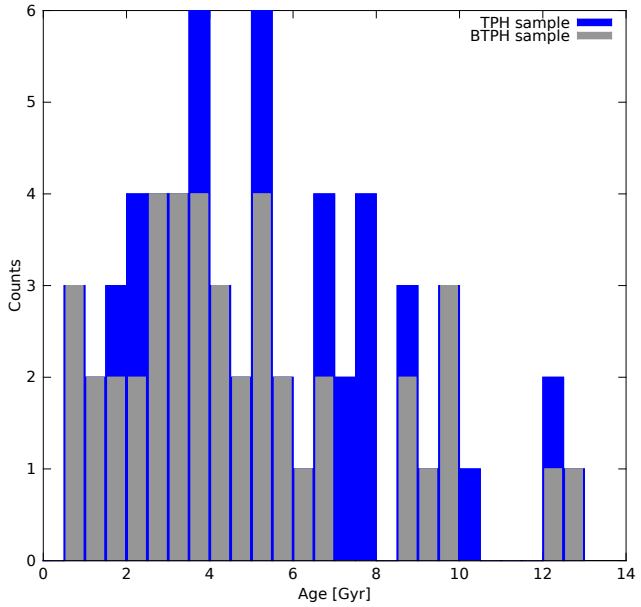

Fig. 5. Grey bars represent age distribution of the 43 stars belonging to the BTPH catalogue. The superset given by TPH catalogue is represented in the background through blue bars.

WASP-18 is age between 0 and 2 Gyr. This is consistent with both of our determinations, but since the different sets of input parameters do not fully agree with Padova theoretical models, we caution that the age estimation is not necessarily reliable. Further photometric investigations or a re-determination of its metallicity are required to correct the inconsistency between the position of the star on the HRD and the theoretical isochrones.

As a term of comparison, we computed the ages of stars taken from SH catalogue. The consequent age distribution is represented in Fig. 6. This age distribution peaks in the [3, 3.5) Gyr bin and its median is ∼ 4.8 Gyr, which is very close to the solar age value. The age distributions in Figs. 5 and 6 are consistent. Differences may arise because of the paucity of the TPH, but, in any case, no significant bias emerges in the comparison between the samples. Actually, we performed a Kolmogorov-Smirnov test (KS test) to investigate whether TPH and BTPH come from the same distribution, which characterizes the larger SH sample. The high p-values (0.5 for the TPH-SH comparison and 0.3 for the BTPH-SH comparison) suggest that we should not reject the null hypothesis based on which the samples come from the same distribution. This emphasizes that even if photometric and spectroscopic targets could be chosen according to different criteria, the confirmation of a candidate exoplanet requires the application of both the transit and radial velocity method. Therefore, similar biases are expected in the two different samples.

All the parameters of the planet-hosting stars derived according to Padova isochrones are listed in Table 2.

4.3. Age comparison with the stars of the solar neighbourhood

Our second step is to investigate whether exoplanet hosts are peculiar with respect to field stars not harbouring planets. The exoplanet hosts known so far are late spectral type stars located in the solar neighbourhood: ∼ 90% of the planet-hosting stars we analysed are closer than 200 pc. The stars contained in the SN catalogue represent an interesting comparison test because

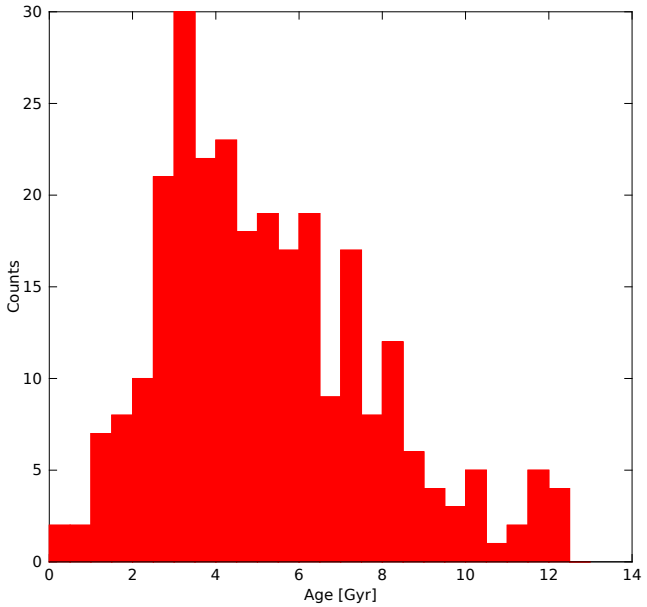

Fig. 6. Age distribution of the 274 stars belonging to the SH catalogue. The median of the distribution is ∼ 4.8 Gyr, which is very close to the age of the Sun.

they represent a numerous sample of late spectral type MS-stars occupying almost the same volume as the exoplanet hosts. The age values reported by Casagrande et al. (2011) (C11 from here on) are computed following their own method, so we checked whether their results were consistent following the VF-SN subsample, which contains all the input parameters needed by our algorithm. We managed to obtain the age for 818 stars. We recall that the cut in spectral type is imposed by both C11 and Valenti & Fischer (2005) limits, and includes basically F, G and K stars. The plot of the expectation age reported by C11 versus our age values is shown in Fig. 7. The scatter of points around the bisector is expected given the high age uncertainties, and, in any case, good statistical agreement characterizes the two determinations.

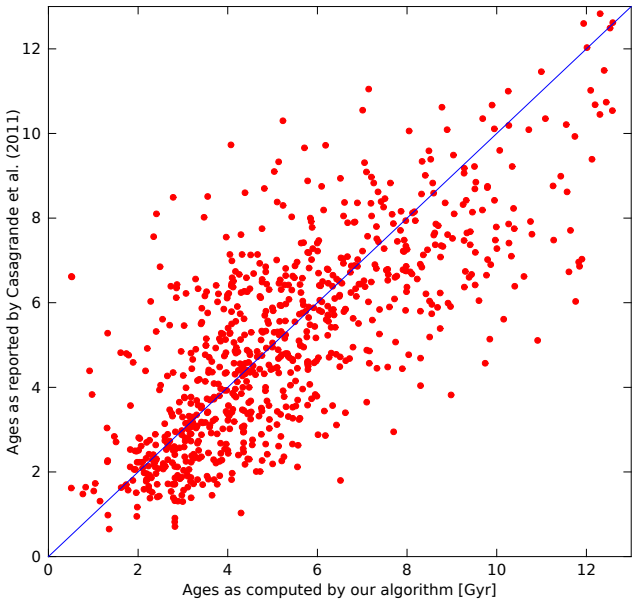

Fig. 7. Age comparison between Casagrande estimation and ours (818 stars). The dispersion between the two measurements can be quantified through the linear correlation coefficient, that is ∼ 0.75.

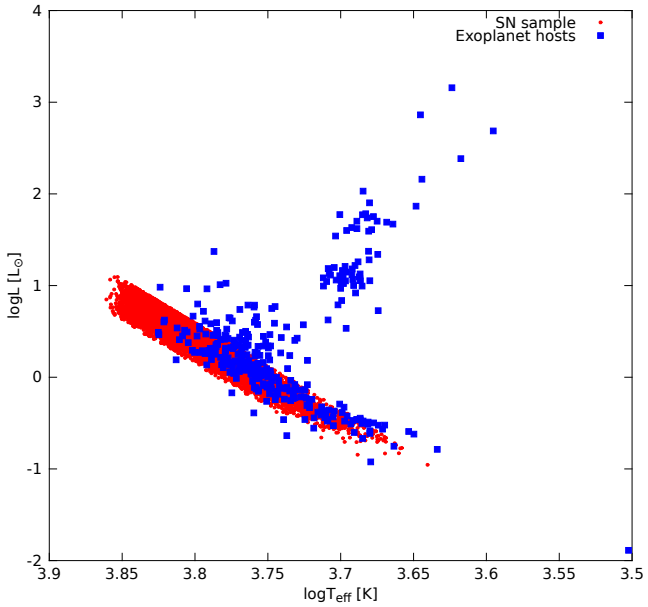

Fig. 8. SN sample on the HRD (red dots). The very straight boundaries of the SN sample is simply a consequence of our identification of the MS through a strip as described in § 2.2. All the planet-hosting stars we analysed are superimposed (blue squares).

The median age for C11 values is ∼ 4.9 Gyr, which is very similar to our median age (∼ 4.8 Gyr) for the common sample. This agreement between the two age determinations suggests that any comparison between C11 ages and ours is consistent. In addition, considering the median age value coming from the VF-SN sample, it is not surprising that the age is similar to the ages found for the samples of stars with planets analysed above. In fact, we obtained the VF-SN catalogue by cross-matching the SN sample with the catalogue of stars reported by Valenti & Fischer (2005). The authors performed high-precision spectroscopy on stars taken from Keck, Lick and AAT planet search programme, thus, their stars present the typical selection effects characterizing stars with planets. Actually the median value we obtained for the VF-SN sample is the same as the SH value.

As C11 age values suggest, the age distribution of all the 7044 stars belonging to the SN catalogue peaks in the [1.5, 2) Gyr bin with a median age value of ∼ 2.6 Gyr. This raw analysis may suggest that field stars are globally younger than planet-hosting stars. Instead, this comparison hides a bias, in fact, the SN catalogue contains a huge number of hot F-type stars with respect to planet-hosting stars, as shown in Fig. 8 (stars with $\log T_{\rm eff} \gtrsim 3.8$). The earlier the spectral type, the faster the evolution of a star, thus, F-type stars are expected to be statistically younger than later spectral type stars.

Analysing Fig. 8, all the stars with $T_{\rm eff} > 6300$ have been removed from the SN catalogue, remaining with 3713 stars (RSN catalogue). In this way, the comparison between the solar neighbourhood stars and the stars with planets is homogeneous in spectral type. The result is given by the age distributions in Fig. 9. They are almost consistent (KS p-value is 0.2): SN age distribution is less peaked, but they both have 4.8 Gyr as median value.

Two considerations should be added.

1. The median age value of the stars with planets is very similar to the solar age value, but very different (∼ 1 Gyr) from the histogram peak because of the extended tail towards old ages. According to their metallicities, there is no evidence that planet-hosting stars with $t \gtrsim 9$ Gyr have population II properties. If we exclude this contamination, we may argue whether such a skew distribution may be due to a real distribution reflecting a prolonged star formation history (Rocha-Pinto et al. 2000) or to an asymmetric propagation of errors.
2. Assuming a solar age of ∼ 4.6 Gyr (Chaussidon 2007), an age of t = 4.6-4.8 Gyr appears older than that currently assumed for most of the thin disc population, where planet-hosting stars and the RSN sample are located. In fact, as summarized by Allende Prieto (2010), Reddy et al. (2006) say that thin disc stars span a range between 1 and 9 Gyr, with the majority of them younger than 5 Gyr. Holmberg et al. (2009) and Haywood (2008) set an older upper limit for the thin disc ages, however they both agree that most of these stars are younger than 4-5 Gyr. Rocha-Pinto et al. (2000), using a different approach based on the stellar activity as age indicator, found three different peaks in the local star formation history, with the highest at very young ages below 1 Gyr. We caution that we limited our sample primarily to G-type stars. The other point is that we are sampling a very limited inter-arms volume (essentially < 200 pc), as most of the recent studies based on single star age measurements. The literature does not present detailed studies of the ages of single disc stars far away from the solar neighbourhood. Thus, this lack of information does not allow us to perform a complete comparison between the evolutionary properties of our samples and those of the entire galactic disc. The extension of the stellar analysis to a distance larger than 200 pc would include younger active star-forming regions, such as the Orion Nebula or Taurus-Auriga complex. As a consequence, in deeper surveys we expect to include significantly younger stars.

5. Conclusions

We analysed a sample of 61 transiting-planet hosts to compute their ages and their peculiar parameters according to Padova isochrones. A priori, one could say that our particular sample

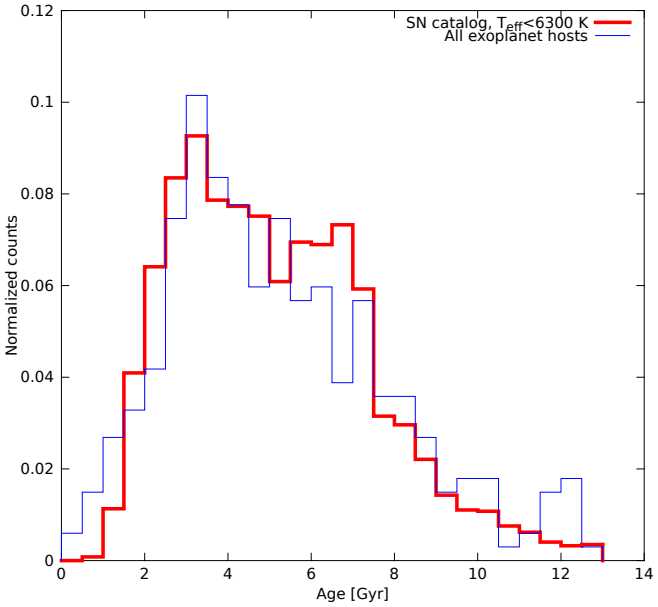

Fig. 9. Age distribution of the MS stars colder than 6300 K belonging to the RSN catalogue (red stairs, 3713 stars) compared with the age distribution of all the planet-hosting stars we analysed (blue stairs, 335 stars).

is expected not to be affected by some typical biases that characterize those planet-hosting stars coming from radial velocity surveys. Spectroscopic targets are often deliberately chosen to be slow rotators and typically inactive. Instead, very high-precision photometry only requires bright stars in the solar neighbourhood for an adequate signal-to-noise ratio. Actually, once a possible transiting planet has been detected, the confirmation process involves spectroscopic analysis. Therefore, similar biases are expected in both spectroscopic and photometric surveys.

We found that the median age of our TPH sample is $\sim$ 5 Gyr. The subsample of TPH brighter than $V = 12$ yields a median age of $\sim$ 4.2 Gyr. This slightly lower value is expected since brighter stars are on average younger. In order to comment the age distribution of TPH, we also considered 274 planet-hosting stars, whose planets have been detected though radial velocity method. Their age distribution peaks in the [3, 3.5) Gyr bin and it is synthesized by a median value of $\sim$ 4.8 Gyr. These three samples of stars are consistent from an evolutionary point of view. Slight differences are due to the paucity of stars belonging to the TPH catalogue and, in fact, a KS test does not suggest that TPH and SH come from a different distribution. Thus, spectroscopic and photometric targets are characterized by almost the same selection effects, and these biases bring the median of their age distribution around the solar age value.

In the second part we checked whether planet-hosting stars have peculiar ages with respect to field stars without planets of the solar neighbourhood. In case of a homogeneous comparison in terms of spectral type, solar neighborhood stars belonging to the RSN catalog have an age distribution very similar to that deriving from the all exoplanet hosts considered in this paper and the median age is $\sim$ 4.8 in both cases. With its age of 4.567 Gyr (as reported by Chaussidon 2007), the Sun appears not to be a peculiar star, if compared with both the planet-hosting stars and the SN stars, whose spectral types span essentially from late-F to early K. However, it looks that we are sampling a limited inter-arms region, possibly older than the average thin disc population.

Acknowledgements. We thank the anonymous referee for the interesting and fruitful comments that improved our paper. A. B. and S.O. acknowledge "contratto ASI-INAF n.2015-019-R0 del 29 luglio 2015" and support from INAF through the "Progetti Premiali" funding scheme of the Italian Ministry of Education, University, and Research. S. O. acknowledge financial support from University of Padova, as well. V. N. acknowledges support from INAF-OAPd through the grant "Studio preparatorio per le osservazioni della missione ESA/CHEOPS" (#42/2013). This research has made use of the Exoplanet Orbit Database and the Exoplanet Data Explorer at exoplanets.org. Moreover it has made use of SWEET-Cat: a catalog of stellar parameters for stars with planets at astro.up.pt (Centro de Astrofisica da Universidade do Porto).

References

Allende Prieto, C. 2010, in IAU Symposium, Vol. 265, IAU Symposium, ed. K. Cunha, M. Spite, & B. Barbuy, 304–312
Barker, A. J. & Ogilvie, G. I. 2009, MNRAS, 395, 2268
Barnes, J. W., van Eyken, J. C., Jackson, B. K., Ciardi, D. R., & Fortney, J. J. 2013, ApJ, 774, 53
Barnes, S. A. 2010, ApJ, 722, 222
Barnes, S. A. & Kim, Y.-C. 2010, ApJ, 721, 675
Bonfanti, A., Ortolani, S., Piotto, G., & Nascimbeni, V. 2015, A&A, 575, A18
Bressan, A., Marigo, P., Girardi, L., et al. 2012, MNRAS, 427, 127
Broeg, C., Fortier, A., Ehrenreich, D., et al. 2013, in European Physical Journal Web of Conferences, Vol. 47, European Physical Journal Web of Conferences, 3005
Casagrande, L., Schönrich, R., Asplund, M., et al. 2011, A&A, 530, A138
Chaplin, W. J., Basu, S., Huber, D., et al. 2014, ApJS, 210, 1
Chaussidon, M. 2007, Formation of the Solar system: a chronology based on meteorites, ed. M. Gargaud, H. Martin, & P. Claeys (Berlin: Springer-Verlag), 45–74
Debes, J. H. & Jackson, B. 2010, ApJ, 723, 1703
Handler, G. 2013, Asteroseismology, ed. T. D. Oswalt & M. A. Barstow, 207
Haywood, M. 2008, MNRAS, 388, 1175
Hellier, C., Anderson, D. R., Collier Cameron, A., et al. 2009, Nature, 460, 1098
Holmberg, J., Nordström, B., & Andersen, J. 2009, A&A, 501, 941
Kasting, J. F. & Catling, D. 2003, ARA&A, 41, 429
Kjeldsen, H. & Bedding, T. R. 1995, A&A, 293, 87
Maeder, A. 1999, A&A, 347, 185
Mamajek, E. E. & Hillenbrand, L. A. 2008, ApJ, 687, 1264
Maxted, P. F. L., Koen, C., & Smalley, B. 2011, MNRAS, 418, 1039
Meibom, S., Barnes, S. A., Platais, I., et al. 2015, Nature, 517, 589
Pätzold, M., Carone, L., & Rauer, H. 2004, A&A, 427, 1075
Rauer, H., Catala, C., Aerts, C., et al. 2014, Experimental Astronomy, 38, 249
Reddy, B. E., Lambert, D. L., & Allende Prieto, C. 2006, MNRAS, 367, 1329
Rocha-Pinto, H. J., Scalo, J., Maciel, W. J., & Flynn, C. 2000, A&A, 358, 869
Santos, N. C., Sousa, S. G., Mortier, A., et al. 2013, A&A, 556, A150
Sfeir, D. M., Lallement, R., Crifo, F., & Welsh, B. Y. 1999, A&A, 346, 785
Silva Aguirre, V., Davies, G. R., Basu, S., et al. 2015, arXiv:1504.07992v2
Soderblom, D. R. 2010, ARA&A, 48, 581
Southworth, J., Hinse, T. C., Dominik, M., et al. 2009, ApJ, 707, 167
Sozzetti, A., Torres, G., Charbonneau, D., et al. 2007, ApJ, 664, 1190
Valenti, J. A. & Fischer, D. A. 2005, ApJS, 159, 141
van Eyken, J. C., Ciardi, D. R., von Braun, K., et al. 2012, ApJ, 755, 42
van Leeuwen, F. 2007, A&A, 474, 653
von Zeipel, H. 1924, MNRAS, 84, 665
Winn, J. N. 2010, arXiv:1001.2010v5

Table 2. Planet-hosting stars parameters determined through Padova isochrones.

Star	t (Gyr)	Δt (Gyr)	$T_{\rm eff}$ (K)	$\Delta T_{\rm eff}$ (K)	L ($L_\odot$)	ΔL ($L_\odot$)	M ($M_\odot$)	ΔM ($M_\odot$)	$\log g$ (cm/s^2)	$\Delta \log g$ (cm/s^2)	R ($R_\odot$)	ΔR ($R_\odot$)	Bin	Tr
11 Com	3.0	0.3	4741	12	109	1	1.37	0.04	2.19	0.02	15.5	0.2	1	0
11 UMi	4.1	1.0	4140	28	243	6	1.4	0.1	1.6	0.04	30.4	0.8	0	0
14 And	5.6	3.0	4775	49	56	1	1.2	0.2	2.4	0.1	11.0	0.3	0	0
14 Her	4.6	1.5	5313	18	0.61	0.01	0.97	0.01	4.48	0.02	0.93	0.01	0	0
16 Cyg B	5.2	1.0	5837	32	1.26	0.01	1.04	0.02	4.37	0.02	1.1	0.02	1	0
18 Del	1.0	0.1	5037	57	35	1	2.1	0.1	2.98	0.04	7.8	0.3	0	0
24 Sex	2.9	0.2	4917	10	16.4	0.1	1.49	0.02	3.11	0.01	5.6	0.04	0	0
30 Ari B	0.4	0.4	6313	24	1.98	0.03	1.25	0.02	4.38	0.01	1.18	0.02	1	0
42 Dra	6.5	1.7	4414	40	145	3	1.1	0.1	1.8	0.1	20.6	0.6	0	0
51 Peg	3.8	1.1	5857	39	1.34	0.03	1.09	0.02	4.37	0.02	1.13	0.03	0	0
55 Cnc	5.1	2.7	5310	32	0.59	0.01	0.95	0.02	4.49	0.03	0.91	0.02	1	1
6 Lyn	3.1	0.4	4973	28	14.8	0.1	1.4	0.1	3.15	0.03	5.2	0.1	0	0
61 Vir	5.2	2.1	5651	36	0.81	0.01	0.96	0.02	4.46	0.03	0.94	0.02	0	0
7 CMa	4.9	1.0	4782	39	11.3	0.2	1.3	0.1	3.17	0.04	4.9	0.1	0	0
70 Vir	8.1	0.4	5560	31	3.0	0.1	1.07	0.01	3.92	0.02	1.9	0.1	0	0
75 Cet	3.3	0.7	4742	14	53.7	0.3	1.4	0.1	2.52	0.03	10.9	0.1	0	0
81 Cet	3.2	0.5	4799	24	59.8	0.4	1.4	0.1	2.49	0.03	11.2	0.2	0	0
91 Aqr	8.1	2.8	4656	26	51	1	1.1	0.2	2.4	0.1	11.0	0.2	0	0
BD +14 4559	6.9	4.2	4948	25	0.32	0.01	0.82	0.02	4.57	0.03	0.78	0.02	0	0
BD +20 2457	10.5	1.7	4504	5	172	12	0.89	0.05	1.71	0.01	21.6	0.8	0	0
CoRoT-18	7.5	4.5	5444	38	0.58	0.04	0.87	0.03	4.5	0.05	0.86	0.04	0	1
CoRoT-19	5.1	0.8	6133	58	3.0	0.3	1.2	0.1	4.12	0.01	1.5	0.1	0	1
CoRoT-7	4.5	4.3	5357	22	0.52	0.05	0.89	0.03	4.54	0.05	0.84	0.05	0	1
HAT-P-11	5.2	3.1	4785	12	0.262	0.004	0.8	0.01	4.59	0.02	0.75	0.01	0	1
HAT-P-13	5.6	0.9	5733	42	2.7	0.2	1.2	0.1	4.071	0.005	1.7	0.1	0	1
HAT-P-14	1.1	0.8	6694	73	4.3	0.3	1.42	0.04	4.21	0.03	1.54	0.08	0	1
HAT-P-17	8.9	2.9	5338	30	0.57	0.01	0.87	0.02	4.48	0.03	0.88	0.02	0	1
HAT-P-22	12.3	0.6	5338	14	0.75	0.01	0.9	0.01	4.37	0.01	1.02	0.01	0	1
HAT-P-24	2.2	1.2	6448	55	2.4	0.2	1.17	0.03	4.30	0.02	1.26	0.06	0	1
HAT-P-26	3.6	0.3	5387	6	0.53	0.01	0.9	0.002	4.541	0.004	0.84	0.01	0	1
HAT-P-27	7.9	2.1	5204	28	0.52	0.01	0.9	0.02	4.49	0.02	0.89	0.01	0	1
HAT-P-36	10.0	0.7	5422	23	0.83	0.01	0.94	0.01	4.37	0.01	1.04	0.02	0	1
HAT-P-4	5.4	0.9	5809	45	2.2	0.1	1.19	0.05	4.169	0.003	1.5	0.1	0	1
HAT-P-7	0.8	0.7	6707	53	5.9	0.7	1.57	0.04	4.12	0.06	1.8	0.1	0	1
HAT-P-9	1.8	0.4	6386	38	2.60	0.04	1.27	0.01	4.29	0.01	1.32	0.03	0	1
HATS-1	7.5	1.1	5705	32	0.95	0.01	0.94	0.01	4.4	0.01	1.00	0.02	0	1
HD 100655	9.4	2.1	4675	4	47	2	1.0	0.1	2.39	0.02	10.4	0.2	0	0
HD 100777	5.9	1.8	5579	37	0.92	0.02	1.00	0.02	4.41	0.03	1.03	0.03	0	0
HD 10180	4.5	1.1	5939	43	1.49	0.03	1.08	0.02	4.34	0.03	1.16	0.03	0	0
HD 101930	5.7	4.3	5144	27	0.42	0.02	0.87	0.03	4.54	0.04	0.82	0.02	1	0
HD 102117	6.1	1.2	5727	47	1.4	0.04	1.07	0.02	4.3	0.03	1.21	0.04	0	0
HD 102195	5.9	3.5	5283	29	0.49	0.01	0.88	0.03	4.53	0.03	0.84	0.02	0	0
HD 102272	11.6	1.2	4794	18	21.5	0.2	0.92	0.03	2.74	0.02	6.7	0.1	0	0
HD 102329	4.1	0.8	4786	39	19.0	0.3	1.4	0.1	2.96	0.04	6.4	0.2	0	0
HD 102365	10.8	2.0	5687	39	0.81	0.01	0.84	0.02	4.42	0.03	0.93	0.02	0	0
HD 102956	2.9	0.2	4892	14	11.9	0.1	1.54	0.02	3.25	0.01	4.8	0.1	0	0
HD 103197	3.4	2.0	5237	18	0.48	0.01	0.91	0.02	4.54	0.02	0.84	0.01	0	0
HD 103774	2.0	0.1	6391	27	3.7	0.1	1.38	0.01	4.183	0.002	1.56	0.03	0	0
HD 104067	9.0	3.4	4961	12	0.31	0.01	0.78	0.01	4.57	0.02	0.75	0.02	0	0
HD 104985	4.9	1.2	4730	41	51	1	1.2	0.1	2.5	0.1	10.6	0.3	0	0
HD 106252	6.4	1.4	5881	47	1.37	0.04	1.02	0.02	4.33	0.03	1.13	0.03	0	0
HD 106270	3.8	0.2	5570	123	5.9	0.3	1.37	0.03	3.74	0.05	2.6	0.2	0	0
HD 10647	1.8	0.9	6159	39	1.56	0.02	1.12	0.02	4.4	0.02	1.1	0.02	0	0
HD 10697	7.5	0.4	5674	93	2.8	0.04	1.12	0.01	4.00	0.03	1.7	0.1	0	0
HD 107148	4.0	1.0	5789	36	1.34	0.05	1.1	0.01	4.35	0.03	1.15	0.03	0	0
HD 108147	1.3	0.5	6211	21	1.88	0.02	1.21	0.01	4.37	0.01	1.19	0.01	0	0
HD 108863	3.3	0.5	4876	29	16.5	0.3	1.4	0.1	3.08	0.03	5.7	0.1	0	0
HD 108874	6.3	0.7	5647	19	1.06	0.01	1.02	0.01	4.37	0.01	1.08	0.01	0	0
HD 109246	2.5	0.8	5887	19	1.15	0.01	1.07	0.01	4.43	0.01	1.03	0.01	0	0
HD 109749	4.1	0.7	5860	39	1.55	0.02	1.14	0.01	4.32	0.02	1.21	0.02	1	0
HD 111232	11.6	1.5	5650	22	0.67	0.01	0.79	0.01	4.47	0.02	0.85	0.01	0	0
HD 113337	1.5	0.9	6622	71	4.18	0.08	1.38	0.03	4.19	0.03	1.56	0.05	0	0
HD 114386	8.8	2.8	4926	13	0.28	0.01	0.76	0.01	4.58	0.02	0.73	0.01	0	0
HD 114613	5.0	0.1	5756	13	4.09	0.03	1.25	0.01	3.91	0.01	2.04	0.02	0	0
HD 114729	9.3	0.6	5939	58	2.33	0.02	0.97	0.01	4.1	0.02	1.44	0.03	1	0
HD 114762	12.4	0.6	6043	22	1.52	0.01	0.82	0.01	4.24	0.01	1.13	0.01	1	0
HD 114783	10.4	2.4	5089	17	0.4	0.01	0.81	0.01	4.53	0.02	0.81	0.01	0	0
HD 11506	2.0	0.6	6119	45	2.1	0.1	1.25	0.01	4.31	0.02	1.29	0.04	0	0
HD 116029	4.9	1.1	4849	39	11.4	0.1	1.3	0.1	3.19	0.04	4.8	0.1	0	0
HD 117207	6.6	1.0	5681	33	1.19	0.02	1.03	0.01	4.34	0.02	1.13	0.02	0	0
HD 117618	4.0	1.3	6019	50	1.6	0.1	1.1	0.02	4.34	0.03	1.17	0.04	0	0
HD 118203	5.4	0.5	5741	35	3.8	0.3	1.23	0.03	3.93	0.02	2.0	0.1	0	0
HD 11964	8.5	0.5	5371	43	2.6	0.1	1.09	0.02	3.92	0.02	1.9	0.1	1	0
HD 11977	2.9	0.2	4851	9	62.1	0.2	1.46	0.03	2.5	0.01	11.2	0.1	0	0
HD 120084	4.4	1.2	4675	11	52	1	1.3	0.1	2.48	0.03	11.0	0.2	0	0
HD 121504	1.9	1.0	6089	47	1.62	0.04	1.16	0.02	4.38	0.03	1.15	0.03	0	0
HD 125595	8.0	3.7	4654	22	0.21	0.01	0.74	0.01	4.61	0.02	0.71	0.02	0	0
HD 125612	3.1	0.3	5818	13	1.205	0.003	1.09	0.01	4.4	0.01	1.08	0.01	1	0
HD 12661	3.3	0.6	5714	22	1.13	0.01	1.09	0.01	4.4	0.01	1.08	0.01	0	0
HD 128311	8.5	3.6	4922	26	0.29	0.01	0.77	0.02	4.58	0.02	0.74	0.02	0	0
HD 130322	6.1	2.9	5410	30	0.56	0.01	0.88	0.02	4.52	0.03	0.85	0.02	0	0
HD 131496	4.0	0.7	4838	43	9.9	0.2	1.4	0.1	3.27	0.04	4.5	0.1	0	0
HD 134987	5.4	0.5	5797	23	1.51	0.01	1.09	0.01	4.3	0.01	1.22	0.01	0	0

Table 2. continued.

Star	t (Gyr)	Δt (Gyr)	$T_{\rm eff}$ (K)	$\Delta T_{\rm eff}$ (K)	L ($L_\odot$)	ΔL ($L_\odot$)	M ($M_\odot$)	ΔM ($M_\odot$)	$\log g$ (cm/s^2)	$\Delta \log g$ (cm/s^2)	R ($R_\odot$)	ΔR ($R_\odot$)	Bin	Tr
HD 136418	5.0	1.0	4997	40	6.9	0.1	1.2	0.1	3.43	0.04	3.5	0.1	0	0
HD 137388	7.3	3.8	5183	25	0.46	0.02	0.87	0.03	4.52	0.03	0.85	0.02	1	0
HD 13908	3.9	0.5	6212	38	4.0	0.1	1.28	0.04	4.06	0.02	1.74	0.04	0	0
HD 13931	5.3	1.3	5902	52	1.48	0.03	1.07	0.02	4.33	0.03	1.17	0.03	0	0
HD 139357	7.2	1.8	4454	39	73.5	1.3	1.1	0.1	2.2	0.1	14.4	0.4	0	0
HD 141937	3.2	0.5	5837	14	1.13	0.01	1.06	0.01	4.42	0.01	1.04	0.01	0	0
HD 142	2.8	0.5	6321	67	2.81	0.05	1.25	0.01	4.24	0.03	1.4	0.04	1	0
HD 142245	3.1	0.3	4831	28	13.1	0.2	1.52	0.05	3.19	0.03	5.2	0.1	0	0
HD 142415	1.6	0.6	5869	12	1.16	0.02	1.1	0.01	4.44	0.01	1.04	0.01	0	0
HD 145377	2.9	1.2	5979	46	1.43	0.04	1.11	0.02	4.38	0.03	1.12	0.03	0	0
HD 145457	2.8	0.6	4772	45	41	1	1.5	0.1	2.66	0.05	9.4	0.2	0	0
HD 1461	4.0	0.7	5807	20	1.20	0.01	1.07	0.01	4.39	0.01	1.08	0.01	0	0
HD 147018	7.3	2.0	5526	29	0.78	0.02	0.94	0.02	4.44	0.03	0.97	0.02	0	0
HD 147513	3.4	0.7	5827	21	1.01	0.01	1.02	0.01	4.45	0.01	0.99	0.01	1	0
HD 148156	1.2	0.5	6156	23	1.84	0.03	1.22	0.01	4.36	0.01	1.19	0.02	0	0
HD 148427	4.3	0.6	4993	44	6.2	0.1	1.32	0.05	3.51	0.03	3.3	0.1	0	0
HD 149026	2.9	0.3	6116	44	2.8	0.1	1.302	0.005	4.2	0.02	1.49	0.04	0	1
HD 149143	4.8	0.8	5792	58	2.2	0.1	1.21	0.03	4.17	0.03	1.5	0.1	0	0
HD 1502	3.0	0.3	5006	25	11.5	0.2	1.46	0.04	3.29	0.02	4.5	0.1	0	0
HD 152581	7.2	2.0	4991	45	16.1	0.2	1.0	0.1	3.0	0.1	5.4	0.1	0	0
HD 153950	4.3	0.8	6136	64	2.24	0.03	1.15	0.02	4.25	0.03	1.33	0.04	0	0
HD 154345	4.1	1.2	5557	15	0.62	0.002	0.9	0.01	4.53	0.01	0.85	0.01	0	0
HD 154672	7.1	0.8	5754	51	1.81	0.02	1.09	0.02	4.2	0.03	1.36	0.03	0	0
HD 154857	5.8	0.5	5740	46	4.4	0.3	1.13	0.03	3.83	0.03	2.1	0.1	0	0
HD 155358	1.9	4.5	5966	53	2.11	0.02	1.1	0.1	4.2	0.04	1.36	0.03	0	0
HD 156279	7.4	2.2	5449	31	0.7	0.01	0.93	0.02	4.45	0.03	0.94	0.02	0	0
HD 156411	4.5	0.3	5886	29	5.1	0.3	1.23	0.02	3.85	0.02	2.2	0.1	0	0
HD 156668	10.2	2.8	4857	18	0.27	0.01	0.75	0.01	4.58	0.01	0.73	0.01	0	0
HD 158038	3.2	0.4	4839	29	11.9	0.1	1.5	0.1	3.23	0.03	4.9	0.1	0	0
HD 159243	2.0	0.3	6071	19	1.45	0.05	1.12	0.01	4.4	0.01	1.09	0.03	0	0
HD 159868	6.3	0.5	5583	54	3.8	0.2	1.13	0.03	3.85	0.03	2.1	0.1	0	0
HD 16141	6.5	0.6	5856	60	2.46	0.03	1.13	0.02	4.12	0.03	1.53	0.04	1	0
HD 16175	4.1	0.8	6009	44	3.35	0.02	1.3	0.05	4.09	0.02	1.69	0.03	0	0
HD 162020	3.1	2.7	4807	17	0.22	0.01	0.75	0.01	4.63	0.01	0.68	0.01	0	0
HD 163607	8.3	0.5	5508	15	2.6	0.1	1.1	0.02	3.98	0.01	1.8	0.1	0	0
HD 16417	6.9	0.4	5818	51	2.74	0.01	1.12	0.01	4.06	0.02	1.63	0.03	0	0
HD 164509	3.2	0.8	5860	31	1.31	0.02	1.1	0.01	4.38	0.02	1.11	0.02	0	0
HD 164922	7.9	2.7	5439	38	0.7	0.01	0.93	0.02	4.45	0.03	0.95	0.02	0	0
HD 167042	3.1	0.3	4989	32	10.7	0.1	1.46	0.05	3.31	0.03	4.4	0.1	0	0
HD 168443	10.0	0.3	5646	36	2.08	0.01	1.02	0.01	4.08	0.01	1.51	0.02	0	0
HD 168746	12.0	0.9	5637	26	1.04	0.01	0.9	0.01	4.32	0.01	1.07	0.01	0	0
HD 169830	2.82	0.03	6276	12	4.656	0.003	1.3975	4.0E-4	4.052	0.004	1.83	0.01	0	0
HD 170469	4.7	0.9	5866	54	1.7	0.1	1.14	0.01	4.28	0.03	1.27	0.05	0	0
HD 171028	8.2	1.1	5771	46	3.9	0.5	0.98	0.04	3.84	0.03	2.0	0.2	0	0
HD 171238	4.0	1.2	5570	21	0.774	0.003	0.99	0.01	4.47	0.01	0.95	0.01	0	0
HD 17156	4.9	0.6	5943	38	2.46	0.05	1.2	0.03	4.17	0.02	1.48	0.03	0	1
HD 173416	1.8	0.7	4790	37	80	2	1.8	0.2	2.5	0.1	13.0	0.3	0	0
HD 175541	2.9	0.2	5093	23	10.0	0.1	1.45	0.03	3.37	0.02	4.07	0.05	0	0
HD 177830	10.2	1.7	4735	31	5.3	0.1	1.1	0.1	3.39	0.04	3.4	0.1	1	0
HD 178911 B	4.8	1.3	5642	29	1.00	0.02	1.03	0.02	4.4	0.02	1.05	0.02	1	0
HD 179079	7.8	0.4	5649	47	2.392	0.004	1.11	0.01	4.06	0.02	1.62	0.03	0	0
HD 179949	1.2	0.6	6220	28	1.95	0.01	1.23	0.01	4.36	0.01	1.2	0.01	0	0
HD 180314	0.9	0.2	4946	55	40	1	2.3	0.1	2.92	0.05	8.7	0.3	0	0
HD 180902	3.3	0.5	5001	44	9.4	0.1	1.4	0.1	3.36	0.04	4.1	0.1	0	0
HD 181342	3.6	0.6	4856	41	12.3	0.4	1.4	0.1	3.2	0.04	5.0	0.2	0	0
HD 181433	7.4	3.4	4909	20	0.34	0.01	0.84	0.02	4.55	0.02	0.8	0.02	0	0
HD 181720	12.4	0.5	5840	49	2.112	0.003	0.87	0.01	4.06	0.02	1.42	0.02	0	0
HD 183263	4.5	0.8	5870	56	1.8	0.1	1.16	0.02	4.28	0.03	1.29	0.05	0	0
HD 185269	4.1	0.5	6023	43	4.5	0.1	1.3	0.04	3.97	0.03	2.0	0.1	1	0
HD 187085	2.7	0.8	6163	53	2.0	0.1	1.19	0.02	4.31	0.03	1.26	0.04	0	0
HD 187123	5.6	1.3	5853	53	1.44	0.02	1.06	0.02	4.32	0.03	1.17	0.03	0	0
HD 18742	3.9	0.8	4956	40	14.0	0.2	1.3	0.1	3.14	0.04	5.1	0.1	0	0
HD 188015	5.9	1.3	5722	52	1.41	0.03	1.08	0.02	4.3	0.03	1.21	0.03	1	0
HD 189733	5.3	3.8	5019	23	0.327	0.003	0.81	0.02	4.58	0.02	0.76	0.01	1	1
HD 190360	7.3	1.6	5628	47	1.12	0.03	1.01	0.02	4.34	0.03	1.12	0.03	1	0
HD 190647	8.7	0.4	5630	48	2.19	0.01	1.07	0.01	4.07	0.02	1.56	0.03	0	0
HD 192263	5.9	3.9	4980	20	0.3	0.01	0.78	0.02	4.59	0.02	0.73	0.01	0	0
HD 192310	8.1	3.2	5153	21	0.4	0.01	0.82	0.02	4.54	0.02	0.79	0.01	0	0
HD 192699	3.1	0.4	5097	36	11.1	0.1	1.39	0.05	3.31	0.03	4.3	0.1	0	0
HD 195019	7.7	0.7	5825	56	2.23	0.02	1.08	0.01	4.13	0.02	1.47	0.04	1	0
HD 196050	5.4	0.7	5884	47	2.09	0.02	1.15	0.02	4.2	0.02	1.4	0.03	1	0
HD 19994	3.1	0.3	6164	62	3.78	0.04	1.35	0.01	4.1	0.02	1.71	0.04	1	0
HD 200964	3.1	0.4	5059	34	12.8	0.2	1.4	0.1	3.23	0.03	4.7	0.1	0	0
HD 202206	2.9	1.0	5719	26	1.04	0.01	1.07	0.02	4.43	0.02	1.04	0.01	0	0
HD 2039	4.4	0.9	5927	60	2.1	0.1	1.19	0.02	4.23	0.04	1.4	0.1	0	0
HD 204313	4.3	1.8	5783	48	1.18	0.03	1.06	0.03	4.39	0.04	1.08	0.03	0	0
HD 204941	3.9	3.3	5072	17	0.297	0.003	0.77	0.02	4.62	0.02	0.71	0.01	1	0
HD 205739	2.9	0.2	6247	40	3.581	0.003	1.335	0.003	4.14	0.01	1.62	0.02	0	0
HD 206610	3.0	0.3	4836	30	18	1	1.51	0.05	3.05	0.03	6.0	0.2	0	0
HD 20782	5.4	1.3	5876	31	1.20	0.03	1.01	0.02	4.39	0.03	1.06	0.03	1	0
HD 207832	1.4	0.8	5676	40	0.82	0.04	1.03	0.02	4.5	0.01	0.94	0.04	0	0
HD 20794	11.6	1.5	5602	20	0.642	0.003	0.8	0.01	4.47	0.02	0.85	0.01	0	0
HD 208487	2.3	0.9	6143	47	1.76	0.05	1.16	0.02	4.36	0.03	1.17	0.03	0	0

Table 2. continued.

Star	t (Gyr)	Δt (Gyr)	$T_{\rm eff}$ (K)	$\Delta T_{\rm eff}$ (K)	L ($L_\odot$)	ΔL ($L_\odot$)	M ($M_\odot$)	ΔM ($M_\odot$)	$\log g$ (cm/s^2)	$\Delta \log g$ (cm/s^2)	R ($R_\odot$)	ΔR ($R_\odot$)	Bin	Tr
HD 20868	8.2	2.7	4769	24	0.25	0.01	0.77	0.01	4.59	0.01	0.73	0.02	0	0
HD 209458	4.4	1.2	6047	62	1.8	0.04	1.11	0.02	4.3	0.04	1.22	0.04	0	1
HD 210277	8.8	1.9	5530	40	0.92	0.03	0.96	0.02	4.37	0.03	1.05	0.03	0	0
HD 210702	3.1	0.3	4946	25	12.9	0.1	1.47	0.04	3.22	0.02	4.9	0.1	0	0
HD 212771	2.9	0.1	5008	14	15.1	0.2	1.45	0.02	3.16	0.02	5.2	0.1	0	0
HD 213240	4.6	0.6	6029	37	2.6	0.1	1.2	0.02	4.17	0.02	1.48	0.03	1	0
HD 215497	9.9	2.8	5128	12	0.47	0.02	0.86	0.02	4.49	0.03	0.87	0.02	0	0
HD 216437	5.2	0.7	5898	37	2.23	0.03	1.17	0.03	4.19	0.02	1.43	0.03	0	0
HD 216770	5.4	2.9	5406	39	0.66	0.01	0.95	0.03	4.48	0.03	0.93	0.02	0	0
HD 217107	4.2	1.0	5676	31	1.14	0.01	1.08	0.01	4.38	0.02	1.11	0.02	0	0
HD 217786	6.8	0.9	6031	55	1.93	0.04	1.03	0.02	4.23	0.03	1.27	0.04	0	0
HD 218566	8.0	3.1	4880	16	0.3	0.01	0.8	0.01	4.57	0.02	0.77	0.02	0	0
HD 219828	5.2	0.8	5921	53	2.74	0.03	1.2	0.04	4.11	0.03	1.58	0.04	0	0
HD 220773	6.3	0.1	5852	26	3.16	0.01	1.154	0.003	4.02	0.01	1.73	0.02	0	0
HD 221287	2.8	0.3	6193	20	2.0	0.1	1.17	0.01	4.33	0.01	1.22	0.03	0	0
HD 222155	8.1	0.4	5814	43	2.9	0.1	1.05	0.01	4.00	0.01	1.7	0.1	0	0
HD 222582	6.2	1.1	5851	32	1.24	0.01	1.01	0.02	4.36	0.02	1.09	0.02	1	0
HD 224693	3.9	0.5	5972	49	4.1	0.1	1.35	0.04	4.01	0.01	1.89	0.05	0	0
HD 22781	7.5	2.9	5152	27	0.32	0.01	0.74	0.02	4.6	0.02	0.71	0.02	0	0
HD 23079	4.1	1.4	6039	44	1.37	0.03	1.03	0.02	4.39	0.03	1.07	0.03	0	0
HD 23127	4.4	0.6	5841	45	3.08	0.02	1.29	0.03	4.07	0.02	1.72	0.03	0	0
HD 231701	3.7	0.5	6211	71	2.94	0.05	1.23	0.01	4.18	0.03	1.48	0.05	0	0
HD 23596	4.0	0.7	5979	68	2.65	0.03	1.25	0.03	4.17	0.03	1.52	0.04	0	0
HD 24040	4.9	0.9	5910	53	1.78	0.05	1.13	0.02	4.27	0.03	1.27	0.04	0	0
HD 25171	4.8	0.9	6131	57	1.94	0.02	1.08	0.02	4.28	0.03	1.24	0.03	0	0
HD 2638	5.1	4.1	5173	26	0.42	0.01	0.87	0.03	4.55	0.03	0.81	0.02	0	0
HD 27894	6.9	4.3	4923	32	0.33	0.01	0.83	0.03	4.56	0.03	0.79	0.02	0	0
HD 28185	5.5	4.2	5615	56	1.17	0.02	1.0	0.1	4.33	0.03	1.15	0.03	0	0
HD 28254	7.8	0.4	5607	37	2.19	0.01	1.11	0.01	4.08	0.02	1.57	0.02	1	0
HD 28678	6.1	1.7	4798	43	24.0	0.4	1.1	0.1	2.8	0.1	7.1	0.2	0	0
HD 290327	11.5	1.3	5543	13	0.74	0.02	0.85	0.01	4.42	0.02	0.93	0.02	0	0
HD 2952	3.1	0.3	4755	18	61.5	0.4	1.5	0.1	2.47	0.02	11.6	0.1	0	0
HD 30177	5.9	1.1	5596	32	1.09	0.01	1.05	0.01	4.36	0.02	1.11	0.02	0	0
HD 30562	3.7	0.5	6000	55	2.8	0.02	1.28	0.02	4.16	0.02	1.55	0.03	0	0
HD 30856	7.3	1.8	4911	41	10.0	0.2	1.1	0.1	3.19	0.05	4.4	0.1	0	0
HD 31253	4.0	0.7	6105	63	2.9	0.1	1.25	0.04	4.16	0.03	1.5	0.1	0	0
HD 32518	5.8	1.5	4610	40	47	1	1.2	0.1	2.4	0.1	10.8	0.3	0	0
HD 330075	6.1	4.0	5127	26	0.4	0.03	0.84	0.02	4.55	0.03	0.8	0.04	0	0
HD 33142	3.3	0.4	4980	37	10.5	0.2	1.4	0.1	3.31	0.03	4.4	0.1	0	0
HD 33283	3.9	0.6	5980	54	4.43	0.02	1.37	0.04	3.98	0.03	1.97	0.04	0	0
HD 34445	3.7	0.6	6038	53	2.1	0.1	1.19	0.01	4.27	0.03	1.32	0.04	1	0
HD 3651	6.9	2.8	5271	26	0.51	0.01	0.88	0.02	4.51	0.02	0.86	0.01	1	0
HD 37124	11.1	1.7	5733	37	0.81	0.01	0.82	0.02	4.42	0.02	0.92	0.02	0	0
HD 37605	4.2	1.4	5364	25	0.62	0.01	0.96	0.01	4.49	0.01	0.91	0.02	0	0
HD 38283	6.5	0.6	6080	59	2.56	0.01	1.07	0.02	4.14	0.03	1.45	0.03	0	0
HD 38529	3.98	0.03	5526	17	5.81	0.03	1.412	0.003	3.74	0.01	2.64	0.02	1	0
HD 38801	4.8	0.3	5323	52	3.7	0.1	1.28	0.02	3.82	0.02	2.3	0.1	0	0
HD 39091	2.8	0.8	6018	31	1.5	0.02	1.12	0.01	4.37	0.02	1.13	0.02	0	0
HD 40307	6.9	4.0	4956	18	0.243	0.003	0.71	0.02	4.63	0.02	0.67	0.01	0	0
HD 40979	1.5	0.6	6163	25	1.82	0.03	1.21	0.01	4.36	0.02	1.19	0.02	1	0
HD 4113	5.8	1.6	5717	46	1.16	0.04	1.03	0.02	4.36	0.03	1.1	0.03	1	0
HD 4203	7.3	0.9	5640	57	1.71	0.02	1.09	0.02	4.2	0.03	1.37	0.04	0	0
HD 4208	7.4	2.4	5678	33	0.71	0.01	0.86	0.02	4.48	0.03	0.88	0.02	0	0
HD 4308	0.4	2.2	5674	51	1.02	0.03	0.96	0.03	4.37	0.02	1.05	0.03	0	0
HD 4313	3.0	0.3	4920	21	14.0	0.2	1.49	0.04	3.18	0.02	5.2	0.1	0	0
HD 43197	4.4	2.1	5457	33	0.75	0.02	1.00	0.02	4.46	0.03	0.97	0.03	0	0
HD 43691	2.1	1.7	6101	67	3.2	0.1	1.33	0.03	4.14	0.03	1.6	0.1	0	0
HD 44219	9.7	0.8	5739	50	1.82	0.02	1.01	0.01	4.16	0.02	1.37	0.03	0	0
HD 45350	7.1	0.9	5683	35	1.43	0.02	1.06	0.01	4.27	0.02	1.24	0.02	0	0
HD 45364	5.8	2.4	5523	28	0.575	0.004	0.86	0.02	4.53	0.02	0.83	0.01	0	0
HD 45652	5.4	2.7	5342	31	0.61	0.01	0.94	0.02	4.49	0.03	0.91	0.02	0	0
HD 46375	11.9	1.1	5379	19	0.77	0.01	0.91	0.01	4.38	0.01	1.01	0.01	1	0
HD 47186	5.3	0.8	5729	24	1.19	0.02	1.05	0.01	4.36	0.02	1.11	0.02	0	0
HD 49674	3.6	0.8	5655	25	0.99	0.02	1.06	0.01	4.42	0.01	1.04	0.02	0	0
HD 50499	2.3	0.4	6112	30	2.26	0.04	1.27	0.01	4.28	0.02	1.34	0.03	0	0
HD 50554	2.1	0.5	6047	17	1.37	0.01	1.1	0.01	4.41	0.01	1.07	0.01	0	0
HD 52265	2.2	0.7	6183	41	2.06	0.03	1.22	0.01	4.32	0.02	1.25	0.02	0	0
HD 5319	6.1	1.4	4888	39	8.2	0.1	1.2	0.1	3.3	0.04	4.0	0.1	0	0
HD 5608	3.0	0.3	4897	25	13.1	0.3	1.5	0.04	3.2	0.02	5.0	0.1	0	0
HD 5891	5.7	1.5	4796	41	39.1	0.4	1.1	0.1	2.57	0.05	9.1	0.2	0	0
HD 60532	3.0	0.2	6188	17	9.3	0.1	1.46	0.03	3.75	0.02	2.66	0.03	0	0
HD 63454	2.4	3.1	4787	12	0.24	0.01	0.79	0.01	4.62	0.02	0.72	0.01	0	0
HD 63765	7.9	3.1	5474	35	0.58	0.01	0.85	0.02	4.51	0.03	0.85	0.02	0	0
HD 6434	12.2	0.7	5907	21	1.208	0.003	0.83	0.01	4.31	0.01	1.05	0.01	0	0
HD 65216	4.6	3.1	5694	45	0.72	0.02	0.91	0.03	4.51	0.04	0.87	0.02	1	0
HD 66428	5.9	0.8	5721	29	1.28	0.02	1.06	0.01	4.33	0.02	1.15	0.02	0	0
HD 6718	6.2	2.0	5805	46	1.06	0.02	0.97	0.02	4.4	0.03	1.02	0.03	0	0
HD 68988	2.1	0.5	5880	21	1.34	0.02	1.15	0.01	4.39	0.01	1.12	0.02	0	0
HD 69830	10.4	2.5	5401	28	0.59	0.01	0.85	0.02	4.47	0.02	0.88	0.02	0	0
HD 70642	3.6	0.9	5675	18	0.92	0.01	1.02	0.01	4.45	0.01	0.99	0.01	0	0
HD 7199	9.2	2.5	5357	39	0.72	0.01	0.93	0.02	4.41	0.03	0.99	0.02	0	0
HD 72659	6.4	0.7	5994	50	2.09	0.02	1.08	0.02	4.21	0.02	1.34	0.03	0	0
HD 73256	4.5	2.3	5514	35	0.75	0.02	0.98	0.03	4.47	0.03	0.95	0.02	0	0

Table 2. continued.

Star	t (Gyr)	Δt (Gyr)	$T_{\rm eff}$ (K)	$\Delta T_{\rm eff}$ (K)	L ($L_\odot$)	ΔL ($L_\odot$)	M ($M_\odot$)	ΔM ($M_\odot$)	$\log g$ (cm/s^2)	$\Delta \log g$ (cm/s^2)	R ($R_\odot$)	ΔR ($R_\odot$)	Bin	Tr
HD 73267	11.8	1.4	5434	18	0.74	0.01	0.89	0.01	4.4	0.02	0.97	0.01	0	0
HD 73526	7.9	0.5	5669	53	2.18	0.01	1.09	0.01	4.1	0.02	1.53	0.03	0	0
HD 73534	7.1	0.8	4958	45	3.4	0.1	1.15	0.03	3.7	0.03	2.5	0.1	0	0
HD 74156	4.3	0.6	6070	56	3.08	0.03	1.24	0.04	4.12	0.03	1.59	0.04	0	0
HD 7449	2.2	1.3	6060	42	1.26	0.02	1.05	0.02	4.44	0.02	1.02	0.02	1	0
HD 75289	1.7	0.4	6143	25	1.97	0.01	1.23	0.01	4.33	0.01	1.24	0.01	1	0
HD 75898	3.8	0.6	6019	66	2.88	0.02	1.28	0.02	4.15	0.03	1.56	0.04	0	0
HD 76700	6.2	0.9	5706	41	1.73	0.03	1.13	0.02	4.22	0.03	1.35	0.03	0	0
HD 77338	7.8	3.4	5261	29	0.57	0.02	0.91	0.03	4.47	0.04	0.91	0.03	0	0
HD 7924	5.4	2.6	5218	12	0.36	0.01	0.79	0.01	4.59	0.02	0.74	0.01	0	0
HD 79498	4.2	0.9	5741	20	1.11	0.02	1.05	0.01	4.4	0.02	1.07	0.02	1	0
HD 80606	2.7	0.7	5558	23	0.81	0.02	1.03	0.01	4.47	0.01	0.97	0.02	1	1
HD 81040	3.6	1.5	5678	24	0.79	0.02	0.96	0.02	4.49	0.02	0.92	0.02	0	0
HD 81688	6.3	2.9	4830	64	54	1	1.1	0.2	2.4	0.1	10.5	0.4	0	0
HD 82886	3.3	0.5	5083	38	13.5	0.2	1.3	0.1	3.21	0.04	4.8	0.1	0	0
HD 82943	3.1	0.4	5944	18	1.54	0.02	1.14	0.01	4.35	0.01	1.17	0.02	0	0
HD 83443	5.2	1.9	5458	28	0.76	0.02	0.99	0.02	4.45	0.03	0.98	0.02	0	0
HD 8535	3.3	0.5	6142	34	1.92	0.01	1.15	0.01	4.31	0.02	1.23	0.02	0	0
HD 85390	6.8	2.9	5174	17	0.39	0.01	0.81	0.02	4.56	0.02	0.78	0.01	0	0
HD 85512	8.2	3.0	4530	8	0.138	0.002	0.64	0.01	4.67	0.01	0.6	0.01	0	0
HD 8574	4.4	0.6	6092	56	2.35	0.04	1.17	0.02	4.22	0.03	1.38	0.04	0	0
HD 86081	5.5	0.9	5887	56	2.51	0.02	1.18	0.04	4.14	0.03	1.53	0.03	0	0
HD 86264	0.8	0.2	6616	39	4.02	0.04	1.46	0.01	4.23	0.02	1.53	0.02	0	0
HD 87883	7.5	3.8	4971	22	0.327	0.004	0.81	0.02	4.56	0.02	0.77	0.01	0	0
HD 88133	5.7	0.3	5468	25	3.4	0.1	1.23	0.02	3.9	0.02	2.1	0.1	0	0
HD 89307	4.6	1.7	6011	59	1.34	0.03	1.02	0.03	4.38	0.03	1.07	0.03	0	0
HD 89744	2.5	0.3	6270	54	6.29	0.01	1.49	0.02	3.95	0.02	2.13	0.04	1	0
HD 90156	5.7	1.7	5721	28	0.74	0.01	0.89	0.02	4.49	0.02	0.88	0.01	0	0
HD 92788	4.2	1.1	5788	38	1.28	0.02	1.09	0.02	4.36	0.02	1.13	0.02	0	0
HD 93083	6.2	4.4	5025	21	0.35	0.02	0.83	0.02	4.57	0.03	0.78	0.02	0	0
HD 9446	3.7	2.0	5790	45	1.06	0.03	1.04	0.03	4.43	0.03	1.03	0.03	0	0
HD 95089	3.0	0.2	4952	19	13.0	0.1	1.48	0.04	3.22	0.02	4.9	0.1	0	0
HD 96063	2.9	0.2	5073	19	12.3	0.1	1.42	0.03	3.27	0.01	4.5	0.1	0	0
HD 96127	7.2	2.1	3943	34	516	22	1.0	0.1	1.1	0.1	48.8	1.9	0	0
HD 96167	4.7	0.6	5753	49	3.7	0.2	1.3	0.1	3.97	0.02	1.9	0.1	0	0
HD 97658	9.7	2.8	5211	16	0.35	0.01	0.74	0.01	4.58	0.02	0.73	0.01	0	1
HD 98219	3.2	0.4	4952	31	11.4	0.3	1.5	0.1	3.27	0.03	4.6	0.1	0	0
HD 99109	6.0	3.0	5270	24	0.56	0.02	0.93	0.02	4.49	0.03	0.9	0.03	0	0
HD 99492	8.1	3.2	4917	21	0.33	0.01	0.82	0.02	4.55	0.02	0.79	0.02	1	0
HD 99706	2.9	0.2	4847	17	15.6	0.1	1.53	0.03	3.12	0.02	5.6	0.1	0	0
HIP 14810	7.1	2.1	5570	47	0.99	0.03	1.00	0.02	4.37	0.04	1.07	0.04	0	0
HIP 5158	4.5	3.2	4571	14	0.19	0.01	0.75	0.01	4.63	0.02	0.69	0.02	0	0
HIP 57050	8.8	3.6	3542	2	0.0068	2.0E-4	0.2	0.0	5.05	0.01	0.219	0.003	0	0
HIP 57274	8.9	2.1	4636	35	0.2	0.01	0.72	0.01	4.61	0.01	0.69	0.03	0	0
kappa CrB	3.2	0.4	4899	30	11.8	0.2	1.5	0.1	3.24	0.03	4.8	0.1	0	0
KELT-3	1.8	1.2	6413	55	3.3	0.1	1.3	0.02	4.2	0.01	1.5	0.1	0	1
KELT-6	2.6	2.8	6267	46	3.8	0.6	1.2	0.1	4.1	0.1	1.7	0.1	0	1
Kepler-21	3.7	0.4	6264	60	5.20	0.04	1.31	0.03	3.97	0.02	1.94	0.04	0	1
Kepler-37	3.3	0.6	5630	9	0.559	0.002	0.85	0.01	4.57	0.01	0.787	0.004	0	1
Kepler-68	6.1	0.5	5868	32	1.62	0.03	1.07	0.01	4.28	0.01	1.23	0.03	0	1
mu Ara	5.4	0.7	5817	44	1.78	0.04	1.14	0.02	4.25	0.03	1.32	0.04	0	0
NGC 2423 3	6.7	3.0	4446	26	73	14	1.2	0.2	2.19	0.01	14.4	1.6	0	0
Qatar-1	6.9	3.8	4730	15	0.24	0.01	0.78	0.02	4.59	0.02	0.73	0.01	0	1
tau Boo	1.8	0.4	6408	45	3.11	0.04	1.33	0.01	4.24	0.02	1.43	0.03	1	0
TrES-1	9.5	3.1	5492	57	0.77	0.02	0.91	0.03	4.42	0.04	0.97	0.03	0	1
TrES-2	5.0	1.0	5958	65	1.7	0.1	1.09	0.03	4.3	0.01	1.2	0.1	0	1
TrES-3	7.9	1.4	5614	29	0.77	0.01	0.9	0.02	4.45	0.01	0.93	0.02	0	1
TrES-4	2.1	0.1	6327	25	3.42	0.04	1.37	0.01	4.192	0.004	1.54	0.02	0	1
TrES-5	7.5	3.7	5087	31	0.41	0.01	0.85	0.03	4.53	0.03	0.82	0.02	0	1
WASP-11	5.7	2.1	4917	18	0.29	0.01	0.79	0.01	4.59	0.01	0.74	0.02	0	1
WASP-14	1.5	1.4	6454	52	4.2	0.5	1.33	0.04	4.13	0.03	1.7	0.1	0	1
WASP-16	8.5	1.2	5633	49	1.09	0.04	0.98	0.02	4.34	0.01	1.1	0.04	0	1
WASP-18	0.9	0.2	6167	7	1.7	0.04	1.2	0.001	4.39	0.01	1.15	0.02	0	1
WASP-19	3.6	1.8	5526	39	0.76	0.01	1.00	0.02	4.47	0.02	0.95	0.02	0	1
WASP-2	0.7	0.3	5345	8	0.47	0.01	0.9	0.001	4.581	0.004	0.8	0.01	0	1
WASP-21	3.7	0.7	6123	38	1.43	0.03	1.03	0.02	4.39	0.01	1.06	0.02	0	1
WASP-25	3.2	1.2	5582	21	0.72	0.02	0.97	0.01	4.5	0.01	0.91	0.02	0	1
WASP-26	3.1	0.4	5881	13	1.26	0.01	1.09	0.01	4.4	0.01	1.08	0.01	0	1
WASP-34	6.8	1.3	5758	55	1.19	0.03	1.01	0.02	4.35	0.02	1.1	0.04	0	1
WASP-37	7.7	1.4	5956	55	1.1	0.04	0.9	0.02	4.39	0.02	0.99	0.04	0	1
WASP-39	6.7	2.4	5466	34	0.57	0.01	0.86	0.02	4.51	0.02	0.85	0.01	0	1
WASP-4	5.5	2.0	5435	31	0.6	0.01	0.91	0.02	4.51	0.02	0.88	0.01	0	1
WASP-41	3.9	1.0	5555	27	0.7	0.02	0.96	0.01	4.5	0.01	0.91	0.02	0	1
WASP-43	2.4	2.3	4756	12	0.215	0.002	0.75	0.01	4.64	0.01	0.68	0.01	0	1
WASP-44	6.8	2.8	5402	31	0.6	0.02	0.9	0.02	4.49	0.03	0.89	0.02	0	1
WASP-48	9.1	0.8	5770	53	2.6	0.2	1.01	0.02	4.03	0.01	1.6	0.1	0	1
WASP-5	2.5	0.7	5611	14	0.79	0.02	1.01	0.01	4.49	0.01	0.94	0.01	0	1
WASP-52	3.8	2.6	5077	14	0.348	0.004	0.83	0.02	4.58	0.02	0.76	0.01	0	1
WASP-54	3.3	0.4	6090	26	1.61	0.02	1.1	0.01	4.36	0.01	1.14	0.02	0	1
WASP-58	12.6	0.1	5874	5	1.23	0.01	0.839	0.002	4.2936	1.0E-4	1.073	0.005	0	1
WASP-60	8.8	1.4	5730	52	1.09	0.03	0.95	0.02	4.36	0.02	1.06	0.04	0	1
WASP-75	2.9	0.2	5862	9	1.1	0.01	1.051	0.004	4.435	0.002	1.02	0.01	0	1
WASP-8	4.2	1.1	5632	34	0.96	0.02	1.04	0.02	4.42	0.01	1.03	0.02	1	1

Table 2. continued.

Star	t (Gyr)	Δt (Gyr)	$T_{\rm eff}$ (K)	$\Delta T_{\rm eff}$ (K)	L ($L_\odot$)	ΔL ($L_\odot$)	M ($M_\odot$)	ΔM ($M_\odot$)	$\log g$ (cm/s^2)	$\Delta \log g$ (cm/s^2)	R ($R_\odot$)	ΔR ($R_\odot$)	Bin	Tr
XO-2	9.6	0.9	5474	54	1.7	0.1	1.04	0.03	4.13	0.01	1.4	0.1	1	1
XO-3	1.7	1.0	6685	45	3.7	0.1	1.26	0.01	4.22	0.01	1.43	0.04	0	1
XO-5	12.4	0.6	5452	12	0.794	0.004	0.89	0.01	4.38	0.01	1.00	0.01	0	1

Chapter 5

Conclusions

Computing the ages of stars is a challenging and difficult task because age is related to the inner stellar core, while we are almost limited to observe the stellar surface. Several indicators enable to evaluate the age of a star, but the sensitivity of some of them can span a different range of age or mass.

This thesis describes the development of two algorithms aiming at determining the ages of single field stars using theoretical evolutionary tracks and isochrones. One is the isochrone placement, that selects the best theoretical age on the basis of the closeness between a star and an isochrone in terms of metallicity, $\log T_{\rm eff}$, $\log L$, $\log g$ and M. If available, additional observables such as $v \sin i$, $\log R'_{\rm HK}$ and $\rho_\star$ are employed to better constrain the output age. The other algorithm, i.e. the Bayesian estimation technique, is based on another statistical approach. It requires to build the posterior probability density function of age starting from a Gaussian likelihood that involves metallicity, temperature and luminosity and a prior initial mass function.

We compared the reliability of the two algorithms by testing them on different coeval samples of synthetic stars, whose ages were a priori known. We found that the isochrone placement technique selects the expected ages in the $\sim 80\%$ of the cases. Instead, the Bayesian estimation technique gives age distributions that are less peaked around the true age and their modal values typically underestimate age. Jørgensen and Lindegren (2005) already pointed out that this technique tends to select the outmost age values available in the grids, nevertheless we mitigated this effect, in fact now it arises for $\sim 15\%$ of the synthetic stars (it was 70% with the Jørgensen and Lindegren 2005 implementation).

The reliability of the output age depends also on the position of a star on the CMD. The age may sensibly differ from the expected one in the case of very dim stars (low-MS region) and very bright stars (RGB region). Given that the analyzed stars are synthetic, problems are due to errors in the in-

terpolation scheme, that enables to retrieve all the needed input parameters. In the very low MS-region, interpolation is difficult because not many points are available in the grid, since we are just at the beginning of the isochrones. In the RGB region furher difficulties arise because the isochrones have a strongly not-linear shape and overlap in several points.

Along the MS, the age is very well determined because the shape of the isochrones is linear. But this happens only because here we are dealing with synthetic stars having input parameters exactly corresponding to the theoretical ones. In the case of real stars, all the input parameters required by the algorithm would likely differ from the theoretical ones. Because of the closeness of MS isochrones, the ages of MS stars would be characterized by quite a high uncertainty.

We also simulate the expected dispersion of a coeval group of stars around the nominal age value by inserting a slight random perturbation in the input parameters. The isochrone placement technique gives distributions that are peaked around the nominal age values and result to be less scattered over the entire age range, if compared with the Bayesian estimation technique. The two algorithms address the age errors in a different way. The age relative uncertainties carried out by the Bayesian estimation technique are generally higher at least by a factor of 2 than the ones given by the isochrone placement. In addition, in the case of the isochrone placement, the median uncertainties of the age of the perturbed synthetic samples are around $\sim$ 20-40%, that are a factor of 10 higher with respect to the typical age uncertainties affecting the unperturbed samples of stars.

We also recall that the age uncertainties given by the algorithms are internal and based upon the error propagation of the input data. In other words, age uncertainties do not take the uncertainties due to stellar theoretical models into account. This means that the actual age uncertainty of a star is likely higher than the formal one given here, especially in the case of the isochrone placement.

Also Lebreton et al. (2014) confirm that it is not easy to provide ages with realistic error bars, because different evolutionary models likely use different input physics. The European working group ESTA-CoRoT has compared the ages given by models that use ten different stellar evolutionary codes. They found that the mean relative differences are in the range 1-12%, while the maximum differences span the 2-43% range. Considering only the codes that adopt, as far as possible, the same input physics and astronomical constants, the differences are reduced by a factor of 2. These conclusions highlight that the ages of an individual star obtained with different sets of theoretical models can be sensibly different. In some research contexts it is necessary to provide the ages of individual stars after a star-by-star analysis of a sam-

ple, like in the case of the characterization of stars for the future CHEOPS mission (Broeg et al., 2013). In that situation, the input physics of different theoretical models would have to be changed to investigate the possible range spanned by the stellar age and then provide realistical ages and error bars. Anyway, because of the homogeneous statistical treatment and the number of input parameters they accept, the algorithms we provide represent a significant step forward towards the evaluation of ages of individual stars. In this regard, our age determinations represent the best estimations of stellar ages, among the ones that are currently available in the literature. In this thesis, in particular, we concentrated on the evolutionary analysis of entire samples of stars, like the one made of stars with planets or the one made of stars of the solar neighbourhood. Comparing the age distributions of the different samples, we provided a relative comparison of the evolutionary stage, without considering the individual ages of stars. Therefore, our results can be judged statistically robust and reliable.

It is also quite hard to find out the input observable that affect the output age most. We considered our Sun as reference and firstly derived its reference age through the isochrone placement. Then, we alternatively perturbed its input magnitude, colour index and surface gravity to test how the output age is sensitive to the input parameters. Variations with respect to the output reference age may amount from zero to $\sim 40\%$. In this particular cases the $B-V$ perturbation produce the most evident age variations, but it is possible that this is also due to the shape of the isochrones on the MS. It is likely that around the "hook" of TO where isochrones appear almost horizontal on the CMD, a slight $B-V$ variation does not impact the age very much. Stellar input magnitude is probably critical in affecting the age of a star located around the TO, while instead Tab. 4.3 shows that an input perturbation $\Delta V = -0.01$ mag does not produce even a variation on the age if the star is located on the MS.

The validation tests applied to our custom-developed algorithms prove the reliability of our isochrone placement technique, that we use for analysing real stars. The data analysis has been divided in two parts. The first one investigates whether stars that harbour transiting planets (TPH) are different from planet-hosting stars taken from radial velocity surveys (SH) from an evolutionary point of view. Even if spectroscopic targets could be chosen according to different criteria with respect to photometric targets, however once a possible transiting planet has been detected, then the confirmation process involves spectroscopic analysis. Therefore, TPH and SH seem to be characterized by the same selection effects, which bring the median ages of the two distribution around the solar age value.

In the second part we compared the age distribution of all the planet-

hosting stars (SWP) with that of a broad sample of stars belonging to the solar neighbourhood (RSN) and that are similar to our SWP in terms of spectral type. We found that SWP show no evolutionary peculiarities if compared with RSN, having both a median age of ~ 4.8 Gyr. So there is no reason to exclude that planets around stars are very common, at least around stars with spectral type ranging from late-F to early-K.

In addition, we saw that planets are found both around young and old stars. This means that any dynamical phenomenon leading to planets disruption does not act (at least on a time-scale of some Gyrs).

We also said that both SWP and RSN have a median age of ~ 4.8 Gyr. This is not fully in agreement with the younger age that is assumed for the thin disc. But, actually, we sampled only a limited portion of the disc and we concentrated our attention almost only to G-type stars. Analysing stars farther than 200 pc, it would be possible to check if the ratio between the number of stars younger and older than the Sun reflects the one we found for $d < 200$ pc. As a preliminary answer, we can say that in deeper surveys we expect to include also young star forming regions, such as the Orion Nebula or the Taurus-Auriga complex. It is likely that many young stars would be added to our sample, bringing the age distribution in agreement with the one expected for thin disc stars. In any case, this kind of analysis will enable to check our knowledge about disc and stellar population evolution.

Appendix. List of publications

1. Bonfanti, A., Ortolani, S., and Nascimbeni, V. Age consistency between exoplanet hosts and field stars. A& A, 585:A5, January 2016. doi: 10.1051/0004-6361/201527297.

2. Rossi, L. J., Ortolani, S., Barbuy, B., Bica, E., and Bonfanti, A. Proper motions and kinematics of selected bulge globular clusters. MNRAS, 450:3270-3288, July 2015. doi: 10.1093/mnras/stv748.

3. Bonfanti, A., Ortolani, S., Piotto, G., and Nascimbeni, V. Revising the ages of planet-hosting stars. A& A, 575:A18, March 2015. doi: 10.1051/0004-6361/201424951.

4. Borsato, L., Bonfanti, A., Tomasella, L., Benetti, S., Cappellaro, E., Elias-Rosa, N., Pastorello, A., and Turatto, M. Asiago spectroscopic observation of PSN J22081243+4110503. The Astronomer's Telegram, 6621, October 2014.

5. Boles, T., James, N., Balam, D. D., Graham, M. L., Hsiao, E. Y., Dennefeld, M., Bonfanti, A., Dervisoglu, A., Narloch, W., and Zejmo, M. Supernova 2013ed = Psn J16162429+5153057. Central Bureau Electronic Telegrams, 3596, July 2013.

Bibliography

Allende Prieto, C. The Stellar Population of the Thin Disk. In Cunha, K., Spite, M., and Barbuy, B., editors, *IAU Symposium*, volume 265 of *IAU Symposium*, pages 304–312, March 2010. doi: 10.1017/S1743921310000785.

Alongi, M., Bertelli, G., Bressan, A., and Chiosi, C. Effects of envelope overshoot on stellar models. *A&A*, 244:95–106, April 1991.

Angulo, C., Arnould, M., Rayet, M., Descouvemont, P., Baye, D., Leclercq-Willain, C., Coc, A., Barhoumi, S., Aguer, P., Rolfs, C., Kunz, R., Hammer, J. W., Mayer, A., Paradellis, T., Kossionides, S., Chronidou, C., Spyrou, K., degl'Innocenti, S., Fiorentini, G., Ricci, B., Zavatarelli, S., Providencia, C., Wolters, H., Soares, J., Grama, C., Rahighi, J., Shotter, A., and Lamehi Rachti, M. A compilation of charged-particle induced thermonuclear reaction rates. *Nuclear Physics A*, 656:3–183, August 1999. doi: 10.1016/S0375-9474(99)00030-5.

Aringer, B., Girardi, L., Nowotny, W., Marigo, P., and Lederer, M. T. Synthetic photometry for carbon rich giants. I. Hydrostatic dust-free models. *A&A*, 503:913–928, September 2009. doi: 10.1051/0004-6361/200911703.

Asplund, M., Grevesse, N., and Sauval, A. J. The Solar Chemical Composition. In Barnes, T. G., III and Bash, F. N., editors, *Cosmic Abundances as Records of Stellar Evolution and Nucleosynthesis*, volume 336 of *Astronomical Society of the Pacific Conference Series*, page 25, September 2005.

Asplund, M., Grevesse, N., Sauval, A. J., and Scott, P. The Chemical Composition of the Sun. *ARA&A*, 47:481–522, September 2009. doi: 10.1146/annurev.astro.46.060407.145222.

Bailey, J. E., Nagayama, T., Loisel, G. P., Rochau, G. A., Blancard, C., Colgan, J., Cosse, P., Faussurier, G., Fontes, C. J., Gilleron, F., Golovkin, I.,

Hansen, S. B., Iglesias, C. A., Kilcrease, D. P., Macfarlane, J. J., Mancini, R. C., Nahar, S. N., Orban, C., Pain, J.-C., Pradhan, A. K., Sherrill, M., and Wilson, B. G. A higher-than-predicted measurement of iron opacity at solar interior temperatures. *Nature*, 517:56–59, January 2015. doi: 10.1038/nature14048.

Baliunas, S. L., Donahue, R. A., Soon, W., Gilliland, R., and Soderblom, D. R. Chromospheric Activity and Age of Solar-Type Stars. In *American Astronomical Society Meeting Abstracts #186*, volume 27 of *Bulletin of the American Astronomical Society*, page 839, March 1995a.

Baliunas, S. L., Donahue, R. A., Soon, W. H., Horne, J. H., Frazer, J., Woodard-Eklund, L., Bradford, M., Rao, L. M., Wilson, O. C., Zhang, Q., Bennett, W., Briggs, J., Carroll, S. M., Duncan, D. K., Figueroa, D., Lanning, H. H., Misch, T., Mueller, J., Noyes, R. W., Poppe, D., Porter, A. C., Robinson, C. R., Russell, J., Shelton, J. C., Soyumer, T., Vaughan, A. H., and Whitney, J. H. Chromospheric variations in main-sequence stars. *ApJ*, 438:269–287, January 1995b. doi: 10.1086/175072.

Barker, A. J. and Ogilvie, G. I. On the tidal evolution of Hot Jupiters on inclined orbits. *MNRAS*, 395:2268–2287, June 2009. doi: 10.1111/j.1365-2966.2009.14694.x.

Barnes, S. A. Gyrochronology and its usage for main sequence field star ages. In Mamajek, E. E., Soderblom, D. R., and Wyse, R. F. G., editors, *IAU Symposium*, volume 258 of *IAU Symposium*, pages 345–356, June 2009. doi: 10.1017/S1743921309032001.

Barnes, S. A. A Simple Nonlinear Model for the Rotation of Main-sequence Cool Stars. I. Introduction, Implications for Gyrochronology, and Color-Period Diagrams. *ApJ*, 722:222–234, October 2010. doi: 10.1088/0004-637X/722/1/222.

Barnes, S. A. and Kim, Y.-C. Angular Momentum Loss from Cool Stars: An Empirical Expression and Connection to Stellar Activity. *ApJ*, 721:675, September 2010. doi: 10.1088/0004-637X/721/1/675.

Basu, S. and Antia, H. M. Revisiting the Issue of Solar Abundances. *Journal of Physics Conference Series*, 440(1):012017, June 2013. doi: 10.1088/1742-6596/440/1/012017.

Böhm-Vitense, E. Über die Wasserstoffkonvektionszone in Sternen verschiedener Effektivtemperaturen und Leuchtkräfte. Mit 5 Textabbildungen. *ZAp*, 46:108, 1958.

Bonfanti, A., Ortolani, S., Piotto, G., and Nascimbeni, V. Revising the ages of planet-hosting stars. *A&A*, 575:A18, March 2015. doi: 10.1051/0004-6361/201424951.

Bonfanti, A., Ortolani, S., and Nascimbeni, V. Age consistency between exoplanet hosts and field stars. *A&A*, 585:A5, January 2016. doi: 10.1051/0004-6361/201527297.

Bressan, A., Fagotto, F., Bertelli, G., and Chiosi, C. Evolutionary sequences of stellar models with new radiative opacities. II - Z = 0.02. *A&AS*, 100: 647–664, September 1993.

Bressan, A., Marigo, P., Girardi, L., Salasnich, B., Dal Cero, C., Rubele, S., and Nanni, A. PARSEC: stellar tracks and isochrones with the PAdova and TRieste Stellar Evolution Code. *MNRAS*, 427:127–145, November 2012. doi: 10.1111/j.1365-2966.2012.21948.x.

Bressan, A. G., Chiosi, C., and Bertelli, G. Mass loss and overshooting in massive stars. *A&A*, 102:25–30, September 1981.

Broeg, C., Fortier, A., Ehrenreich, D., Alibert, Y., Baumjohann, W., Benz, W., Deleuil, M., Gillon, M., Ivanov, A., Liseau, R., Meyer, M., Oloffson, G., Pagano, I., Piotto, G., Pollacco, D., Queloz, D., Ragazzoni, R., Renotte, E., Steller, M., and Thomas, N. CHEOPS: A transit photometry mission for ESA's small mission programme. In *European Physical Journal Web of Conferences*, volume 47 of *European Physical Journal Web of Conferences*, page 3005, April 2013. doi: 10.1051/epjconf/20134703005.

Broggini, C., Bemmerer, D., Guglielmetti, A., and Menegazzo, R. LUNA: Nuclear Astrophysics Deep Underground. *Annual Review of Nuclear and Particle Science*, 60:53–73, November 2010. doi: 10.1146/annurev.nucl.012809.104526.

Brown, D. J. A. Discrepancies between isochrone fitting and gyrochronology for exoplanet host stars? *MNRAS*, 442:1844–1862, August 2014. doi: 10.1093/mnras/stu950.

Burgers, J. *Flow equations for composites gases.* Academic Press, New York, 1969.

Caffau, E. and Ludwig, H.-G. The forbidden 1082 nm line of sulphur: the photospheric abundance of sulphur in the Sun and 3D effects. *A&A*, 467: L11–L14, May 2007. doi: 10.1051/0004-6361:20077234.

Caffau, E., Steffen, M., Sbordone, L., Ludwig, H.-G., and Bonifacio, P. The solar photospheric abundance of phosphorus: results from CO^5BOLD 3D model atmospheres. *A&A*, 473:L9–L12, October 2007. doi: 10.1051/0004-6361:20078370.

Caffau, E., Ludwig, H.-G., Steffen, M., Ayres, T. R., Bonifacio, P., Cayrel, R., Freytag, B., and Plez, B. The photospheric solar oxygen project. I. Abundance analysis of atomic lines and influence of atmospheric models. *A&A*, 488:1031–1046, September 2008. doi: 10.1051/0004-6361:200809885.

Caffau, E., Maiorca, E., Bonifacio, P., Faraggiana, R., Steffen, M., Ludwig, H.-G., Kamp, I., and Busso, M. The solar photospheric nitrogen abundance. Analysis of atomic transitions with 3D and 1D model atmospheres. *A&A*, 498:877–884, May 2009. doi: 10.1051/0004-6361/200810859.

Caffau, E., Ludwig, H.-G., Bonifacio, P., Faraggiana, R., Steffen, M., Freytag, B., Kamp, I., and Ayres, T. R. The solar photospheric abundance of carbon. Analysis of atomic carbon lines with the CO5BOLD solar model. *A&A*, 514:A92, May 2010. doi: 10.1051/0004-6361/200912227.

Caffau, E., Ludwig, H.-G., Steffen, M., Freytag, B., and Bonifacio, P. Solar Chemical Abundances Determined with a CO5BOLD 3D Model Atmosphere. *Sol. Phys.*, 268:255–269, February 2011. doi: 10.1007/s11207-010-9541-4.

Canuto, V. M. and Mazzitelli, I. Stellar turbulent convection - A new model and applications. *ApJ*, 370:295–311, March 1991. doi: 10.1086/169815.

Canuto, V. M., Goldman, I., and Mazzitelli, I. Stellar Turbulent Convection: A Self-consistent Model. *ApJ*, 473:550, December 1996. doi: 10.1086/178166.

Casagrande, L., Schönrich, R., Asplund, M., Cassisi, S., Ramírez, I., Meléndez, J., Bensby, T., and Feltzing, S. New constraints on the chemical evolution of the solar neighbourhood and Galactic disc(s). Improved astrophysical parameters for the Geneva-Copenhagen Survey. *A&A*, 530: A138, June 2011. doi: 10.1051/0004-6361/201016276.

Cassisi, S., Potekhin, A. Y., Pietrinferni, A., Catelan, M., and Salaris, M. Updated Electron-Conduction Opacities: The Impact on Low-Mass Stellar Models. *ApJ*, 661:1094–1104, June 2007. doi: 10.1086/516819.

Castellani, V., degl'Innocenti, S., and Marconi, M. Theoretical stellar models for old galactic clusters. *MNRAS*, 303:265–274, February 1999. doi: 10.1046/j.1365-8711.1999.02193.x.

Chaboyer, B., Fenton, W. H., Nelan, J. E., Patnaude, D. J., and Simon, F. E. Heavy-Element Diffusion in Metal-poor Stars. *ApJ*, 562:521–527, November 2001. doi: 10.1086/323872.

Chabrier, G. The Galactic Disk Mass Budget. I. Stellar Mass Function and Density. *ApJ*, 554:1274–1281, June 2001. doi: 10.1086/321401.

Chaplin, W. J., Basu, S., Huber, D., Serenelli, A., Casagrande, L., Silva Aguirre, V., Ball, W. H., Creevey, O. L., Gizon, L., Handberg, R., Karoff, C., Lutz, R., Marques, J. P., Miglio, A., Stello, D., Suran, M. D., Pricopi, D., Metcalfe, T. S., Monteiro, M. J. P. F. G., Molenda-Żakowicz, J., Appourchaux, T., Christensen-Dalsgaard, J., Elsworth, Y., García, R. A., Houdek, G., Kjeldsen, H., Bonanno, A., Campante, T. L., Corsaro, E., Gaulme, P., Hekker, S., Mathur, S., Mosser, B., Régulo, C., and Salabert, D. Asteroseismic Fundamental Properties of Solar-type Stars Observed by the NASA Kepler Mission. *ApJS*, 210:1, January 2014. doi: 10.1088/0067-0049/210/1/1.

Chapman, S. and Cowling, T. G. *The mathematical theory of non-uniform gases. an account of the kinetic theory of viscosity, thermal conduction and diffusion in gases*. Cambridge: University Press, 1970, 3rd ed.

Chaussidon, M. *Formation of the Solar system: a chronology based on meteorites*, pages 45–74. Gargaud, M. and Martin, H. and Claeys, P., Berlin: Springer-Verlag, 2007.

Christensen-Dalsgaard, J., Monteiro, M. J. P. F. G., Rempel, M., and Thompson, M. J. A more realistic representation of overshoot at the base of the solar convective envelope as seen by helioseismology. *MNRAS*, 414: 1158–1174, June 2011. doi: 10.1111/j.1365-2966.2011.18460.x.

Collier Cameron, A., Davidson, V. A., Hebb, L., Skinner, G., Anderson, D. R., Christian, D. J., Clarkson, W. I., Enoch, B., Irwin, J., Joshi, Y., Haswell, C. A., Hellier, C., Horne, K. D., Kane, S. R., Lister, T. A., Maxted, P. F. L., Norton, A. J., Parley, N., Pollacco, D., Ryans, R., Scholz, A., Skillen, I., Smalley, B., Street, R. A., West, R. G., Wilson, D. M., and Wheatley, P. J. The main-sequence rotation-colour relation in the Coma Berenices open cluster. *MNRAS*, 400:451–462, November 2009. doi: 10.1111/j.1365-2966.2009.15476.x.

De Marchi, G., Panagia, N., and Romaniello, M. Photometric Determination of the Mass Accretion Rates of Pre-main-sequence Stars. I. Method and Application to the SN 1987A Field. *ApJ*, 715:1–17, May 2010. doi: 10.1088/0004-637X/715/1/1.

De Marchi, G., Panagia, N., Romaniello, M., Sabbi, E., Sirianni, M., Prada Moroni, P. G., and Degl'Innocenti, S. Photometric Determination of the Mass Accretion Rates of Pre-main-sequence Stars. II. NGC 346 in the Small Magellanic Cloud. *ApJ*, 740:11, October 2011. doi: 10.1088/0004-637X/740/1/11.

degl'Innocenti, S., Fiorentini, G., and Ricci, B. Helioseismology and $p+p \rightarrow d+e^{+}+\nu_e$ in the sun. *Physics Letters B*, 416:365–368, January 1998. doi: 10.1016/S0370-2693(97)01197-0.

Denissenkov, P. A. A Model of Magnetic Braking of Solar Rotation that Satisfies Observational Constraints. *ApJ*, 719:28–44, August 2010. doi: 10.1088/0004-637X/719/1/28.

Dorren, J. D. and Guinan, E. F. HD 129333: The Sun in its infancy. *ApJ*, 428:805–818, June 1994. doi: 10.1086/174289.

Dullemond, C. P., Hollenbach, D., Kamp, I., and D'Alessio, P. Models of the Structure and Evolution of Protoplanetary Disks. *Protostars and Planets V*, pages 555–572, 2007.

Duncan, D. K., Vaughan, A. H., Wilson, O. C., Preston, G. W., Frazer, J., Lanning, H., Misch, A., Mueller, J., Soyumer, D., Woodard, L., Baliunas, S. L., Noyes, R. W., Hartmann, L. W., Porter, A., Zwaan, C., Middelkoop, F., Rutten, R. G. M., and Mihalas, D. CA II H and K measurements made at Mount Wilson Observatory, 1966-1983. *ApJS*, 76:383–430, May 1991. doi: 10.1086/191572.

Eggenberger, P., Maeder, A., and Meynet, G. Effects of rotation and magnetic fields on the lithium abundance and asteroseismic properties of exoplanet-host stars. *A&A*, 519:L2, September 2010. doi: 10.1051/0004-6361/201014939.

Ekström, S., Georgy, C., Eggenberger, P., Meynet, G., Mowlavi, N., Wyttenbach, A., Granada, A., Decressin, T., Hirschi, R., Frischknecht, U., Charbonnel, C., and Maeder, A. Grids of stellar models with rotation. I. Models from 0.8 to 120 $M_{\odot}$ at solar metallicity (Z = 0.014). *A&A*, 537: A146, January 2012. doi: 10.1051/0004-6361/201117751.

Fontaine, G., Brassard, P., and Bergeron, P. The Potential of White Dwarf Cosmochronology. *PASP*, 113:409–435, April 2001. doi: 10.1086/319535.

Formicola, A. and LUNA Collaboration. Re-investigation of the ^{14}N(p,γ)^{15}O reaction within LUNA collaboration. In Hillebrandt, W. and Müller, E., editors, *Nuclear Astrophysics*, pages 111–114, April 2002.

Formicola, A., Imbriani, G., Costantini, H., Angulo, C., Bemmerer, D., Bonetti, R., Broggini, C., Corvisiero, P., Cruz, J., Descouvemont, P., Fülöp, Z., Gervino, G., Guglielmetti, A., Gustavino, C., Gyürky, G., Jesus, A. P., Junker, M., Lemut, A., Menegazzo, R., Prati, P., Roca, V., Rolfs, C., Romano, M., Rossi Alvarez, C., Schümann, F., Somorjai, E., Straniero, O., Strieder, F., Terrasi, F., Trautvetter, H. P., Vomiero, A., and Zavatarelli, S. Astrophysical S-factor of ^{14}N(p,γ)^{15}O. *Physics Letters B*, 591:61–68, July 2004. doi: 10.1016/j.physletb.2004.03.092.

Fu, X., Bressan, A., Molaro, P., and Marigo, P. Lithium evolution in metal-poor stars: from pre-main sequence to the Spite plateau. *MNRAS*, 452: 3256–3265, September 2015. doi: 10.1093/mnras/stv1384.

Giardino, G., Pillitteri, I., Favata, F., and Micela, G. The X-ray luminosity of solar-mass stars in the intermediate age open cluster NGC 752. *A&A*, 490:113–123, October 2008. doi: 10.1051/0004-6361:200810042.

Girardi, L., Dalcanton, J., Williams, B., de Jong, R., Gallart, C., Monelli, M., Groenewegen, M. A. T., Holtzman, J. A., Olsen, K. A. G., Seth, A. C., Weisz, D. R., and ANGST/ANGRRR Collaboration. Revised Bolometric Corrections and Interstellar Extinction Coefficients for the ACS and WFPC2 Photometric Systems. *PASP*, 120:583–591, May 2008. doi: 10.1086/588526.

Goupil, M. J. and Talon, S. Radial and Nonradial Pulsations as Probes of Stellar Physics. In Aerts, C., Bedding, T. R., and Christensen-Dalsgaard, J., editors, *IAU Colloq. 185: Radial and Nonradial Pulsationsn as Probes of Stellar Physics*, volume 259 of *Astronomical Society of the Pacific Conference Series*, page 306, 2002.

Grevesse, N. and Sauval, A. J. Standard Solar Composition. *Space Sci. Rev.*, 85:161–174, May 1998. doi: 10.1023/A:1005161325181.

Güdel, M., Guinan, E. F., and Skinner, S. L. The X-Ray Sun in Time: A Study of the Long-Term Evolution of Coronae of Solar-Type Stars. *ApJ*, 483:947–960, July 1997.

Guenther, D. B., Demarque, P., Kim, Y.-C., and Pinsonneault, M. H. Standard solar model. *ApJ*, 387:372–393, March 1992. doi: 10.1086/171090.

Guinan, E. F. and Engle, S. G. The Sun in time: age, rotation, and magnetic activity of the Sun and solar-type stars and effects on hosted planets. In Mamajek, E. E., Soderblom, D. R., and Wyse, R. F. G., editors, *IAU Symposium*, volume 258 of *IAU Symposium*, pages 395–408, June 2009. doi: 10.1017/S1743921309032050.

Guinan, E. F., Ribas, I., and Harper, G. M. Far-Ultraviolet Emissions of the Sun in Time: Probing Solar Magnetic Activity and Effects on Evolution of Paleoplanetary Atmospheres. *ApJ*, 594:561–572, September 2003. doi: 10.1086/376859.

Hall, J. C., Henry, G. W., and Lockwood, G. W. The Sun-like Activity of the Solar Twin 18 Scorpii. *AJ*, 133:2206–2208, May 2007. doi: 10.1086/513195.

Handler, G. *Asteroseismology*, page 207. 2013. doi: 10.1007/978-94-007-5615-1_4.

Hartmann, L., Calvet, N., Gullbring, E., and D'Alessio, P. Accretion and the Evolution of T Tauri Disks. *ApJ*, 495:385–400, March 1998. doi: 10.1086/305277.

Haywood, M. Radial mixing and the transition between the thick and thin Galactic discs. *MNRAS*, 388:1175–1184, August 2008. doi: 10.1111/j.1365-2966.2008.13395.x.

Henry, T. J., Soderblom, D. R., Donahue, R. A., and Baliunas, S. L. A Survey of Ca II H and K Chromospheric Emission in Southern Solar-Type Stars. *AJ*, 111:439, January 1996. doi: 10.1086/117796.

Holmberg, J., Nordström, B., and Andersen, J. The Geneva-Copenhagen survey of the Solar neighbourhood II. New uvby calibrations and rediscussion of stellar ages, the G dwarf problem, age-metallicity diagram, and heating mechanisms of the disk. *A&A*, 475:519–537, November 2007. doi: 10.1051/0004-6361:20077221.

Holmberg, J., Nordström, B., and Andersen, J. The Geneva-Copenhagen survey of the solar neighbourhood. III. Improved distances, ages, and kinematics. *A&A*, 501:941–947, July 2009. doi: 10.1051/0004-6361/200811191.

Huber, D., Carter, J. A., Barbieri, M., Miglio, A., Deck, K. M., Fabrycky, D. C., Montet, B. T., Buchhave, L. A., Chaplin, W. J., Hekker, S., Montalbán, J., Sanchis-Ojeda, R., Basu, S., Bedding, T. R., Campante, T. L., Christensen-Dalsgaard, J., Elsworth, Y. P., Stello, D., Arentoft, T., Ford, E. B., Gilliland, R. L., Handberg, R., Howard, A. W., Isaacson, H., Johnson, J. A., Karoff, C., Kawaler, S. D., Kjeldsen, H., Latham, D. W., Lund, M. N., Lundkvist, M., Marcy, G. W., Metcalfe, T. S., Silva Aguirre, V., and Winn, J. N. Stellar Spin-Orbit Misalignment in a Multiplanet System. *Science*, 342:331–334, October 2013. doi: 10.1126/science.1242066.

Iben, I., Jr. Thermal pulses; p-capture, alpha-capture, s-process nucleosynthesis; and convective mixing in a star of intermediate mass. *ApJ*, 196: 525–547, March 1975. doi: 10.1086/153433.

Jørgensen, B. R. and Lindegren, L. Determination of stellar ages from isochrones: Bayesian estimation versus isochrone fitting. *A&A*, 436:127–143, June 2005. doi: 10.1051/0004-6361:20042185.

Kasting, J. F. and Catling, D. Evolution of a Habitable Planet. *ARA&A*, 41:429–463, 2003. doi: 10.1146/annurev.astro.41.071601.170049.

Kjeldsen, H. and Bedding, T. R. Amplitudes of stellar oscillations: the implications for asteroseismology. *A&A*, 293:87–106, January 1995.

Komatsu, E., Smith, K. M., Dunkley, J., Bennett, C. L., Gold, B., Hinshaw, G., Jarosik, N., Larson, D., Nolta, M. R., Page, L., Spergel, D. N., Halpern, M., Hill, R. S., Kogut, A., Limon, M., Meyer, S. S., Odegard, N., Tucker, G. S., Weiland, J. L., Wollack, E., and Wright, E. L. Seven-year Wilkinson Microwave Anisotropy Probe (WMAP) Observations: Cosmological Interpretation. *ApJS*, 192:18, February 2011. doi: 10.1088/0067-0049/192/2/18.

Kovács, G. Are the gyro-ages of field stars underestimated? *A&A*, 581:A2, September 2015. doi: 10.1051/0004-6361/201525920.

Kraft, R. P. Studies of Stellar Rotation. V. The Dependence of Rotation on Age among Solar-Type Stars. *ApJ*, 150:551, November 1967. doi: 10.1086/149359.

Kroupa, P., Tout, C. A., and Gilmore, G. The distribution of low-mass stars in the Galactic disc. *MNRAS*, 262:545–587, June 1993. doi: 10.1093/mnras/262.3.545.

Laughlin, G. and Chambers, J. E. Short-Term Dynamical Interactions among Extrasolar Planets. *ApJ*, 551:L109–L113, April 2001. doi: 10.1086/319847.

Lebreton, Y., Goupil, M. J., and Montalbán, J. How accurate are stellar ages based on stellar models?. I. The impact of stellar models uncertainties. In *EAS Publications Series*, volume 65 of *EAS Publications Series*, pages 99–176, November 2014. doi: 10.1051/eas/1465004.

Lodders, K., Palme, H., and Gail, H.-P. Abundances of the Elements in the Solar System. *Landolt Börnstein*, page 44, 2009. doi: 10.1007/978-3-540-88055-4_34.

Loidl, R., Lançon, A., and Jørgensen, U. G. Spectra of carbon-rich asymptotic giant branch stars between 0.5 and 2.5 mu m: Theory meets observation. *A&A*, 371:1065–1077, June 2001. doi: 10.1051/0004-6361:20010400.

Ludwig, H.-G., Caffau, E., Steffen, M., Bonifacio, P., and Sbordone, L. Accuracy of spectroscopy-based radioactive dating of stars. *A&A*, 509:A84, January 2010. doi: 10.1051/0004-6361/200810780.

Maeder, A., Meynet, G., Lagarde, N., and Charbonnel, C. The thermohaline, Richardson, Rayleigh-Taylor, Solberg-Høiland, and GSF criteria in rotating stars. *A&A*, 553:A1, May 2013. doi: 10.1051/0004-6361/201220936.

Magic, Z., Weiss, A., and Asplund, M. The Stagger-grid: A grid of 3D stellar atmosphere models. III. The relation to mixing length convection theory. *A&A*, 573:A89, January 2015. doi: 10.1051/0004-6361/201423760.

Mamajek, E. E. and Hillenbrand, L. A. Improved Age Estimation for Solar-Type Dwarfs Using Activity-Rotation Diagnostics. *ApJ*, 687:1264–1293, November 2008. doi: 10.1086/591785.

Marigo, P. and Aringer, B. Low-temperature gas opacity. ÆSOPUS: a versatile and quick computational tool. *A&A*, 508:1539–1569, December 2009. doi: 10.1051/0004-6361/200912598.

Marques, J. P., Goupil, M. J., Lebreton, Y., Talon, S., Palacios, A., Belkacem, K., Ouazzani, R.-M., Mosser, B., Moya, A., Morel, P., Pichon, B., Mathis, S., Zahn, J.-P., Turck-Chièze, S., and Nghiem, P. A. P. Seismic diagnostics for transport of angular momentum in stars. I. Rotational splittings from the pre-main sequence to the red-giant branch. *A&A*, 549:A74, January 2013. doi: 10.1051/0004-6361/201220211.

Marzari, F. Impact of planet-planet scattering on the formation and survival of debris discs. *MNRAS*, 444:1419–1424, October 2014. doi: 10.1093/mnras/stu1544.

Mathis, S. Studying Stellar Rotation and Convection. In Goupil, M., Belkacem, K., Neiner, C., Ligniéres, F., and Green, J. J., editors, *Lecture Notes in Physics, Berlin Springer Verlag*, volume 865 of *Lecture Notes in Physics, Berlin Springer Verlag*, page 23, 2013. doi: 10.1007/978-3-642-33380-4.

Maxted, P. F. L., Koen, C., and Smalley, B. UBV(RI)$_C$ photometry of transiting planet hosting stars. *MNRAS*, 418:1039–1042, December 2011. doi: 10.1111/j.1365-2966.2011.19554.x.

Mayor, M. and Queloz, D. A Jupiter-mass companion to a solar-type star. *Nature*, 378:355–359, November 1995. doi: 10.1038/378355a0.

Meibom, S., Barnes, S. A., Platais, I., Gilliland, R. L., Latham, D. W., and Mathieu, R. D. A spin-down clock for cool stars from observations of a 2.5-billion-year-old cluster. *Nature*, 517:589–591, January 2015. doi: 10.1038/nature14118.

Mestel, L. On the theory of white dwarf stars. I. The energy sources of white dwarfs. *MNRAS*, 112:583, 1952.

Meynet, G., Ekstrom, S., and Maeder, A. Studying Stellar Rotation and Convection. In Goupil, M., Belkacem, K., Neiner, C., Ligniéres, F., and Green, J. J., editors, *Lecture Notes in Physics, Berlin Springer Verlag*, volume 865 of *Lecture Notes in Physics, Berlin Springer Verlag*, page 3, 2013. doi: 10.1007/978-3-642-33380-4.

Micela, G. Evolution of Stellar Coronal Activity on the Main Sequence. In Montesinos, B., Gimenez, A., and Guinan, E. F., editors, *The Evolving Sun and its Influence on Planetary Environments*, volume 269 of *Astronomical Society of the Pacific Conference Series*, page 107, 2002.

Micela, G., Sciortino, S., Kashyap, V., Harnden, F. R., Jr., and Rosner, R. ROSAT Observations of the Pleiades. I. X-Ray Characteristics of a Coeval Stellar Population. *ApJS*, 102:75, January 1996. doi: 10.1086/192252.

Middelkoop, F. Magnetic structure in cool stars. IV - Rotation and CA II H and K emission of main-sequence stars. *A&A*, 107:31–35, March 1982.

Mucciarelli, A., Caffau, E., Freytag, B., Ludwig, H.-G., and Bonifacio, P. The solar photospheric abundance of europium. Results from CO5BOLD

3D hydrodynamical model atmospheres. *A&A*, 484:841–845, June 2008. doi: 10.1051/0004-6361:20079327.

Nordström, B., Mayor, M., Andersen, J., Holmberg, J., Pont, F., Jørgensen, B. R., Olsen, E. H., Udry, S., and Mowlavi, N. The Geneva-Copenhagen survey of the Solar neighbourhood. Ages, metallicities, and kinematic properties of ∼14 000 F and G dwarfs. *A&A*, 418:989–1019, May 2004. doi: 10.1051/0004-6361:20035959.

Noyes, R. W., Hartmann, L. W., Baliunas, S. L., Duncan, D. K., and Vaughan, A. H. Rotation, convection, and magnetic activity in lower main-sequence stars. *ApJ*, 279:763–777, April 1984. doi: 10.1086/161945.

Pätzold, M., Carone, L., and Rauer, H. Tidal interactions of close-in extrasolar planets: The OGLE cases. *A&A*, 427:1075–1080, December 2004. doi: 10.1051/0004-6361:20040258.

Rauer, H., Catala, C., Aerts, C., Appourchaux, T., Benz, W., Brandeker, A., Christensen-Dalsgaard, J., Deleuil, M., Gizon, L., Goupil, M.-J., Güdel, M., Janot-Pacheco, E., Mas-Hesse, M., Pagano, I., Piotto, G., Pollacco, D., Santos, Ċ., Smith, A., Suárez, J.-C., Szabó, R., Udry, S., Adibekyan, V., Alibert, Y., Almenara, J.-M., Amaro-Seoane, P., Eiff, M. A.-v., Asplund, M., Antonello, E., Barnes, S., Baudin, F., Belkacem, K., Bergemann, M., Bihain, G., Birch, A. C., Bonfils, X., Boisse, I., Bonomo, A. S., Borsa, F., Brandão, I. M., Brocato, E., Brun, S., Burleigh, M., Burston, R., Cabrera, J., Cassisi, S., Chaplin, W., Charpinet, S., Chiappini, C., Church, R. P., Csizmadia, S., Cunha, M., Damasso, M., Davies, M. B., Deeg, H. J., Díaz, R. F., Dreizler, S., Dreyer, C., Eggenberger, P., Ehrenreich, D., Eigmüller, P., Erikson, A., Farmer, R., Feltzing, S., de Oliveira Fialho, F., Figueira, P., Forveille, T., Fridlund, M., García, R. A., Giommi, P., Giuffrida, G., Godolt, M., Gomes da Silva, J., Granzer, T., Grenfell, J. L., Grotsch-Noels, A., Günther, E., Haswell, C. A., Hatzes, A. P., Hébrard, G., Hekker, S., Helled, R., Heng, K., Jenkins, J. M., Johansen, A., Khodachenko, M. L., Kislyakova, K. G., Kley, W., Kolb, U., Krivova, N., Kupka, F., Lammer, H., Lanza, A. F., Lebreton, Y., Magrin, D., Marcos-Arenal, P., Marrese, P. M., Marques, J. P., Martins, J., Mathis, S., Mathur, S., Messina, S., Miglio, A., Montalban, J., Montalto, M., Monteiro, M. J. P. F. G., Moradi, H., Moravveji, E., Mordasini, C., Morel, T., Mortier, A., Nascimbeni, V., Nelson, R. P., Nielsen, M. B., Noack, L., Norton, A. J., Ofir, A., Oshagh, M., Ouazzani, R.-M., Pápics, P., Parro, V. C., Petit, P., Plez, B., Poretti, E., Quirrenbach, A., Ragazzoni, R., Raimondo, G., Rainer, M., Reese, D. R., Redmer, R., Reffert, S., Rojas-Ayala, B., Roxburgh, I. W., Salmon,

S., Santerne, A., Schneider, J., Schou, J., Schuh, S., Schunker, H., Silva-Valio, A., Silvotti, R., Skillen, I., Snellen, I., Sohl, F., Sousa, S. G., Sozzetti, A., Stello, D., Strassmeier, K. G., Švanda, M., Szabó, G. M., Tkachenko, A., Valencia, D., Van Grootel, V., Vauclair, S. D., Ventura, P., Wagner, F. W., Walton, N. A., Weingrill, J., Werner, S. C., Wheatley, P. J., and Zwintz, K. The PLATO 2.0 mission. *Experimental Astronomy*, 38:249–330, November 2014. doi: 10.1007/s10686-014-9383-4.

Reddy, B. E., Lambert, D. L., and Allende Prieto, C. Elemental abundance survey of the Galactic thick disc. *MNRAS*, 367:1329–1366, April 2006. doi: 10.1111/j.1365-2966.2006.10148.x.

Ribas, I., Guinan, E. F., Güdel, M., and Audard, M. Evolution of the Solar Activity over Time and Effects on Planetary Atmospheres. I. High-Energy Irradiances (1-1700 Å). *ApJ*, 622:680–694, March 2005. doi: 10.1086/427977.

Rocha-Pinto, H. J., Scalo, J., Maciel, W. J., and Flynn, C. Chemical enrichment and star formation in the Milky Way disk. II. Star formation history. *A&A*, 358:869–885, June 2000.

Salasnich, B. *PhD Thesis*. PhD thesis, Universitá degli Studi di Padova, 1999.

Santos, N. C., Sousa, S. G., Mortier, A., Neves, V., Adibekyan, V., Tsantaki, M., Delgado Mena, E., Bonfils, X., Israelian, G., Mayor, M., and Udry, S. SWEET-Cat: A catalogue of parameters for Stars With ExoplanETs. I. New atmospheric parameters and masses for 48 stars with planets. *A&A*, 556:A150, August 2013. doi: 10.1051/0004-6361/201321286.

Schlaufman, K. C. Evidence of Possible Spin-orbit Misalignment Along the Line of Sight in Transiting Exoplanet Systems. *ApJ*, 719:602–611, August 2010. doi: 10.1088/0004-637X/719/1/602.

Schmidt, M. The Rate of Star Formation. *ApJ*, 129:243, March 1959. doi: 10.1086/146614.

Silva Aguirre, V., Davies, G. R., Basu, S., Christensen-Dalsgaard, J., Creevey, O., Metcalfe, T. S., Bedding, T. R., Casagrande, L., Handberg, R., Lund, M. N., Nissen, P. E., Chaplin, W. J., Huber, D., Serenelli, A. M., Stello, D., Van Eylen, V., Campante, T. L., Elsworth, Y., Gilliland, R. L., Hekker, S., Karoff, C., Kawaler, S. D., Kjeldsen, H., and Lundkvist, M. S. Ages and fundamental properties of Kepler exoplanet host stars from asteroseismology. *ArXiv e-prints*, April 2015.

Skumanich, A. Time Scales for CA II Emission Decay, Rotational Braking, and Lithium Depletion. *ApJ*, 171:565, February 1972. doi: 10.1086/151310.

Soderblom, D. R. The Ages of Stars. *ARA&A*, 48:581–629, September 2010. doi: 10.1146/annurev-astro-081309-130806.

Southworth, J., Hinse, T. C., Dominik, M., Glitrup, M., Jørgensen, U. G., Liebig, C., Mathiasen, M., Anderson, D. R., Bozza, V., Browne, P., Burgdorf, M., Calchi Novati, S., Dreizler, S., Finet, F., Harpsøe, K., Hessman, F., Hundertmark, M., Maier, G., Mancini, L., Maxted, P. F. L., Rahvar, S., Ricci, D., Scarpetta, G., Skottfelt, J., Snodgrass, C., Surdej, J., and Zimmer, F. Physical Properties of the 0.94-Day Period Transiting Planetary System WASP-18. *ApJ*, 707:167, December 2009. doi: 10.1088/0004-637X/707/1/167.

Sozzetti, A., Torres, G., Charbonneau, D., Latham, D. W., Holman, M. J., Winn, J. N., Laird, J. B., and O'Donovan, F. T. Improving Stellar and Planetary Parameters of Transiting Planet Systems: The Case of TrES-2. *ApJ*, 664:1190–1198, August 2007. doi: 10.1086/519214.

Spezzi, L., de Marchi, G., Panagia, N., Sicilia-Aguilar, A., and Ercolano, B. Photometric determination of the mass accretion rates of pre-mainsequence stars - III. Results in the Large Magellanic Cloud. *MNRAS*, 421:78–97, March 2012. doi: 10.1111/j.1365-2966.2011.20130.x.

Stern, R. A., Schmitt, J. H. M. M., and Kahabka, P. T. ROSAT All-Sky Survey Observations of the Hyades Cluster. *ApJ*, 448:683, August 1995. doi: 10.1086/175997.

Straniero, O., Chieffi, A., and Salaris, M. The influence of the galactic early nucleosynthesis on age and distance determinations for globular clusters. *Mem. Soc. Astron. Italiana*, 63:315–320, 1992.

Strigari, L. E., Barnabè, M., Marshall, P. J., and Blandford, R. D. Nomads of the Galaxy. *MNRAS*, 423:1856–1865, June 2012. doi: 10.1111/j.1365-2966.2012.21009.x.

Talon, S., Zahn, J.-P., Maeder, A., and Meynet, G. Rotational mixing in early-type stars: the main-sequence evolution of a $9M_{sun-}$ star. *A&A*, 322: 209–217, June 1997.

Thoul, A. A., Bahcall, J. N., and Loeb, A. Element diffusion in the solar interior. *ApJ*, 421:828–842, February 1994. doi: 10.1086/173695.

Tinetti, G., Drossart, P., Eccleston, P., Hartogh, P., Isaak, K., Linder, M., Lovis, C., Micela, G., Ollivier, M., Puig, L., and et al. The EChO science case. *Experimental Astronomy*, November 2015. doi: 10.1007/s10686-015-9484-8.

Torres, G. On the Use of Empirical Bolometric Corrections for Stars. *AJ*, 140:1158–1162, November 2010. doi: 10.1088/0004-6256/140/5/1158.

Trampedach, R. and Stein, R. F. The Mass Mixing Length in Convective Stellar Envelopes. *ApJ*, 731:78, April 2011. doi: 10.1088/0004-637X/731/2/78.

Van Saders, J. L., Ceillier, T., Metcalfe, T. S., Silva Aguirre, V., Pinsonneault, M. H., García, R. A., Mathur, S., and Davies, G. R. Weakened magnetic braking as the origin of anomalously rapid rotation in old field stars. *ArXiv e-prints*, January 2016.

Vaughan, A. H., Preston, G. W., and Wilson, O. C. Flux measurements of CA II H and K emission. *PASP*, 90:267–274, June 1978. doi: 10.1086/130324.

Winn, J. N. Transits and Occultations. *ArXiv e-prints*, January 2010.